UNCLASSIFIED

MARTIN MARIETTA ENERGY SYSTEMS LIBRARIES
3 4456 0049742 4

ORNL-2272
Progress cy. 8

CENTRAL RESEARCH LIBRARY
DOCUMENT COLLECTION

HOMOGENEOUS REACTOR PROJECT

QUARTERLY PROGRESS REPORT

FOR PERIOD ENDING JANUARY 31, 1957

CENTRAL RESEARCH LIBRARY
DOCUMENT COLLECTION

LIBRARY LOAN COPY

DO NOT TRANSFER TO ANOTHER PERSON

If you wish someone else to see this document, send in name with document and the library will arrange a loan.

OAK RIDGE NATIONAL LABORATORY
OPERATED BY
UNION CARBIDE NUCLEAR COMPANY
A Division of Union Carbide and Carbon Corporation
UCC
POST OFFICE BOX X · OAK RIDGE, TENNESSEE

UNCLASSIFIED

Printed in USA. Price 110 cents. Available from the

Office of Technical Services
U. S. Department of Commerce
Washington 25, D. C.

LEGAL NOTICE

This report was prepared as an account of Government sponsored work. Neither the United States, nor the Commission, nor any person acting on behalf of the Commission:

A. Makes any warranty or representation, express or implied, with respect to the accuracy, completeness, or usefulness of the information contained in this report, or that the use of any information, apparatus, method, or process disclosed in this report may not infringe privately owned rights; or

B. Assumes any liabilities with respect to the use of, or for damages resulting from the use of any information, apparatus, method, or process disclosed in this report.

As used in the above, "person acting on behalf of the Commission" includes any employee or contractor of the Commission to the extent that such employee or contractor prepares, handles or distributes, or provides access to, any information pursuant to his employment or contract with the Commission.

UNCLASSIFIED

ORNL-2272

Contract No. W-7405-eng-26

HOMOGENEOUS REACTOR PROJECT

QUARTERLY PROGRESS REPORT

For Period Ending January 31, 1957

Project Director – R, B. Briggs
Associate Director – C. E. Winters

Homogeneous Reactor Test – S. E. Beall
Reactor Design and Analysis – J. A. Lane
Engineering Development – J. A. Lane
Reactor Materials Research – E. G. Bohlmann
Chemical Engineering Development – F. R. Bruce
Supporting Chemical Research – E. H. Taylor
Analytical Chemistry – M. T. Kelley

DATE ISSUED APR 3 1957

OAK RIDGE NATIONAL LABORATORY
Operated by
UNION CARBIDE NUCLEAR COMPANY
A Division of Union Carbide and Carbon Corporation
Post Office Box X
Oak Ridge, Tennessee

UNCLASSIFIED

MARTIN MARIETTA ENERGY SYSTEMS LIBRARIES
3 4456 0049742 4

ORNL-2272
Progress

INTERNAL DISTRIBUTION

1. C. E. Center
2. Biology Library
3. Health Physics Library
4. Metallurgy Library
5-6. Reactor Experimental Engineering Library
Central Research Library
10-14. Laboratory Records Department
15. Laboratory Records, ORNL R.C.
16. G. M. Adamson
17. J. E. Baker
18. S. E. Beall
19. A. M. Billings
20. D. S. Billington
21. E. P. Blizard
22. E. G. Bohlmann
23. C. J. Borkowski
24. G. E. Boyd
25. J. C. Bresee
26. F. R. Bruce
27. W. D. Burch
28. C. A. Burchsted
29. A. D. Callihan
30. D. W. Cardwell
31. W. L. Carter
32. G. H. Cartledge
33. R. A. Charpie
34. R. D. Cheverton
35. H. C. Claiborne
36. W. E. Clark
37. T. E. Cole
38. E. L. Compere
39. D. D. Cowen
40. S. Cromer
41. F. L. Culler
42. J. S. Culver
43. J. S. Drury
44. W. K. Eister
45. L. B. Emlet (K-25)
46. D. E. Ferguson
47. J. H. Frye, Jr.
48. C. H. Gabbard
49. J. L. Gabbard
50. W. R. Gall
51. H. E. Goeller
52. A. T. Gresky
53. J. C. Griess
54. E. Guth
55. P. H. Harley
56. P. N. Haubenreich
57. J. W. Hill
58. C. J. Hochanadel
59. A. Hollaender
60. A. S. Householder
61. G. H. Jenks
62. W. H. Jordan
63. S. I. Kaplan
64. P. R. Kasten
65. C. P. Keim
66. M. T. Kelley
67. R. B. Korsmeyer
68. A. S. Kitzes
69. K. A. Kraus
70. J. A. Lane
71. W. J. Leonard
72. R. E. Leuze
73. S. C. Lind
74. R. B. Lindauer
75. R. S. Livingston
76. M. I. Lundin
77. R. N. Lyon
78. J. L. Marsh (C&CCC, South Charleston)
79. H. F. McDuffie
80. J. P. McBride
81. R. A. McNees
82. J. R. McWherter
83. O. Menis
84. E. C. Miller
85. K. Z. Morgan
86. E. J. Murphy
87. M. L. Nelson
88. E. O. Nurmi
89. J. P. Murray (Y-12)
90. L. F. Parsly
91. Sigfred Peterson
92. M. L. Picklesimer
93. L. R. Quarles
94. W. D. Reel
95. P. M. Reyling
96. A. M. Rom
97. M. W. Rosenthal
98. W. L. Ross

99. H. C. Savage
100. C. H. Secoy
101. C. L. Segaser
102. E. D. Shipley
103. M. J. Skinner
104. R. W. Stoughton
105. A. H. Snell
106. I. Spiewak
107. C. D. Susano
108. J. A. Swartout
109. E. H. Taylor
110. D. G. Thomas
111. P. F. Thomason
112. M. Tobias
113. D. S. Toomb
114. W. E. Unger
115. R. Van Winkle
116. B. Weaver
117. A. M. Weinberg
118. E. P. Wigner (consultant)
119. G. C. Williams
120. J. C. Wilson
121. C. E. Winters
122. F. C. Zapp
123. ORNL – Y-12 Technical Library, Document Reference Section
124. HRP Director's Office, Y-12

EXTERNAL DISTRIBUTION

125. Houdry Corporation (Attn: G. A. Mills)
126. Division of Research and Development, AEC, ORO
127-133. TISE for P.A.R.P.
134-709. Given distribution as shown in TID-4500 (12th ed.) under Engineering category (200 copies – OTS)

Reports previously issued in this series are as follows:

ORNL-527	Date Issued, December 28, 1949
ORNL-630	Period Ending February 28, 1950
ORNL-730	Feasibility Report – Date Issued, July 6, 1950
ORNL-826	Period Ending August 31, 1950
ORNL-925	Period Ending November 30, 1950
ORNL-990	Period Ending February 28, 1951
ORNL-1057	Period Ending May 15, 1951
ORNL-1121	Period Ending August 15, 1951
ORNL-1221	Period Ending November 15, 1951
ORNL-1280	Period Ending March 15, 1952
ORNL-1318	Period Ending July 1, 1952
ORNL-1424	Period Ending October 1, 1952
ORNL-1478	Period Ending January 1, 1953
ORNL-1554	Period Ending March 31, 1953
ORNL-1605	Period Ending July 31, 1953
ORNL-1658	Period Ending October 31, 1953
ORNL-1678	Period Ending January 31, 1954
ORNL-1753	Period Ending April 30, 1954
ORNL-1772	Period Ending July 31, 1954
ORNL-1813	Period Ending October 31, 1954
ORNL-1853	Period Ending January 31, 1955
ORNL-1895	Period Ending April 30, 1955
ORNL-1943	Period Ending July 31, 1955
ORNL-2004	Period Ending October 31, 1955
ORNL-2057	Period Ending January 31, 1956
ORNL-2096	Period Ending April 30, 1956
ORNL-2148	Period Ending July 31, 1956
ORNL-2222	Period Ending October 31, 1956

HRP QUARTERLY PROGRESS REPORT

SUMMARY

PART I. HOMOGENEOUS REACTOR TEST

1. HRT Operations

During November and December numerous modifications were made to the differential-pressure control system and the oxygen-metering system. The flanged joints on the core outlet and the rupture-disk pot were reworked, and a number of critical valves were replaced. Short water runs were made to check leak-tightness and operability of the modified components and to simulate conditions for low-temperature criticality runs. Successful tests of remote maintenance practices were conducted, including some underwater operations.

Two extended water runs were made during January, in which 294 hr was accumulated at 1500 psi and 280°C, making a total of 441 hr at 280°C. During the tests (1) the core-blanket differential pressure during venting and dumping was controlled within satisfactory limits; (2) the reactor temperature was controlled satisfactorily for criticality tests by using cooling water on the shell side of the steam generator; (3) no further leakage around the rupture disks, or disk failure, was observed after the installation of the gold disks, rated at 200 psig; (4) chloride ion concentration in the reactor and in the leak-detector system was held to 1 ppm or less; and (5) performance of the water-filled leak-detector system was judged to be acceptable for operation with a radioactive system.

During operation, difficulties were encountered with erratic diaphragm-pump performance, which was traced to leaking check valves and phasing valves, and in one case, a ruptured diaphragm. Also, seven valve replacements had to be made, one because of faulty construction, two because of improper stem travel adjustment, and four because of erosion or corrosion of the trim materials.

Several flanges and sections of leak-detector tubing were removed for further study of the effects of the chloride contamination reported last quarter. The cracks in the leak-detector system were shown by the HRP Metallurgy Group to be caused by stress corrosion from a chloride impurity left in the tubing. This chloride had leached from the leak-detector tubing and caused similar cracking in the main flanges and O-rings. Severe pitting was found in all flanges examined. Replacement of all these components has been recommended by the Metallurgy Group.

Improper heat treatment was shown to be the cause of several cracks found in the bolts and ferrules from the HRT flanges. Suitable inspection techniques for revealing these cracks were developed.

2. HRT Design

Amsco 125-82 was recommended as the secondary refrigerant for the HRT, replacing Freon-11. The use of hydrazine for the control of oxygen concentration and coordinated phosphate treatment for control of pH in the HRT steam-system feed water was recommended. Criteria for radiation protection necessitated by the changes to the cooling-water system were established. Some possibility of overstressing the steam outlet piping of the fuel heat exchanger exists during warmup of the heat exchanger. Reinvestigation of the deuterium recombination problem indicates that with the presently installed pressurizer bleed valves a 2-min delay is required during a reactor dump to minimize the explosion hazard due to the concentrations of deuterium and oxygen. Investigation of the possibility of precipitation of uranyl peroxide in the fuel circulating pump indicated that no danger from such an occurrence is to be expected as long as the purge flow continues. Preliminary conclusions drawn from the operation of the flange test loop confirm the need of careful selection, handling, and installation of ring-joint flanges and gaskets and the need for more reliable means of determining bolt loading.

3. HRT Component Development

The 400A-1 and 400A-2 pumps continued to circulate 0.04 *m* UO_2SO_4 solution without difficulty. The 300A-1 pump operated in the HRT mockup for a total of 5541 hr without incident; inspection following this period, however, revealed excessive bearing wear and extensive cracking in the thermal-barrier seal weld. After repair, the pump operated for 482 hr before similar troubles were experienced.

Diaphragm-pump development loops continued to operate without any diaphragm failures. Protection of diaphragms from dirt particles was improved by use of 100-mesh screen filters.

The prototype HRT sampler was operated to determine its "memory" in taking successive samples of different mediums. In tests of ½-in.-pipe freezer coils it was found that, at constant temperature, variations in pressure had no appreciable effect on the leak rate at which water could be frozen. Flow and pressure-drop measurements were made on a model of the proposed HRT core sample holder.

The HRT mockup completed a 1925-hr run with 0.04 *m* UO_2SO_4 without incident. Following some modifications, 1.3 *m* UO_2SO_4 was circulated for 200 hr before circulating-pump trouble forced termination of the run.

4. HRT Reactor Analysis

The development of maintenance procedures for the HRT requires an estimate of the radiation escaping through biological-shield openings. For this purpose the biological dose rate associated with the leakage of gamma rays was calculated as a function of gamma-source position and size of shield opening. These results were obtained in the form of design charts for 8-, 14-, and 16-in.-dia openings and apply to the HRT 4 hr after shutdown.

5. HRT Controls and Instrumentation

A differential-expansion-type control valve was installed to replace the fuel-system oxygen-metering valve, which developed severe leakage past the seat. The new valve has performed satisfactorily for four weeks.

A study of pressure and temperature effects on the pressurizer-level transmitters was made to define errors in the level indication which can occur during periods of heating or cooling of the reactor system.

Excellent performance in 5000 hr of operation was obtained from the HRT-model letdown valve installed on the HRT mockup in uranyl sulfate service. However, similar valves installed on the reactor suffered corrosive attack from the rinse solutions and water circulated to date.

A high-level gamma ionization chamber was developed to measure reactor-cell ambient radiation levels as high as 10^7 r/hr.

A controls system was designed for the revised HRT closed-circuit cooling-water system. The controls provide for supplying emergency cooling water from the cooling tower if the reserve in the closed circuit becomes exhausted. Valve and pilot solenoid actions have been selected to give "fail-safe" action, with activity containment considerations given precedence over system operation and equipment protection.

6. HRT Processing Plant

Testing operations in the HRT chemical plant high-pressure (hydroclone) system with simulated corrosion-product solids were successfully completed. Concentration factors as high as 1700 were achieved, but the material balances were low (approximately 70%) because of solids deposition on the piping walls. Solids concentration fell off logarithmically at a rate corresponding to a half life of about 11 hr (attributed to deposition) without the hydroclone and 1 to 2½ hr with the hydroclone.

The hydroclone retainer plug, which galled during attempts to remove the hydroclone, will be replaced with one of improved design. The thrust bearing of the 1-gpm canned-rotor pump displayed excessive wear, and the thermal-barrier gasket and scroll gaskets leaked, but these closures are designed for seal welding.

The fuel-processing pilot plant has been shut down for the installation of dissolver equipment, which is scheduled for completion and initial testing in March.

PART II. REACTOR DESIGN AND ANALYSIS

7. Reactor Analysis

Two-group, two-region nuclear calculations have been extended for 10- and 12-ft-dia spherical reactors containing D_2O-ThO_2-$U^{233}O_2$ in both the core and blanket regions. For these reactors the critical concentration of U^{233} in the core increased with increasing core thorium concentration, decreased with increasing core diameter, and varied only slightly with changes in blanket thickness, blanket U^{233} concentration, and blanket thorium concentration. The fraction of total power generated in the blanket increased nearly linearly with increasing blanket U^{233} concentration and decreased with increasing core diameter and increasing core and blanket thorium concentrations. The U^{233}/Th

core concentration required for criticality passed through a minimum with increasing core thorium concentration; this minimum occurred at core thorium concentrations between 100 and 200 g of thorium per liter for the cases studied.

Preliminary results have been obtained for steady-state fuel costs in two-region thorium breeder reactors (thorium in both core and blanket). Results indicate that fuel costs will lie between 1 and 2 mills/kwhr if inventory charges are between 4 and 12% per year.

The effects upon breeding ratio of neutron leakage and neutron resonance absorption in fuel were studied for single-region ThO_2-D_2O-$U^{233}O_2$ reactors. For a given reactor size, increasing the thorium concentration decreased the leakage but increased the neutron resonance absorption in fuel. Thus, if the resonance value of η^{23} were less than the thermal value, a finite thorium concentration would exist for which the breeding ratio would be a maximum. If η_{res}/η_{th} were 0.9, the breeding ratio in a 14-ft-dia reactor would have a maximum value at a thorium concentration near 500 g/liter.

The cost of electrical power associated with the use of $Th(N^{15}O_3)_4$ in a two-region thorium-breeder power reactor has been estimated. Because of the high costs associated with replacing the decomposed nitrate, use of an N^{15} solution appears uneconomical based on present data. If 5% of the fission power were generated within a blanket containing 1000 g of thorium per liter, the power cost associated with nitrate decomposition would be about 4 mills/kwhr if the effective cost of $DN^{15}O_3$ were \$3 per pound (3¢ per gram of N^{15}).

An economic evaluation of organic-moderated homogeneous power-breeder reactors was made. Based on present data the use of deuterated hydrocarbons appears uneconomical for both one- and two-region systems. The power cost associated with the radiation damage suffered by organic materials appears to be particularly high (>10 mills/kwhr) for one-region reactors. The use of an organic material in the blanket of a two-region reactor appears to be more promising; even so, the power cost associated with the radiation damage and the accompanying blanket-processing cycle time appears to be greater than 1 mill/kwhr.

An Oracle code was written for calculating the steady-state fuel costs in two-region, thorium breeder reactors.

PART III. ENGINEERING DEVELOPMENT

8. Development of Fuel-System Components

The high-pressure recombiner loop completed a 200-hr run in which titanium and zirconium alloy specimens were exposed; some of the specimens absorbed large amounts of hydrogen. Battelle Memorial Institute completed their investigation of the reaction limits of the H_2-O_2-H_2O system. Syracuse University completed an investigation of the behavior of rupture disks exposed to detonations. Experimental and calculated detonation pressures in the H_2-O_2-H_2O system were reported.

The 20-cfm canned-motor blower was operated for 13 hr, and excessive wear was observed in its hydrostatic bearings. After successful performance through the report period, operation of three 5-gpm ORNL pumps was discontinued. The 4000-gpm pump suffered two can failures.

Further delays in procurement of titanium-lined equipment were caused by vendors' difficulties in obtaining suitable material.

Some cracking was experienced in a small heat exchanger containing nickel-plated tubing exposed for 600 hr to a Cl–O_2–boiling-water environment.

9. Development of Reactor Slurry Systems

A heat transfer system was constructed to check the validity of the Lawson heat transfer equation for slurries.

Values of yield stress for slurry circulated for 1994 hr in a 200-gpm loop, run 200A-5B, were found to be about 40% higher than any value obtained at the same concentration with similar slurries pumped for a shorter length of time.

Hard cakes produced in the 200-gpm loop have been partially disintegrated in laboratory tests by being flooded with dilute electrolytes after they were air-dried at 110°C.

A thorium-uranium oxide slurry prepared by simple mixing of thoria and $UO_3 \cdot H_2O$, containing 2% uranium and 2000 ppm sulfate based on the thorium oxide, was circulated at 300°C in a 100-gpm loop. No difficulties were encountered in pumping the slurry, and the generalized attack rate on stainless steel was not significantly different from that of pure thoria slurries. The same type of mixed oxide slurry, containing 3% uranium, was circulated in

the 200-gpm loop for 775 hr at 250°C without incident. The generalized corrosion rate was about 0.5 mpy in the loop piping.

A new type of continuous density meter, called the "pressure bridge," was tested successfully in a low-temperature loop.

The first slurry run was started in the blanket test system following removal of the heat exchangers which had plugged in previous slurry runs. During the 1350 hr that the run has been in progress, water high in chloride was removed from the pressurizer, presumably due to leaching of chloride impurities from the thoria; the larger part of the thoria apparently lay in the blanket without significant circulation; the thoria concentration in the circulating stream varied inversely with the loop temperature and at all times was below the concentration calculated from the material charged; there was a steady downward drift in stream concentration with time, not attributable to temperature; and the stream concentration was extremely sensitive to temperature rises just above about 180°C.

10. Valve Development

A type 347 stainless steel bellows of the type used in the HRT for sealing valve stems was gold-plated in an attempt to improve its corrosion resistance. The bellows failed after 3500 cycles with a stroke of $\frac{1}{8}$ in. in uranyl sulfate at 2000 psi and 300°C, but since it had been overstressed to permit the plating solution to penetrate to the inner folds, the test is not considered conclusive.

A valve trim, designed for tight shutoff, incorporating a gold gasket recessed in a groove in the plug and mating with an annular ring on the seat, performed well on the valve test loop.

PART IV. REACTOR MATERIALS RESEARCH

11. Solution Corrosion

A second test of the mockup of the Zircaloy–stainless steel transition joint used in the HRT reactor vessel was completed. The unit has now received 104 thermal cycles, and the bellows has withstood 148 mechanical deflections. The joint and bellows have functioned properly, and corrosion damage has been negligible, except for a small area on the bellows which has undergone pitting attack.

Long-term runs with uranyl sulfate solutions of the concentration proposed for use in the HRT (0.04 *m* UO_2SO_4, 0.02 *m* H_2SO_4, and 0.005 *m* $CuSO_4$) showed the solution to be stable at 300°C. Critical velocities on stainless steel were 15 to 20 fps at 200°C, 25 to 35 fps at 250°C, and 35 to 40 fps at 300°C. Substituting heavy water for normal water caused no difference in either corrosion or solution stability.

Experiments in which chromic acid was used to pretreat stainless steel showed that, under certain conditions, the pretreatment film can exist for relatively long periods of time in uranyl sulfate solutions at flow rates in excess of the critical velocity.

The practicability of using titanium inserts in highly turbulent areas of stainless steel loops to minimize corrosion was demonstrated. One 100A loop was operated for 9900 hr with titanium inserts in regions which normally suffer heavy corrosion damage. The titanium was essentially unattacked, and the crevice between the stainless steel and the titanium caused no undue corrosion of either the titanium or the stainless steel.

The corrosiveness of beryllium sulfate solutions containing dissolved uranium trioxide was determined at 250 and 280°C. The solutions showed no advantage over uranyl sulfate solutions of the same concentration. In fact, at low flow rates the attack was greater in the beryllium-containing solution. On the other hand, at 250 and 300°C, 0.04 *m* UO_2SO_4 containing equimolal beryllium sulfate showed approximately the same corrosion behavior as 0.04 *m* UO_2SO_4 containing 0.02 *m* H_2SO_4 at the same temperature.

Laboratory studies of stress-corrosion cracking have shown that highly stressed type 347 stainless steel will crack in boiling uranyl sulfate solutions containing 25 and 50 ppm chloride ions. At chloride concentrations of 0, 5, 10, and 100 ppm, cracking has not been observed; at the 500-ppm chloride level, possible incipient cracking was observed after a 500-hr exposure. Neither bromide nor iodide ions incorporated in uranyl sulfate solutions produced cracking.

Cold-formed type 347 stainless steel pipes developed stress-corrosion cracks when steam (153°C) was passed through them and chloride-containing potable water was sprayed on their surfaces. Either annealing or shot peening the pipes after bending prevented cracking during a 1000-hr test, but stress-relief treatments between 600 and 1250°F were ineffective in preventing

cracking. Cold-formed titanium and modified type 430 stainless steel showed no tendency to crack.

A number of different zirconium-base alloys prepared by the HRP Metallurgy Group were tested in uranyl sulfate solutions. Although all alloys tested showed good corrosion resistance to uranyl sulfate solutions, none of the alloys were as resistant as Zircaloy-2.

Corrosion studies related to the chemical processing plant of the HRT have primarily involved testing stabilized Carpenter 20-Cb stainless steel specimens which are representative of the material being used in fabrication of the plant. Most of the tests have been run in boiling 4 *M* H_2SO_4 containing simulated corrosion and fission products. All specimens showed adequate corrosion resistance, with two exceptions: One specimen showed apparent stress-corrosion cracks, and one welded specimen showed knife-line attack and some selective attack of the weld metal itself.

12. Slurry Corrosion

Dynamic-corrosion data and operating experiences are reported for four thorium oxide slurry runs made at 300°C in 100A pump loops at concentrations of 347 to 635 g of thorium per kilogram of H_2O, with operating times of 139 to 335 hr. Two different batches of thoria were used.

One thoria batch formed slurry spheroids up to 80 μ in diameter and formed hard deposits in the pump. Corrosion of metal specimens was normal, but an aluminum oxide pump bearing was damaged. A subsequent run, also with oxygen atmosphere, and with Na_2SO_4 added, showed somewhat higher corrosion rates for austenitic stainless steels and titanium, smaller spheroids, no deposits of thoria, and no damage to Graphitar bearings.

Two runs with a different batch of thoria, under a hydrogen-argon atmosphere with excess hydrazine added to remove trace oxygen, formed very small or no spheroids and no deposits, showed lower corrosion rates on austenitic stainless steels, and did not damage aluminum oxide pump bearings. Some embrittlement of thin sheet titanium pump seal rings appeared to be associated with hydrogen pickup.

Stress-corrosion cracking, apparently as a result of chloride associated with thorium oxide, was shown to have occurred in a type 347 stainless steel toroid after approximately 4000 hr of circulating aqueous thoria slurries. An apparently identical toroid of somewhat similar operating history gave no evidence of stress-corrosion cracking, however.

Relatively large attack rates on type 347 stainless steel and titanium were obtained for 50-hr circulating times with raw slurries in toroids. During this same period the size of the oxide was decreased significantly. Slurries of relatively small and constant-size oxide, obtained by precirculating the slurry for at least 50 hr, gave rates for short exposures that were distinctly lower than those obtained with raw slurries.

Batch LO-14 thorium oxide yielded slurries that often behaved quite similarly to previously studied slurries whose behavior was accepted as normal. On one occasion, however, entirely different characteristics were observed, chiefly a growth of particles to giant proportions (from about 3-μ particles to 150- by 200-μ ellipsoids).

During the past quarter, emphasis shifted from an in-pile slurry loop to an in-pile slurry toroid. Preliminary tests have been made on an experimental model.

13. Radiation Corrosion

The construction and operational testing of in-pile loop L-4-16 were completed, and it is presently in operation in beam hole HB-4 of the LITR. Loop L-2-14 (titanium) is undergoing operational testing prior to insertion into beam hole HB-2. The construction of loops L-2-17 and L-4-18 is under way.

One of the Byron-Jackson 5-gpm pumps successfully completed a 943-hr test in which a uranyl sulfate solution was circulated.

Design and development work for a dynamic-loop radiation-corrosion facility in the ORR has continued. The ORR loop installation is being modeled after the LITR in-pile loop facilities. Some changes have been necessitated by the higher radiation intensities which will be encountered at the ORR.

The eighth in-pile loop experiment, L-2-10, type 347 stainless steel, has been completed. This was the first loop exposed in LITR beam hole HB-2. The solution composition was the same as that proposed for use in the HRT, except that H_2O rather than D_2O was employed as the solvent. The main-stream operating temperature was 280°C. One result was a very low over-all stainless steel corrosion rate, 0.4 mpy, based on oxygen data. The rate based on nickel data was 0.2 mpy.

Zircaloy-2 corrosion rates varied from 3.6 mpy at 1.7 w/ml to 9.1 mpy at 3.6 w/ml power density. There was no evidence of solution instability.

Exposure of loop L-4-13, type 347 stainless steel, in beam hole HB-4 at the LITR has been completed. The solution, 0.17 *m* UO_2SO_4, was the first made up with heavy water. The main-stream operating temperature was 250°C. The over-all stainless steel corrosion rate during the final 670 hr was 1.0 mpy based on oxygen data and 0.4 mpy based on nickel data.

Exposure of loop L-2-15, type 347 stainless steel, has been completed. This was the second loop experiment in LITR beam hole HB-2. The UO_2SO_4 concentration of 0.17 *m* was four times the L-2-10 concentration. The main-stream operating temperature was 278°C. The over-all stainless steel corrosion rate was 1.5 mpy based on oxygen data and 0.5 mpy based on nickel data.

A mockup of the new multiple-bomb facility, which will replace the present single-bomb facility in beam hole HB-5 of the LITR, has been completed. Operational tests of the facility, which includes instrument panel, shielding-plug assembly, autoclave assemblies, and rocking mechanism, are being carried out prior to installation of the equipment in the LITR. Testing and pretreatment of the in-pile autoclaves will be carried out at the Y-12 site prior to in-pile operation.

Recent tests indicate an effect on radiation-induced corrosion of Zircaloy-2 by the inclusion of nitrogen gas in the system. The effect seems to be complementary to the effect of excess acid; that is, no change is observed in systems including excess acid, but the corrosion rate is reduced when nitrogen is included in systems without excess acid. Analyses of one solution indicate that the nitrogen gas is fixed during exposure in the reactor but not as nitrate or ammonia.

Three Zircaloy-2 experiments are discussed. One, Z-26, was designed to demonstrate the effect on corrosion when $MgSO_4$ was added to a 0.17 *m* UO_2SO_4 solution. The observed corrosion was slightly more than that predicted for a similar system without the inert sulfate. Experiment Z-27, containing 0.04 *m* UO_2SO_4, 0.03 *m* excess sulfuric acid, and 0.005 *m* $CuSO_4$, operated at 250, 280, 300, and 330°C. An apparent anomalous dependence of corrosion rate on temperature was observed. Experiment L6Z-101 provides needed data in the study of corrosion rate vs power density in 0.17 *m* UO_2SO_4 solution containing excess acid (0.04 *m*).

One type 347 stainless steel experiment was designed to show the effect on radiation-induced corrosion of adding $MgSO_4$ to the solution. The effect appears negligible.

The out-of-pile corrosion behavior of pin-type specimens of type 347 stainless steel was determined at 250 and 290°C in solutions containing 0.17 *m* UO_2SO_4 but of varying acid concentrations. After varying rates of attack and penetrations, a protective film was formed under all conditions. The effect of increasing acidity at the lower temperature, 250°C, was to increase the amount of metal involved in film formation and also to increase the rate of attack prior to the formation of a protective film. Increasing the temperature from 250 to 290°C markedly decreased the amount of metal involved in film formation. At the higher temperature, an increase in acidity appeared to have little effect on the amount of metal involved in film formation.

Irradiation studies performed on triethyl phosphate and Amsco 125-82 indicate that either of these materials may be satisfactorily employed as the HRT secondary refrigerant in the cold traps. It was recommended that the refrigerant should be replaced periodically and the lines flushed out with fresh material to dissolve and remove any "polymer" formed. Problems which may arise from the use of either of these materials in the freeze-plug sections have not been completely evaluated.

14. Metallurgy

Hardness-time-temperature curves determined for Zr-Nb base alloys with ternary additions of Fe, Pd, and Pt indicate that the formation of "omega" phase on quench-and-reheat heat treatment is delayed by the addition of the ternary alloying elements. Additional data are needed to determine whether the delay is sufficient to permit welding of the alloys. The Widmanstätten platelet phase observed in the quenched specimens is redissolved on heating at and above 300°C and seems to be a metastable transition phase.

The stability of all-alpha and all-beta zirconium-base alloys is being investigated by Armour Research Foundation. Results to date indicate that unalloyed zirconium is superior to sponge Zr; 1.8% Sn has little effect on the strengths of iodide Zr, but 1.7% Sn improves the tensile impact strength of sponge Zr. Iodide Zr–15% Nb alloys

are brittle in the as-quenched and quenched-and-aged conditions, while the addition of 2% Pd to the Zr–15% Nb alloy causes the alloy to show fairly high strengths and some ductility.

Subsize impact testing of A55 titanium has shown no adverse effect of aging at 300°C on the impact values, even with hydrogen additions. A considerable reduction in impact strength occurs when small quantities of hydrogen are added, but these values are not changed by aging.

In drop-weight tests, A55 titanium was shown to be ductile at temperatures as low as –196°C; A75 titanium was brittle at –70°C.

A procedure has been developed by Armour Research Institute for roll cladding titanium on steel with vanadium and copper as transition materials.

An apparatus which permits elevated-temperature irradiation of a large number of subsize tensile and impact specimens has been designed and is operating successfully in the MTR.

Tensile tests of irradiated Zircaloy-2 and austenitic stainless steels have shown that a greater loss of ductility occurs in the weld area than in samples of wrought material.

A reduction in Charpy V impact-test values of A212 steel was found after irradiation to a total fast dose of 4×10^{18} *nvt*.

PART V. CHEMICAL ENGINEERING DEVELOPMENT

15. Fuel Processing

Particle-size analyses of solids taken from the hydroclone underflow pot on the HRT mockup showed that these solids were coarser than the synthetic corrosion-product solids injected into the loop. This implies that particle growth and agglomeration processes may prevent a buildup of submicron-sized particles in the fuel system of a homogeneous reactor.

The stability of iodate in simulated fuel solution under gamma irradiation was decreased by the presence of H_2-O_2 mixtures with H_2/O_2 ratios higher than 2/1 and by increasing the temperature to 120°C.

The extractability of iodine by a circulating gas stream from simulated fuel solution at 285°C was not affected by the presence of iron in the solution. The absorption of iodine by platinized alundum pellets from an atmosphere of oxygen and steam decreased with increased temperature. With hydrogen present in the gas stream, the amount of iodine absorbed was 4 to 14 times larger than with no hydrogen present. Iodine absorbed by silver-alundum pellets from the vapor phase at 300°C did not exchange with other iodine until the temperature was above 350°C.

In circulating loop tests on fission-product behavior, zirconium plated out almost quantitatively on metal surfaces when introduced into 0.04 *m* UO_2SO_4 at 300°C as zirconium sulfate solution. Contrasted with this result, essentially 100% of precipitated ZrO_2 injected into the loop was recovered in suspension.

16. Uranyl Sulfate Blanket Processing

Plutonium formed in the uranyl sulfate blanket of the HRT can be expected to distribute itself as follows: (1) in solution as Pu(IV) and Pu(VI), (2) as a loose precipitate, primarily PuO_2, and (3) attached to vessel walls either as adsorbed ionic plutonium or as PuO_2. The amount of plutonium in each form cannot be estimated, since the behavior depends on a large number of variables.

Out-of-pile experiments were carried out to determine the effect of some of these variables on plutonium behavior in 1.4 *m* UO_2SO_4 at 250°C. The solubility of Pu(IV) decreases from 20 to <3 mg per kilogram of H_2O as the initial plutonium concentration increases from 20 to 100 mg per kilogram of H_2O. The addition of preformed PuO_2 also decreased the apparent solubility.

When heated to 250°C in pyrex containers, Pu(IV) dissolved in 1.4 *m* UO_2SO_4 was readily oxidized to Pu(VI) under an O_2 overpressure but not under a stoichiometric O_2 plus H_2 overpressure. When heated in stainless steel containers, Pu(IV) was readily oxidized by either an O_2 or a stoichiometric H_2 plus O_2 overpressure. This oxidation is catalyzed by dissolved chromium from corrosion of stainless steel.

When 1.4 *m* UO_2SO_4 solutions containing plutonium were heated to 250°C in stainless steel, the apparent solubility of plutonium was 6 to 16 mg per kilogram of H_2O. Plutonium that came out of solution either formed a loose PuO_2 precipitate or was adsorbed on the wall. The fraction adsorbed and the fraction that precipitated depended on the initial plutonium concentration. For example, with an initial concentration of 17.5 mg per kilogram of H_2O, all the plutonium

removed from solution was adsorbed, giving 0.3 $\mu g/cm^2$. With an initial concentration of 70 mg per kilogram of H_2O, plutonium adsorption was 10 $\mu g/cm^2$; however, this was only 55% of the plutonium removed from solution.

Simulated hydroclone–underflow-pot contents from HRT chemical processing were evaporated to dryness and completely dissolved in anhydrous phosphoric acid at 230°C.

Tentative procedures for plutonium and neptunium analyses in irradiated UO_2SO_4 were developed.

In initial tests, blanket processing loop P-1 operated satisfactorily. Tests on the prototype of the pressurizer indicated that it will withstand the proposed operating overpressures of 100 psi of both oxygen and hydrogen.

The titanium canned-rotor pump, the core tank, and the heat exchanger for loop P-2 performed satisfactorily in preliminary tests.

17. Thorium Oxide Slurry Development

Two slurries of pure thorium oxide and seven slurries of thorium–0.5% uranium oxide (93% enriched uranium) which had been irradiated at 300°C in the LITR were recovered for examination. The thorium concentrations of all slurries were 750 to 1000 g per kilogram of H_2O. None appeared to have been grossly affected by the irradiation. The calculated power density under irradiation for the slurries containing the enriched uranium was approximately 5 kw/liter (the average power density expected in the TBR blanket).

Out-of-pile studies on the catalytic recombination of hydrogen and oxygen by thorium-uranium oxide slurries containing 0.05 *m* molybdenum oxide were continued, with studies on the effects of sulfate and rare-earth additions on the reaction rate. A slurry that contained 2000 ppm of sulfate (based on ThO_2) and that had been activated by heating for 70 min at 70°C under H_2 (1000 psi at room temperature) gave a hydrogen combination rate of 36 moles/hr/liter at 171°C and a hydrogen partial pressure of 500 psi. Increasing the sulfate concentration to 4000 and to 6000 ppm resulted in only a 20% decrease in recombination under the same conditions of temperature and hydrogen partial pressure. The addition of 634 ppm (based on ThO_2) of rare earths to a slurry that had been activated by heating with hydrogen did not decrease its catalytic activity, a hydrogen recombination rate of 30 moles/hr/liter being observed both in the presence and absence of the rare earths under similar conditions. Doubling the rare-earth concentration decreased the rate about 30%.

The effect of silicate addition on the chemical and physical properties of thorium oxide slurries was investigated. The adsorption of silicon on the thoria surface from sodium metasilicate solution was disproportionately greater than that of sodium. At silicate and thoria concentrations of interest in the slurry development program, the silicate was almost completely adsorbed by the thoria. Autoclaving the silicated slurry at 285°C changed a large fraction of the silica to a form not readily soluble. The addition of 1000 ppm of SiO_2 (based on ThO_2) as sodium metasilicate to a thorium oxide and a thorium-uranium oxide slurry and subsequent autoclaving at 285°C yielded slurries with slow settling rates at temperatures less than 100°C, but above this temperature (to 300°C) the treated slurries settled at rates little different from those of the untreated slurries. The treated slurries were, however, less viscous than the untreated slurries, as indicated by the faster stirrer operation under set conditions, when they were stirred in the dash-pot irradiation bomb. Slurries of thorium and thorium-uranium oxide (750 g of thorium per kilogram of H_2O) showed a decrease in viscosity with increasing sodium metasilicate concentration (0 to 7000 ppm SiO_2, based on ThO_2) in the temperature range 100 to 300°C. At all silicate concentrations and comparable temperatures the thorium-uranium oxide slurry was much more viscous than the thorium oxide slurry. In studies on the effect of silicate addition on the settling rate of a standard slurry, the settling rate markedly decreased at 100°C and SiO_2 concentrations of 5000 and 10,000 ppm. Similar changes in settling rate were observed at slurry temperatures of 150 and 200°C for SiO_2 concentrations of 6500 and 10,000 ppm, respectively.

The addition of aluminum oxide to thorium oxide, at aluminum concentrations of 250, 500, 1000, and 10,000 ppm, based on thorium, by the coprecipitation of the oxalates and subsequent thermal decomposition resulted in oxide products with increased crystallite sizes, proportionately lower specific surface areas, and smaller, more uniform particles when compared with pure oxide similarly prepared. The settling characteristics of aqueous slurries of the thorium-aluminum oxides were similar to those of pure oxide slurries.

The effect of method of preparation on the properties of thorium-uranium oxides with a uranium/thorium mole ratio of 0.005/1 was studied. Three methods were examined: simple addition of UO_3 to ThO_2 followed by autoclaving in water, thermal decomposition of the coprecipitated thorium-uranous oxalates, and hydrothermal decomposition of thorium-uranium nitrate solution. All products appeared to be suitable slurry materials. The mixed oxide prepared by thermal decomposition of the coprecipitated oxalates was much more abrasive than either the pure oxide similarly prepared or the other mixed-oxide products. No gross change was observed in the slurry properties of aqueous suspensions of any of the mixed oxides when they were autoclaved at 300°C with O_2, H_2, and CO_2 atmospheres and in the presence of 1000 to 10,000 ppm of sulfate.

Work is continuing on the preparation of thoria sols and gels suitable for the preparation of microspheres. Quick-setting gels have been prepared by coagulating thoria sols with hexamethylenetetramine solution.

18. Thorium Oxide Blanket Processing

Simple methods of processing thorium oxide slurries that can be incorporated as part of each reactor operation are being investigated. Calculation shows that the recoil energy of fission fragments is sufficient to eject most fission products into the aqueous phase of a ThO_2 slurry if the ThO_2 particles are less than 10 μ in diameter. It may be possible to remove fission-product neutron poisons without destroying or dissolving the ThO_2 particles. However, scouting tests indicate that fission products will be irreversibly adsorbed on the ThO_2 unless the oxide is pretreated in some manner. In tests with ThO_2 pretreated with dilute H_2SO_4, only 10% as much uranium was adsorbed as by untreated ThO_2. Treatment of ThO_2 with silicate increased the uranium adsorption, but about 90% of this adsorbed uranium was readily eluted with dilute acid. By coating the thorium oxide particle with molecular sulfur (~50 ppm S), it was possible to eliminate adsorption of uranium from uranyl sulfate solutions.

19. Equipment Decontamination

Chromous sulfate solution for use in descaling and removing fission products from type 347 stainless steel was readily prepared by electrolytic reduction of chromic sulfate. In the nine-chamber cell used, the alternating anodes and cathodes were separated by an anion exchange membrane. Chromium(VI) was reduced to Cr(III) by electrolysis, but precipitation of lead chromate interfered with operation. Reduction of Cr(VI) to Cr(III) with SO_2 was rapid and quantitative, making it possible to use chromates or dichromates, which are much less expensive than chromic sulfate.

PART VI. SUPPORTING CHEMICAL RESEARCH

20. Aqueous Systems at Elevated Temperatures

Temperatures of appearance of a second liquid phase have been determined as a function of UO_2SO_4 and $CuSO_4$ concentrations in solutions containing 29.11 mole % excess acid based on the total salt content. Precipitates appear in the more dilute solutions at temperatures below the two-liquid phase region. The approximate position of the boundary between precipitate formation and second liquid phase formation has been established.

Study of the homogeneous reaction of hydrogen with oxygen, catalyzed by dissolved copper salts in aqueous solutions, was resumed after a lapse of several years. Interest is presently focused upon the effects of temperature, acidity, and copper concentration because of the interim developments with respect to the mechanism of the reaction and the needs of the Project. Tests performed at 200°C are reported in which the effects of 0.025 to 0.100 *M* sulfuric acid upon the catalytic activity of 0.01 *M* cupric sulfate solutions were determined; increasing the acidity lowered the activity, but the effect was not so strong as that previously found at 250°C. Hydrogen was found to be more reactive than deuterium at 200°C, as had been found at 250°C.

21. Radiation Chemistry

Results of two experiments are reported which are useful in determining the molecular and radical yields in heavy water. The ferric-ion yield from an air-saturated heavy-water solution of 10^{-3} *M* Fe^{++}, 10^{-3} *M* NaCl, and 0.4 *M* H_2SO_4 was determined to be 17.44 ± 0.08 molecules of ferrous ions oxidized per 100 ev of absorbed energy.

The deuterium gas yield for a 0.4 *M* H_2SO_4 heavy-water solution 10^{-4} *M* in KBr was found to be 0.39 ± 0.01 molecule of D_2 produced for each 100 ev absorbed.

The radiation fixation of nitrogen with oxygen or hydrogen in the liquid phase is estimated to be $<10^{-3}$ molecule of nitrogen fixed per 100 ev absorbed.

PART VII. ANALYTICAL CHEMISTRY

22. Analytical Chemistry

Significant progress is reported on the development and improvement of methods for use in the analysis of the HRT fuel and of the material used in the breeding phase, with particular emphasis placed on the estimation of the additives, contaminants, and fission products in the latter. With regard to the former, a constant-potential coulometer, which appears to be quite satisfactory for application to the estimation of both copper and uranium in the HRT fuel material, has been developed and was tested on solutions of UO_2SO_4. Methods for use in the determination of aluminum, molybdenum, titanium, lanthanum, and hydrazine in the analysis of slurries of thorium oxide have been developed or improved and were tested under a variety of conditions, but, even so, further studies are to be continued in an effort to improve the scope of such methods in the presence of certain other interfering constituents. Brief statements are also given of the progress which has been made in the correlation of certain physical attributes of slurries of thorium oxide, particularly with regard to particle-size distribution, surface area, and exchange capacity. Modifications in the methods of activation analysis have been made that now make it possible to evaluate the particle-size distribution of ThO_2 to particles with diameters of the order of 0.7 micron. It is also indicated that the method can be applied to dispersions of other solid materials.

CONTENTS

SUMMARY v

PART I. HOMOGENEOUS REACTOR TESTS

1. HRT OPERATIONS 3
   - 1.1 Reactor Operations 3
     - 1.1.1 Dump Tests 4
   - 1.2 Metallurgical Service 4
     - 1.2.1 Metallurgical Inspection of HRT Flanges and Leak-Detector Tubing 4
     - 1.2.2 Cracks in HRT Flange Bolts and Ferrules 9
   - 1.3 Maintenance of Radioactive Components 10
2. HRT DESIGN 22
   - 2.1 Refrigeration System 22
   - 2.2 Water Treatment 22
   - 2.3 Cooling-Water System 23
   - 2.4 Fuel Heat Exchanger Steam Piping 23
   - 2.5 Deuterium Recombination 24
   - 2.6 Precipitation of Uranyl Peroxide in Fuel Circulating Pump 24
   - 2.7 Flange Test Program 25
3. HRT COMPONENT DEVELOPMENT 28
   - 3.1 HRT Pump Development 28
     - 3.1.1 400A-1 Pump and Loop 28
     - 3.1.2 400A-2 Pump and Loop 28
     - 3.1.3 300A-1 Pump 28
   - 3.2 Diaphragm Pumps 29
     - 3.2.1 Feed-Pump Loop No. 1 29
     - 3.2.2 Feed-Pump Loop No. 2 29
     - 3.2.3 Purge Pump 29
   - 3.3 HRT Sampler 30
   - 3.4 Freeze Jackets 30
   - 3.5 HRT Core Sample Holder 30
   - 3.6 HRT Mockup 30
4. HRT REACTOR ANALYSIS 32
   - 4.1 Gamma Radiations Escaping from Openings in the HRT Shield 32
5. HRT CONTROLS AND INSTRUMENTATION 34
   - 5.1 Component and System Testing 34
     - 5.1.1 Oxygen-Injection Systems 34
     - 5.1.2 Pressurizer-Level Transmitter 34
     - 5.1.3 Letdown Valves 35
     - 5.1.4 Heat-Balance Flowmeters 35
     - 5.1.5 Reactor-Cell Ambient Radiation Measurement 35
   - 5.2 Design 36
     - 5.2.1 Controls for the HRT Demineralized-Cooling-Water System 36

6. HRT PROCESSING PLANT 37
6.1 High-Pressure-System Testing Operations 37
6.1.1 Solids Disappearance from Feed Loop 37
6.1.2 Hydroclone Performance with Solids of Low Concentrations 37
6.1.3 Draining of the Underflow Receiver 38
6.1.4 Hydroclone Performance 38
6.1.5 Equipment Performance During Testing Operations 39
6.2 Dissolver-System Installation 41
6.3 Flange Tests – Belleville Springs 41

PART II. REACTOR DESIGN AND ANALYSIS

7. REACTOR ANALYSIS 49
7.1 Nuclear Characteristics of Two-Region Slurry Reactors 49
7.2 Fuel Costs for Two-Region Slurry Reactors 49
7.3 Effect of $\eta^{23}_{res}/\eta^{23}_{th}$ Upon Breeding Ratio in Single-Region Slurry Reactors 51
7.4 Power Costs Associated with Use of N^{15} in Breeder Reactors 52
7.5 Power Costs Associated with Use of Deuterated Hydrocarbons in Breeder Reactors 53
7.6 Mathematics and Computation 54

PART III. ENGINEERING DEVELOPMENT

8. DEVELOPMENT OF FUEL-SYSTEM COMPONENTS 57
8.1 Recombiner Development 57
8.1.1 High-Pressure Recombiner Loop 57
8.1.2 Battelle and Syracuse Contracts 57
8.2 Small Reactor Components 57
8.2.1 20-cfm Canned-Motor Blower 57
8.2.2 Small Circulating Pumps 58
8.3 4000-gpm Loop 58
8.4 Titanium Program 59
8.5 Heat-Exchanger Tube-Joint Test 59

9. DEVELOPMENT OF REACTOR SLURRY SYSTEMS 61
9.1 Heat-Transfer Measurements 61
9.2 Slurry Rheology 61
9.3 Disintegration of ThO_2 Cakes 64
9.4 Circulating-Slurry Behavior 64
9.4.1 Circulation of Thorium-Uranium Oxide Slurries in 100-gpm Loop 64
9.4.2 Circulation of Thorium-Uranium Oxide Slurries in 200-gpm Loop 64
9.4.3 Pressure-Bridge Density Meter 67
9.5 Blanket-System Development 68
9.5.1 Test-System Operation 68
9.5.2 Gamma-Survey Work 71
9.5.3 Settling Tests 71
9.5.4 Analytical Data 71

10. VALVE DEVELOPMENT 73
10.1 Sealing Bellows 73
10.2 Valve Trim 73

PART IV. REACTOR MATERIALS RESEARCH

11. SOLUTION CORROSION 77
11.1 Pump Loop Test Results 77
11.1.1 Mockup of the Zircaloy–Stainless Steel Transition and Expansion Joint 77
11.1.2 Studies with the Proposed HRT Fuel Solution 79
11.1.3 Studies on the Effectiveness of Pretreatments 80
11.1.4 Use of Titanium Inserts in Stainless Steel Loops 81
11.1.5 Corrosion of Stainless Steel in Beryllium Sulfate Solutions Containing Uranium 81
11.1.6 Effect of Cr(VI) on the Corrosion of Stainless Steel 84
11.1.7 Effect of Copper Sulfate on the Corrosion of Stainless Steel 84
11.2 Laboratory Corrosion Studies 84
11.2.1 Stress-Corrosion Cracking in Chloride-Containing Uranyl Sulfate Solutions 84
11.2.2 Stress-Corrosion Cracking Produced by Tap Water 84
11.2.3 Stress-Corrosion Cracking in High-Temperature, Chloride-Containing Water 85
11.2.4 Testing of Zirconium Alloys 86
11.2.5 Effect of Heat Treatment and Surface Finish on the Corrosion of Elgiloy 88
11.2.6 Corrosion Tests Related to the HRT Chemical Processing Plant 88

12. SLURRY CORROSION 90
12.1 Pump Loops 90
12.1.1 100A Pump Loops 90
12.2 Toroids 93
12.2.1 Toroid Examination 93
12.2.2 Effect of Circulation Time 95
12.2.3 Batch LO-14 Thorium Oxide 97
12.3 In-Pile Slurry Toroid Development 100

13. RADIATION CORROSION 102
13.1 In-Pile Loops 102
13.1.1 Development and Construction 102
13.1.2 General Description of In-Pile Loop Experiment L-2-10 104
13.1.3 Qualitative Results of Inspection and Evaluation of Loop L-2-10 105
13.1.4 Quantitative Results of Inspection and Evaluation of Loop L-2-10 106
13.1.5 Discussion of Results from Loop L-2-10 107
13.1.6 In-Pile Loop L-4-13 108
13.1.7 In-Pile Loop L-2-15 109
13.1.8 In-Pile Loop L-4-16 109
13.2 In-Pile Autoclave Tests, LITR 110
13.2.1 Development and Construction 110
13.2.2 In-Pile Tests 110
13.3 Supporting Research 115
13.3.1 Corrosion of Type 347 Stainless Steel in a System Free from the Products of Corrosion 115
13.3.2 Radiation Stability of Triethyl Phosphate and Amsco 125-82 118

14. METALLURGY 119
14.1 Physical Metallurgy 119
14.1.1 Zirconium-Alloy Development 119
14.1.2 Special Zirconium Alloys – Mechanical Properties 123
14.1.3 Zirconium-Hydrogen System 124
14.2 Mechanical Metallurgy 124
14.2.1 Effect of Hydrogen on Embrittlement of Titanium at 300°C 124
14.2.2 Drop-Weight and Charpy V Impact Studies of Steel, Titanium, and Zirconium 124
14.3 Welding Development 126
14.4 Metallurgical Development and Service 126
14.4.1 Roll Cladding Titanium on Steel 126
14.5 Inspection Development 127
14.5.1 Development of an Eddy-Current Test for Heat Exchanger Tubing 127
14.6 Effects of Radiation on Structural Metals and Alloys 127
14.6.1 Equipment and Facilities 127
14.6.2 Results of Irradiation Experiments 127

PART V. CHEMICAL ENGINEERING DEVELOPMENT

15. FUEL PROCESSING 133
15.1 Behavior of Solids in the HRT Mockup 133
15.2 Iodine Chemistry 133
15.3 Volatility of Iodine Under Reactor Conditions 135
15.4 Behavior of Fission Products in Circulating Loop Tests 136

16. URANYL SULFATE BLANKET PROCESSING 138
16.1 Plutonium Behavior in UO_2SO_4 Solution at 250°C 138
16.2 Blanket Solids Dissolution 139
16.3 Analysis of Irradiated Uranyl Sulfate 140
16.4 Loop P-1 Tests 140
16.5 Loop P-2 Component Tests 141
16.5.1 Titanium Canned-Rotor Pump 141
16.5.2 Core Tank 142
16.5.3 Heat Exchanger 142
16.6 Electrolysis as a Method of H_2-O_2 Addition for Loops P-1 and P-2 143
16.7 Hydroclone Development Studies 143

17. THORIUM OXIDE SLURRY DEVELOPMENT 144
17.1 Slurry Irradiation Studies 144
17.1.1 Slurry Irradiations in the LITR 144
17.1.2 Postirradiation Examination of Slurries 144
17.1.3 Corrosion-Erosion Effects in Operation of the Dash-Pot-Stirred Irradiation Bomb 144
17.2 Gas-Recombination Studies 144
17.2.1 Effect of Sulfate 146
17.2.2 Effect of Rare Earths 146
17.3 Studies with Thorium Oxide Slurries Containing Sodium Silicate 147
17.3.1 Adsorption Studies 147
17.3.2 Equilibrium Studies 148

17.3.3 Viscosity Studies 149
17.3.4 High-Temperature Hindered-Settling-Rate Studies 150
17.4 Effect of Aluminum Oxide on Thorium Oxide Properties 151
17.5 Preparation and Properties of Thorium-Uranium Oxide 153
17.5.1 Characteristic Properties of Thorium-Uranium Oxides 155
17.5.2 Abrasive Properties of Thorium-Uranium Mixed Oxides 155
17.5.3 Room-Temperature Settling Properties of Aqueous Thorium-Uranium Oxide Slurries 156
17.6 Preparation of Thoria Sols and Gels 156

18. THORIUM OXIDE BLANKET PROCESSING 159
18.1 Adsorption on ThO_2 159

19. EQUIPMENT DECONTAMINATION 160

PART VI. SUPPORTING CHEMICAL RESEARCH

20. AQUEOUS SYSTEMS AT ELEVATED TEMPERATURES 163
20.1 The System UO_2SO_4-$CuSO_4$-H_2SO_4-H_2O 163
20.2 Homogeneous Catalysis of the Hydrogen-Oxygen Reaction in Aqueous Solutions 165
20.2.1 Cupric Perchlorate 166
20.2.2 Cupric Sulfate 168
20.2.3 The Deuterium-Oxygen Reaction 170

21. RADIATION CHEMISTRY 172
21.1 Fundamental Processes in the Radiation Chemistry of Heavy Water 172
21.2 Fixation of Nitrogen by Radiation 172

PART VII. ANALYTICAL CHEMISTRY

22. ANALYTICAL CHEMISTRY 177
22.1 Analysis of Thorium Oxide 177
22.2 Determination of Submicron Particle Sizes by an Activation Analysis–Centrifugation Method 178
22.3 Determination of Uranium by Means of a Constant-Potential Integrating Coulometer 178

Part I

HOMOGENEOUS REACTOR TEST

S. E. Beall

1. HRT OPERATIONS

S. E. Beall

H. F. Bauman
N. A. Brown[1]
J. R. Buchanan
N. W. Curtis[2]
J. R. Engel
J. D. Flynn
D. F. Frech
T. H. Gladney[1]
R. H. Guymon
P. N. Haubenreich
J. W. Hill, Jr.
R. W. Jurgensen[3]
S. I. Kaplan
J. O. Kolb
H. M. McLeod
G. W. Rivenbark
H. K. Search[1]
R. Van Winkle
R. R. Wiethaup

1.1 REACTOR OPERATIONS

The initial operating test period, reported last quarter,[4] resulted in recommendations for revisions in the piping of the pressurizers and their liquid-level control elements. These revisions, completed early in November, included a pressure-equalizing valve (see Sec. 1.1.1) and new, gold rupture disks rated at 200 psig. After the usual 2500-psig hydrostatic test the reactor was operated with distilled water at 230°C and 600 psi for 24 hr in preparation for a dump test, which concluded the short run.

The next run was started immediately and was continued for a period of 100 hr at 280°C and 1700 psig before another dump test (Sec. 1.1.1) was performed. At the end of this run it was found that oxygen, which was being used to pressurize the leak-detector system, was leaking through cracks in some of the leak-detector tubing. The cracks were found to be typical of stress-corrosion cracking and were attributed to a combination of temperature, stress, chloride contamination which could not be completely removed from the tubing by the flushing operations reported previously,[4] and the use of oxygen as a pressurizing medium when combined with the method of operation of the leak-detector system. Although it was decided to dismantle part of the reactor to inspect the flanges for similar cracking, the reactor was filled and operated for 48 hr at 100°C to determine the limits of temperature control at temperatures as low as 25°C. Control was effected within ±3°C by circulating cooling water through the steam generators. During this period it was established that the blanket pressurizer-purge-pump diaphragm was ruptured, requiring that the pump head be replaced.

To investigate further the chloride-induced stress-corrosion picture, several flanges were cut from the system and others unbolted for examination. Much of the disassembly at this time was accomplished by remote means, as reported in Sec. 1.3. Results of the metallurgical inspection are reported in Sec. 1.2.1.

While the reactor was partially dismantled, the fuel and blanket dump valves, two letdown valves, and the two oxygen flow-control valves were replaced because of leakage past the seats. Erosion of the stem and seat material (type 347 stainless steel for the dump valves and Stellite 6 for the letdown and oxygen-throttling valves) was observed after disassembly. The pressurizer vent valves were replaced with valves of higher capacity. Special closed circulating loops were installed to provide a continuous flush for the leak-detector annuli of the fuel and blanket steam-generator head gaskets and for the pressure-vessel dome gasket. The loops are treated continuously with an oxygen scavenger (hydrazine) in an effort to prevent further attack at these three vulnerable places.

By January 4 the reactor was ready for further operation with distilled water. Run No. 3 covered 189 hr at 1500 psig and 280°C. Difficulty was experienced with the fuel feed pumps, and at the end of the run one pumping head was replaced and the other fitted with a new suction-check-valve assembly. Later examination showed that the Stellite balls and seats of the check valves in both pumps had corroded sufficiently to permit leakage through the valves.

Run No. 4 followed and was continued for 105 hr at 280°C and 1500 psig without difficulty, making a total operating time of 441 hr at full temperature.

---

[1]On loan from TVA.

[2]On loan from Pennsylvania Power and Light Co.

[3]On loan from American Gas and Electric Company.

[4]S. E. Beall *et al.*, *HRP Quar. Prog. Rep. Oct. 31, 1956*, ORNL-2222, p 3.

1.1.1 Dump Tests

Dump tests were carried out which demonstrated the successful operation of the pressure-balancing control system. Figure 1.1 shows results of the first test with the rupture disks in place between the two pressurizers. This test was carried out at a moderate temperature and pressure to reduce the likelihood of damage in the event of failure of the control system. The vent valves controlled the differential pressure very satisfactorily during the first stage of the dump. During the second stage, with the dump valves open, the vent valves exercised little control; however, the fuel dump valve responded rapidly to prevent excessive differential pressure at the time when all the liquid had drained from the core and some flashing liquid still remained in the blanket.

In a subsequent test from 1700 psig and 280°C, the control system proved adequate, although the rate of pressure reduction by venting was very slow. The vent valves still contained the original small trim [valve capacity (C_v) = 0.07], and as a result of the test it was obvious that larger trim would be necessary for the desired 2-min venting time. Furthermore, it was decided to install a pilot-operated equalization valve between the two pressurizers and in parallel with the rupture disks so that an unbalance of as much as ±50 psig could be corrected by the valve.

Following the installation of the pressure-equalizing valve and the enlargement (to $C_v = 0.34$) of the trim in the vent valves, a dump test was conducted from 1500 psi and 280°C. Pressures during this test are shown in Fig. 1.2. The larger vent valves permitted a much more rapid pressure reduction during the first stage. The equalizing valve opened once at the initiation of the dump, and twice later when vapor began to flow through the fuel dump line. The performance of the entire dump-control system was highly satisfactory.

1.2 METALLURGICAL SERVICE[5]

1.2.1 Metallurgical Inspection of HRT Flanges and Leak-Detector Tubing

During HRT run No. 2, six different leak-detector lines were found to leak. Four of the leaks were through pinholes in the ¼-in., 16-gage tubing and were within 2 in. of the flanges. Several sections of the type 304 stainless steel tubing were removed and examined metallographically. The cracks in this tubing originated at the inside surface and were fine, branching, transgranular cracks, of the type usually associated with chloride stress corrosion. Typical cracks are shown at both high and low magnification in Fig. 1.3. Several lengths of tubing that had been placed in the system, but never used, were then removed and examined. As shown in Fig. 1.4, the inner surface of this tubing is very rough, with cavities up to 2 mils deep; at high magnification it is evident that these penetrations are narrow in proportion to the depth. Figure 1.5 (specimen etched to reveal carbides) shows that the inner surface of the tubing had been severely carburized. After discussions with the tubing manufacturer it was concluded that the chloride contaminant had originated from the organic drawing compound and had not been removed by the cleaning treatment. Furthermore, it is thought that the tubing was carburized during annealing and that the subsequent pickling treatment etched out many of the carbides, making a rough surface available to the chloride compound. Replacement of the tubing in the reactor was recommended.

A series of inspections was then initiated to determine whether cracking had occurred in the HRT flanges. Most of the flanges came from the high-pressure, high-temperature system, but two were from low-pressure, low-temperature service. The most effective testing medium used was postemulsified fluorescent penetrant and a dry-powder developer.

Initially, three flange pairs and their O-rings from the high-pressure system were examined. In the penetrant inspection, flange A-111 showed no significant indications, A-213 gave questionable results, and A-101 showed several pinholes and many of what appeared to be short cracks (Fig. 1.6). Circumferential cracks were found in the O-rings. A metallographic examination revealed severe pitting but no cracking in flanges A-111 and A-213. A large number of short, shallow cracks were found in the groove of flange A-101. As shown in Fig. 1.7, these cracks were located mainly at the corners of the groove, but some could be found on each side and on the bottom. Scattered areas of pits were found in all the flanges, including those which did not show

[5]This work performed by G. M. Adamson, J. P. Hammond, T. M. Kegley, Jr., and J. K. White of the HRP Metallurgy Group.

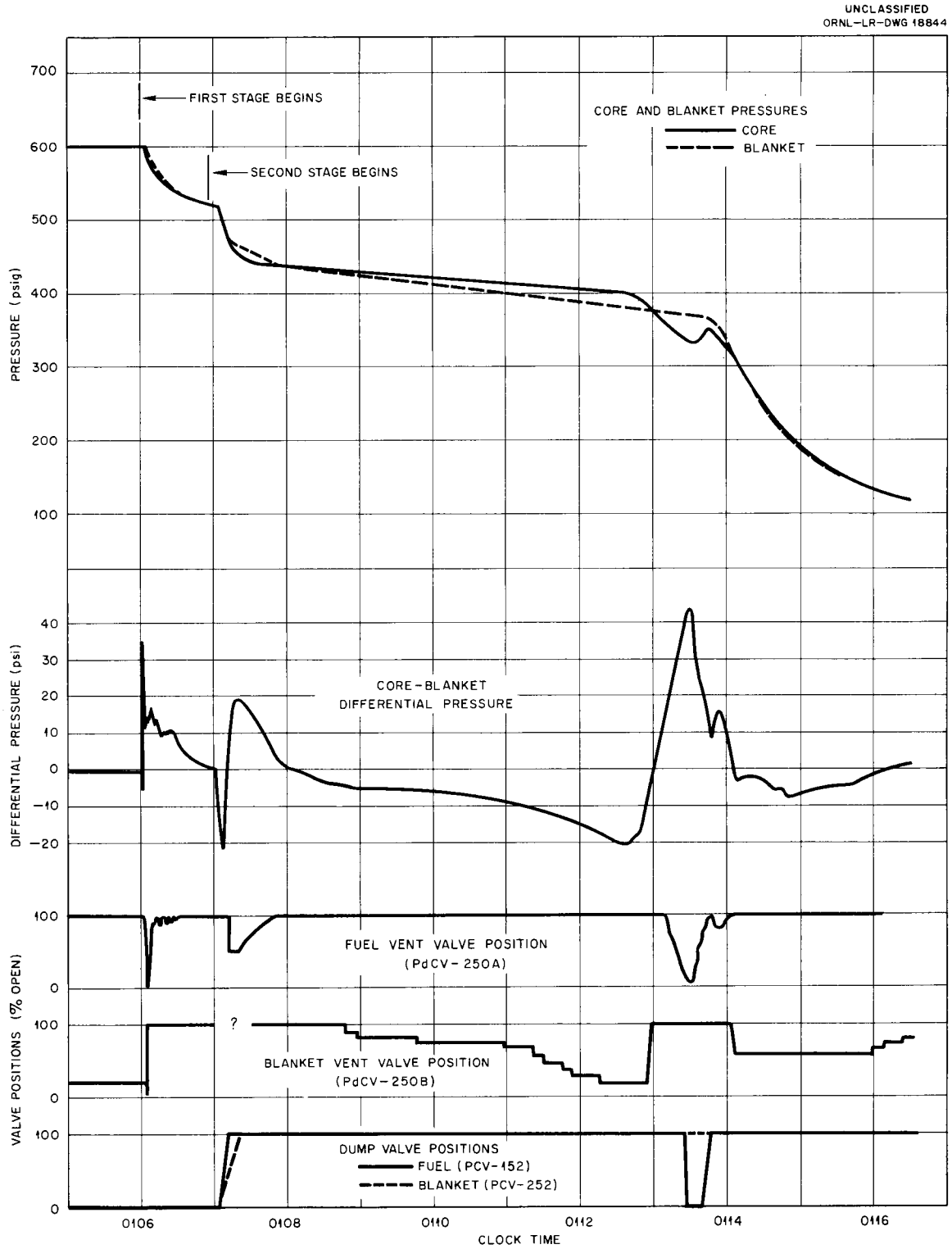

Fig. 1.1. Pressures and Valve Positions During Dump Test No. 3.

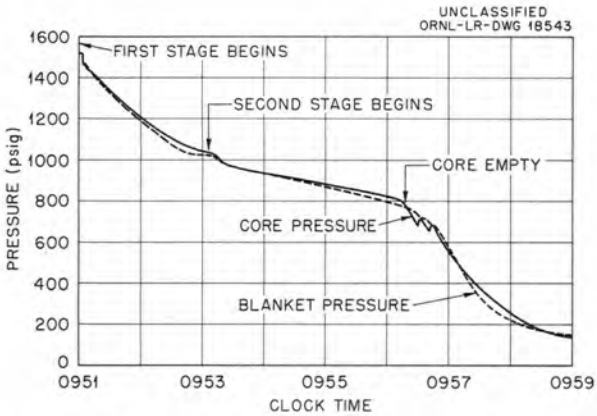

Fig. 1.2. Core and Blanket Pressures During Dump Test No. 6.

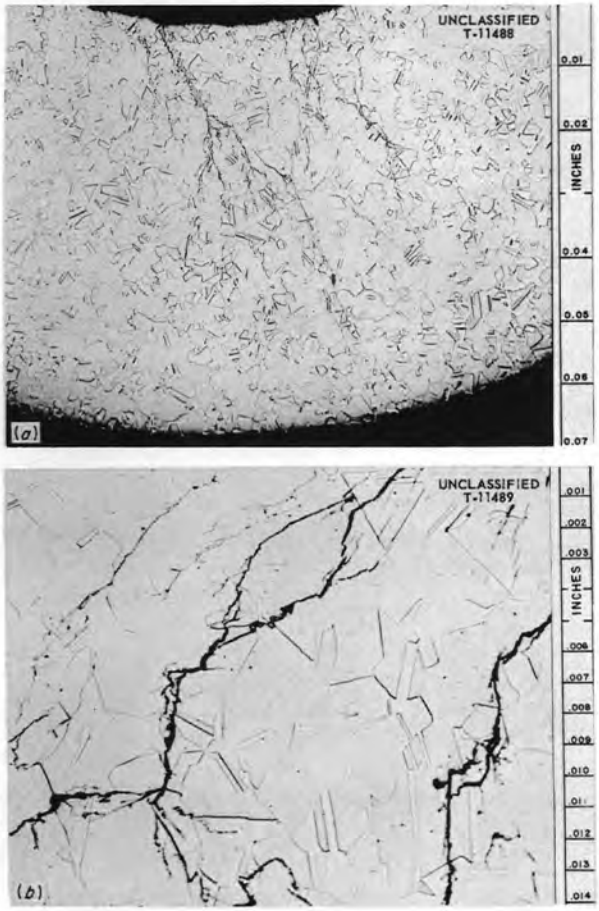

Fig. 1.3. Typical Transgranular Cracks in HRT Leak-Detector Tubing. (*a*) 50X; (*b*) 250X. Reduced 32%.

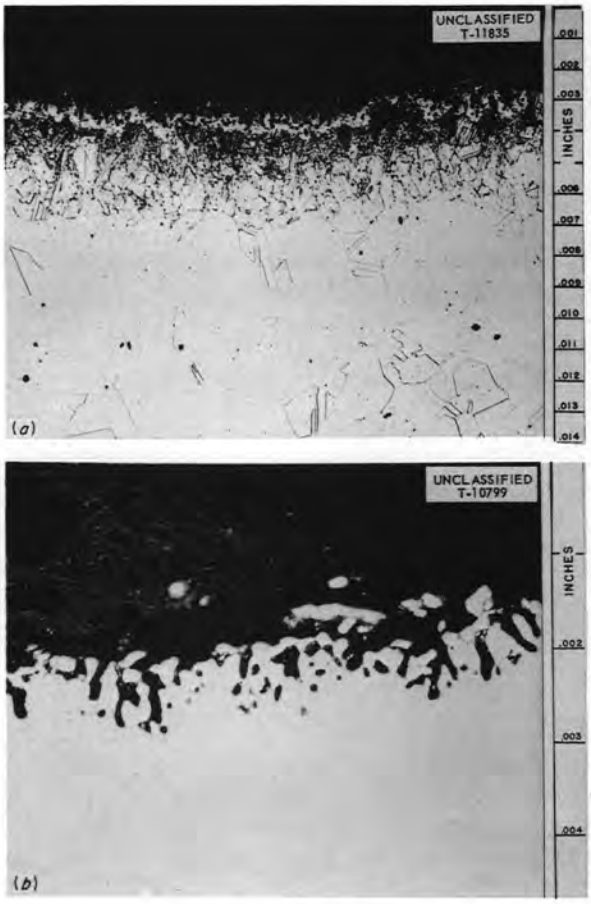

Fig. 1.4. Inner Surface Defects in As-Received Leak-Detector Tubing. (*a*) 250X; (*b*) 750X. Reduced 36%.

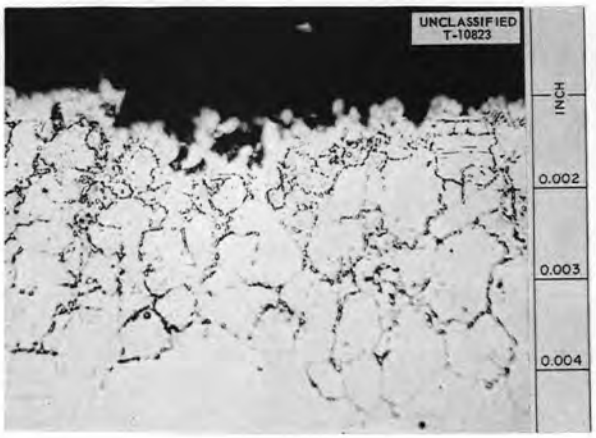

Fig. 1.5. Carburization on Inner Surface of Leak-Detector Tubing. Etched with Vilella's reagent. 750X. Reduced 34%.

cracking. Figure 1.8 shows a pitted area in the groove of flange A-101. While no particular effort was made to study these pits, depths of 0.020 in. were measured in making the sections for the crack study. A recommendation was made that the flanges be replaced because all had been exposed to the chloride solution from the leak-detector tubing.

The initial penetrant examination of the bottom

Fig. 1.6. Penetrant Indications in Groove of Flange A-101.

Fig. 1.7. Typical Cracks in Groove of Flange A-101. 15X. Reduced 32%.

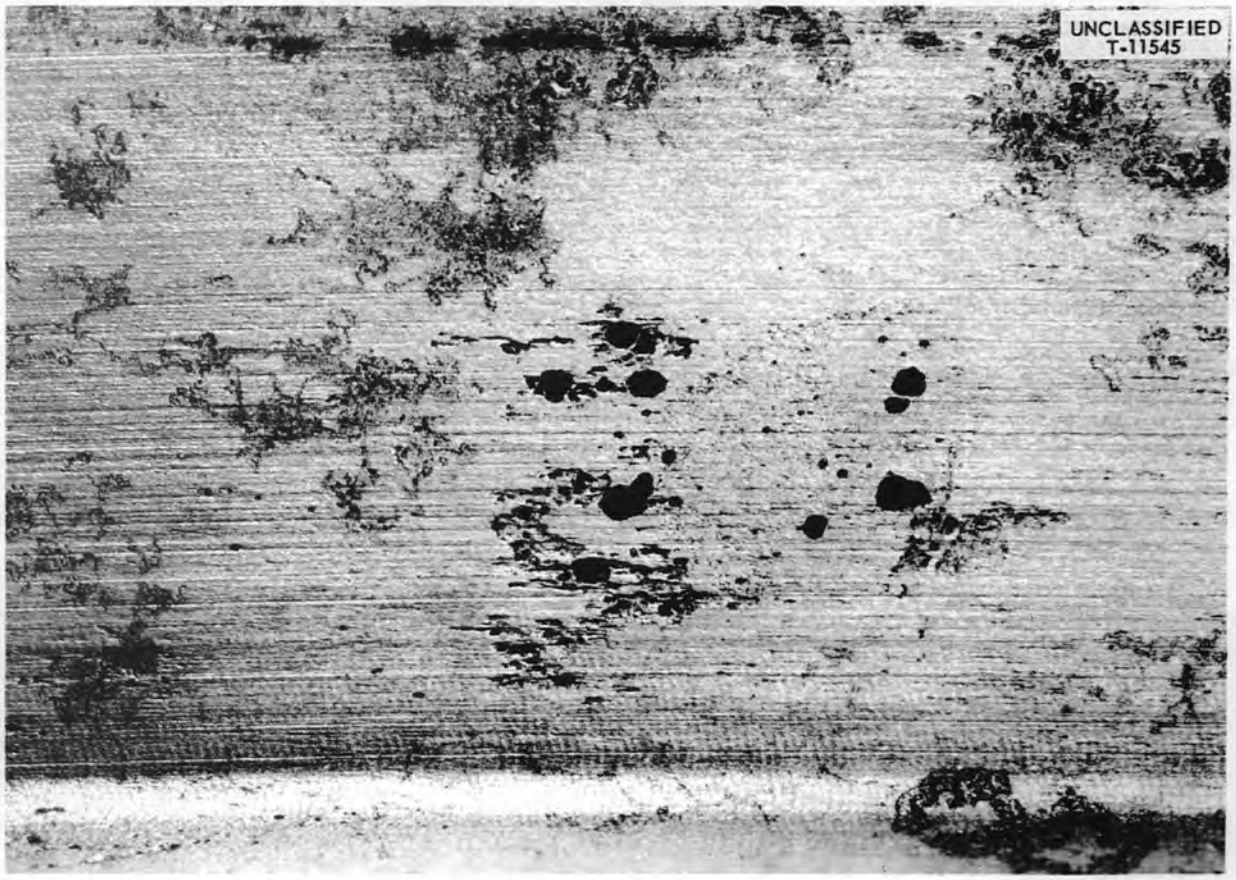

Fig. 1.8. Pitted Area in Groove of Flange A-101.

half of the pressure-vessel dome flange (B-1) showed pitting and porosity. A crack was located near the leak-detector hole. After the first lapping operation, which removed approximately 0.005 in. of metal, no crack was found near the leak-detector hole, but a $1\frac{1}{2}$-in.-long crack was indicated at the 3 o'clock position. After a second lapping the indication at 3 o'clock was gone, but several short pitlike imperfections showed up at the 6 o'clock position. By alternate examination and abrasion it was possible to remove all indication of cracks. The top half of the flange initially showed pitting, porosity, and one imperfection suggestive of a possible crack. After the surface of the groove was machined 0.005 in., it was again given a penetrant examination, which showed no significant indications. Another machine operation was necessary later to correctly shape the groove to the new gasket, but inspection after this examination did not show anything significant either. The O-ring from this flange contained several long circumferential cracks, which were revealed both by penetrant and metallographic inspection (Fig. 1.9).

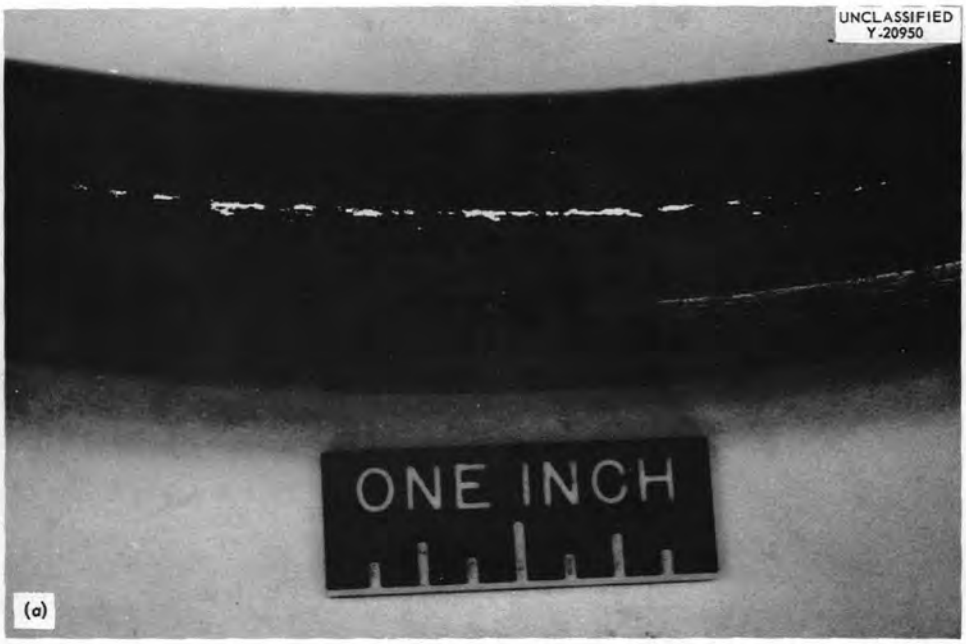

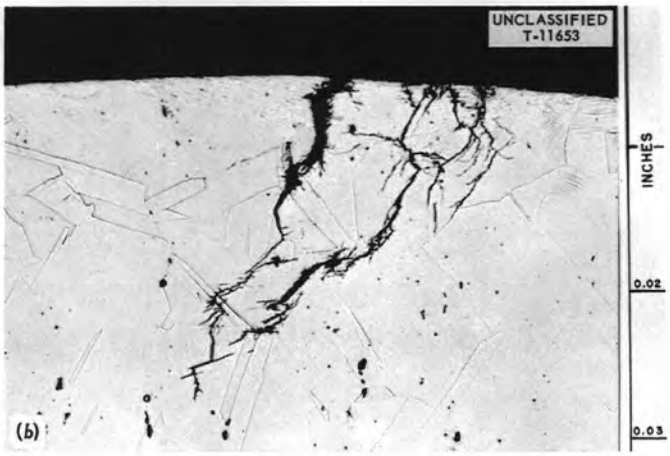

Fig. 1.9. Crack in O-Ring from Dome Flange B-1. (*a*) Penetrant inspection; (*b*) metallographic inspection (100X). Reduced 23%.

While this flange was open, exposing the core tank, numerous photographs were made to record the condition of the inner surface of the Zircaloy-2 alloy of the core.

The rupture-disk flange and several flanges from the low-temperature system were also penetrant inspected. Several deep pits were found but no definite cracks were located.

On the basis of these flange examinations it was recommended that all the flanges (~200 pairs), as well as all the leak-detector tubing (~15,000 ft), be replaced.

1.2.2 Cracks in HRT Flange Bolts and Ferrules

Two HRT flange bolts of a lot of 16 spares were found to be severely cracked, and a program was launched to determine the cause for the cracking and to find methods for nondestructive testing of the remainder of the 672-bolt shipment, a large portion of which had been installed in the HRT. Shortly thereafter, inspection of eight ferrules removed from the flange in line 246 of the HRT disclosed hairline cracking in four of them. Specifications had called for the bolts and ferrules to be fabricated of AISI 4140 steel, cadmium plated to 0.0002 in., the bolts to be tempered to Rockwell C 32–38 hardness, and the ferrules to be tempered to a minimum yield strength of 105,000 psi.

Of several methods attempted, Magnaglo proved to be the most suitable for examining the bolts, even though it required their removal. Out of a total of 208 bolts tested by this method, 5 showed serious cracks and 13 contained surface seams in the hexagonal head. The latter were not considered to be serious defects.

Figure 1.10 is a macrograph showing four of the HRT bolts with varying degrees of defection. Those in the first, third, and fourth positions from the left have deep cracks which appear to originate at the sharp change in cross section below the head. The crack in the second is a surface seam. In the most serious case the crack traverses completely around the head and goes some distance into the shank of the bolt. The cracks in the ferrules (Fig. 1.11) were very fine, ranged from $^{2}/_{16}$ to $^{7}/_{16}$ in. in length, and were aligned along the axis of the part.

The evidence gathered from the bolt examinations pointed to a case of quench cracking. The

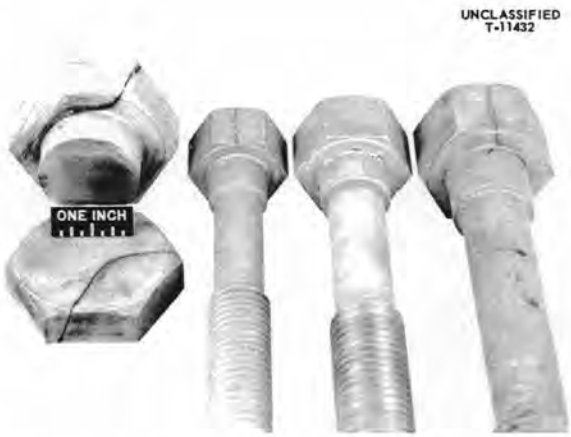

Fig. 1.10. Cracking in HRT Bolts.

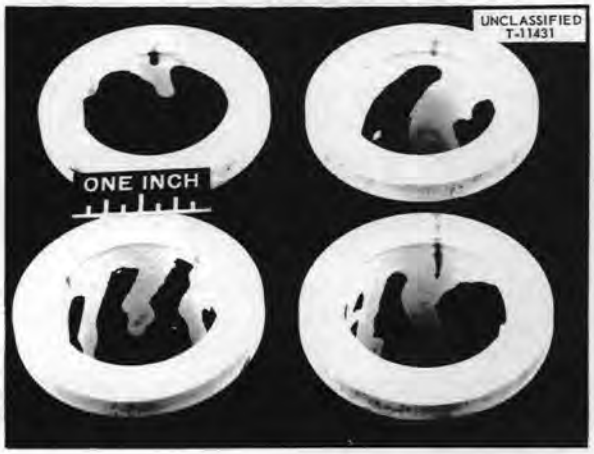

Fig. 1.11. Cracking in HRT Ferrules.

fillet called for below the head of the bolt was often sharp, and in some cases undercutting in the shank at this location was found. Nothing abnormal was disclosed in regard to the microstructure or chemical analyses of the bolts, and the parts were through-hardened in all cases. Embrittlement by hydrogen did not appear to be a factor in the cracking. A trace of the plating metal found at the interface of one of the cracks clearly showed that the cracking had occurred prior to plating. Spectrographic analysis revealed this plating to be zinc instead of the specified cadmium. However, zinc is considered suitable.

The findings in regard to the ferrules were similar to those for the bolts; however, a case

for ascribing the defects to quench cracking was not so clear.

It was recommended that all remaining HRT bolts and ferrules be examined by Magnaglo and that all parts showing evidence of cracking be replaced. Although the existing material and heat-treatment specifications were considered suitable for these parts, it was recommended that future bolts and ferrules be plated with zinc to 0.0002-in. thickness, immediately hydrogen-relieved by boiling in water for 3 hr, and finally given a bichromate chemical dip (Cronak or approved equal).

1.3 MAINTENANCE OF RADIOACTIVE COMPONENTS

The numerous maintenance devices that have been designed for the HRT can be categorized as follows: jigs, fixtures (positioning frames for components), lifting bails, disconnects, tongs, and auxiliary facilities. To date two remote-maintenance practice periods have been held, to afford an opportunity to test the adequacy of the devices and the accompanying job procedures and to familiarize HRT personnel with their use. During the first period the work was performed with the special long-handled tools, but the reactor cell was not flooded, as it will be in later operations. Altogether, seven valves, two feed-pump head assemblies, and the blanket circulating pump were removed. It was shown during the first trials that several tools were too fragile or were impractical to use, and numerous design and procedure changes resulted.

In the second remote-maintenance period, during the latter part of December, the reactor cell was filled with filtered plant water to a depth of 11 ft, thereby allowing the formation of freeze plugs in process lines with the freezer coils submerged. In order to ensure that no chloride-contaminated water leaked into the reactor piping, no flanges were completely unbolted while submerged; however, the freeze plugs were maintained while the water level was lowered, so that their performance could be checked after the flanges were opened. Equipment removed and replaced remotely included high- and low-pressure valve assemblies, a space cooler, one condensate-tank weigh-cell assembly, and the blanket circulating pump. Prior to this maintenance period the spare blanket circulating pump had been fabricated on its jig (Fig. 1.12).

Fig. 1.12. Blanket Circulating Pump Scroll Assembly in Jig.

The spare assembly was successfully installed during this practice period to check the dimensional reproducibility of the jig.

The 16 different replacement jobs practiced to date encompass the various devices and procedures required for the replacement of 74 different

components. Eighteen additional jobs remain to be practiced.

Some of the maintenance devices utilized during the practice periods are illustrated in Figs. 1.13 through 1.24 and are described below:

Tool Cart – Fig. 1.13: A device provided for the safe storage of uncontaminated tools, facilities, and handle sections.

High-Pressure Valve Jig – Fig. 1.14: A universal-type jig for locating valve flanges, capable of handling 21 different high-pressure valves comprising 18 different configurations; universal feature accomplished by utilizing various brackets in the several locations indicated by the holes in the base plate.

Lifting Bail – Fig. 1.15: Consists of three rods and a lifting plate, and is shown attached to one of the pressurizer liquid-level indicator assemblies.

Thermocouple-Disconnect Tool – Fig. 1.16: Female half of the thermocouple disconnect shown held by tool after having been separated from its male half at the disconnect station.

Air-Line-Disconnect Tool – Fig. 1.17: Remotely disengages or engages the Snap-Tite disconnects used in air lines to replaceable equipment in the reactor cell.

Torque-Multiplier Wrench – Fig. 1.18: Used for applying torques up to 2000 ft-lb; input supplied by hand through an extension handle into the cylinder (shown in the center of the photograph) which contains a 4:1 gear reduction unit.

Spinner Wrench – Fig. 1.19: Used for removing bolts quickly after they are loosened with one of the high-torque wrenches, for spinning the bolts snug before final tightening, and, by use of a right-angle bevel-gear attachment (not shown), for handling bolts in a horizontal position; has a chain-driven offset to fit bolts not accessible by direct drive, such as bolts hidden under pipe fittings and bends.

Hydraulic Retriever Tool – Fig. 1.20: Used for picking up various items from the cell floor; the fingers are actuated by the hydraulic cylinder through rack and pinion gears, and the tool is connected to the handle through a bevel-gear set which allows 360-deg rotation of the head.

Flange-Spreader Tool – Fig. 1.21: Used to spread low-pressure valve flanges to prevent damage to the ring gaskets during removal or insertion of the valves; tool shown in place with flanges spread and the valve assembly moved back on its cell fixture.

Pump-Mover Tool – Fig. 1.22: A scissors-jack type of tool (shown in position on the feed-pump head assembly), used for moving the feed-pump and purge-pump head assemblies back and forth on their respective cell fixtures so that the two halves of the mating flange can be positioned.

Hydraulic Torque Wrench – Fig. 1.23: Used to lighten or loosen bolts on flanges larger than 2-in. pipe size; is actuated by a hydraulic (water-operated) cylinder and is capable of applying 2000 ft-lb force.

Electrical-Wiring Disconnect Tool – Fig. 1.24: Designed to loosen the gripper nut and to remove the male half of the disconnect of the collet-type clamp assembly associated with the power leads to the circulating pumps, space-cooler motors, and pressurizer heaters.

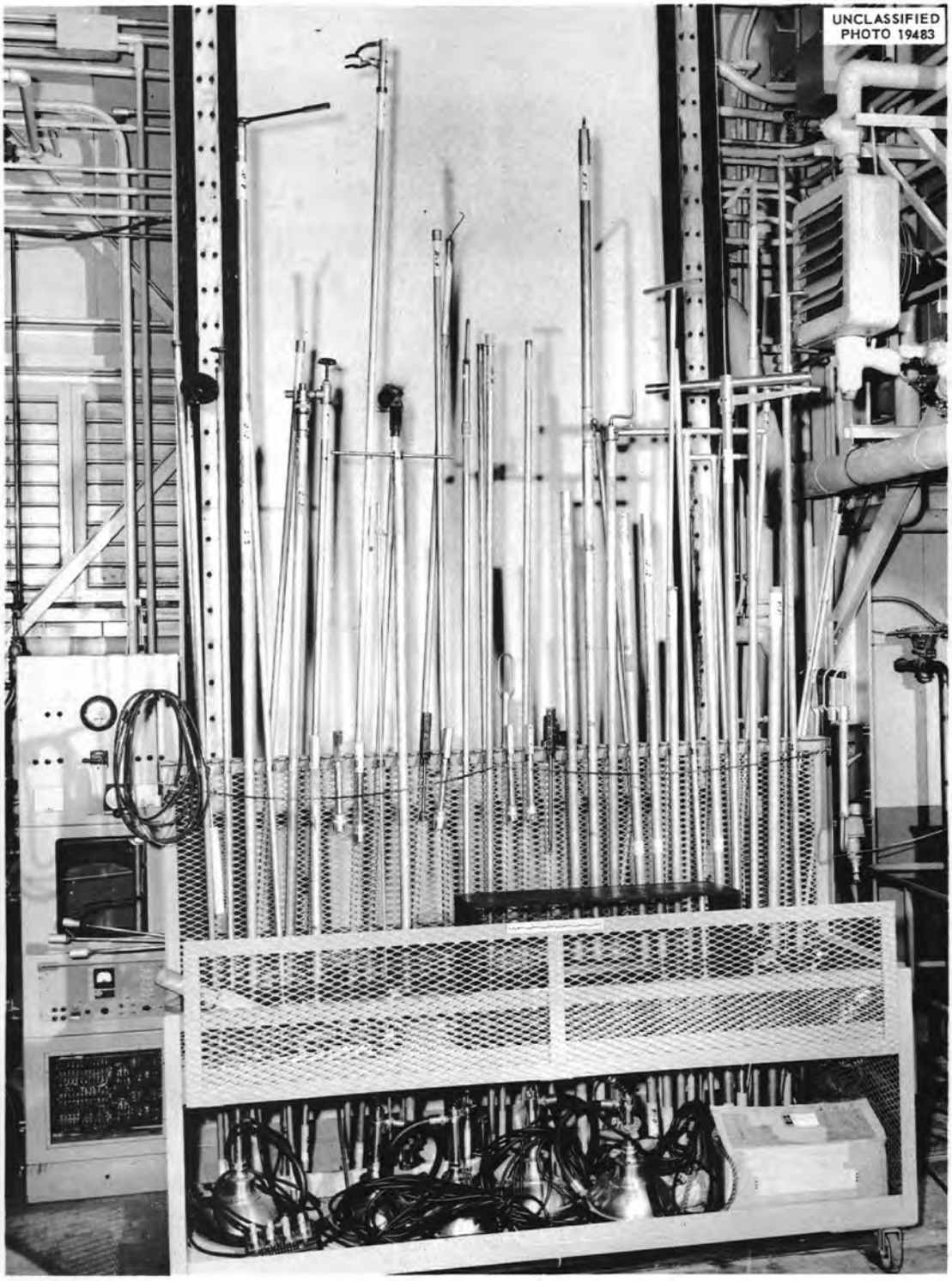

Fig. 1.13. Tool Cart.

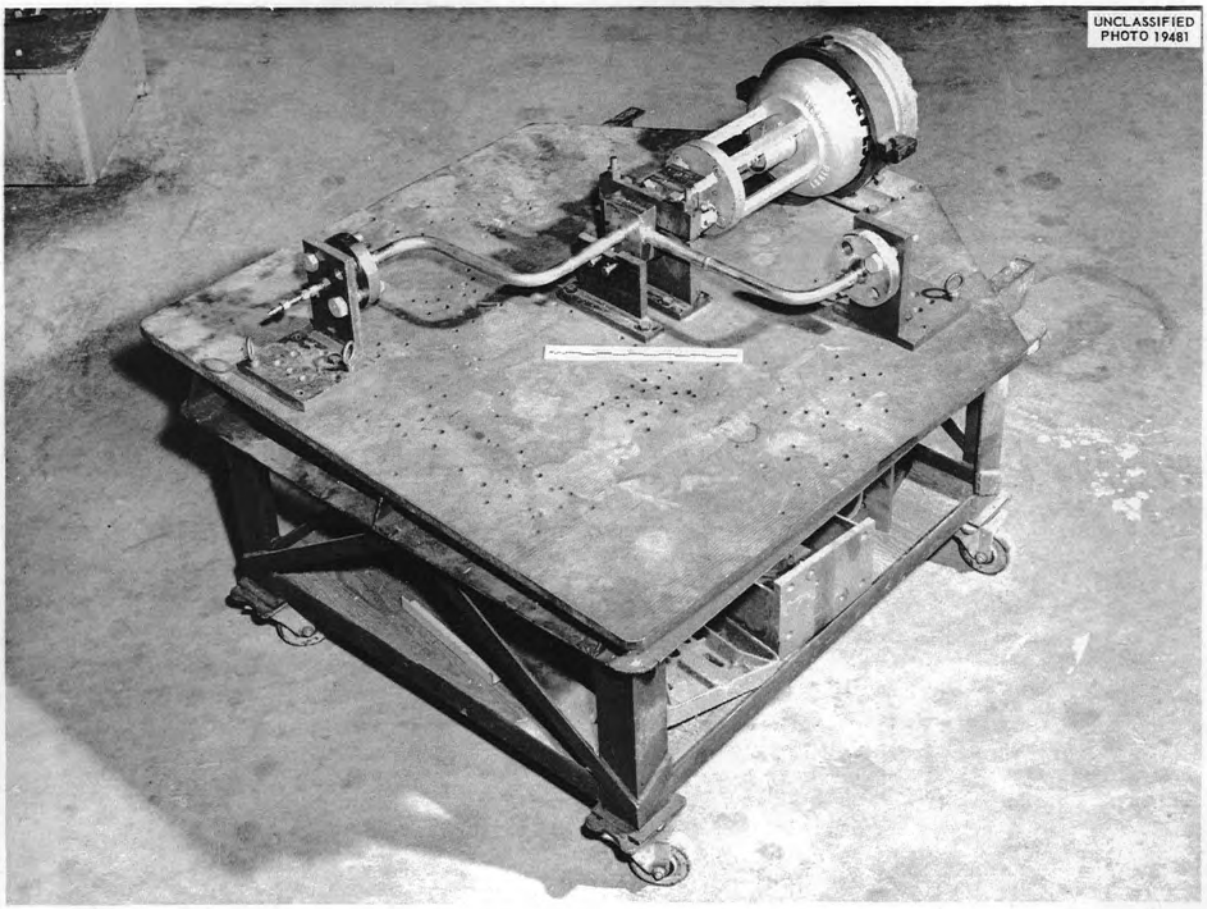

Fig. 1.14. High-Pressure Valve Jig.

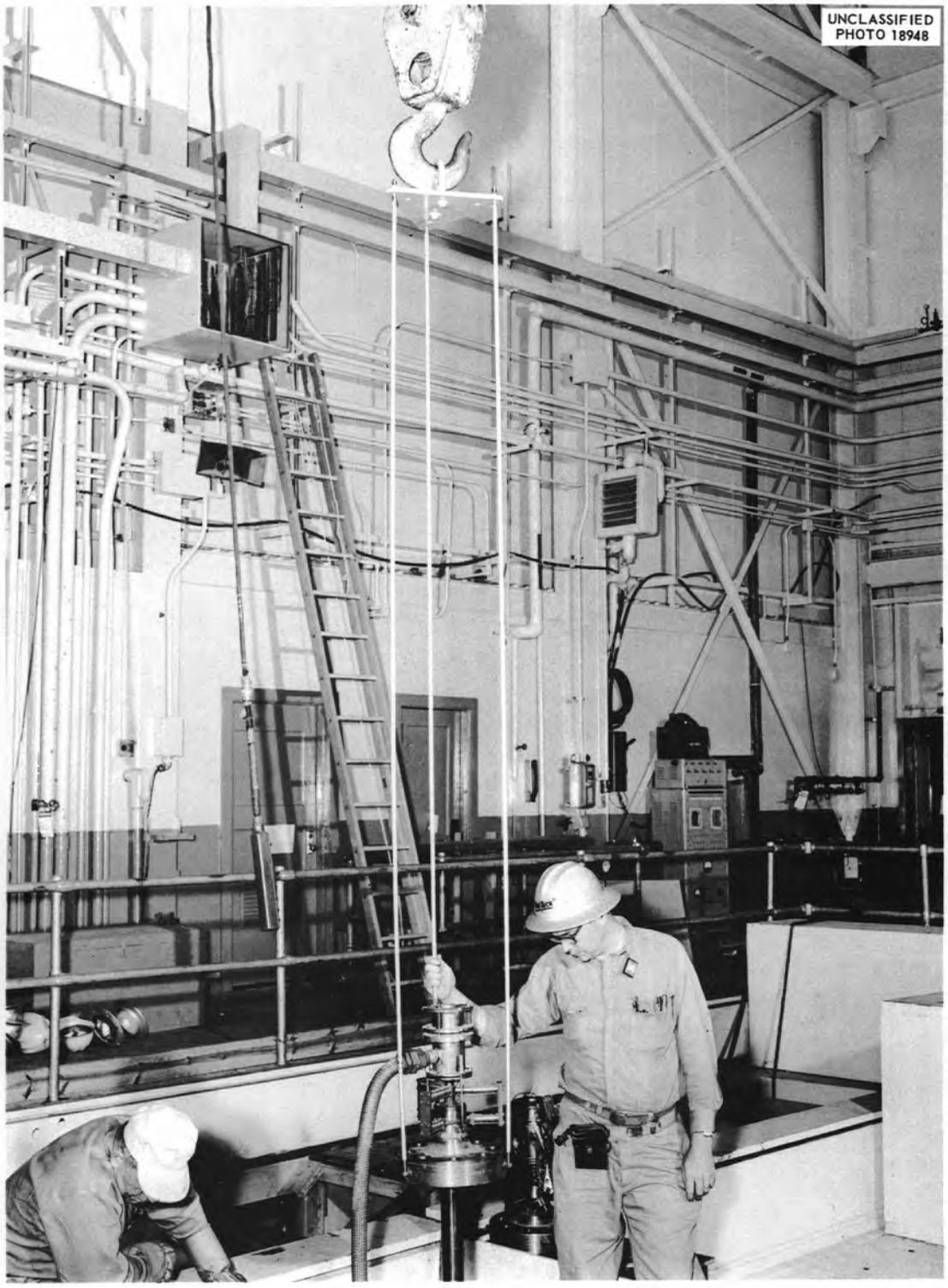

Fig. 1.15. Lifting Bail.

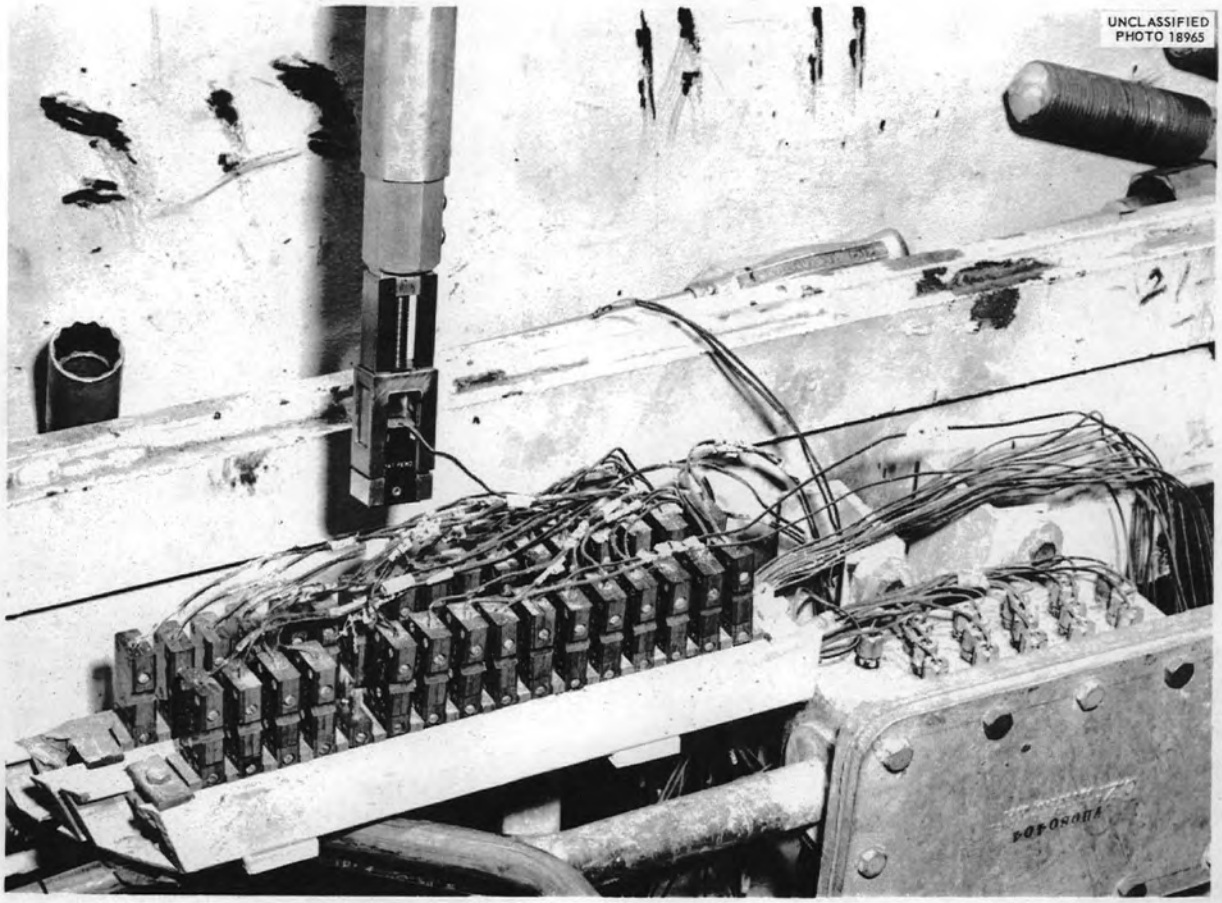

Fig. 1.16. Thermocouple-Disconnect Tool.

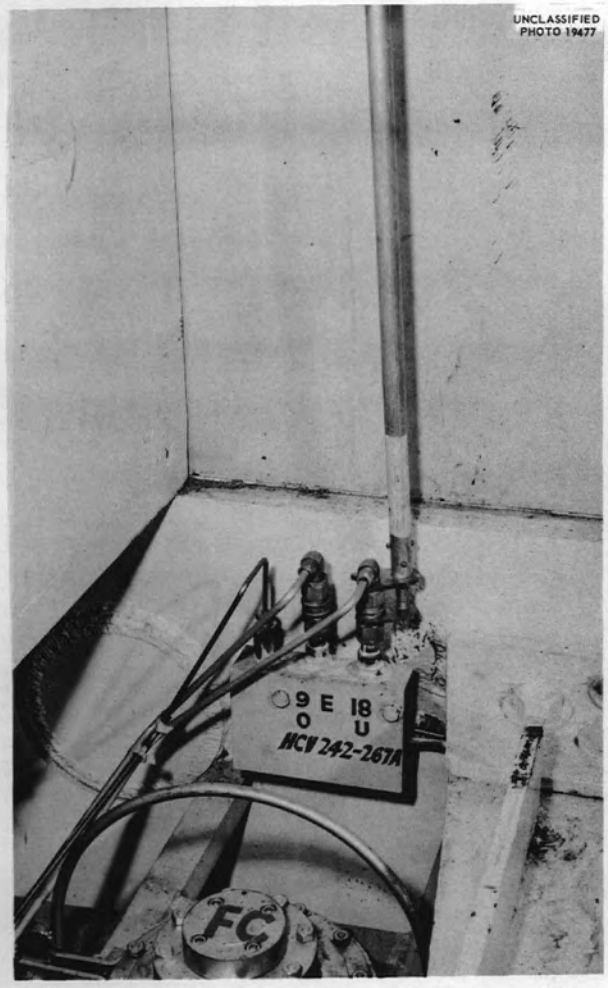

Fig. 1.17. Air-Line-Disconnect Tool.

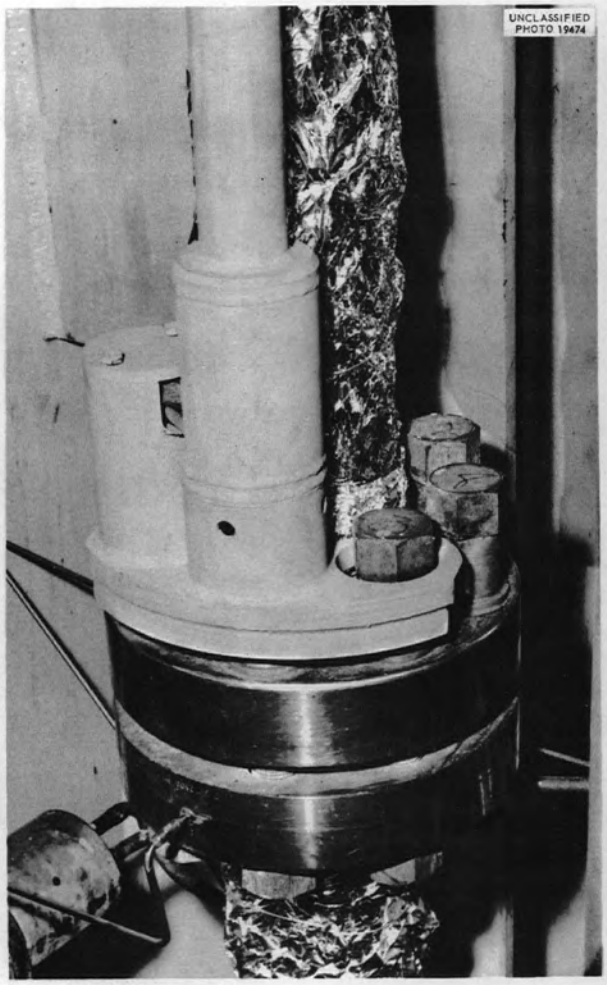

Fig. 1.18. Torque-Multiplier Wrench.

UNCLASSIFIED
PHOTO 19484

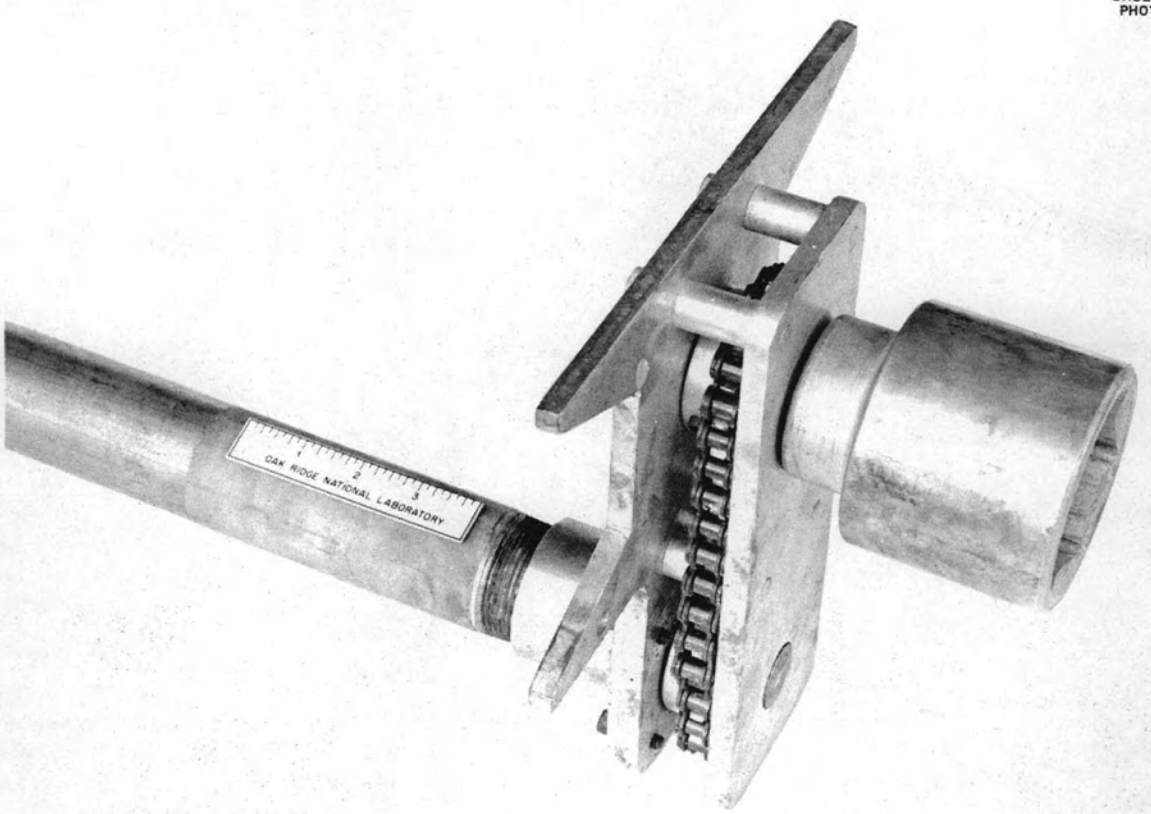

Fig. 1.19. Spinner Wrench.

UNCLASSIFIED
PHOTO 19478

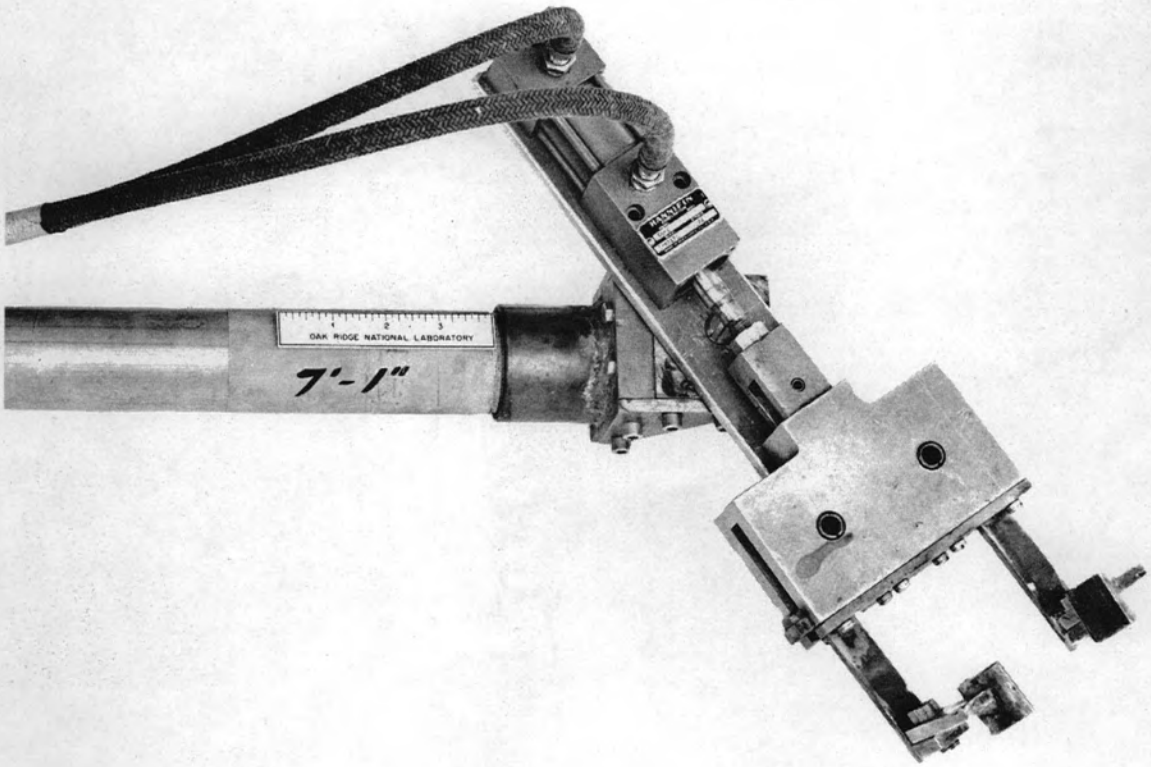

Fig. 1.20. Hydraulic Retriever Tool.

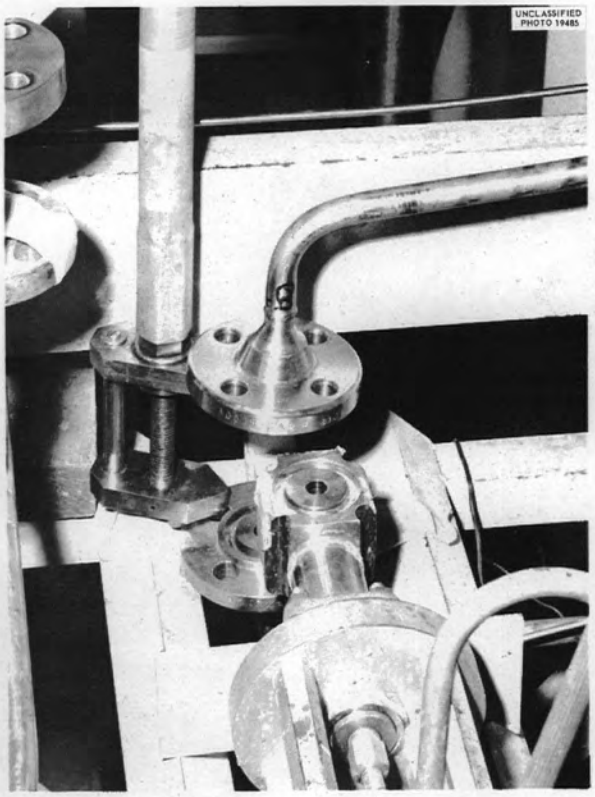

Fig. 1.21. Flange-Spreader Tool.

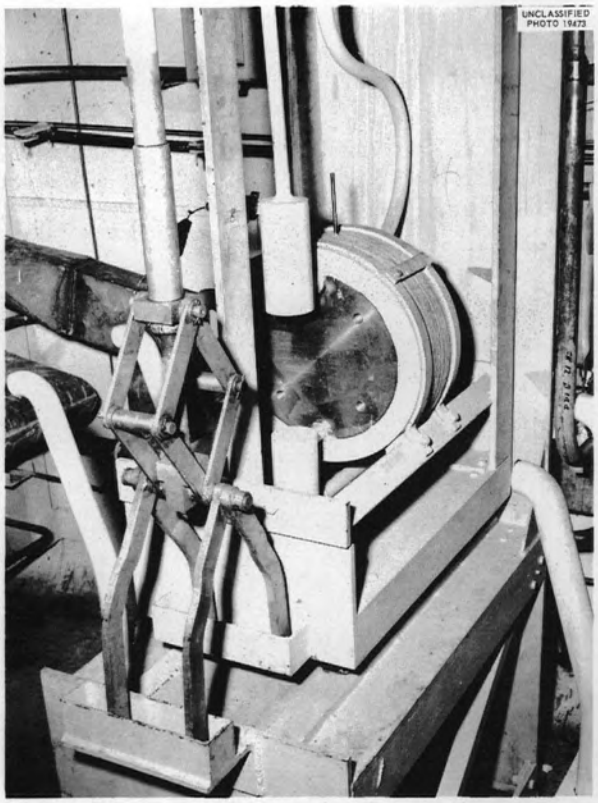

Fig. 1.22. Pump-Mover Tool.

Fig. 1.23. Hydraulic Torque Wrench.

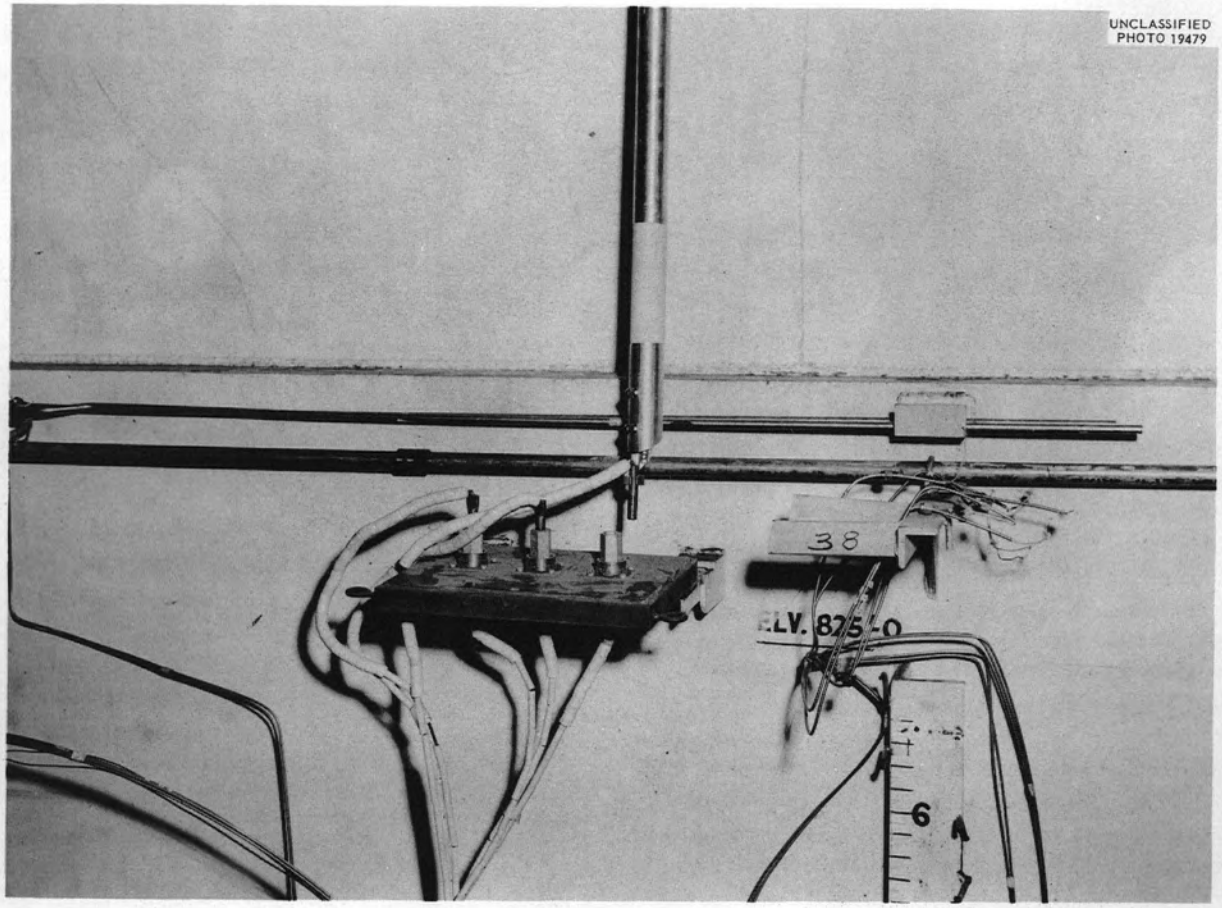

Fig. 1.24. Electrical-Wiring Disconnect Tool.

2. HRT DESIGN

W. R. Gall

C. A. Burchsted
R. D. Cheverton
C. J. Claffey
C. W. Collins
E. H. Gift
P. H. Harley
R. F. Hughes[1]
M. I. Lundin
H. A. McLain
R. C. Moren[2]
R. C. Robertson
J. N. Robinson
W. Robinson
H. C. Roller
R. E. Schappel
C. L. Segaser
I. Spiewak
W. Terry
T. H. Thomas
F. C. Zapp

2.1 REFRIGERATION SYSTEM

Amsco 125-82, an odorless mineral spirit resembling kerosene in its physical properties, was recommended[3] as the secondary refrigerant, replacing Freon-11, for the refrigeration systems in both the reactor and the chemical processing plant. Several other refrigerants, including ethanol, tributyl phosphate, triethyl phosphate, and Cellosolve, were also investigated, but they failed to meet one or more of the specifications. To be suitable for service within the HRT reactor cell, a refrigerant must have a freezing point of –40°F or lower, be resistant to radiation damage, have good heat transfer properties, be relatively noncorrosive, nontoxic, and nonexplosive, be free of chloride or fluoride ions, have a vapor pressure at room temperature of 100 psig or lower, and be amenable to low-temperature pumping.

Amsco has a freezing point of –67°F and a viscosity at the operating temperature (–40°F) of 8.2 centipoises. It appears to be compatible with the materials in the system, is not subject to excessive decomposition under radiation, is reasonably nontoxic, and has suitable heat transfer characteristics. In addition, Amsco showed no tendency to form insoluble residues at the high temperatures (550°F) which may be attained in certain freeze jackets, has a low chloride content in the commercial grades (1 ppm), and is considerably less expensive than the other materials investigated (~25¢/gal). Some gassing of Amsco was evidenced under radiation[4] but was no more than could be handled by the existing vent system. The installation of a ventilating fan and CO_2 fire extinguishers in the proximity of the Amsco circulating pump was recommended because of the relatively low flash point (128°F) of the material. No further additions or changes to the refrigeration system would be necessitated by the use of Amsco; it will be necessary only to drain the Freon-11 and flush the system. The continued use of the silica-gel drier was recommended for the removal of free water from the system.

2.2 WATER TREATMENT

Following an extensive investigation of feedwater treatment, hydrazine and coordinated phosphate treatment were recommended for the conditioning of the HRT steam-system feed water.[5] Hydrazine, a material widely used in large central-station practice, was recommended as an oxygen scavenger, although its behavior under the conditions which will be experienced in the HRT is conjectural. If it should break down excessively under irradiation or if its reaction time with oxygen should be too slow, the use of a sodium or potassium sulfite treatment would be recommended. A high rate of consumption would be expected with either sulfite under radiation, requiring frequent blowdown. In addition, there is the possibility that foaming with sulfite could cause an appreciable carry-over of solids and radioactivity to the valve pit.

A coordinated phosphate treatment was recommended for pH control. Coordination is effected by balancing the quantities of tri-, di-, and monosodium phosphate added to the system to maintain the ratio of phosphate concentration to pH at the empirical level below which caustic embrittlement is not expected to occur. The use of morpholine

[1]On loan from Kaighan & Hughes, Inc.

[2]On loan from Westinghouse Electric Corp.

[3]R. C. Robertson and H. A. McLain, *Secondary Refrigerant for HRT Refrigeration System*, ORNL CF-57-1-88 (Jan. 24, 1957).

[4]M. D. Silverman, *The HRT Refrigerating System*, ORNL CF-57-1-28 (Jan. 9, 1957).

[5]H. A. McLain, *Treatment of the HRT Steam System Water*, ORNL CF-56-11-132 (Nov. 29, 1956).

was deemed inadvisable because of its probable polymerization under radiation.

The initial charge and the makeup for the steam system will be steam condensate of less than 5 ppm total hardness and less than 1 ppm chloride concentration.

2.3 COOLING-WATER SYSTEM

The change to a double-loop cooling-water system with a closed cooling loop serving in-cell components[6,7] required several control-circuit modifications to provide adequate radiation protection in the event of disturbances within the reactor cell. The redesigned cooling-water system has a storage tank from which normal or emergency makeup water may be supplied to the internal loop, with a connection from the cooling-tower basin to provide additional makeup water should the storage tank become exhausted during an emergency.

The criteria for the control-circuit modifications required that, should a leak occur in the reflux or recombiner condensers, as indicated by the detection of radiation in the cooling-water returns from those condensers, the contaminated water would be diverted to the cell floor, with emergency makeup of cooling water to the internal loop being supplied from the storage tank or cooling tower. Should the level of radiation in the cooling water be excessively high, an emergency dump would be initiated and cooling water from all in-cell components would be diverted to the cell floor, again with an emergency supply of makeup cooling water from the storage tank or cooling-tower basin to protect reactor components from overheating. In the former case a normal shutdown in the event of a minor leak in the condensers would avoid the excessive pressure buildups in the low-pressure system which would be occasioned by an emergency reactor dump.

Should an explosion occur within the reactor cell, it would be necessary not only to contain the entire body of cooling water in the internal loop but also to prevent a back-surge of contaminated water to external components (i.e., the storage tank, cooling tower, heat exchanger, etc.), necessitating the blockage of all lines leading to that equipment. The criteria for system controls also required protection against pressure buildups within the closed cooling loop itself, and provision to permit intentional shutdown of the closed-loop circulating pump without actuating block or diversion valves to drain the closed loop.[8]

2.4 FUEL HEAT EXCHANGER STEAM PIPING

Figure 2.1 shows the configuration of the steam outlet piping at the fuel heat exchanger. When steam from the package boiler is fed to the heat exchanger, during warmup of the heat exchanger, the pipes can be expected to be initially hotter than the shell of the exchanger. This temperature difference between the steam outlet header and the exchanger shell will result in differential expansion between these members. Because the vertical nozzles are rigidly fixed to both header and shell, it is possible, if the temperature difference becomes too great, that excessive stresses could be developed in those nozzles. The total combined stress in the nozzles includes the stresses due to (1) the working pressure (1500 psig max), (2) expansion of the steam main connecting the outlet header and the steam drum, and (3) the differential expansion noted above. It was estimated that a temperature difference in the order of 20 to 40°F could cause a total combined stress in the nozzles in excess of the 40,000 psi allowed by the Code.[9]

It was recommended therefore that thermocouples be installed to measure the temperature difference and that careful measurements of piping expansion be made during one or two heat exchanger warmups to determine whether this may actually be a problem. If temperature differentials of as much as 30 to 40°F are discovered, it is further recommended that a permanent thermocouple installation, with annunciation, be provided. If temperature differentials in excess of 40 to 50°F are discovered, it is recommended that some consideration be given to the use of a single steam outlet nozzle, as on the blanket heat exchanger, although this would entail some sacrifice in efficiency of the entrainment separators located within the heat exchanger steam space.

---

[6] W. R. Gall *et al.*, *HRP Quar. Prog. Rep. Oct. 31, 1956*, ORNL-2222, p 7.

[7] H. A. McLain, R. E. Aven, and R. C. Robertson, *HRT Cooling Water System Modifications*, ORNL CF-56-8-152 (Aug. 23, 1956).

[8] R. L. Moore, *Proposed Control Circuitry for Revised HRT Cooling Water System*, memorandum dated November 12, 1956.

[9] *ASA Code for Pressure Piping*, ASA B31.1-1955, Par. 622(c).

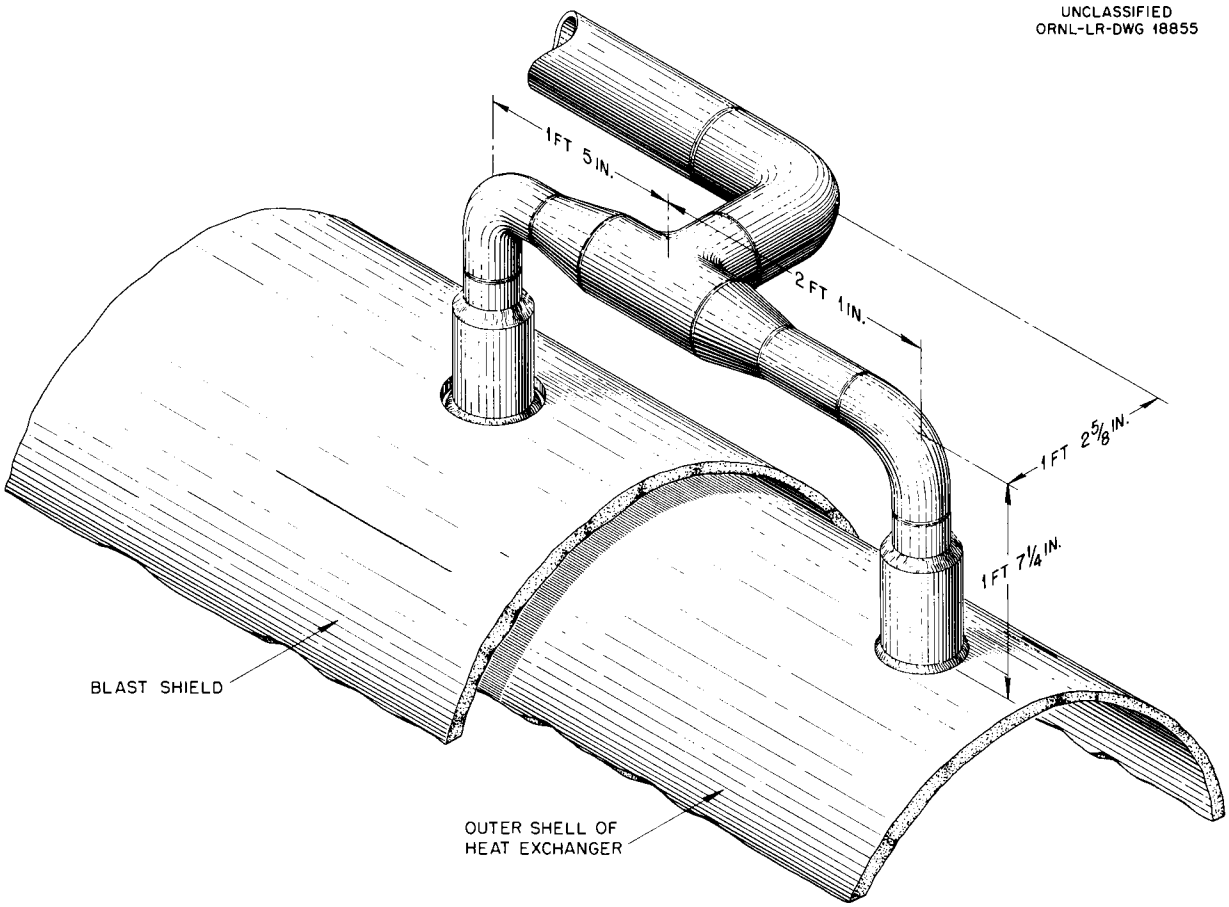

Fig. 2.1. Section of Fuel Heat Exchanger Showing Configuration of Outlet Steam Piping.

2.5 DEUTERIUM RECOMBINATION

The conclusions from the original investigation of the delay time required to minimize the deuterium explosion hazard during a dump of the HRT were predicted on the pessimistic assumption that the gas-liquid equilibrium between the vapor and the total volume of reactor fluid was achieved instantaneously upon initiating a dump.[10] Re-evaluation of the problem, taking into account the rate of pressure release, the rate of deuterium recombination, the rate at which deuterium can be supplied to the vapor space in the pressurizers, and the solubility of deuterium confirms that with the present pressurizer gas bleed valves a delay period of approximately 2 min will be required to allow for internal recombination of deuterium and oxygen to prevent the accumulation of an explosive mixture. The delay primarily assures that the concentration of deuterium in the reactor will always be lower than the solubility limit of deuterium during the rapid drop of system pressure. The solubility of deuterium appears to be the decisive factor, since, if only gas-liquid equilibria, rate equations, and material-energy balances in the system are considered, no delay period is necessary.[11]

2.6 PRECIPITATION OF URANYL PEROXIDE IN FUEL CIRCULATING PUMP

Because of the relatively low temperatures which will be encountered in the motor portion of the fuel circulating pump, some concern was expressed regarding the precipitation of uranyl peroxide in that area should fuel solution leak into it from the

[10] R. E. Aven and M. W. Rosenthal, *Delay Time Required to Reduce D_2 Explosion Hazard During HRT Dump*, ORNL CF-56-5-40 (May 1, 1956).

[11] E. H. Gift and H. A. McLain, *Delay Time Prior to Dumping the HRT*, ORNL CF-57-1-103 (Jan. 10, 1957).

pump scroll. A purge stream is admitted to the back of the fuel circulating pump under a pressure somewhat in excess of the fuel circulating pressure; this stream serves to cool the pump to some extent and to prevent excessive leakage from the scroll into the motor portion of the pump. This purge will not be 100% effective in preventing leakage from the scroll, and some contamination of the purge water will take place.

It has been observed that at low temperatures uranyl peroxide will precipitate from radioactive aqueous fuel solutions.[12] Under the operating conditions of the HRT mockup, the maximum purge-water temperature obtained in the circulating pump was approximately 60°C (at the mechanical seal between the scroll and rotor chamber); the minimum was 46°C. Calculations indicated that for a 100% solution of active reactor fuel at a reactor power level of 5 Mw uranyl peroxide would precipitate at temperatures lower than 62°C. However, since essentially any leakage will be in-leakage to the fuel solution rather than leakage of the fuel into the purge stream, the concentration of fuel solution and fission products in the purge stream should be considerably less than that in the circulated fuel solution. On the assumption that concentrations of uranium and fission products in the purge stream will be a factor of 10 lower than those in the fuel solution (i.e., 1 g of uranium per liter), uranyl peroxide would not precipitate unless the temperature should drop below 40°C. Since, in practice, the purge dilution should be much greater than this, no precipitation of uranyl peroxide would be expected as long as the purge flow continues. As any "dead" areas in the purge volume within the pump would be at a temperature considerably above the precipitation threshold, precipitation in such areas is not considered to be a problem.

[12] M. D. Silverman, G. M. Watson, and H. F. McDuffie, *Reactor Sci. Technol.* 3(3), 43–61 (1953) (TID-2010) (Classified).

2.7 FLANGE TEST PROGRAM

A thermal-cycling test facility to aid in the investigation of flanged joints was constructed and placed in operation. Essentially, the facility (Fig. 2.2) consists of a 40-kw boiler which supplies saturated steam under regulated conditions to eight vertically mounted flange joints of varying sizes. A vacuum leak-detector system, in which leak rates are measured by determining the pressure rise in calibrated vacuum tubes mounted between each flange pair and an air-actuated vacuum valve, is used to determine flange leakage as factors affecting the integrity of the flanged joints are varied. The loop is normally cycled from room temperature to 335°C (the saturation temperature at 2000 psi) at a rate of 55°C per hour, at which temperature it is held for about 2 hr and then returned to room temperature at the same rate of temperature change.

A summary of test data and the results of the first five cycles are given in Table 2.1. Several

Table 2.1. Flange Leak Rates During Five Thermal Cycles

Flange Size	Ring Type	Average Per Cent of Required Bolt Loading for a Given Torque Wrench	Maximum Leak Rate First Five Cycles (cc/day) (1500 psi diff)
2 in., 2500 lb	Oval	73	2.8
1 in., 2500 lb	Oval	99	3.6
1 in., 2500 lb	Oval	73	3.2
2 in., 2500 lb	Octagonal	68	2.9
3½ in., 2500 lb	Octagonal	49	7.1
½ in., 1500 lb	Oval	95	4.6
½ in., 1500 lb	Oval	92	Large*
3½ in., 2500 lb	Oval	68	4.1

*Posttest inspection of flange grooves revealed several defects.

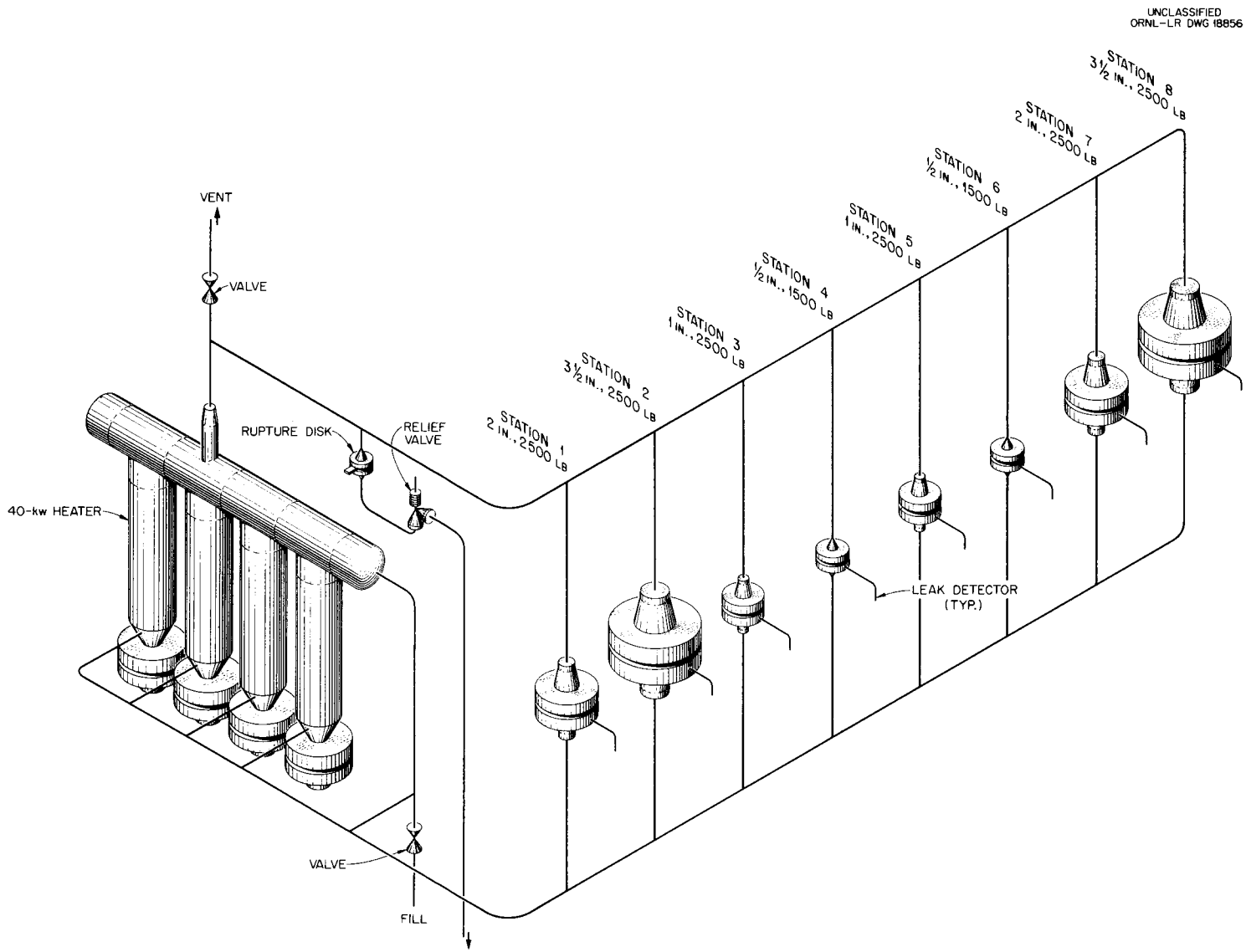

Fig. 2.2. Flange Test Facility Flow Diagram.

preliminary conclusions regarding flanged joints may be drawn as the result of observations made during the initial runs:

1. The torque wrench is not an adequate means of determining bolt loading. In spite of careful calibration, readings obtained from torque wrenches correlated no closer than 50% with pin extensometer readings.

2. Bolts should be retightened (without prior loosening) at least twice following the initial tightening, the system being thermally cycled at least three times between each such operation.

3. Leakage difficulties can be expected to increase with increasing flange size because of the increased area to be sealed, the increased difficulty in machining groove or ring without warpage or "scalloping," and the larger temperature differentials experienced between flange and bolts.

4. The resiliency and uniformity of flange bolting are definite factors in maintaining leak-tightness in flanged joints; resiliency can be increased by the use of ferrules in the bolt assembly.

5. Great care should be taken in handling and installing ring-joint flanges and gaskets to protect the seating surfaces. Nearly microscopic scratches have been found sufficient to cause leakage in a flanged joint.

3. HRT COMPONENT DEVELOPMENT

I. Spiewak

J. M. Baker
R. Blumberg
J. S. Culver
B. D. Draper[1]
C. H. Gabbard
B. A. Hannaford
P. H. Harley
P. G. Herndon
E. C. Hise
J. C. Moyers
P. F. Pasqua[2]
W. L. Ross
D. E. Willis

3.1 HRT PUMP DEVELOPMENT

3.1.1 400A-1 Pump and Loop

The 400A-1 Westinghouse pump, which contains a titanium impeller and a stainless steel thermal barrier with a titanium wear-ring insert, has operated for 6650 hr since the thermal barrier was welded to the stator flange. For 6407 hr, a solution of 0.04 *m* UO_2SO_4, 0.005 *m* $CuSO_4$, and 50 mole % excess H_2SO_4 was circulated at 255°C. Heat-balance checks on the pump cooling water indicated no leakage around the thermal barrier. Chemical analyses indicated low corrosion rates during the run.

3.1.2 400A-2 Pump and Loop

The 400A-2 Westinghouse pump was fitted with a $\frac{1}{16}$-in.-wide gold-plated stainless steel thermal-barrier gasket, held in place by type 322 annealed cap screws. The pump has circulated 0.04 *m* UO_2SO_4 and 0.005 *m* $CuSO_4$, with 50 mole % excess H_2SO_4, for 1170 hr at 250°C. Heat-balance checks on the pump cooling water indicated no leakage around the gasket.

3.1.3 300A-1 Pump

The 300A-1 pump operated in the HRT mockup for a total of 5541 hr, including 5148 hr in 0.04 *m* UO_2SO_4 solution at 280 to 300°C, after its thermal barrier was seal-welded. Pump performance throughout this period was excellent, as judged by power consumption, sound, and output. However, when the unit was dismantled early in the quarter so that it could be modified for service in 1.3 *m* UO_2SO_4 solution, it was found that the thermal-barrier seal weld had cracked. The back hub of the stainless steel impeller and the mating recess in the thermal barrier were badly eroded, and the pump bearings showed considerable wear.

The pump was reassembled with a seal-welded stainless steel thermal barrier containing a titanium labyrinth insert. The 230-gpm impeller and the scroll liner were also constructed of titanium.

Operation with water and with 1.3 *m* UO_2SO_4 solution was commenced and was continued for 482 hr, when a shutdown was necessitated by evidence of considerable leakage around the thermal barrier and by irregularities in pump power demand. An examination showed that the irregularities in power demand had been caused by momentary seizures of the lower radial bearing and that the thermal-barrier seal weld had cracked in several places, with one crack extending through the weld. Figure 3.1 shows corrosion cracking and pits found in the stagnant area between the main closure gasket and the seal-weld lips, located as shown in Fig. 3.2. The titanium impeller and wear-ring insert both had bare-metal erosive attack at the top of the impeller wear rings, as indicated in Figs. 3.2 and 3.3. The impeller suffered a weight loss of 1.7 g.

The lower radial bearing and journal have been replaced, the scroll housing has been drilled to provide for a circulating hydrazine leak-detector system in the area of the corrosion cracking, and

Fig. 3.1. Corrosion Cracking in Pump Stator. 9X. Reduced 32%.

[1]On loan from TVA.
[2]Consultant.

UNCLASSIFIED
ORNL-LR-DWG 18857

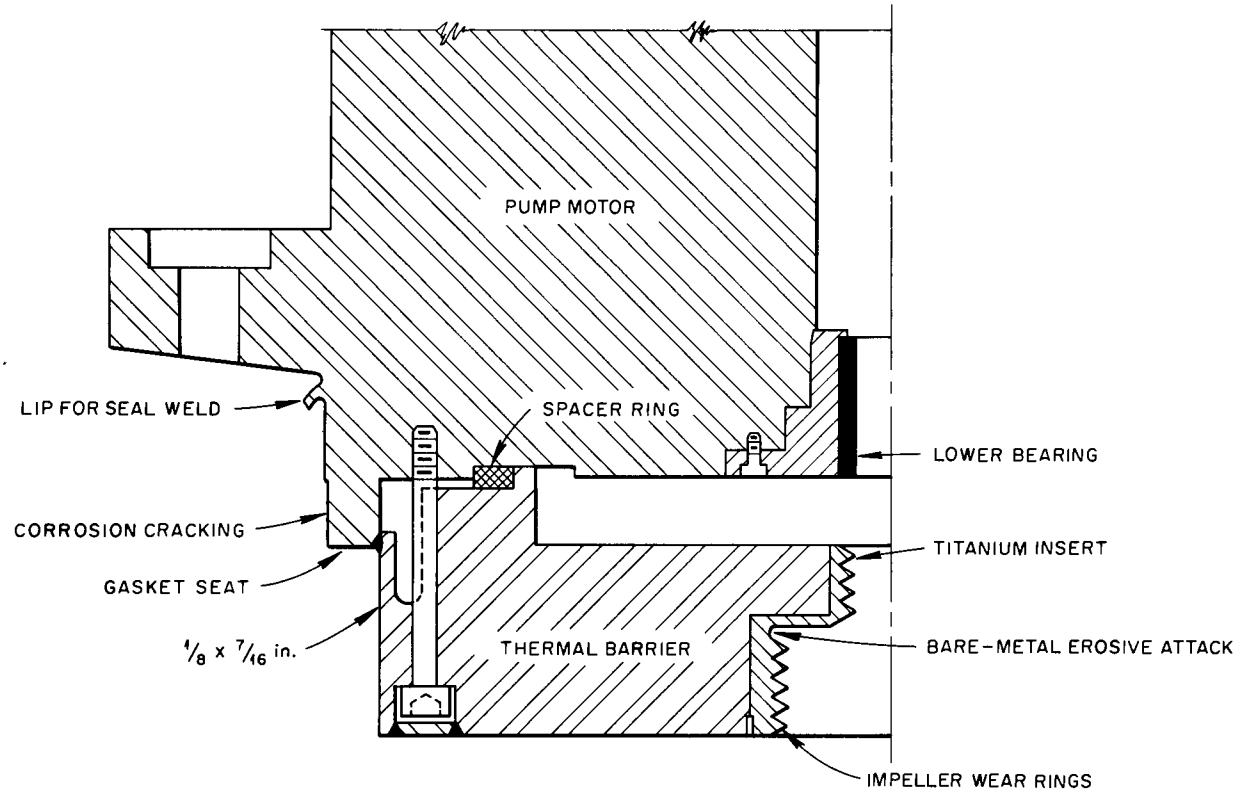

Fig. 3.2. Revised Thermal-Barrier Seal Weld.

the thermal barrier has been remachined (as shown in Fig. 3.2) to provide more flexibility to the seal weld.

3.2 DIAPHRAGM PUMPS

3.2.1 Feed-Pump Loop No. 1

Endurance tests of type 347 stainless steel diaphragms in water have continued concurrently with various performance tests of feed-pump components. The 0.019-in. annealed diaphragm and the $\frac{1}{4}$-hard 0.031-in. diaphragm have operated for 2314 and 1308 hr, respectively.

A preliminary test was conducted for 600 hr to compare the effectiveness of 100-mesh screens with that of the present 30-mesh screens in protecting diaphragms from dirt particles. The finer screens were, of course, more efficient particle filters and fortunately had very little effect on pump performance. They did not seem to be subject to plugging or fatigue failure and are therefore recommended for replacement HRT pumps.

3.2.2 Feed-Pump Loop 2

After operating for 856 hr with an experimental bolted head, feed-pump loop 2 was shut down because of a fatigue failure in a reducing fitting which had been machined from bar stock. A discussion of this failure and of the experience obtained with this head was reported.[3]

3.2.3 Purge Pump

A prototype HRT purge pump is continuing to run at 200 strokes/min, pumping 25 gph at 2000 psi in an endurance test. The diaphragm has been operated for 6670 hr, or approximately 58 million cycles, to date. The original discharge check valve with type 17-4 PH seats and type 440 stainless steel balls is still in operation and has given much better service in water than the standard valves with Stellite trim.

[3] E. C. Hise, *Evaluation of Experimental Pump Head Design*, ORNL CF-57-1-77 (Jan. 14, 1957).

Fig. 3.3. 230-gpm Titanium Impeller.

3.3 HRT SAMPLER

The prototype HRT sampler was operated to determine the "memory" of the device in taking successive samples of different media. It was found that 50 to 70 liters of distilled-water rinse was required to give a decontamination factor of 5000. Development work on the sampler was discontinued, and a final report on the testing was issued.[4]

3.4 FREEZE JACKETS

Additional tests were made on the 7½-in.-long, 5/16-in.-OD, type 347 stainless steel freezer coil welded around a ½-in. vertical pipe, which is an appendage on a piping system through which water was circulated at temperatures up to 300°C and pressures up to 2000 psi.[5,6] It was determined that at constant temperature (tests were made at 300, 200, 100, and 60°C) variations in pressure had no appreciable effect on the leak rate at which water could be frozen, although previously there had been some evidence of an effect. In these tests the pressure was varied from saturation pressure for each temperature up to 2000 psi.

A 12-in.-long, 5/16-in.-OD stainless steel coil was installed in place of the 7½-in.-long coil, and tests at 2000 psi and 300 and 200°C revealed that the maximum leak rate at which water could be frozen doubled in each instance to 22 and 35 cc/min, respectively. These data indicate that some freeze jackets on the HRT should be made 12 in. long if possible.

3.5 HRT CORE SAMPLE HOLDER

The sample holder[7] designed for use in the HRT core vessel was loaded with samples and inserted into a full-scale mockup of the vessel. Water was circulated at several flow rates in order to measure the pressure drop caused by the holder and to observe the flow pattern adjacent to the holder.

At a flow rate of 442 gpm (the nominal discharge flow from the HRT core), the additional pressure drop caused by the holder was 17.7 ft of fluid.

Dye which was injected into the core disclosed downward flow currents adjacent to the holder. This region extended upward two-thirds of the distance from the screens to the core outlet and outward to a maximum radius of 4 to 5 in. In order to make a qualitative determination of the effectiveness of natural-convention currents in opposing this downward flow, a dyed methanol solution, specific gravity 0.98, was circulated through the core followed by circulation of water. Visual observation indicated upward velocities of the order of 1 fps in the 98% density region adjacent to the holder. Upward flow persisted for approximately 10 sec after the flow of methanol was stopped. It was concluded that natural convection would supply adequate flow of fuel solution around the HRT core samples to keep them below the boiling point.

3.6 HRT MOCKUP

The HRT mockup operated for 1053 hr during the period covered by this report. In a continuation of a run started previously,[8] the mockup operated for

[4] B. A. Hannaford, *HRT Sampler Development*, ORNL CF-57-1-87 (Jan. 22, 1957).

[5] I. Spiewak *et al.*, *HRP Quar. Prog. Rep. Oct. 31, 1956*, ORNL-2222, p 17.

[6] B. D. Draper, *Test of Stainless Steel Freeze Jacket to be Used on ½-in. High Pressure and High Temperature Process Lines*, ORNL CF-57-1-89 (Jan. 21, 1957).

[7] ORNL Dwg. D-25625, "Corrosion Specimen Fuel Assembly."

[8] I. Spiewak *et al.*, *HRP Quar. Prog. Rep. Oct. 31, 1956*, ORNL-2222, p 18.

572 hr at 1400 psi and 280°C, with a 0.04 *m* UO_2SO_4, 0.024 *m* H_2SO_4, 0.02 *m* $CuSO_4$ solution containing 500 ppm O_2. This run was terminated on November 5, 1956, after a total of 1925 hr so that the loop could be inspected and then modified for operation with 1.3 *m* UO_2SO_4. Since the last inspection, 1925 operating hours had elapsed.

No major component failures occurred during the 1925-hr run, although the south feed-pump head developed a leak (after 2330 hr of service on the mockup) and the circulating pump experienced thermal-barrier and impeller damage (see Sec 3.1.3). The leak in the feed-pump head was caused by a crack at the junction of a capped ¾-in. pipe nozzle in the bottom of the intermediate side of the head. The pipe was cut off, the crack ground out, and the entire hole plugged with weld metal. The crack resulted from poor penetration where the pipe was welded to the head.

The high-pressure loop, as inspected from the tee between the pressurizer and the main loop, was in good condition. Again, however, there was a silt deposit along the bottom of the horizontal line going to the pressurizer.

The tubes of the 37-tube steam-heated loop heat exchanger were coated with a very heavy scale, possibly a result of solids added as slurry during tests on the performance of the HRT chemical plant hydroclone, but the tubes appeared to be sound (after 7500 hr of exposure).

The letdown heat exchanger was removed, and heavy corrosive attack was noted in the portions that had contacted fuel solution at 200 to 225°C. Consequently, the exchanger was replaced with a duplicate unit.

Stainless steel corrosion coupons removed from the high-pressure loop showed a corrosion rate of 0.13 mpy. The type 347 stainless steel coupons in the vertical leg from the loop to the pressurizer showed rates varying from 0.02 to 0.35 mpy. These rates contrast with the generalized rate of 1.3 to 1.5 mpy, based on nickel analysis of the solution.

Several modifications were made in the loop before the high-concentration uranyl sulfate run was started. All existing small high-pressure lines were removed; these included sample lines and the chemical plant hydroclone loop. A ½-in. line was installed from the pump discharge to the pressurizer vertical leg to simulate HRT line 230. A high-pressure-gas leak-detector system was installed on two flanges in the main loop and on one flange in the pressurizer boiler.

The loop was then pretreated for 119 hr at 260°C and 1400 psi with water containing 150 ppm of chromium as chromic acid. Then UO_2SO_4 and H_2SO_4 were added to bring the solution concentration to 0.04 *m* UO_2SO_4 and 50 mole % excess acid. After 115 hr of operation at this level, UO_2SO_4 was added over a 48-hr period to bring the solution to 1.3 *m*. The run was continued for 200 hr at the higher concentration before being terminated because of the circulating-pump trouble described in Sec 3.1.3. The generalized corrosion rate during the 200-hr run with the concentrated solution was 23 mpy.

4. HRT REACTOR ANALYSIS

P. R. Kasten

H. C. Claiborne T. B. Fowler

4.1 GAMMA RADIATION ESCAPING FROM OPENINGS IN THE HRT SHIELD

Maintenance of the HRT will require openings in the biological shield. An estimate of the radiation escaping through the maintenance portholes is necessary for designing temporary shielding and developing maintenance procedures.

After reactor shutdown the sources of gamma radiation in the reactor cell will be associated with the induced activity in the biological shield and equipment and with the fission products adhering to the inner surfaces of the equipment and piping. The biological dose rate associated with gamma radiation escaping from a maintenance porthole was calculated, taking into consideration line-of-sight from equipment, piping, and shield wall; scatter of gamma rays by porthole walls, cell walls, and equipment; and air scatter within the reactor cell. The results were used to prepare simplified design charts of the form illustrated in Fig. 4.1. These charts permit estimation of the biological dose rate near the porthole opening and are based on the assumptions that the HRT had previously operated at 5 Mw for several weeks and had been shut down for 4 hr before the shield was opened and that 50% of the total generated fission products had adhered to the surfaces exposed to fuel solution. Only 1 ft^2 of this exposed surface was considered in the calculations, and this was treated as a point source.

In using Fig. 4.1, it is necessary to reduce all equipment and pipes to equivalent point sources and to locate these sources in terms of the perpendicular distance from the porthole axis and the perpendicular distance from the wall containing the opening. The number of equivalent point sources to use will depend on the size and location of the particular equipment or piping and will be a matter of judgment. The total dose at the

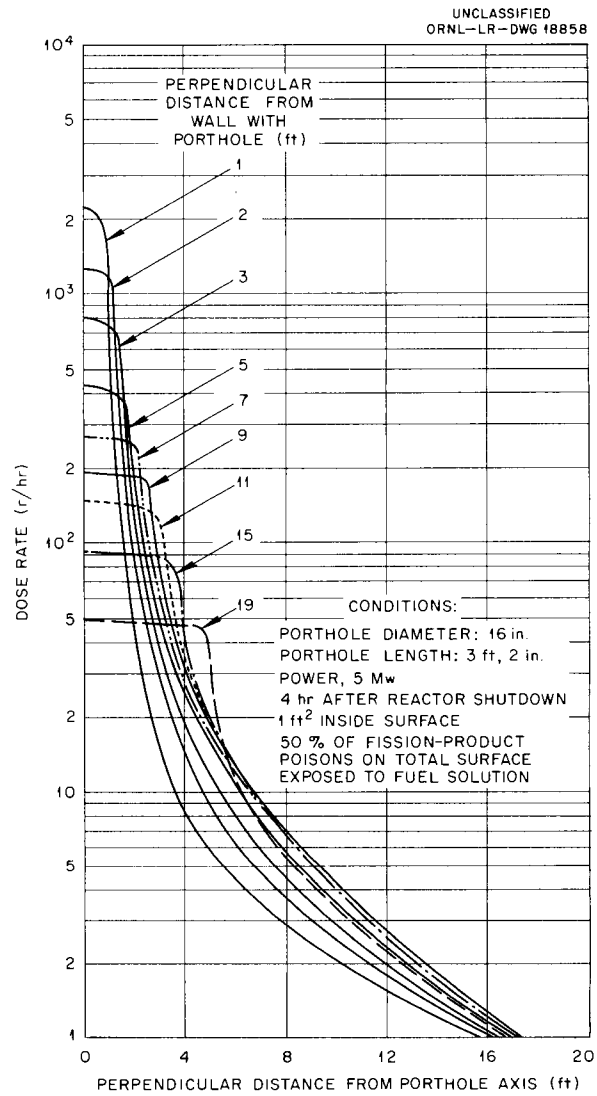

Fig. 4.1. Biological Dose Rate at Outer Edge of HRT Shield Due to Gamma Leakage Through Maintenance Porthole.

outer edge of the porthole will be the sum of the individual contributions of the point sources.

To use these charts for other than the stipulated conditions, the total dose can be calculated by the equation

$$D_2 = D_1 (2f) \left(\frac{P}{5}\right) \left(\frac{4}{t}\right)^{0.2} ,$$

where

D_1 = dose calculated from Fig. 4.1,

D_2 = dose for new conditions,

f = fraction of total fission products adhering to surface exposed to fuel solution,

P = operating power, Mw,

t = time after shutdown, hr.

In calculating doses at points away from the shield opening, the value of the total dose as obtained from Fig. 4.1 should be decreased by the appropriate geometrical factor.

5. HRT CONTROLS AND INSTRUMENTATION

D. S. Toomb

A. M. Billings
J. R. Brown
J. D. Grimes[1]
J. C. Gundlach
R. L. Moore
L. R. Quarles[2]
W. P. Walker[2]
K. W. West
H. D. Wills

5.1 COMPONENT AND SYSTEM TESTING

5.1.1 Oxygen-Injection Systems[3]

The HRT oxygen metering valve regulates the flow of oxygen gas to the reactor high-pressure fuel system. During the HRT shakedown operation, control was unsatisfactory because of leakage past the seat. Examination revealed that a black film of nickel oxide had built up on the plug and caused galling between the extremely close-fitting Stellite 6 plug and the integral type 347 stainless steel body. This mechanical valve was replaced with a differential-expansion-type control valve[4] (Fig. 5.1), which has performed satisfactorily for four weeks but is inherently more susceptible to plugging by liquids and foreign material. Porous metallic filters will be used to protect these valves.

5.1.2 Pressurizer-Level Transmitter

The level of liquid in the HRT pressurizer is regulated by pneumatic control of the letdown valve, which throttles a mixture of gas and liquid from the high-pressure circulating system into the low-pressure storage tanks and gas recombiners. The continuously operating feed pump provides a constant flow of makeup liquid. To provide information on the performance of this level control system, the frequency response was analyzed[5]

[1] On loan from TVA.

[2] Consultant from University of Virginia.

[3] D. S. Toomb *et al.*, *HRP Quar. Prog. Rep. Oct. 31, 1956*, ORNL-2222, p 23.

[4] W. M. Breazeale *et al.*, *HRP Quar. Prog. Rep. July 1, 1952*, ORNL-1318, p 19.

[5] R. Gelman and C. S. Robertson, Jr., *Frequency Response Analysis of HRT Mockup Pressurizer-Level Controller Loop*, KT-240 (EPS-X-272) (Oct. 19, 1956).

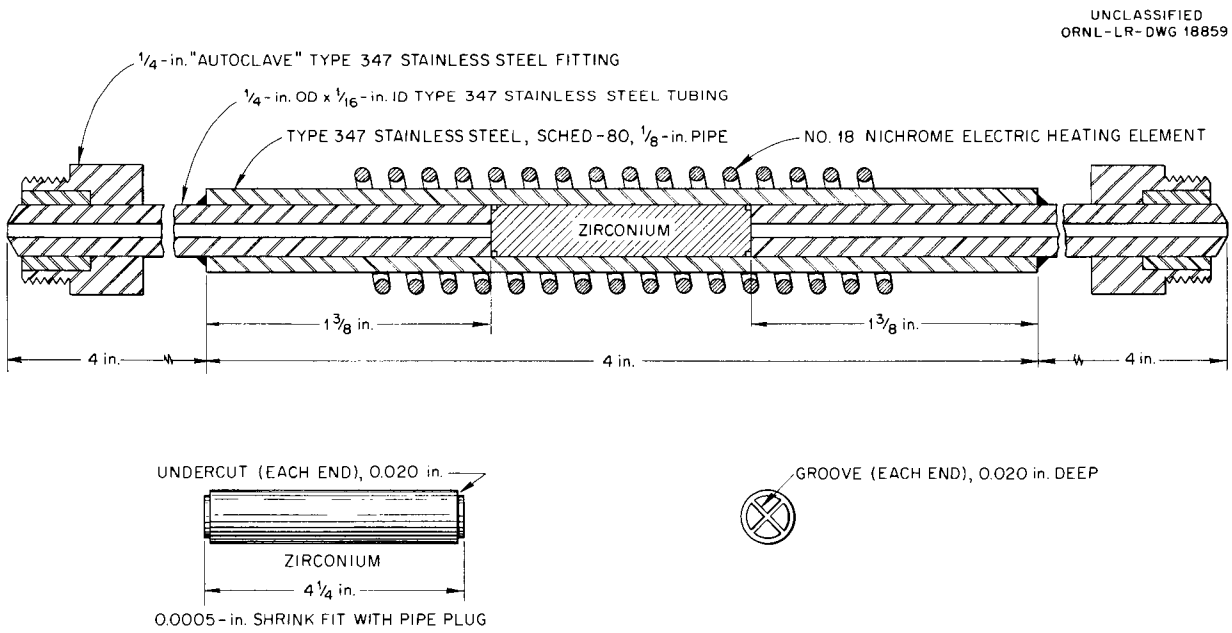

Fig. 5.1. Differential-Expansion-Type Oxygen-metering Valve.

and a systematic study was made of pressure and temperature effects on the operating range and zero point of the level transmitter.[6] The shift of indication with pressure was linear and amounted to 1% of the full-scale reading (5 in. of water) per 500-psi change in pressure. Temperature effects on the level indication are greater and are due to density changes in the vapor and liquid, differential expansions, changes in the modulus of elasticity of the spring material, and electrical resistance changes in the displacer-motion-sensing coil. These effects are most serious when temporary local temperature differences occur in the transmitter during periods of heating or cooling of the reactor system.

5.1.3 Letdown Valves

The HRT-model letdown valve in service on the HRT mockup showed no visible damage upon inspection after 4500 hr of service. No leakage could be measured in two 15-min leakage checks at 1500 psi after 5000 hr of service. The valve was opened and then reclosed between the tests.

During preliminary tests of the HRT, some corrosive attack by rinse solutions and 50 to 60°C water on the Stellite 6 plugs in three letdown valves was noted. Figure 5.2 indicates the type of wear which occurred on the metering and sealing portions of the valve plugs. A thin black film, not visible in the photograph, was analyzed as Stellite 6 and nickel oxide. Bellows-stem assemblies are being fabricated with type 17-4 PH stainless steel and Hadsfield metal (Frogalloy) plugs for evaluation as to suitability for the water operations.

5.1.4 Heat-Balance Flowmeters

An instrument has been installed to continuously compute heat balances on the feed- and purge-pump coolers and heaters. By performing a division operation on the pneumatic temperature-difference signals, an output is obtained which is proportional to the pump flow rates. The signals from the various pumping systems are displayed on a multipoint recorder.

[6] D. A. Camerson and J. C. Bolger, *HRT Pressurizer Level Instrument, Range and Zero Shifts*, KT-242 (EPS-X-285) (Nov. 27, 1956).

Fig. 5.2. Attack on HRT-Letdown-Valve Plug.

5.1.5 Reactor-Cell Ambient Radiation Measurement

A high-level gamma ionization chamber has been developed to measure radiation levels inside the HRT reactor cell (see Fig. 5.3). This information is needed to evaluate the effectiveness of shielding, to assess the rate of radiation damage to reactor components, to measure radiation levels during maintenance operations, and to provide data for future reactor designs. Preliminary tests indicate that the chamber will measure levels to 10^7 r/hr and that it is sensitive down to background radiation levels. The output at 10^7 r/hr is 21 μa with the 120-cc volume saturated at 600 v. The design temperature is 130°F. The chamber is of an inexpensive design, and units are to be discarded upon failure.

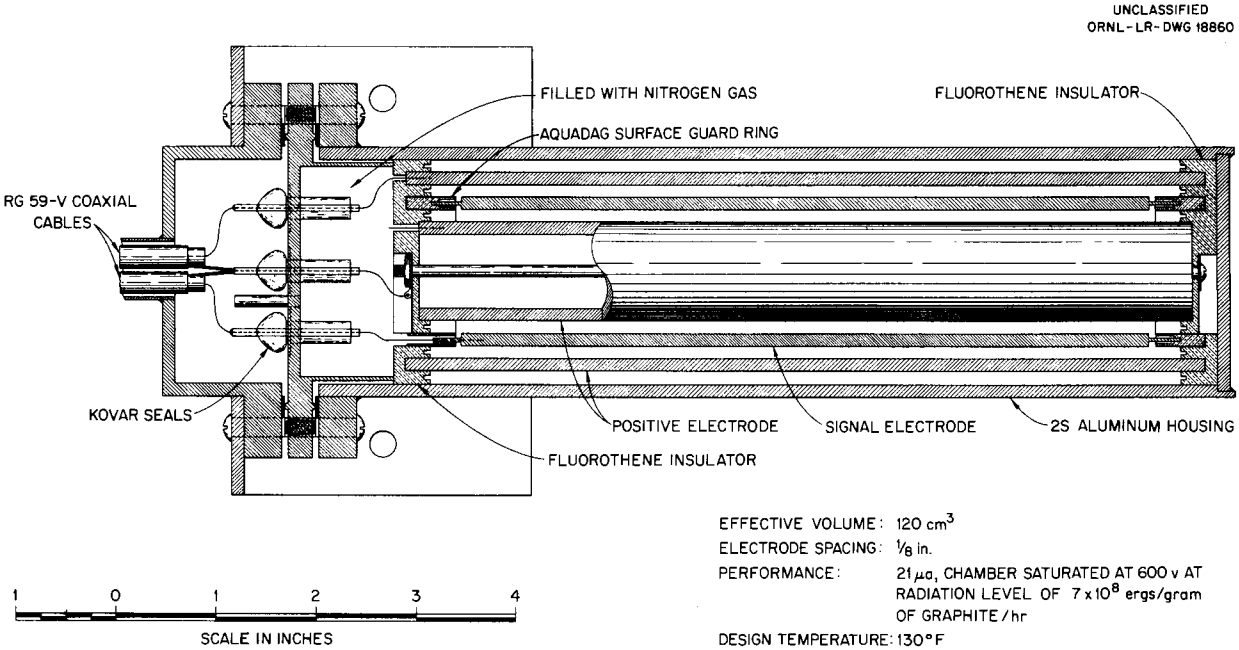

Fig. 5.3. High-Level Gamma Ionization Chamber.

5.2 DESIGN

5.2.1 Controls for the HRT Demineralized-Cooling-Water System

The control system for the revised HRT cooling-water system[7] was completed. Provisions are included for containment of activity resulting from an explosion or from a leak from the reactor into the cooling-water system, for emergency cooling-water supply in case of failure of pumps in either the internal or the external loops, and for automatic relief of excess pressure in the closed demineralized-cooling-water system.

In the case of cooling-water contamination resulting from a leak of reactor solution, the activity will be contained within the shielded area by the return lines being blocked and the cooling-water flow being diverted into the reactor cell. Makeup water will be obtained from a 500-gal demineralized-water storage tank until the supply is exhausted, at which time makeup water will be automatically supplied from the 10,000-gal cooling-tower basin. Contamination in the water from the recombiner-condensers will divert only that water to the reactor cell and will not affect the cooling of other equipment. This permits a slow shutdown of the reactor and avoids dumping and the resultant pressure buildup in the low-pressure system, which would increase the leak rate. Control actions of pneumatic and electric components were selected to give "fail-safe" action for pneumatic and electrical failures and to avoid initiation of emergency cooling from spurious signals, with reactivity-containment considerations being given precedence over system operations and equipment protection.

[7] R. L. Moore, *Control System for HRT Cooling Water*, ORNL CF-57-2-5 (in press).

6. HRT PROCESSING PLANT

W. E. Unger

W. L. Albrect[1]
T. A. Arehart
G. B. Berry
B. F. Bottenfield
N. C. Bradley
N. A. Brown
W. D. Burch
L. H. Chase
S. D. Clinton
W. J. Clossey
J. L. Gory
P. A. Haas
C. C. Haws
R. H. Horton
C. S. Lisser
F. C. McCullough
E. O. Nurmi
A. M. Rom
W. F. Schaffer
H. O. Weeren
R. H. Winget

Testing operations in the high-pressure system of the HRT chemical plant were concluded during the first month of this report period with a series of runs in which simulated corrosion products were injected into the solids feed loop[2] and removed from the circulating stream by the hydroclone in the chemical plant. Modification of the low-pressure system to incorporate a dissolver and decay storage tanks proceeded during December and January and was approximately 80% complete on January 31.

6.1 HIGH-PRESSURE-SYSTEM TESTING OPERATIONS

Following a period of operation in which it was demonstrated that all components of the high-pressure system and solids feed loop could be operated at elevated temperatures and pressures (280°C, 1500 psi) with water, a series of ten 2- to 3-day runs were initiated with 10-g/liter uranyl sulfate solution. In the first two runs, uranium concentrations were followed carefully to ascertain solution stability. No changes in concentration were observed; so the program was continued through eight more runs, the results of which are reported in detail separately.[3–9] Simulated corrosion products were added in varying quantities to the solids feed loop. The disappearance of these solids, through deposition on walls and removal by the hydroclone, was followed by periodic sampling of the flowing stream. Complete draining of the loop and chemical plant between runs permitted material balances to be made (see below).

6.1.1 Solids Disappearance from Feed Loop

Before the rate of removal of solids by the hydroclone was measured, the rate of disappearance from the circulating stream in the solids feed loop was determined in two runs (HRT-CP-3 and -4). Ten grams of solids was injected into the loop at the beginning of each run, and the circulating stream was sampled every 4 hr for 72 hr. Samples were captured in the 500-cc solids addition bombs, through which a flow of 2 to 3 gpm was attained. A plot of the results of run HRT-CP-4 in Fig. 6.1 shows the erratic behavior of solids in the circulating stream. Solids concentrations decreased with a half-period of about 11 hr over time intervals of up to nearly 24 hr, with sudden and unexplained increases in concentration following these periods.

Results of these tests could not be expected to apply directly to the reactor system because of the disparity in dimensions of the systems. The reactor-system wall areas will be much greater than those of the test loop, and the reactor-to-chemical-plant volume ratio will be much higher.

6.1.2 Hydroclone Performance with Solids of Low Concentrations

In runs HRT-CP-5, -6, -7, and -7A, approximately 10 g of solids was added during each 48-hr run, with the hydroclone and other components of the high-pressure system in operation. Figure 6.2 shows typical results, from run HRT-CP-6. In this run about 2 g of solids was added every 8 hr, and two samples were obtained between each addition.

---

[1] On loan from TVA.

[2] W. E. Unger *et al.*, *HRP Quar. Prog. Rep. July 31, 1956*, ORNL-2148, p 24.

[3] R. H. Winget, *Run Summary of Run HRT-CP-3 and 4*, ORNL CF-56-11-136 (Nov. 28, 1956).

[4] R. H. Winget, *Run Summary of HRT-CP-5*, ORNL CF-56-11-137 (Nov. 29, 1956).

[5] R. H. Winget, *Summary of Run HRT-CP-6*, ORNL CF-56-12-49 (Dec. 3, 1956).

[6] R. H. Winget, *Run Summary of HRT-CP-7*, ORNL CF-56-12-48 (Dec. 12, 1956).

[7] R. H. Winget, *Run Summary of HRT-CP-7A and 8*, ORNL CF-56-12-81 (Dec. 17, 1956).

[8] R. H. Winget, *Run Summary of HRT-CP 9*, ORNL CF-56-12-109 (Dec. 19, 1956).

[9] R. H. Winget, *Run Summary of HRT-CP 10*, ORNL CF-56-12-110 (Dec. 19, 1956).

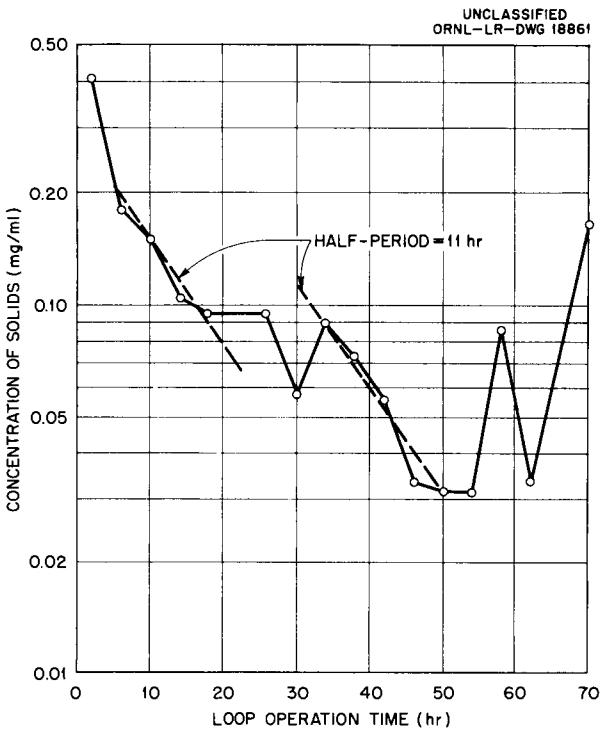

Fig. 6.1. Run HRT-CP-4, Solids Concentration vs Operating Time of Feed Loop (Hydroclone Not in Loop).

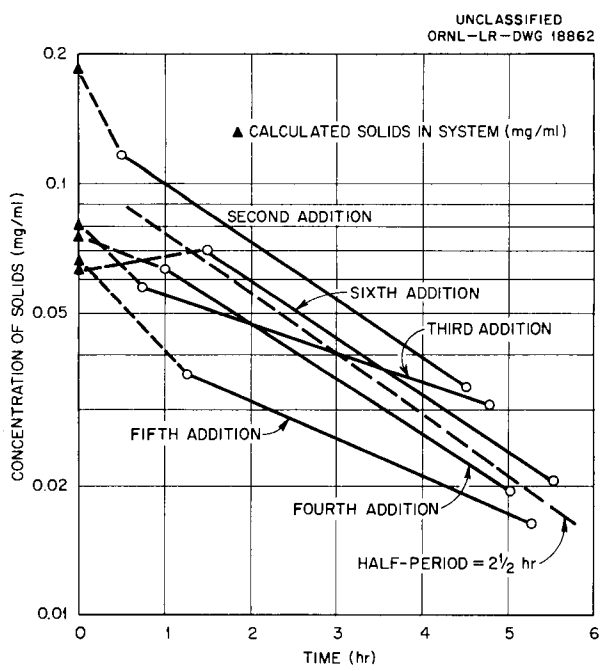

Fig. 6.2. HRT-CP-6 Solids Concentration vs Time of Hydroclone Operation.

Solids removal by the hydroclone was rather uniform, with half-periods for concentration decreases of 2½ hr. From loop volumes and flow rate it can be shown that this corresponds to hydroclone efficiencies of only 4%. However, the particles injected were extremely fine, 50 wt % being less than 0.7 μ. In other runs efficiencies were as high as 13%, averaging about 10% in more concentrated slurries. These efficiencies would be expected to vary with the size distribution of the particular batch of solids. Hydroclone efficiencies have been determined and reported previously for a large range of particle sizes by the Unit Operations Section.[10]

6.1.3 Draining of the Underflow Receiver

The objective of the last three runs (HRT-CP-8, -9, and -10) was to determine whether gross quantities of solids could be removed by the hydroclone and then removed from the underflow receiver without plugging the line which permits drainage to the low-pressure system. This ¼-in. sched-80 line is closed during normal operation by a freeze plug just beneath the underflow pot. In these runs, 225, 266, and 1468 g of solids were added, respectively, and over-all material balances of 68, 75, and 83% were obtained. The material balances were typical of other runs in this series and in similar experiments on other loops. In none of the drains was there indication of plugging. Usually, only about half the total solids recovered came from the initial drain of the underflow receiver; the remainder was removed by subsequent rinses. Drainage was accomplished at atmospheric pressure.

At the end of run 10, the solids concentration in the underflow receiver was more than 1700 times as great as that in the circulating stream. Over 1200 g was recovered, three times that for which the system was designed.

6.1.4 Hydroclone Performance

The performance of the hydroclone was completely satisfactory, with no indication of plugging during operation. A view of the sectioned clone in Fig. 6.3 shows the interior surface to be slightly roughened but otherwise free from excessive wear.

[10] P. A. Haas, *Chemical Technology Division Unit Operation Section Monthly Progress Report May 1956*, ORNL CF-56-5-197, p 26 (Classified).

UNCLASSIFIED
PHOTO 19643

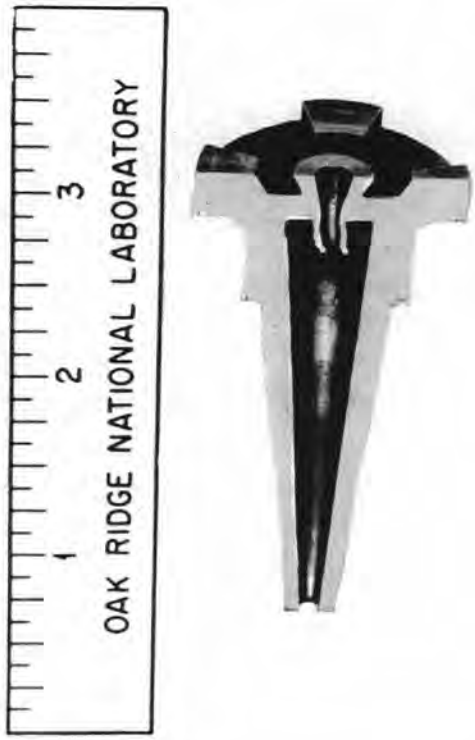

Fig. 6.3. Interior of Sectioned Hydroclone.

Attempts to remove the clone from the specially machined flange by normal procedures proved futile when the retainer plug which seats the hydroclone galled severely while being removed. To remove the hydroclone it was necessary to cut the flange from the underflow receiver and drill out the retainer-plug threads.

It had been assumed that galling had taken place on the threads of the plug. However, the retainer-plug surfaces below the threads (where the clearance between plug and flange was 11 mils) were galled severely and may have been responsible for the plug seizure.

The retainer plug has been redesigned (see Fig. 6.4) to incorporate a bayonet-type closure, which was suggested by a solution to a similar problem on the reactor pressurizer rupture-disk assembly. After insertion of the hydroclone, the hydroclone retainer-plug assembly is dropped into position and the spider engaged by a 60-deg turn. The pressure screw is then turned by means of its hexagonal head to force the hydroclone into position against its gold wire gaskets. The cap plug prevents the inflow of shielding water until the closure flange is in place. The spider has acme threads and is fabricated of precipitation-hardenable stainless steel to minimize galling.

The $1\frac{1}{2}$-in. 2500-psi flange which sealed the hydroclone contained dozens of very small pits beneath the gasket sealing surfaces. Subsequent examination by dye-penetrant methods showed no indication of cracks emanating from the pits. The flange surfaces that had been exposed to solution were covered with the typical blank adherent film. There was no sign of localized corrosion.

6.1.5 Equipment Performance During Testing Operations

During the high-pressure-system tests all equipment was operated for over 1000 hr, with the shakedown loop in operation for over 1250 hr. From this period of operation some indication of equipment performance for long-term operation could be obtained.

(a) 400A Pump. – Although the 400A pump on the solids feed loop is not a component of the chemical plant, its performance is of general interest. After 300 hr of operation the thrust bearing of this pump failed and was replaced. After about 550 additional hours, leakage across the thermal-barrier gasket became excessive, and the hollow stainless steel O-ring gasket was replaced with a Teflon gasket of solid rectangular cross section, which held with no leakage for the final 400 hr of operation. (Teflon would not, of course, be suitable for operation in radioactive service.) Leakage at the main flange terminated run HRT-CP-7 and made it necessary to install a new gasket at the flange.

(b) 1-gpm Chemical Plant Pump. – Following installation of the gold-plated thermal-barrier gasket, reported last quarter,[11] the Westinghouse 1-gpm canned-motor pump (P-1) operated satisfactorily until run HRT-CP-9, when recurring difficulties with overheating in the motor end made it necessary to replace the pump with the spare (titanium) pump. Examination of the stainless steel pump

[11] W. E. Unger *et al.*, *HRP Quar. Prog. Rep. Oct. 31, 1956*, ORNL-2222, p 31.

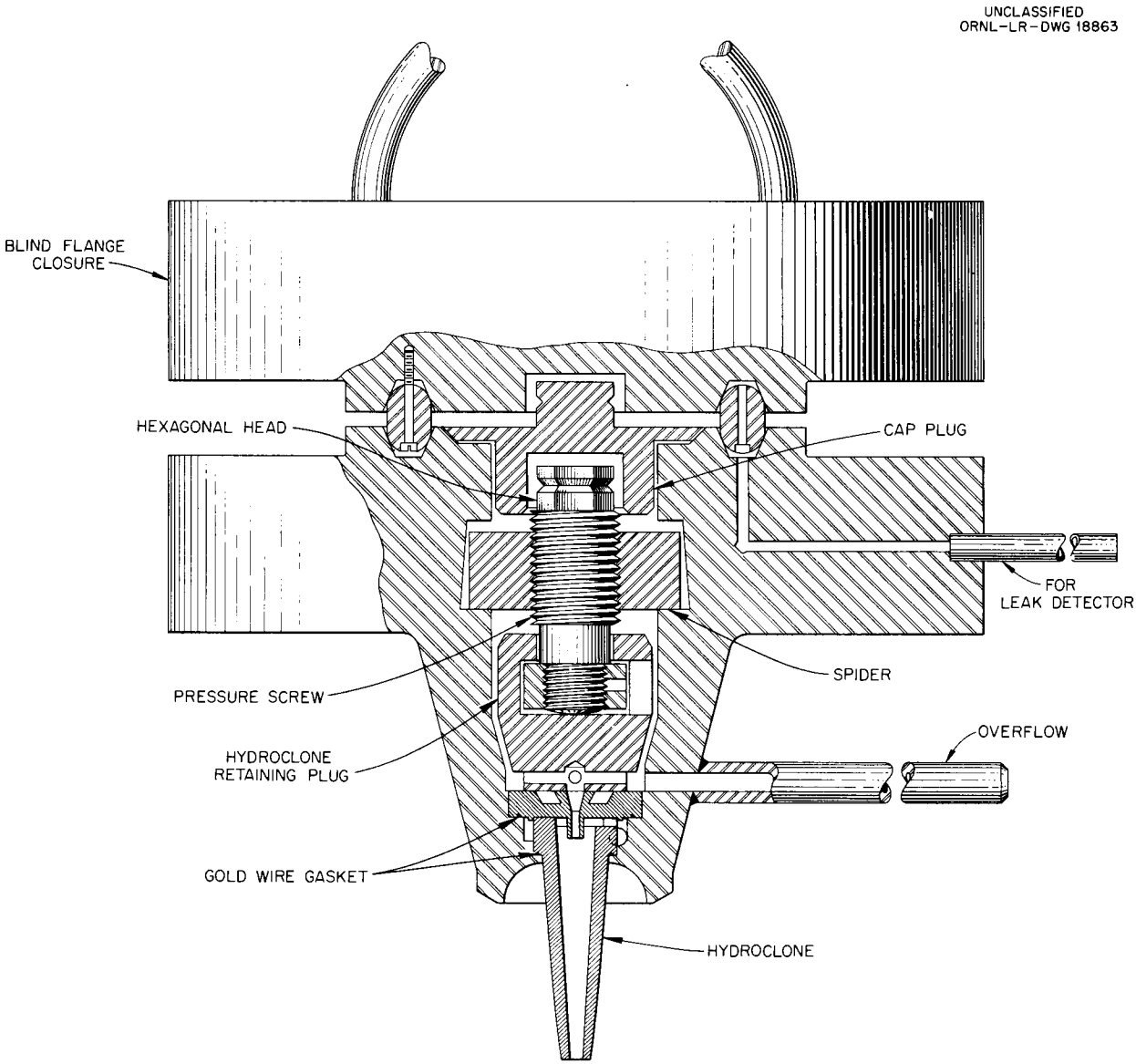

Fig. 6.4. Hydroclone Retainer-Plug Modification.

showed the overheating to be due to leakage across the thermal-barrier gasket. Subsequently, this gasket was reduced in width to decrease gasket loading areas and bolt load required for sealing. The thrust bearings (edge of the radial bearings) of this pump, which had operated for 950 hr, were worn severely, allowing the impeller to rub on the thermal barrier.

The main flange of the replacement pump leaked after 65 hr of operation and terminated the final run. Neither this difficulty nor the thermal-barrier leakage would have occurred had the flange and thermal barrier been seal-welded as is planned for hot operation.

(c) High-Pressure Valves. – None of the seven high-pressure valves required service during the testing operations, although three were noted to be leaking across the seat, with one leaking at least 100 cc/min at a 2000-psi differential. However, since the valves were backed up with freeze plugs, this leakage did not impair operation.

(d) Flange Leakage. – Only two flange leaks of any consequence were noted on the 17 high-pressure flange pairs. On the cool-down cycle following one

shutdown of the system, the inlet flange to heater H-3 leaked severely. The leak was stopped by tightening the flange bolts. The other leak occurred on the pump-vent valve flange during run 9, when frequent pump venting subjected this flange to many, though not severe, thermal cycles. During the course of the runs, nearly all the original oval-ring gaskets were replaced with octagonal-ring gaskets. Both leaks occurred on flanges sealed with oval-ring gaskets. Examination of ring and gasket surfaces following final shutdown disclosed a few small pits, but in general the flanges and gaskets were in excellent condition.

(e) Freeze Plugs. – Except for the previously reported difficulty[11] with freezing plugs after the system was heated, performance of the freeze plugs, both when used to back up normal valves and as valves within the high-pressure system, was satisfactory. One minor piping revision at freeze plug 12 on the side outlet line from the underflow receiver halted the tendency of this plug to thaw. It was believed that this difficulty was due to a convection loop set up in adjacent piping.

6.2 DISSOLVER-SYSTEM INSTALLATION[12]

Installation of the dissolver and related components in the chemical plant low-pressure system is nearing completion, and testing of this equipment will be started on about March 1.

Components added to the system include the 5-gal tantalum-lined dissolver vessel (shown with the flange removed in Fig. 6.5), two 100-gal decay storage tanks, nine new valves, ten additional freeze plugs, a sampling facility, two transfer tanks, and nine double-pipe heat exchangers. The decay tanks, the transfer tanks, all the valves, and seven heat exchangers are fabricated of Carpenter-20 stainless steel to provide good corrosion resistance to the sulfuric acid dissolver solution.

Figure 6.6 shows a photograph (taken on January 21) of the south half of cell C, in which the new equipment is located. The decay tanks are just visible in the lowest portion of the cell. The dissolver will be installed in the "open" space to the right of the three valves visible in the lower center portion of the picture.

A new valve rack (Fig. 6.7) has been installed on the south wall in the service cell A to handle new steam, water, and refrigerant valves and flowmeters. Solenoid valves in lines to the new freeze plugs are visible on the manifold at the bottom of the rack. A new instrument rack, which will contain transmitters for level and specific-gravity measurements on the decay storage tanks, will be located just to the left of the valve rack.

These modifications necessitated changes to the main graphic control panel. The two panels depicting the original low-pressure system have been replaced with three new panels. Installation of new instruments is under way.

6.3 FLANGE TESTS – BELLEVILLE SPRINGS

Belleville (dished-washer type) springs are being tested to determine the effectiveness of their deflection in accommodating the differential thermal expansion between stainless steel flanges and the high-tensile-steel closure studs. Despite the deflection of the washers, the increase in bolt load (as indicated by the bolt extension over and above the known thermal expansion of the bolt) is still excessive when the flange-assembly temperature is increased. Washers have been stacked in series to increase the deflection-vs-load characteristic but without materially affecting the hot bolt load. The bolt thermal expansion and the effect of temperature on the spring characteristics of the washers are being checked in an effort to explain the unsatisfactory performance of the washers.

Figure 6.8 is the measured deflection-vs-load characteristic of the Belleville springs. Table 6.1 lists the initial and hot bolt loadings with Belleville washers being used in various combinations of parallel and series stacking.

[12] *Ibid.*, p 28.

UNCLASSIFIED
PHOTO 19640

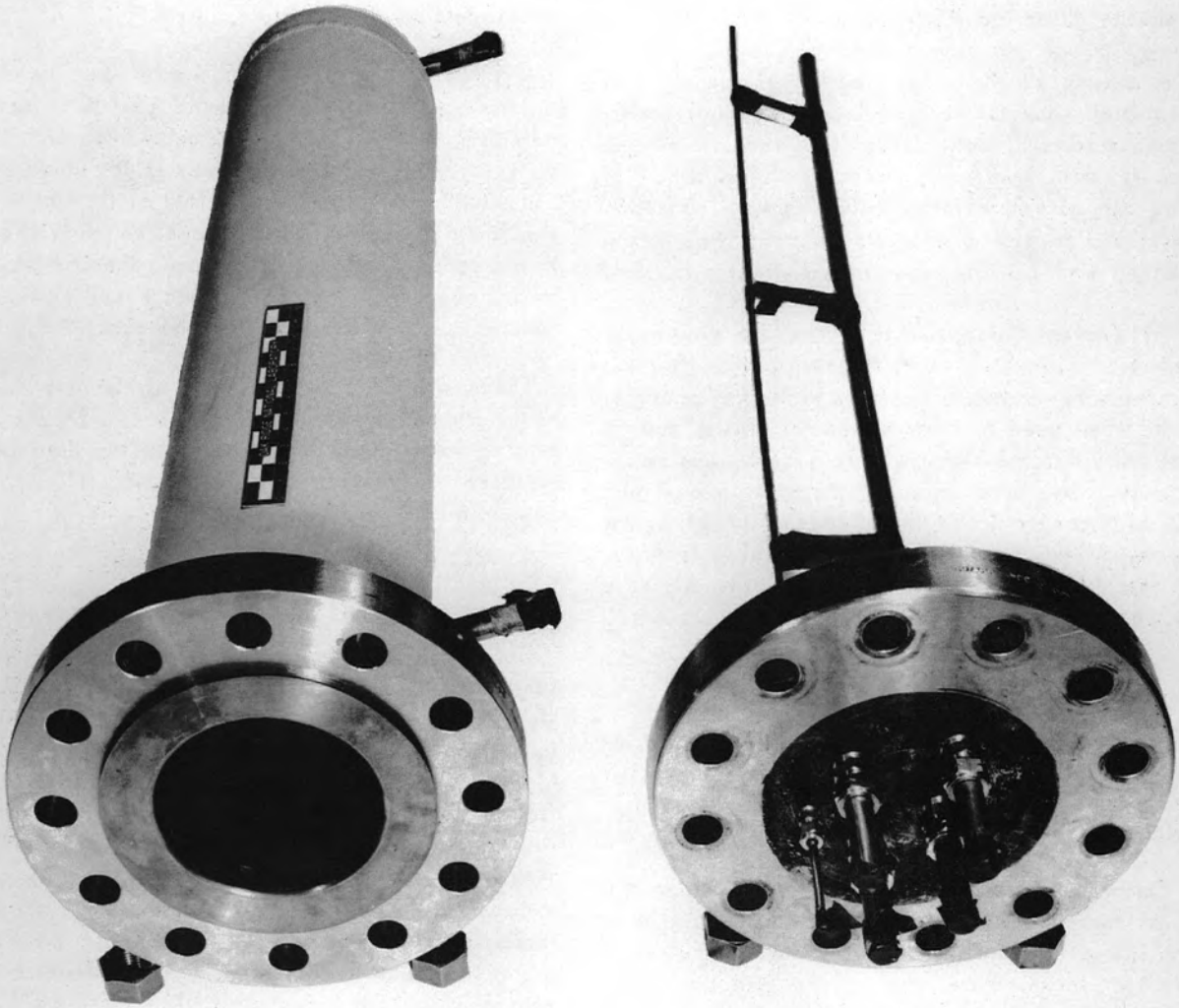

Fig. 6.5. Tantalum-Lined Dissolver.

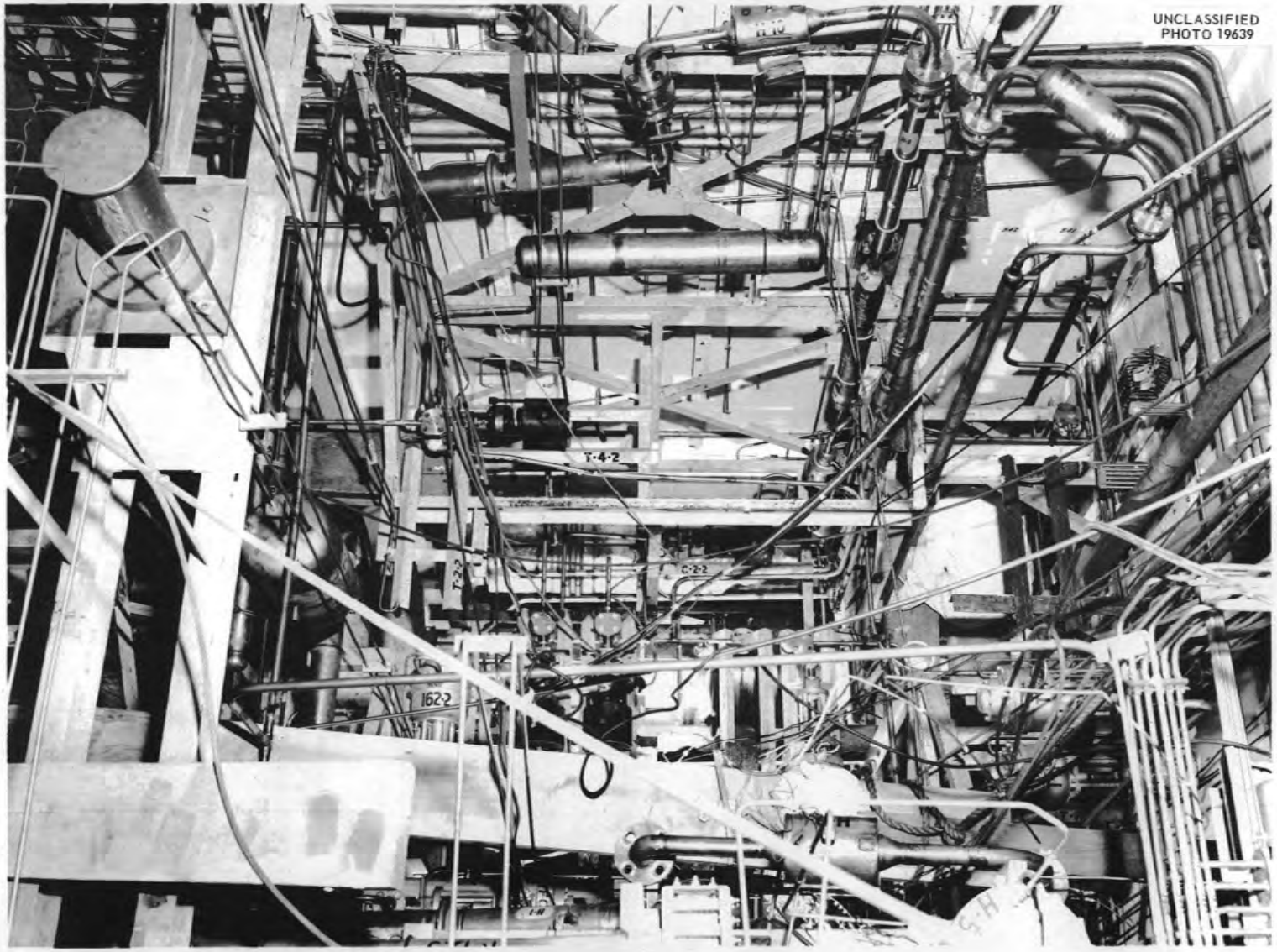

Fig. 6.6. HRT-CP Cell C.

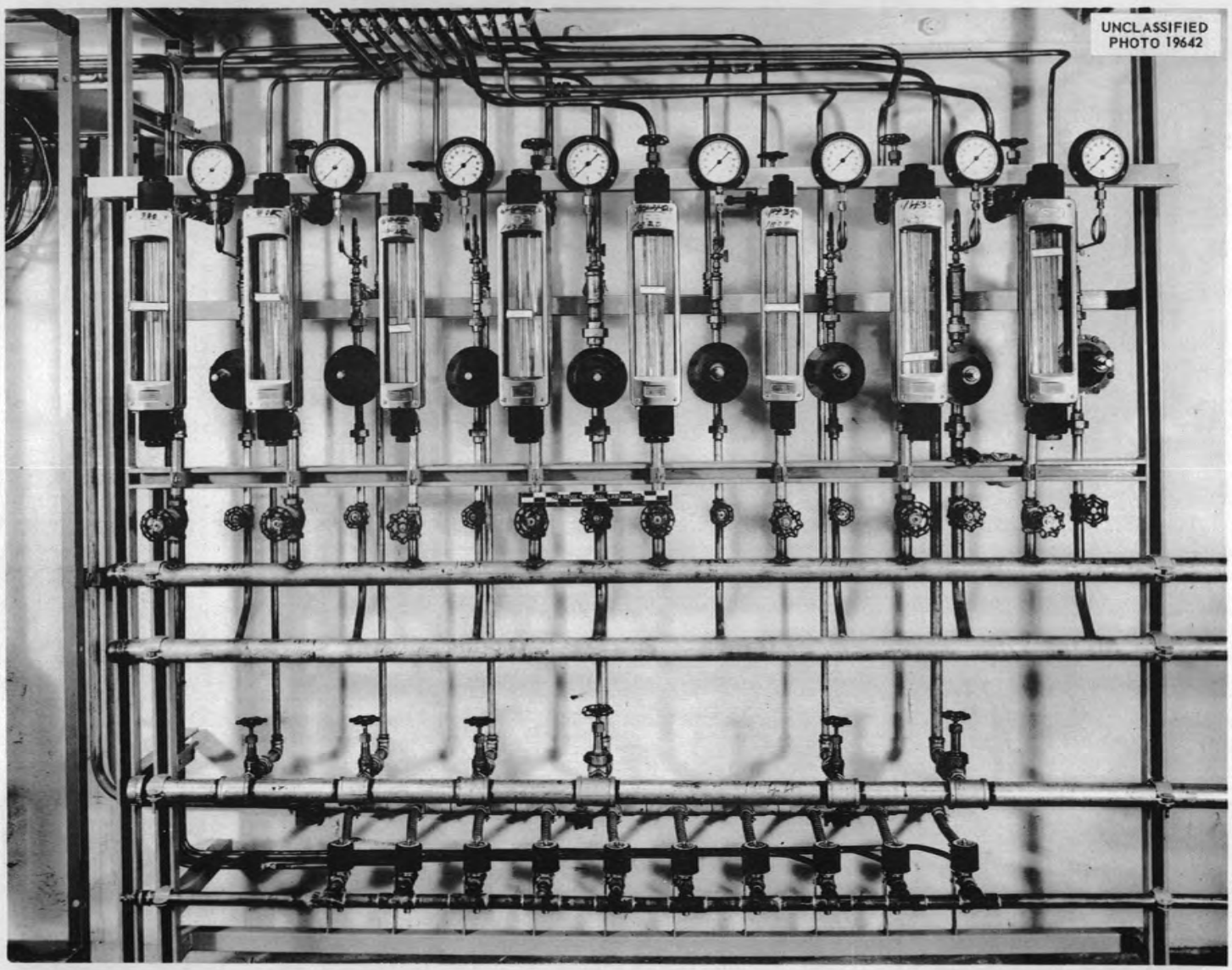

Fig. 6.7. HRT-CP Valve Rack.

Table 6.1. Flange Bolt Loads with Belleville Springs

Bolt No.	Flange Assembly No.	Initial Bolt Loading (lb)	Hot Bolt Loading (lb)	Arrangement
*1	1	7800	17,500	Assemblies made up of two springs in parallel
*2	1	7300	16,200	with two assemblies in series
S7	3	7300	20,300	Assemblies made up of three springs in parallel
S8	3	7200	16,500	with one assembly at each end of bolt
X1	4	6800	14,100	Assemblies made up of two springs in parallel
X4	4	7300	15,100	with one assembly at each end of bolt

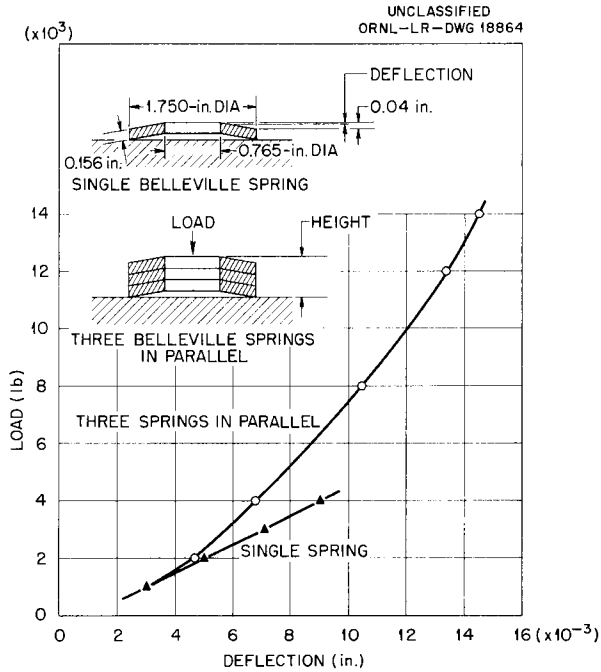

Fig. 6.8. Load-Deflection Characteristics for Two Arrangements of Belleville Springs (Room Temperature, No Lubricant).

Part II

REACTOR DESIGN AND ANALYSIS

J. A. Lane

7. REACTOR ANALYSIS

P. R. Kasten

T. B. Fowler
S. Jaye
M. W. Rosenthal
M. Tobias

7.1 NUCLEAR CHARACTERISTICS OF TWO-REGION SLURRY REACTORS

Additional nuclear characteristics have been computed[1] for some two-region reactors having D_2O-ThO_2-$U^{233}O_2$ in both regions. As in previous studies,[2] two-group calculations were applied to systems having pressure vessels with inside diameters of 10 and 12 ft and core tanks (½-in.-thick Zircaloy-2) of various diameters. Isotope buildup was not considered. The value of η^{23} was taken as 2.25 and that of $\sigma_f^{23}/\sigma_a^{23}$ as 0.90. The reactor temperature was assumed to be 280°C.

In the previous studies there was no allowance for the poisoning effects of fission and corrosion products. A method was therefore developed[1] for estimating the effects of neutron absorptions in poisons and protactinium on breeding ratio and critical concentration. Comparison of this rather simple method with the results of some two-group computations for reactors containing poisons revealed it to be dependable for the slurry systems studied.

The variation of critical concentration of U^{233} with core and blanket thorium concentrations and core diameter is plotted in Fig. 7.1 for reactors having 10-ft-ID pressure vessels. The fraction of total power which would be generated in the blanket is shown in Fig. 7.2 as a function of the same parameters.

In Fig. 7.3 the U^{233}/Th ratio required in the core for criticality is plotted vs core thorium concentration for a 10-ft-dia pressure vessel and various core sizes. These curves are of value in determining the reactivity change that would occur if there were a rapid change in core thorium concentration. If the reactor operating conditions were such that the flat region of the appropriate curve applied, small changes in core thorium concentration would have a negligible effect upon reactor criticality. The location of the minimum in the curves of Fig. 7.3 did not change appreciably with changes in blanket thickness, blanket thorium concentration, or blanket fuel concentration.

7.2 FUEL COSTS FOR TWO-REGION SLURRY REACTORS

Some preliminary results have been obtained for fuel costs in reactor systems containing slurries of D_2O-ThO_2-$U^{233}O_2$ in the core and blanket regions.

In the system analyzed, it was assumed that materials from the core and blanket were fed to a Thorex plant for chemical processing; that thoria was returned to both regions; that fuel was returned to the core as needed to maintain criticality; and that the fissionable material produced in excess of

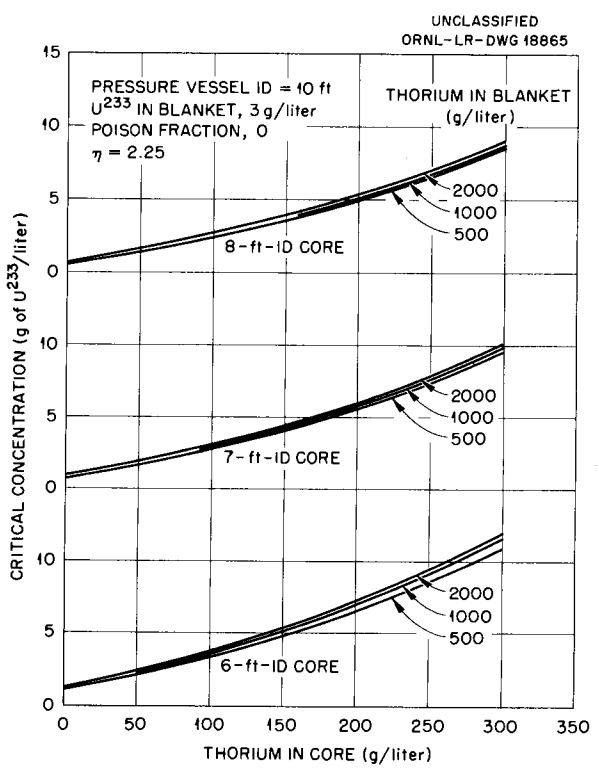

Fig. 7.1. Effect of Core Thorium Concentration on Critical Concentration of U^{233} in Core of Two-Region Slurry Reactors.

[1] M. W. Rosenthal and M. Tobias, *Nuclear Characteristics of Two-Region Slurry Reactors*, ORNL CF-56-12-82 (Dec. 20, 1956).

[2] P. R. Kasten *et al.*, *HRP Quar. Prog. Rep. Oct. 31, 1956*, ORNL-2222, p 41–43.

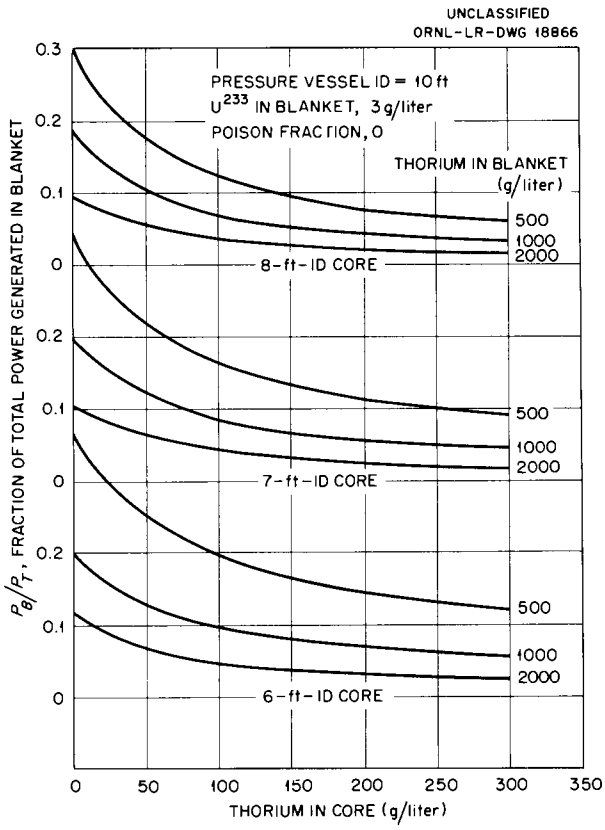

Fig. 7.2. Effect of Core Thorium Concentration on Fraction of Total Power Generated in Blanket of Two-Region Slurry Reactors.

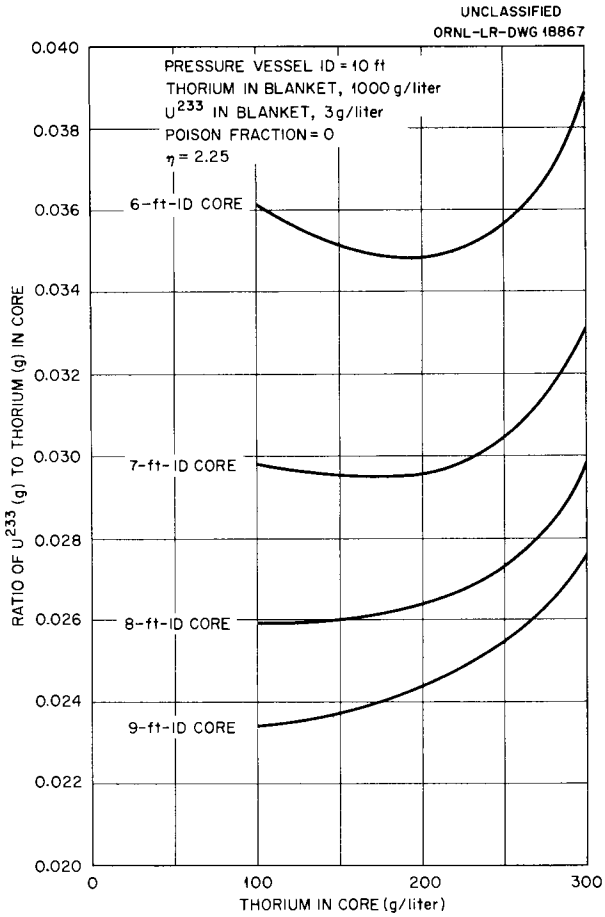

Fig. 7.3. Effect of Core Thorium Concentration and Core Diameter upon Ratio of $(U^{233}/Th)_{core}$ Required for Criticality in Two-Region Slurry Reactors.

that required was sold. The fuel product was computed to be a mixture of U^{233}, U^{235}, and other uranium isotopes, as determined by the isotope equations and the critical equation. The system was assumed to operate under equilibrium conditions.

The major design variables are core diameter, blanket thickness, thorium concentrations in core and blanket, U^{233} concentration in blanket, and poison fraction in the core. Processing-cycle times for both regions are dependent functions of other specified conditions. Costs of the reactor and turbine plants, chemical processing charges, operating and maintenance charges, load factor, and power level were the same as those used in earlier studies[3,4] of homogeneous systems.

Table 7.1 gives the power-cost breakdown for selected values of the parameters. In all cases the power costs associated with reactor and turbine investment and with operation and maintenance were assumed to be constant. The fuel cost was considered to include all costs other than the above. The total cost may be compared with the 6.22-mill/kwhr power cost obtained for a solution-type-core reactor,[4] assuming a 12% inventory charge.

[3] R. B. Briggs, *Aqueous Homogeneous Reactors for Producing Central-Station Power*, ORNL-1642 (May 4, 1954) (Classified).

[4] H. C. Claiborne and M. Tobias, *Some Economic Aspects of Thorium Breeder Reactors*, ORNL-1810 (Oct. 12, 1955).

Table 7.1. Cost Breakdown for Some Two-Region Slurry Reactors

Electrical power, Mw	125	125	125	125	125
Pressure vessel inside diameter, ft	10	10	10	10	10
Core diameter, ft	7	7	7	7	7
Core thorium concentration, g/liter	100	100	300	100	100
Blanket thorium concentration, g/liter	750	750	1500	750	750
Blanket U^{233} concentration, g/liter	3	3	5	3	3
Inventory charge, %	4	12	4	4	4
Fuel value, \$/g of $U^{233,235}$	16	16	16	16	16
η^{23}	2.25	2.25	2.25	2.25	2.25
Core poison fraction	0.07	0.07	0.07	0.12	0.05
Critical concentration, g of U^{233} per liter	3.70	3.70	13.64	4.20	3.54
Net breeding ratio	1.036	1.036	1.116	0.991	1.053
Core-wall power density, kw/liter	29.4	29.4	30.0	30.2	29.0
Core cycle time, days	233	233	812	527	136
Blanket cycle time, days	224	224	372	231	222
Inventory of U^{233} and U^{235}, kg	211	211	522	203	237
Inventory of D_2O, lb	96,200	96,200	94,900	96,100	96,300
Net U^{233} production, g/day	16.3	16.3	54.1	−4.22	24.0
Net U^{235} production, g/day	1.1	1.1	2.4	0	1.7
Estimated cost, mills/kwhr					
Fixed charges	3.73	3.73	3.73	3.73	3.73
Operation and maintenance	0.75	0.75	0.75	0.75	0.75
Uranium inventory	0.16	0.46	0.38	0.15	0.17
D_2O inventory and losses	0.28	0.52	0.27	0.28	0.27
Thorium inventory and feed	0.01	0.03	0.02	0.01	0.01
Fixed chemical processing	0.76	0.76	0.76	0.76	0.76
Core processing	0.20	0.20	0.15	0.16	0.30
Blanket processing	0.09	0.09	0.07	0.08	0.09
Uranium sale (credit)	0.12	0.12	0.38	−0.03	0.17
Net fuel cost	1.38	1.95	1.28	1.47	1.44
Net power cost	5.86	6.43	5.76	5.95	5.92

7.3 EFFECT OF $\eta_{res}^{23}/\eta_{th}^{23}$ UPON BREEDING RATIO IN SINGLE-REGION SLURRY REACTORS

The breeding ratio in single-region D_2O-ThO_2-$U^{233}O_2$ reactors is dependent upon the reactor size and the value of η^{23} in the resonance region relative to that in the thermal region. To determine these relations, nuclear calculations were performed for spherical reactors at 300°C, with reactor size, thorium concentration, and $\eta_{res}^{23}/\eta_{th}^{23}$ treated as parameters. The results are given in Fig. 7.4, in which breeding ratio is plotted vs $\eta_{res}^{23}/\eta_{th}^{23}$, with thorium concentration and reactor diameter as parameters. For finite reactor diameters the curves for different thorium concentrations tend to cross as the value for $\eta_{res}^{23}/\eta_{th}^{23}$ is decreased. This implies that for $\eta_{res}^{23}/\eta_{th}^{23} < 1$, a finite thorium concentration exists for which the breeding ratio is a maximum. Such an effect is shown more clearly in Fig. 7.5, in which the results for the 14-ft-dia reactor are plotted as a function

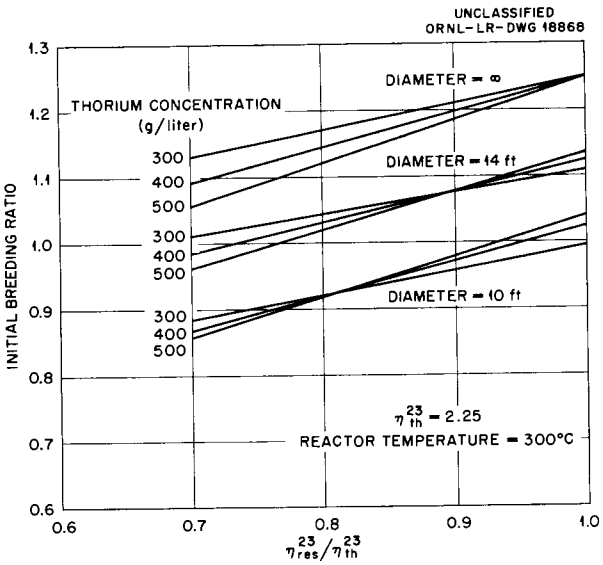

Fig. 7.4. Breeding Ratio as a Function of $\eta_{res}^{23}/\eta_{th}^{23}$, Reactor Diameter, and Thorium Concentration.

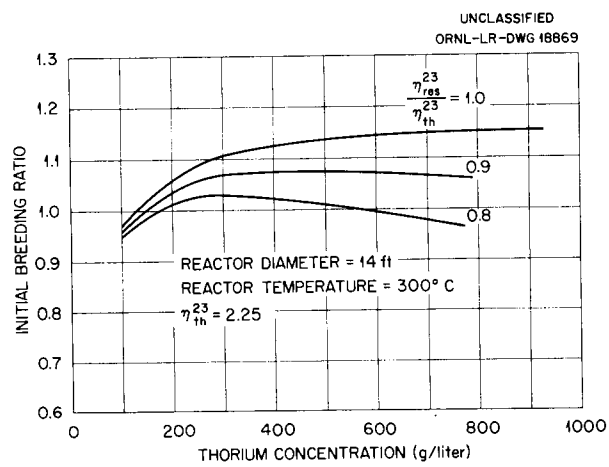

Fig. 7.5. Breeding Ratio as a Function of Thorium Concentration and $\eta_{res}^{23}/\eta_{th}^{23}$ for a 14-ft-dia Reactor.

of thorium concentration. As the thorium concentration was increased, the U^{233} concentration required for criticality increased, leading to an increase in neutron resonance absorption in fuel. For $\eta_{res}^{23}/\eta_{th}^{23} < 1$, a thorium concentration existed above which the detrimental effect of resonance absorption in fuel upon breeding ratio more than outweighed any decrease in neutron leakage.

7.4 POWER COSTS ASSOCIATED WITH USE OF N^{15} IN BREEDER REACTORS

Although thorium nitrate solutions are very soluble, they are unstable when exposed to reactor radiations. In addition, because of the relatively high neutron-absorption cross section of normal nitrogen, it is necessary to use expensive N^{15} in thorium breeder reactors containing nitrate solutions. Thus the power cost[5] associated with the use of N^{15} is a function of the cost of N^{15} and the rate of nitrate decomposition.

The decomposition rate of nitrates under irradiation can be used to define a "decomposition constant," K, such that

$$K \equiv \frac{G_{N_2}}{m} ,$$

where G_{N_2} = molecules of N_2 evolved per 100 ev absorbed by solution and m = molality of Th in $Th(NO_3)_4$ solution. Assuming an over-all thermal efficiency of 25%, the power cost associated with replacement of the decomposed nitrogen is

$$C_r = 185KCN^{02} ,$$

where

C_r = replacement cost, mills/kwhr, based on power generated within nitrate solution,

C = cost of resynthesizing or replacing N^{15}, \$/g,

N^{02} = concentration of thorium, g/liter.

With the values of K obtained by Boyle and Mahlman[6] and with C = \$1.00 per gram (ref. 7) or 3¢ per gram, the results given in Table 7.2 were obtained for a two-region reactor with $Th(NO_3)_4$ in the blanket region. These results indicate that the use of N^{15} would be economically feasible if the nitrate decomposition rate were as low as that associated with a gamma exposure and if the N^{15} could be resynthesized at an effective cost of less than 3¢ per gram. It would be necessary that $DN^{15}O_3$ rather than $HN^{15}O_3$ be resynthesized from the decomposed nitrates. However, a gamma-

[5] P. R. Kasten, *Power Cost Associated with Use of N^{15} in Breeder Reactors*, ORNL CF-56-12-38 (Dec. 7, 1956).

[6] J. W. Boyle and H. A. Mahlman, *HRP Quar. Prog. Rep. Jan. 31, 1955*, ORNL-1853, p 201; *HRP Quar. Prog. Rep. July 31, 1956*, ORNL-2148, p 139.

[7] D. A. Hayford *et al.*, *Feasibility of Large-Scale Nitrogen-15 Production for Nuclear Reactors*, K-1232 (Aug. 17, 1955).

Table 7.2. Effective Cost of N^{15} Replacement if 5% of Total Energy Generated Is Deposited Within Nitrate Solution (Cost Based on Total Electrical Power)

Thorium concentration, g/liter		250	500	1000
Case*				
A	K (fission exposure)	0.03	0.023	0.015
	C = \$1.00 per gram			
	C_r, mills/kwhr	69	106	138
B	K (gamma exposure)	0.003	0.0023	0.0015
	C = \$1.00 per gram			
	C_r, mills/kwhr	6.9	10.6	13.8
C	K (fission exposure)	0.03	0.023	0.015
	C = 3¢ per gram			
	C_r, mills/kwhr	2.1	4.2	5.5
D	K (gamma exposure)			
	C = 3¢ per gram			
	C_r, mills/kwhr	0.21	0.42	0.55

*In cases A and B it is assumed that decomposed N^{15} will be replaced with new N^{15}, and in cases C and D that N^{15} will be resynthesized as $DN^{15}O_3$.

only field implies immediate removal of fuel formed within the blanket, which would require a fast blanket-processing cycle time and would result in high blanket-processing costs.

With a gamma-only field, less than 5% of the total energy generated would be deposited within the blanket solution, and the fraction deposited would be dependent upon the blanket thorium concentration. If breeding is important, however, it would be necessary to have thorium concentrations of 500 g/liter or greater, and so about 3% of the total energy would be deposited in the blanket as a result of gamma-ray absorption; also, at such thorium concentrations, blanket-processing costs would dictate that some fuel remain in the blanket. If 1 g of U^{233} per liter were in the blanket, about 10% of the total power would be generated within the blanket region; about 70% of the amount generated in the blanket would be due to fission power.

[8] P. R. Kasten, *A Preliminary Economic Evaluation of Organic Moderated, Homogeneous Power Reactors*, ORNL CF-56-11-52 (Nov. 2, 1956) (Classified).

7.5 POWER COSTS ASSOCIATED WITH USE OF DEUTERATED HYDROCARBONS IN BREEDER REACTORS

Because of the relatively high pressures associated with aqueous reactors, it would be desirable to replace the water with a material having the same nuclear and coolant properties but a much higher boiling point. Hydrocarbons have some of the desired features but decompose and polymerize when exposed to reactor radiations; also, because of the high cross section of ordinary hydrogen, it would be necessary to use deuterated hydrocarbons if breeder reactors were required. The power cost associated with the use of deuterated hydrocarbons would involve the rate at which these materials are damaged, the effect of this damage on reactor operation, the effective cost of deuterated hydrocarbons, and the fuel-processing cycle time (if it is controlled by radiation damage of the deuterated hydrocarbons).

In this study[8] the radiation damage was defined in terms of the number of high-molecular-weight polymers formed and was based on experimental studies by Atomics International.[9] The studies indicated that

$$G_p = 0.055 ,$$

where G_p is defined as first-order polymers formed per 100 ev absorbed by fluid.

Studies at ANL[10] indicated that heat transfer coefficients associated with organic materials containing decomposition products will be lower than those associated with pure organic materials. It was assumed that this effect would limit the permissible exposure; specifically, it was assumed that the permissible radiation exposure would be ten times greater than the exposure which would transform all the original material to higher polymers.

It was further assumed that the cost of the deuterated hydrocarbons would be essentially the cost of the deuterium alone (as obtained from a D_2O cost of \$28 per pound), which resulted in a cost of about \$14 per pound for makeup material. However, it may be possible to resynthesize

[9] S. Nakazato and R. H. J. Gercke, *Organic In-Pile Loop NAA-18*, NAA-SR-1592 (July 1, 1956).

[10] *Reactor Engineering Division Quarterly Report — Section II, October, November, and December 1955*, ANL-5562 (May 1956) (Classified).

deuterated hydrocarbons from deuterium recovered by burning the polymerized material; the cost of the deuterated hydrocarbons under such conditions was assumed to be $1.4 per pound. In calculating fuel-processing costs, unit costs were considered to be 50¢ per gram of fissionable material processed and $3.50 per kilogram of fertile material processed. Power costs were based on an 80% load factor and a net thermal efficiency of 25% for the D_2O system and 30% for the all-organic reactor.

In all cases studied, the process cycle time was controlled by the necessity of removing the radiation-damaged material. Fuel-processing costs were therefore high, being about 10 mills/kwhr for one-region reactors having an average power density of 10 kw/liter. The power cost associated with replacement of the polymerized material was about 75 mills/kwhr, based upon an effective cost for the deuterated hydrocarbons of $14 per pound. In the case of a slurry perhaps not all the fission energy would contribute to polymer formation. If only 20% of the fission energy were considered to produce radiation damage and if the effective cost of the deuterated hydrocarbons were $1.4 per pound, the above 75-mill/kwhr cost would be decreased to about 2 mills/kwhr.

The high incremental power cost associated with high core power density and radiation-damage effects would prohibit the use of deuterated hydrocarbons within the core region of a two-region reactor, but if the power density within the blanket region were kept low, their use in the blanket might be economically feasible. However, low blanket power density implies a fast blanket cycle time, and so an optimum cycle time would exist, dependent upon costs for blanket processing and the cost of replacing the polymerized deuterated hydrocarbons. If the deuterated hydrocarbons cost $14 per pound, the effective cost of radiation damage would be about 4 mills/kwhr; if they cost $1.4 per pound, the effective cost would be about 1 mill/kwhr.

7.6 MATHEMATICS AND COMPUTATION

An Oracle code was written for calculating the steady-state fuel costs in two-region thorium breeder reactors, taking into consideration the concentration of U^{233}, U^{234}, U^{235}, U^{236}, Th^{232}, Pa^{233}, and fission-product poisons. Included in the input numbers (which may be considered parameters) are unit fuel value, unit inventory charge, unit chemical-processing charges, reactor power level, poison fraction, reactor diameter (core and over-all), thorium concentration (core and blanket), and nuclear values.

Part III

ENGINEERING DEVELOPMENT

J. A. Lane

8. DEVELOPMENT OF FUEL-SYSTEM COMPONENTS

I. Spiewak

J. S. Culver
C. H. Gabbard
B. A. Hannaford
P. H. Harley
P. P. Holz
I. K. Namba
W. L. Ross

8.1 RECOMBINER DEVELOPMENT

8.1.1 High-Pressure Recombiner Loop

A 200-hr run in which titanium and zirconium alloy samples were exposed to recombiner vapors was completed in the high-pressure recombiner loop. The loop was operated at 500 psi and a maximum recombiner temperature of 425°C. During the run the loop was shut down six times because of leakage due to stress-corrosion cracks in type 347 stainless steel piping.

The titanium and zirconium samples showed signs of recrystallization and grain growth similar to observations in a previous test.[1] Large amounts of hydrogen were absorbed in some of the specimens. The observed recrystallization was unexpected at the comparatively low recombiner-loop temperatures. To investigate possible mechanisms through which the temperatures may have been raised, some titanium tubing was checked for catalytic properties at 380°C in a hydrogen-air mixture; it was inactive. It is still possible that the surface film of the loop specimens was an active catalyst.

8.1.2 Battelle and Syracuse Contracts

Battelle Memorial Institute completed an investigation of the reaction limits of the H_2-O_2-H_2O system,[2] which indicated that mixtures containing over 20% $H_2 + O_2$ ignited readily. Varying the H_2/O_2 molar ratio between 0.25 and 7 affected the reaction limits only slightly, although it did affect the violence of the reactions. Additions of nitrogen to the system raised the limits, argon had little effect, and helium lowered the limits.

Syracuse University has found that rupture disks can withstand greater dynamic loading (such as that produced in detonations) than static loading. Dynamic yield stresses were reported for type 304 stainless steel, nickel, phosphor, bronze, and cold-rolled steel.[3]

The incident and reflected detonation pressures in mixtures of stoichiometric H_2-O_2 and steam were computed for initial pressures up to 150 atm and initial temperatures up to 300°C. Supporting experimental work was carried out at up to 60 atm and 200°C. It was found experimentally[4] that the presence of water vapor damped the predicted detonation pressures by as much as a factor of 3.

For example, with initial conditions of 30 atm, 200°C, and 54% water vapor, the calculated detonation pressure was 290 atm; 100 atm was observed. With initial conditions of 30 atm, 25°C, and no water vapor, the calculated detonation pressure was 620 atm; 510 atm was observed.

Work is still in progress at Syracuse on the dampening of shock waves, the explosion limits of H_2-O_2-H_2O systems, and transient loading by detonations.

8.2 SMALL REACTOR COMPONENTS

8.2.1 20-cfm Canned-Motor Blower

The 20-cfm canned-motor blower was installed in the blower test loop and was operated for a total of 13 hr, including approximately 50 starts and stops, with various loop pressures up to 650 psi. At that time undue noise was detected, and the blower was dismantled for inspection. Excessive wear was found on the hydrostatic radial bearings, the lower thrust plate, and the impeller hub labyrinth (see Figs. 8.1 and 8.2). Indications are that the wear resulted from loss of bearing supply pressure, caused either by low water level in the motor or by improper assembly of some O-ring seals in the blower. Additional

[1] M. L. Picklesimer, *Examination of Recombiner Loop Specimens of Zr and Ti Alloys*, ORNL CF-56-10-37 (Oct. 2, 1956).

[2] E. F. Stephan *et al.*, *Ignition Reactions in the Hydrogen-Oxygen-Water System at Elevated Temperatures*, BMI-1138 (Oct. 2, 1956).

[3] M. J. Leibson, *Dynamic Loading of Rupture Discs*, SURI-Ch. E.-273-567F5 (July 31, 1956).

[4] P. L. McGill, *Detonation Pressures of Hydrogen-Oxygen Mixtures Saturated with Water at High Initial Temperatures and Pressures*, SURI-Ch. E.-273-5611F (Dec. 3, 1956).

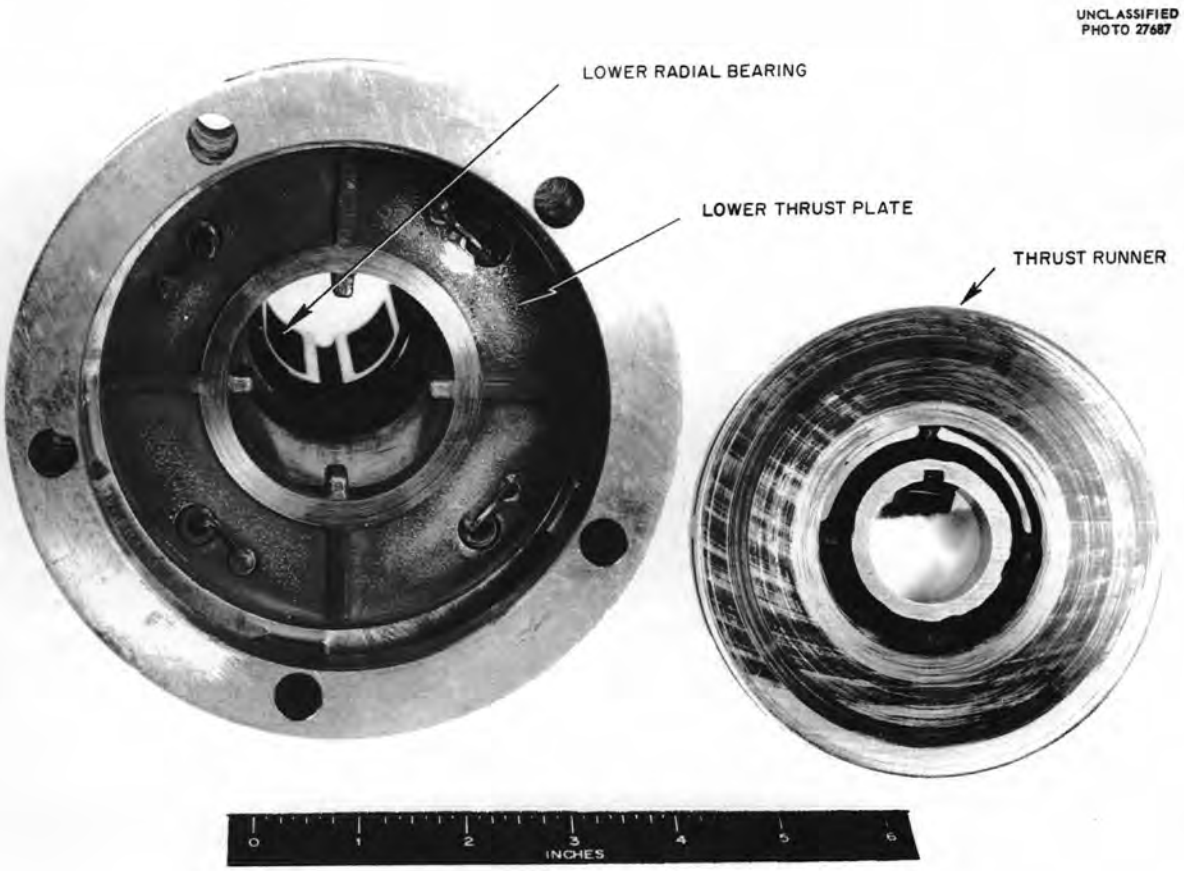

Fig. 8.1. 20-cfm Blower Bearing Parts.

level instrumentation has been installed and the unit reassembled, prior to further testing.

8.2.2 Small Circulating Pumps

Operation of three 5-gpm canned-rotor ORNL pumps with series-connected stator windings was continued. The pump operating on cold water has run for a total of 15,500 hr without incident. One of the pumps completed a 2100-hr run on 10-g/liter UO_2SO_4 solution at 250°C; inspection at the end of the run revealed no appreciable wear. The other pump was operated for a total of 2000 hr during the quarter, 750 hr of which was with 10-g/liter UO_2SO_4 solution at 250°C. After a high-pressure leak in the test loop necessitated termination of the run, the pump was inspected; no appreciable wear was detected. Operation of the three 5-gpm pumps was terminated at the end of the report period.

8.3 4000-gpm LOOP

Two can failures occurred in the Byron Jackson 4000-gpm pump. The rotor can failed 40 hr after startup with the new type 347 stainless steel wear rings.[5] A liquid-penetrant examination of the can after failure showed several pinholes where the can was welded to the end caps. It is believed that failure was caused by the rotor can expanding against the stator as a result of water leaking into the rotor assembly.

The rotor was recanned with 0.025-in. type 347 stainless steel, and the radial-bearing clearance was reduced by shrinking a new journal on the upper bearing and replacing the lower Graphitar bearing.

[5] I. Spiewak *et al.*, *HRP Quar. Prog. Rep. Oct. 31, 1956*, ORNL-2222, p 51.

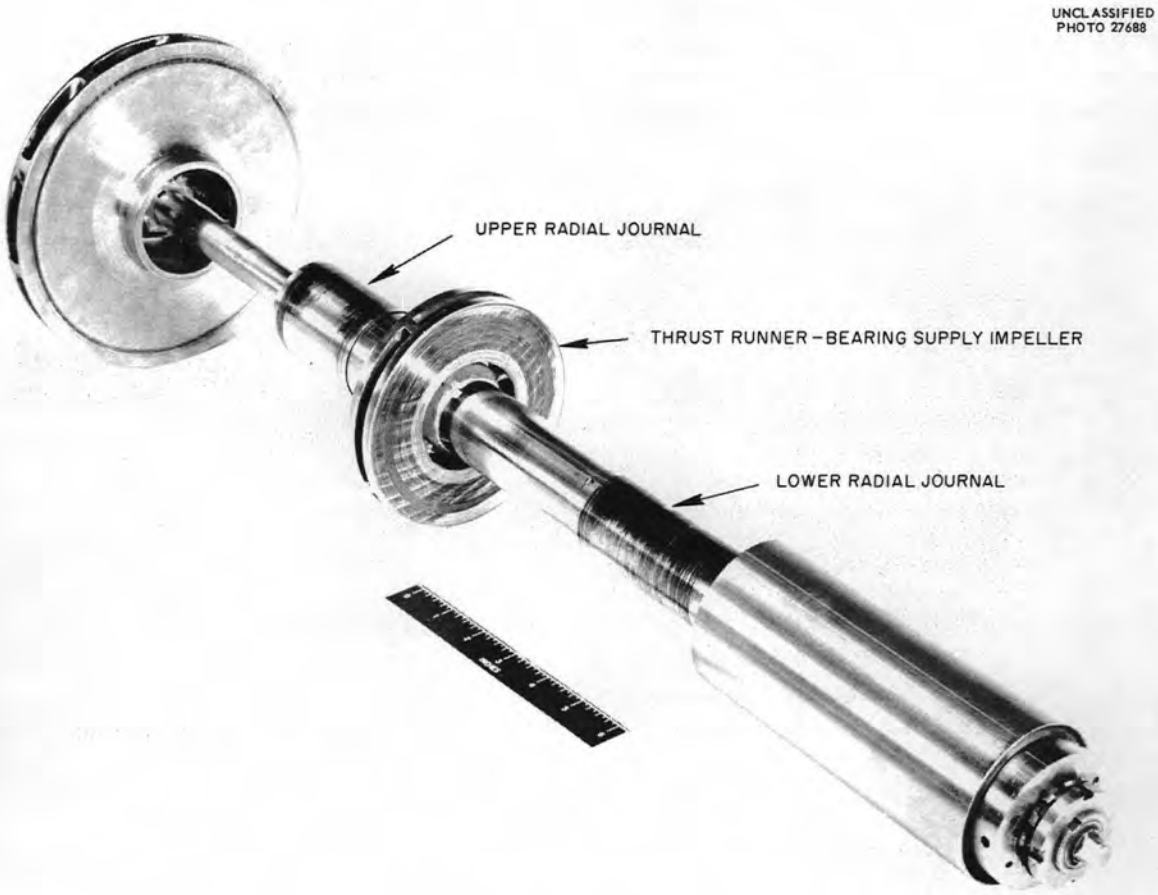

Fig. 8.2. 20-cfm Blower Rotating Assembly.

The pump was reassembled and during startup suffered the second can failure. Inspection revealed that an oil line, used to balance pressure in the stator, was plugged, resulting in a high differential pressure across the stator liner. The liner was ruptured along the seam weld, and one convolution of the stator expansion bellows was ruptured. Methods of repairing the pump are now being investigated.

8.4 TITANIUM PROGRAM

The tubing for the small titanium-lined heat exchanger was received by The Pfaudler Co. and found to be defective. The delivery date of the exchanger will depend on the availability of acceptable tubing, sources of which are being investigated by Pfaudler. The construction of titanium-lined pipe by Crane Co. is also being delayed because of lack of materials. The latest information indicates a delivery date of March 1957.

Titanium A-110-AT pipe, flanges, and fittings have been requisitioned for a 400-gpm pump loop.

8.5 HEAT-EXCHANGER TUBE-JOINT TEST[6]

The first unit tested in this facility contained nickel-plated type 347 stainless steel tubes expanded into a weld-clad tube sheet and seal-welded. It was thermally cycled for 600 hr with 250-psi steam in the tubes for 5 min and off for 3 min. The shell side of the unit was partially filled with water containing 50 ppm of O_2 and 5 ppm of Cl.

[6] *Ibid.*, p 52–53.

Figures 8.3 and 8.4 show sections of two of the five tube-to-tube sheet welds. The metal at the top of the pictures is the tube wall, with nickel plating on its lower surface. The lower mottled area is the weld-cladding. Figure 8.3 shows a crack which has penetrated the nickel plate into the tube wall. The plate did not prevent cracking, as had been hoped. Figure 8.4 shows cracks in the seal-weld root, which may have been the result of stress-corrosion cracking.

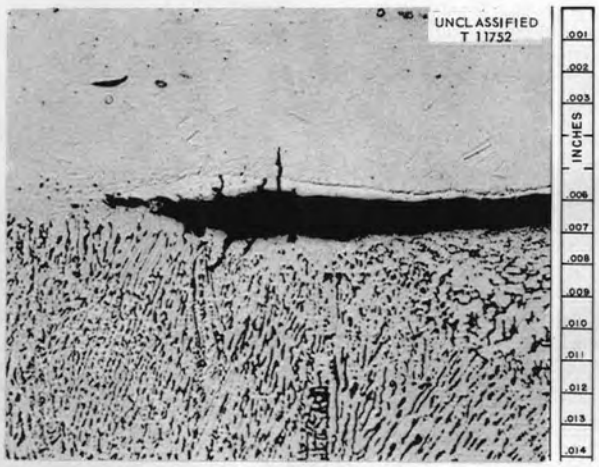

Fig. 8.3. Section of Tube-to-Tube Sheet Weld, Showing a Crack Which Has Penetrated the Nickel Plate. 250X. Reduced 31%.

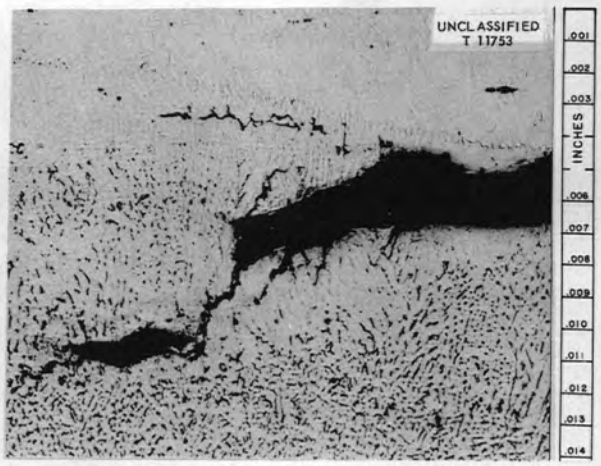

Fig. 8.4. Section of Tube-to-Tube Sheet Weld, Showing Cracks in the Seal-Weld Root. 250X. Reduced 31%.

9. DEVELOPMENT OF REACTOR SLURRY SYSTEMS

R. B. Korsmeyer

D. G. Davis
H. L. Falkenberry[1]
R. B. Gallaher
A. S. Kitzes
C. G. Lawson
I. M. Miller
C. S. Morgan
R. H. Nimmo
L. F. Parsly
M. Richardson
A. N. Smith
D. G. Thomas
C. F. VandenBulck[2]
R. P. Wichner

9.1 HEAT TRANSFER MEASUREMENTS

A heat transfer system (Figs. 9.1 and 9.2) was constructed to check the validity of the Lawson slurry heat transfer equation.[3] Particular features of the system are listed below:

1. The copper heat exchange sections provide for length-to-diameter ratios from 90 to 480 for tubes of ¼- and 1-in. inside diameter.
2. Slurry flow rate will be determined from weigh-tank measurements.
3. Heat transfer coefficients can be estimated (a) from axial temperature-drop measurements, (b) by collecting condensate from the inner steam jacket of the heat exchange system, and (c) by thermocouples embedded in the pipe walls.
4. Heat transfer coefficients can be determined over a velocity range of 0.5 to 35 fps.

The Moyno pump circulated ThO_2 slurry (at 1000 g of thorium per kilogram of H_2O) through the bypass line for over 150 hr with no apparent difficulty during installation of the heat-transfer system. Construction has been completed, and heat transfer tests with water are in progress to provide a basis of comparison with forthcoming slurry tests.

9.2 SLURRY RHEOLOGY

The room-temperature properties of the thorium oxide slurry circulated for 1994 hr in loop run 200A-5B[4] were determined in a capillary-tube viscometer for slurry concentrations from 115 to 875 g of thorium per kilogram of H_2O (Table 9.1). The yield-stress values for this slurry were about 40% higher than any value obtained at the same concentration with similar slurries pumped for a shorter length of time.[5] Values of the coefficient of rigidity were in the same range as values observed for similar slurries pumped for shorter times. End-effect corrections were made in the same manner as previously described[6] by use of the data from tubes having length-to-diameter ratios of 490 and 980. Corrected and uncorrected values of the yield stress and coefficient of rigidity were within ±15%, and there appeared to be no trends (in the corrections) with concentration.

[1] On loan from TVA.

[2] On loan from Union Carbide Nuclear Company.

[3] R. B. Korsmeyer *et al.*, *HRP Quar. Prog. Rep. Oct. 31, 1956*, ORNL-2222, p 59.

[4] R. B. Gallaher, *HRP Quar. Prog. Rep. July 31, 1956*, ORNL-2148, p 58–62.

[5] D. G. Thomas, *Solids Dispersed in Liquids*, ORNL CF-56-10-35 (Oct. 1, 1956).

[6] R. H. Nimmo, *HRP Quar. Prog. Rep. July 31, 1956*, ORNL-2148, p 52.

Table 9.1. Rheological Properties of Thorium Oxide Slurry Produced in Loop Test 200A-5B

Slurry Concentration		Yield Stress (lb/ft^2)	Coefficient of Ridigity (centipoises)
Grams of Th per Kilogram of H_2O	Volume Per Cent of ThO_2		
115	1.33	0.0053	1.5
295	3.34	0.026	2.1
488	5.41	0.075	2.9
625	6.82	0.16	3.5
875	9.29	0.51	4.1

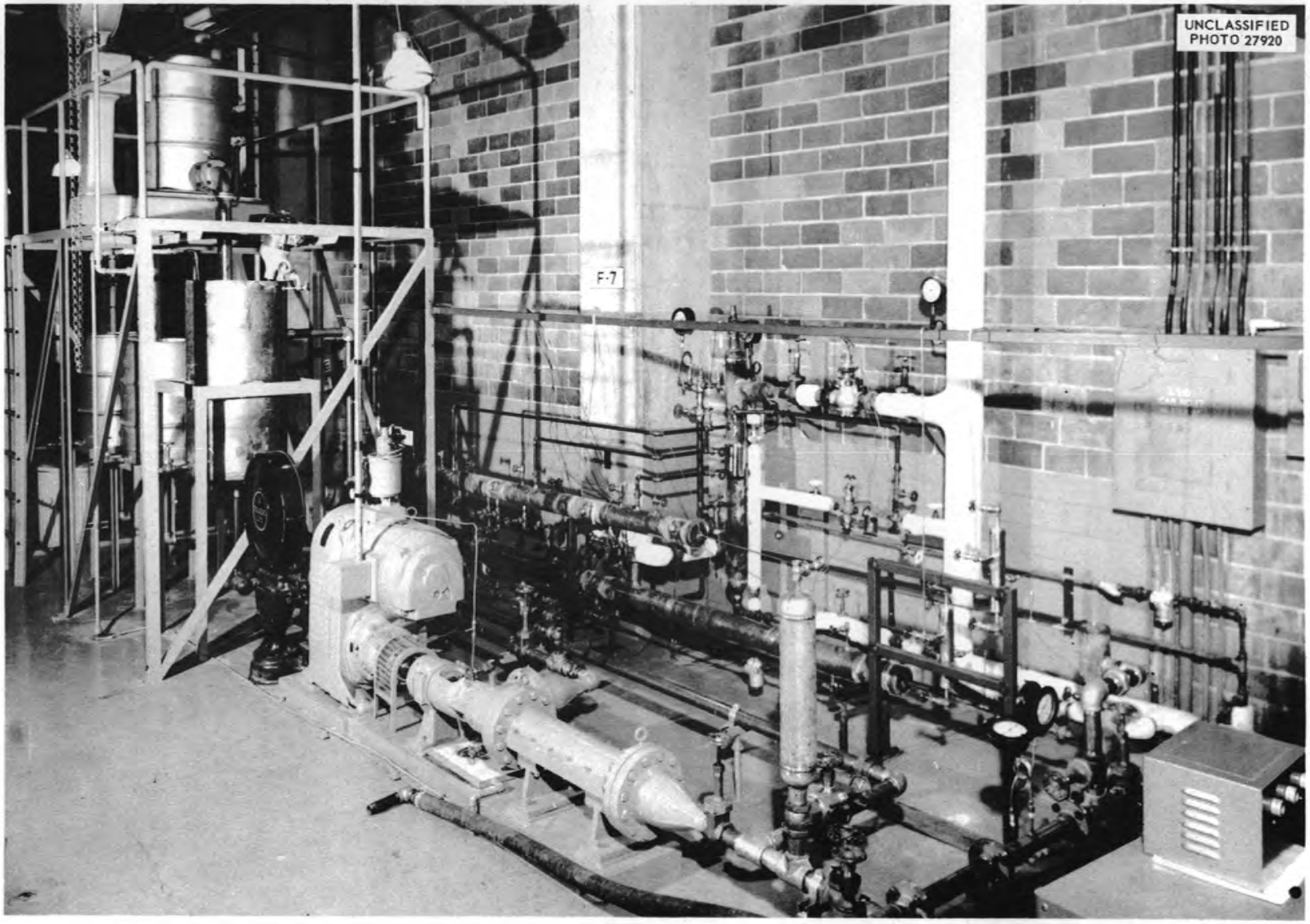

Fig. 9.1. Slurry Heat Transfer System Showing Moyno Pump and Steam-jacketed Heat Transfer Sections.

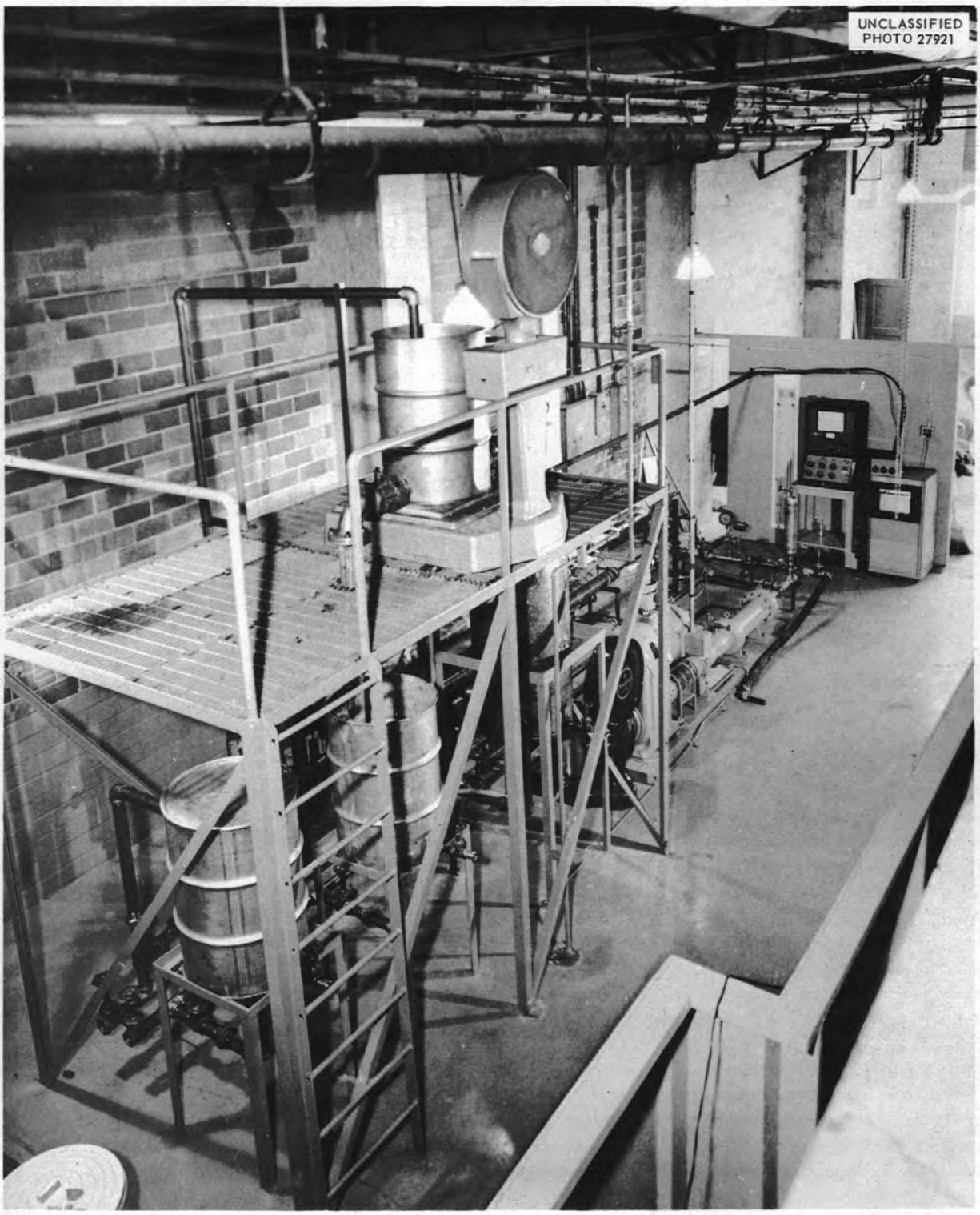

Fig. 9.2. Slurry Heat Transfer System Showing Weigh Tank and Storage Tank Farm.

Studies of the effect of system geometry on the reproducibility of slurry measurements have shown that a pressure tap located in the inlet to the viscometer tube gives reliable and reproducible pressure-drop–flow data, provided that water and air flushing lines are included in the pressure tap. Pressure measurements made with such a tap eliminate the fluid-head corrections necessary when gas-pressure measurements are used to calculate the pressure drop.

9.3 DISINTEGRATION OF ThO_2 CAKES

Hard ThO_2 cakes produced in the 200-A loop[7] were partially disintegrated in laboratory tests by flooding them with dilute electrolytes after they had been air-dried at 110°C. Chunks of cake broke into smaller pieces usually within 10 sec after addition of the electrolyte, and disintegration always stopped in less than 10 min. The sizes of resulting pieces of cake were not dependent on the size of the cake treated but varied between approximately $\frac{1}{32}$ and $\frac{1}{2}$ in. for the longest dimension, with a thickness of $\frac{1}{32}$ to $\frac{1}{4}$ in. Electrolytes used were H_2SO_4, HNO_3, NaOH, KCl, Na_2SiO_3, and Na_4PO_7 in concentrations to 6 *N*.

The effectiveness of different electrolytes and different concentrations was somewhat obscured by variations in the cake from piece to piece. However, the cake from run 200A-3 appeared to disintegrate more readily in 0.1 *N* H_2SO_4. The extent of cake disintegration was a function of the compactness, or extent of bonding, in the cake (which varied substantially even for pieces of cake from the same run) and of the length of drying time. A drying time of 24 to 48 hr was usually sufficient to achieve extensive disintegration upon treatment with electrolyte, but the tendency of the cake to disintegrate slowly increased with increasing drying time. Best results were obtained with a drying temperature in the range 90 to 150°C. Higher temperatures appeared to be deleterious. Evacuation of the cake following air drying increased the extent of disintegration. Large pieces remaining after disintegration were further reduced in size by again drying and submerging in the electrolyte.

[7] D. G. Thomas and R. B. Gallaher, *HRP Quar. Prog. Rep. April 30, 1956*, ORNL-2096, p 67.

9.4 CIRCULATING-SLURRY BEHAVIOR

9.4.1 Circulation of Thorium-Uranium Oxide Slurries in 100-gpm Loop

Run S-94 was completed during the quarter to determine the generalized attack on stainless steel and to determine the handling characteristics of the admixed thorium-uranium oxide slurry at 300°C. In this run a slurry containing 1000 g of thorium per kilogram of H_2O, 2% uranium as $UO_3 \cdot H_2O$ and 2000 ppm sulfate as $Th(SO_4)_2$ (both based on the thorium content), and 500 ppm oxygen was circulated for 301 hr. The two oxides and the thorium sulfate were mixed with a Lightnin mixer for 3 hr before being charged to the loop.

No difficulties were encountered in pumping the slurry. After 160 hr of circulation at 300°C the color of the slurry changed from a deep orange to a green-gray-orange. A check of the gas showed a depletion of oxygen. The deep-orange color was restored when oxygen was added to the system, indicating that the green-gray-orange color was probably due to the reduction of U^{6+} to U^{4+}.

A summary of the run is given in Table 9.2. Included in the table are results from run S-69, in which a pure thorium oxide slurry was circulated at 300°C in the same loop. The apparently low sulfate analysis in run S-94 is consistent with the calculated charge, within the analytical error.

Based on these data, the attack on the system components by both the pure ThO_2 and the admixed thorium-uranium oxide slurries is comparable. No large spheres of oxide[8] were found in the mixed-oxide slurry. Samples have been submitted for petrographic and x-ray diffraction studies to determine the thorium-uranium association.

9.4.2 Circulation of Thorium-Uranium Oxide Slurries in 200-gpm Loop

Run 200A-10 was completed in the 200-gpm loop to check the new components which were added[9] and to determine the handling characteristics of an admixed thorium-uranium oxide slurry at 250°C. The loop was loaded initially to give a thorium concentration of 500 g of thorium per kilogram of H_2O, 3400 ppm of sulfate (based on ThO_2)

[8] R. B. Gallaher and A. S. Kitzes, *Preparation of Standard Oxide*, ORNL CF-56-10-8 (Oct. 3, 1956); R. B. Korsmeyer *et al.*, *HRP Quar. Prog. Rep. Oct. 31, 1956*, ORNL-2222, p 54.

[9] R. B. Korsmeyer *et al.*, *HRP Quar. Prog. Rep. Oct. 31, 1956*, ORNL-2222, p 63.

Table 9.2. Comparison of Thorium-Uranium Oxide and Thorium Oxide Slurries Circulated at 300°C

	S-69(ThO_2)	S-94(Th-U Oxide)
Length of run at 300°C, hr	288	301
Average concentration, g of Th per kg of H_2O	872	1180
Average sulfate analysis based on ThO_2, ppm	720	1850
Average pH of slurry	5.2	4.9
Range of pH	5.5 to 5.0	5.4 to 4.4
Weight loss of $^3/_4$-in.-ID, stainless steel orifice, g	1.476	1.215
Weight loss of impeller, g	18.5	23.5
Average wear on front titanium hub of impeller, in.	0.003	0.005
Generalized attack based on iron contamination in slurry, mpy	6	8

as thorium sulfate, and 500 ppm of oxygen. The concentration was increased over a 116-hr interval to 800 g of thorium per kilogram of H_2O, with the sulfate content of the slurry being maintained at the 3400-ppm level.

The initial charge of slurry was circulated at 250°C and 1000 psig for 112 hr to check the operation of the new components. All components operated satisfactorily at the slurry level of 500 g of thorium per kilogram of H_2O. Slurry was then added to increase the concentration from 500 to 800 g of thorium per kilogram of H_2O. The 800-g/kg slurry was next circulated for 165 hr at 250°C. During the course of the runs with the 500- and 800-g/kg slurries the solids were examined microscopically for formation of spheres, but none were evident. The particles appeared to be dispersed, with an average particle size of less than 1 μ. Results of particle-size determinations from settling-rate measurements confirmed the microscopic observations. After 17 hr of circulation the particles were degraded so that 70% of them were less than 2 μ.

Slurries containing up to 900 g of thorium per kilogram of H_2O were added through the addition system to the circulating loop without incident. Slurries at a higher concentration tended to plug the lines, probably because the head available for this operation was less than 20 ft and was insufficient to move the concentrated slurries through the $^1/_4$-in. tubes.

Increasing the concentration to 800 g of thorium per kilogram of H_2O did not affect the operation of the capillary tube or the in-line sampling systems; however, the readings for the venturi flowmeter became erratic at the increased concentration. The venturi appeared to resume smooth operation when uranium was added to the slurry. No satisfactory explanation has been found for the unexpectedly erratic behavior of the venturi.

To determine the effect of uranium on the handling characteristics of thorium oxide slurries at 250°C, $UO_3 \cdot H_2O$ was added to the system after a total circulation time of 393 hr. The uranium content of the slurry was increased to 3 wt % (based on the ThO_2 content) in increments of 0.5, 1.0, and 1.5% at 24-hr intervals. After the final uranium addition the slurry was circulated satisfactorily for 331 hr at temperature. The oxide did not form spheres; the solids were well dispersed and appeared on the average to be less than 1 μ in size.

The run was terminated after a total of 775 hr of circulation at 250°C for a scheduled shutdown and inspection. No caking or unusual accumulations were found in the pressurizer or main circulating lines, and the solids were easily washed from the system.

The velocity of the slurry in the pipes was about 12 fps, and the generalized loop attack averaged about 0.5 mpy, based on the iron contamination found in the slurry. A greater localized attack occurred in areas of high velocity, as evidenced by the rates of attack listed in Table 9.3 for the stainless steel orifice plates and the titanium impeller; however, these localized rates are comparable to those obtained with the pure thorium oxide slurries.[4]

Table 9.3. Localized Attack on Components in Run 200A-10

Component	Slurry Velocity (fps)	Attack Rate (mpy)
Stainless steel orifice 1	37	36
Stainless steel orifice 2	65	246
Titanium impeller		5

Some pump components, such as the titanium seal rings, suffered wear. Although the stainless steel thermal barrier was not attacked, portions in contact with circulating slurry acquired a minor polish (Fig. 9.3). The titanium impeller was not pitted (Fig. 9.4), although it lost 3.5 g in weight and was highly polished. There was no damage to the Kingsbury thrust bearing; however, the lower Graphitar radial bearing was worn 0.004 in., and the upper one was cracked. Several small cracks were also found in the upper Stellite 19 journal, which may have been the cause of the damage to the upper Graphitar bearing.

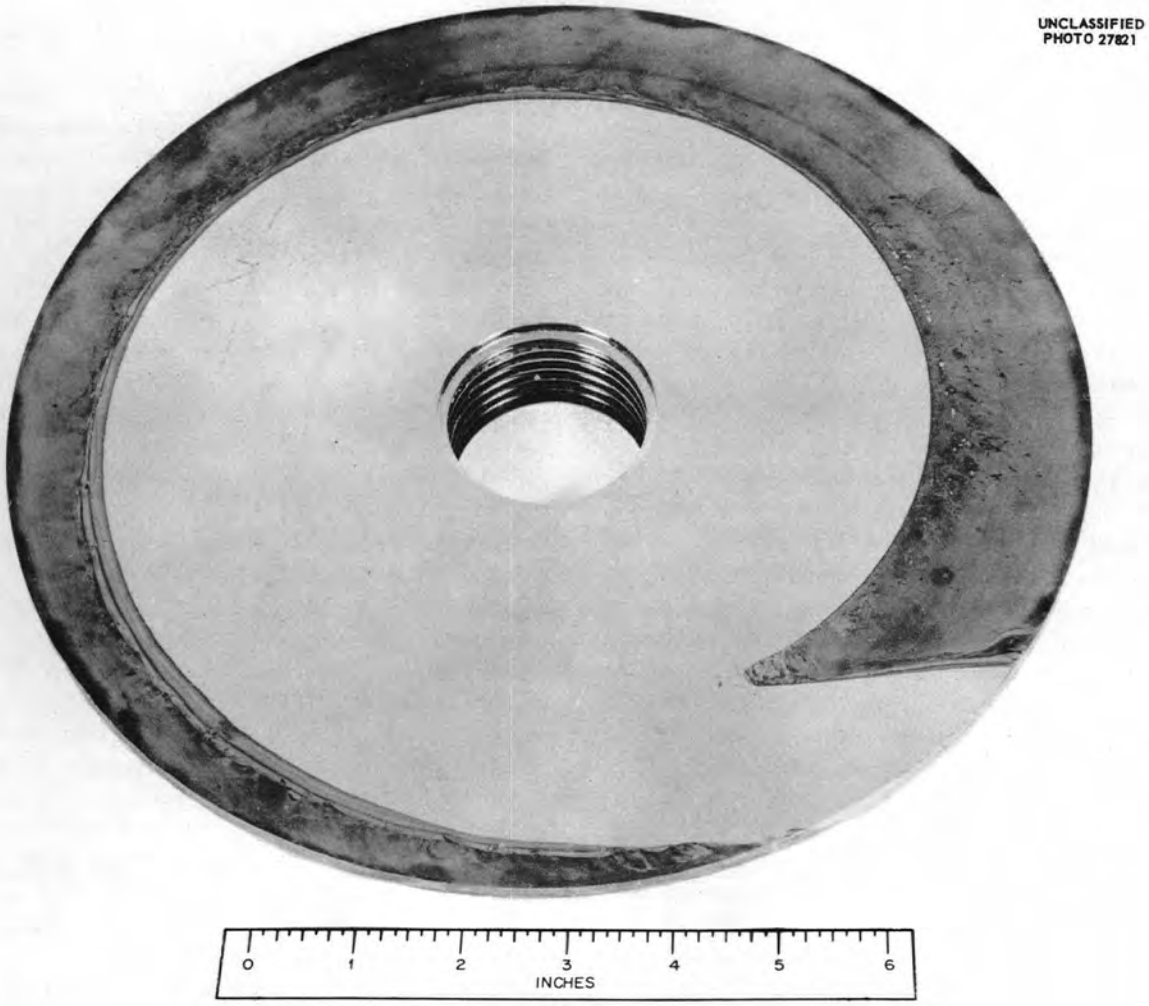

Fig. 9.3. Thermal Barrier from 200-gpm Pump, Run 200A-10.

UNCLASSIFIED
PHOTO 27820

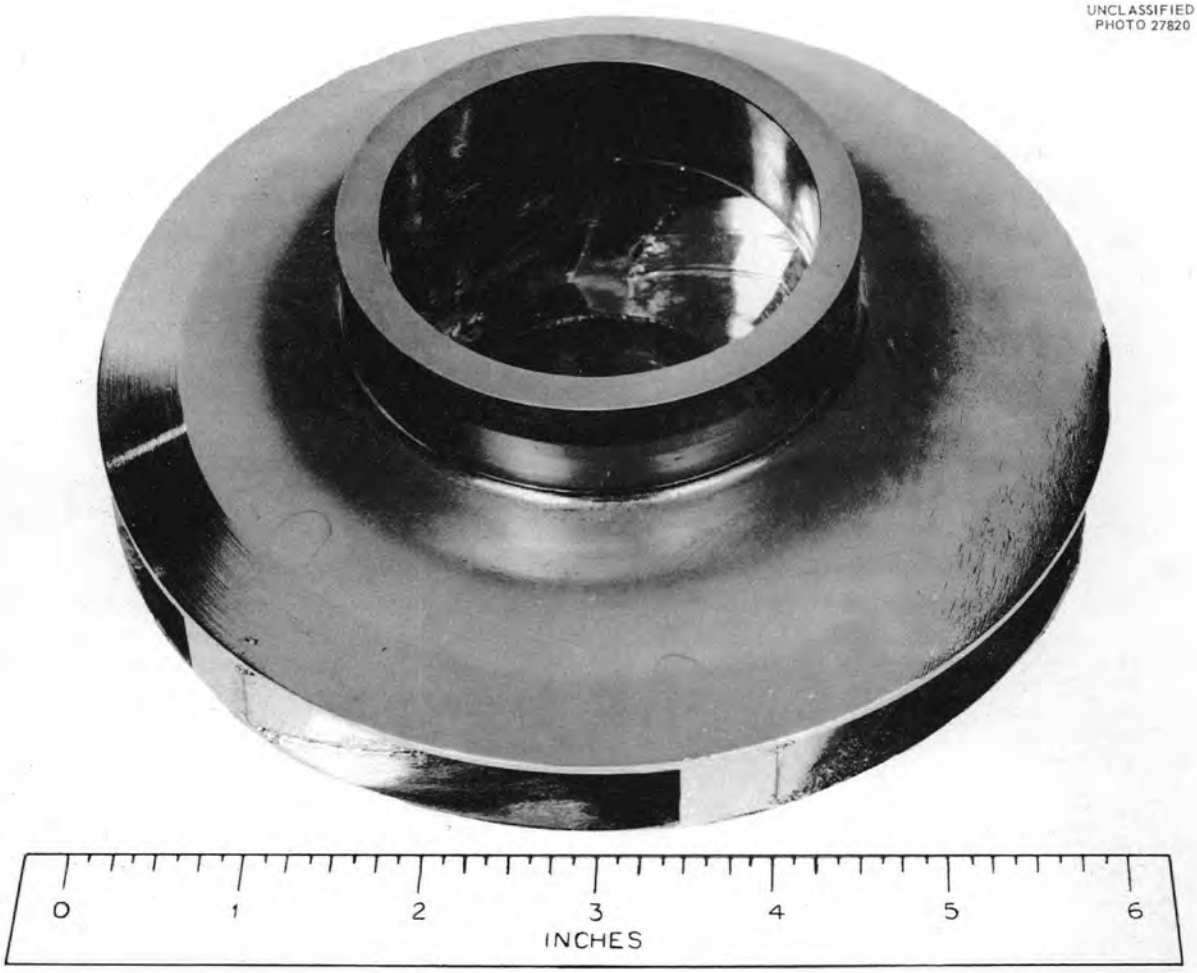

Fig. 9.4. Titanium Impeller from 200-gpm Pump, Run 200A-10.

9.4.3 Pressure-Bridge Density Meter

A new type of continuous density meter, applicable for use with thorium oxide slurry in high-temperature, high-pressure systems, was tested successfully in a low-temperature slurry loop.[10] The instrument, called the "pressure bridge," is shown in Fig. 9.5. Fluid enters, flows through, and exits from the bridge as indicated. The average density of the fluid is determined from the equation

$$\Delta P = (\rho - \rho_m)Z \ , \tag{1}$$

where

ΔP = differential pressure,
ρ = fluid density,
ρ_m = manometer fluid density,
Z = height between taps.

The bridge tested in the low-temperature slurry loop was constructed of 1-in. sched-40 pipe with screwed fittings and had a height of $35\frac{3}{4}$ in. Water was used as the manometer fluid, in which case Eq. 1 becomes:

$$h_w = 35.75\rho - 35.70 \ , \tag{2}$$

where $h_w = \Delta P$, in. H_2O and ρ = fluid density, g/cc.

Figure 9.6 shows the experimental data. The straight line is a plot of Eq. 2. The slurry density

[10] R. P. Wichner and C. F. VandenBulck, *The Pressure Bridge Density Meter for Continuously Metering Densities of Flowing Streams*, ORNL CF-57-1-49 (Jan. 10, 1957).

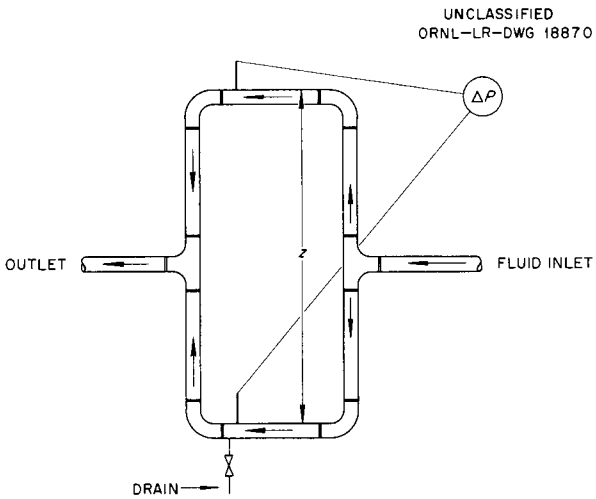

Fig. 9.5. Pressure-Bridge Density Meter.

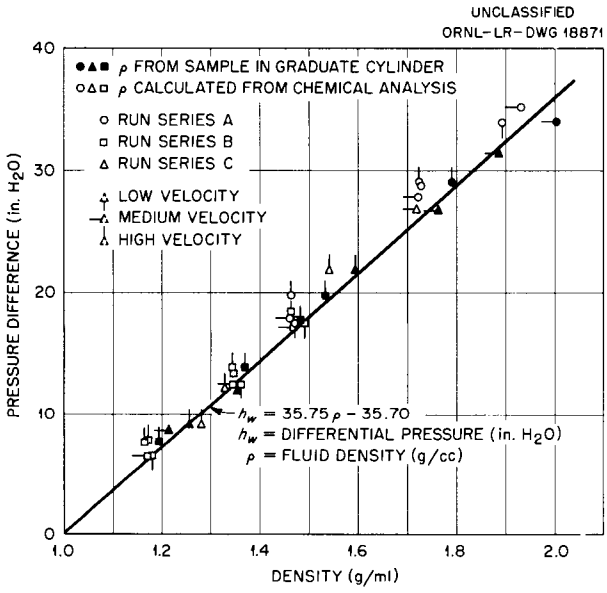

Fig. 9.6. Pressure-Bridge Measurements, Pressure Differences vs Slurry Density.

as determined by sampling into a tared graduated cylinder is indicated, as is the slurry density determined by calculation from chemical analysis, with 9.69 g/cc used as the density of ThO_2.

In these tests the slurry concentration was varied from 100 to 1100 g of thorium per kilogram of H_2O, for which the average deviation between the density predicted and that determined by sampling into a tared graduated cylinder was 0.019 g/ml, or equivalent to an average deviation of 1.2%.

The slurry velocity in the bridge was varied from 1 to 7½ fps (equivalent to throughputs of 5 to 40 gpm) without causing any measurable error.

9.5 BLANKET-SYSTEM DEVELOPMENT

9.5.1 Test-System Operation

A fourth water run, of 277 hr duration, was carried out in the blanket test system pending the arrival of platinum rupture disks and a relief valve for installation downstream from the rupture disks in the vent line. During this run the revised slurry feed system[11] was tested with sulfated slurry (3000 ppm SO_4^{--}, based on thorium) at concentrations up to 1150 g of thorium per kilogram of H_2O and was found to be satisfactory.

After this run two continuous-flow samplers with a common cooling jacket were installed on the upper and lower hemispheres of the blanket vessel as indicated on Fig. 9.7, and three samplers were installed on the 3½-in. pipe between the blanket outlet and the circulating-pump suction. One of these samplers comes off the top of the horizontal pipe upstream from the loop flow nozzle. The other two samplers, downstream from the flow nozzle, consist of two ¼-in. stainless steel tubes located at one-third and two-thirds the distance from the top of the pipe to the bottom. The purpose of the sampler arrangement is to detect settling in the horizontal pipes during slurry operation.

Calculations and experience based on the plugging of the high-pressure heat exchanger indicated that the heat exchanger in use (the former HRE spare heat exchanger), with ¼-in.-OD tubes, was likely to plug in slurry service. This exchanger was disconnected from the system.

The first slurry run (SM-2) without the heat exchangers was started on November 19 to test the slurry behavior in the blanket. The system was filled with distilled water and gradually loaded with thorium oxide during operation. The slurry was prepared at ORNL from specially purified thorium nitrate by thermal decomposition of an oxalate precipitate with a final firing at 800°C. Sulfuric acid was added to give 3000

[11] H. L. Falkenberry, L. F. Parsly, and I. M. Miller, *HRP Quar. Prog. Rep. July 31, 1956*, ORNL-2148, p 65 and Fig. 9.17.

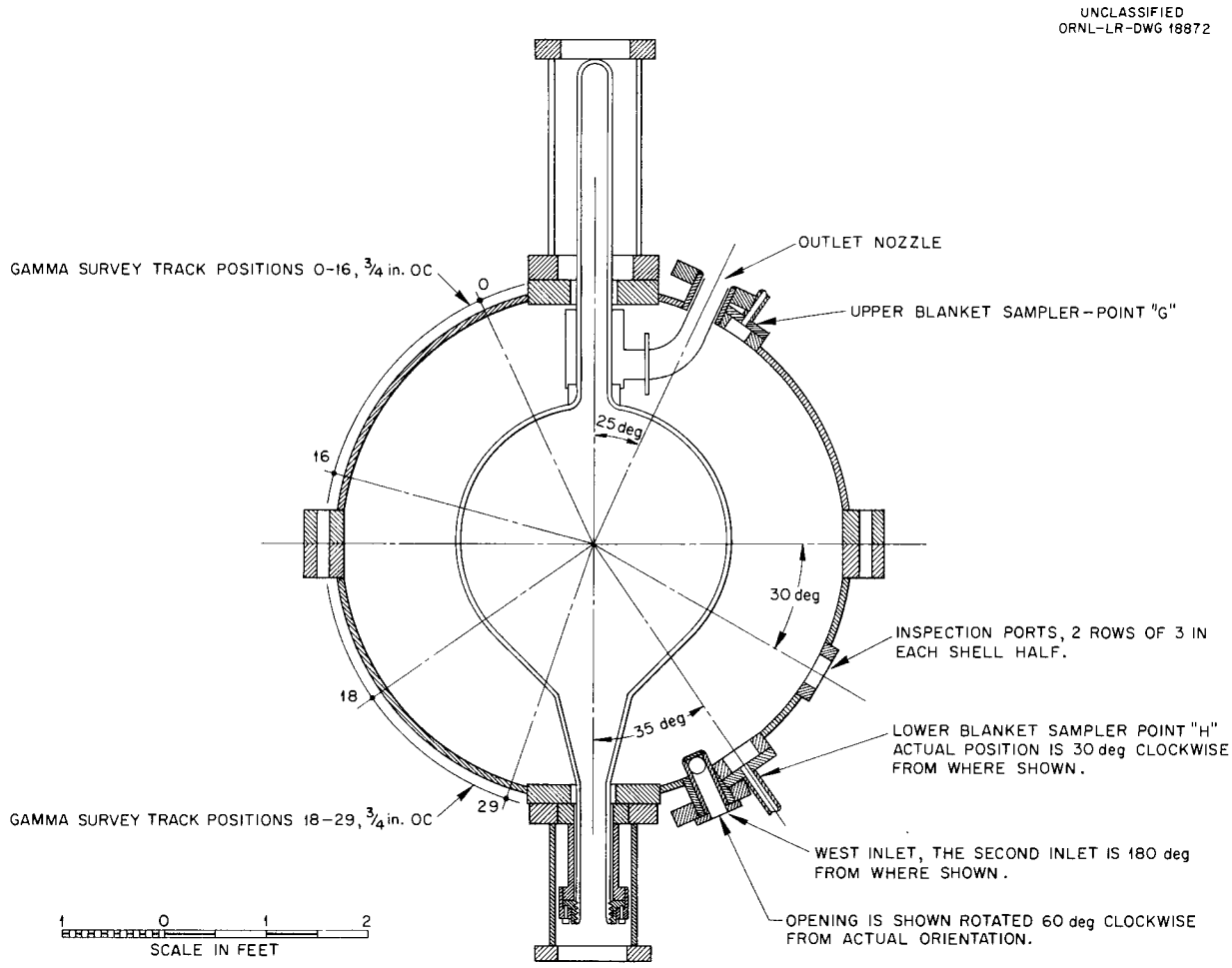

Fig. 9.7. Blanket Assembly.

ppm SO_4^{--} based on the thorium. After operating conditions of 225 psi and 170°C were reached, 650 liters of oxygen was charged to the system at a rate of 1 liter/min. After approximately 300 liters of O_2 had been added, indications were observed that are now recognized as signs of oxygen saturation. Continued oxygen addition led to gas binding in various parts of the system, requiring repeated venting to the atmosphere. Eighty-three kilograms of thorium oxide was charged 94 hr after the startup on water, and charging was continued intermittently until a total of 705 kg of thorium had been added, to give a calculated slurry concentration of 500 g of thorium per kilogram of H_2O. Since the system operates at constant volume, water was removed, as slurry was charged, by decanting through the upper pressurizer sampler.

After about 400 hr of operation the liquid samples drawn from the upper part of the pressurizer were found to be high in chloride. This sample point is above the slurry-liquid interface. Other sample points on the loop and at the lower part of the pressurizer, but still above the slurry interface, indicated 10 ppm or less. It is concluded that the chloride was being leached from the circulating slurry. Distilled water was pumped into the main loop at a rate of approximately 300 cc/min, and a corresponding flow was withdrawn from the upper part of the pressurizer to remove the chloride. The chloride concentration in the liquid withdrawn dropped from an initial value of 130 ppm to a final value of 1 ppm in 2 hr and 20 min of this operation.

The chloride concentration following this flush operation was observed to be less than 10 ppm in the circulating slurry and generally less than

10 ppm in the top of the pressurizer. However, the pressurizer was again flushed, because of progressive discoloration of the liquid.

Figure 9.8 is a plot of the loop temperature and the indicated flowmeter reading vs time during the operating interval from 700 to 1350 hr, or from just after the last thoria addition to the end of the report period. As the flowmeter reads directly in inches of water, the reading is sensitive to changes in density and hence to thoria concentration for comparatively small temperature changes. Since the pump provides substantially constant volume flow for varying head in the flow range utilized, the flowmeter reading is considered to be a fairly reliable indication of the relative concentration of the stream. This belief is supported by analyses of samples withdrawn from time to time, as shown in the figure.

The data revealed the following four phenomena:

1. an inverse relation between the loop temperature and the thoria concentration in the stream,
2. a long-term downward trend in the stream concentration which is not explained by variations in temperature,
3. extreme sensitivity of the stream concentration to temperature variations occurring just above about 180°C, at least during the latter part of the operating interval shown,
4. a concentration lag in response to upward temperature changes just above 180°C, followed by extremely rapid fallout.

When these phenomena were observed, a sample of the slurry was withdrawn from the stream for settling-rate measurements (by J. P. McBride *et al.*) over the range from room temperature to 300°C. These measurements indicate that the settling rate increases markedly between about 165 and 190°C, but it has not been possible to correlate the settling-rate measurements quantitatively with the loop behavior.

Since the circulating stream never exceeded a concentration of about 310 g of thorium per kilogram of H_2O and usually was in the range of 200 g/kg, substantially all the thoria was located in the blanket itself, and settling data (reported below) revealed that the slurry in the lower part of the blanket was of much higher concentration than the calculated charge. It has not been possible to determine the degree of mixing or interchange between the flowing stream and the great bulk of material in the blanket. However, it can be surmised that the rate of mixing could not have been very great, for a change in the sulfate

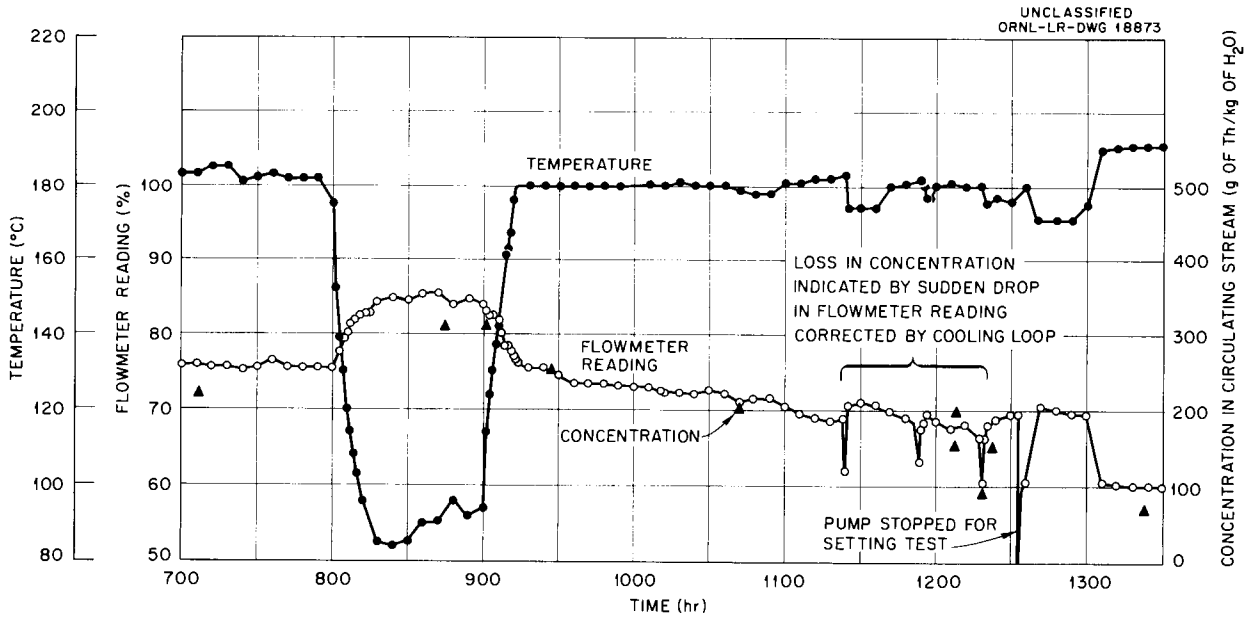

Fig. 9.8. Slurry Blanket Test, Variation of Flowmeter Reading, Temperature, and Concentration in Circulating Stream with Time.

content of the final slurry charge from that previously used apparently did not reach its maximum effect on the circulating stream until some 100 hr later.

The run has continued for a total of 1350 hr since startup. The pump has been shut down several times for periods of up to 15 min for a variety of reasons, including venting to relieve gas binding, accidental loss of panel power, and deliberate shutdowns to make changes on the panel or to run scheduled tests. There has been no difficulty in resuming operation. The running time with slurry in the loop is 1270 hr, and the time at the present charge level (500 g of thorium per kilogram of H_2O) is 670 hr.

9.5.2 Gamma-Survey Work

Previous work has indicated that the distribution of thorium oxide in pipes and pressure vessels can be determined in a qualitative way by use of gamma-ray traverses with a cobalt source and a scintillation head.[12] Accordingly, a 65-mc cobalt source has been placed in the center of the sphere, and a semicircular steel track with 29 positions for a scintillator head has been installed from the top to the bottom of the sphere on the outside of the insulation as shown in Fig. 9.7. Also, two moving-table units have been installed for the purpose of making gamma traverses of a horizontal section of 3½-in., 0.469-in.-wall pipe near the circulating-pump suction and of a vertical section of 3-in. sched-40 pipe at the outlet of the blanket sphere. Several traverses of both pipe and sphere have been taken by means of a Hewlett-Packard counter; they indicate that, owing to the radiation from the thorium present in the blanket, further improvement in technique is necessary to obtain acceptable results.

9.5.3 Settling Tests

Some information concerning the density of a settled bed of slurry in the mockup sphere was obtained by stopping the circulating pump for 5 min and withdrawing samples continuously from the sampler in the lower hemisphere of the blanket vessel. The results of this test are plotted in Fig. 9.9. Since this sampling point is located almost directly in the path of one of the two inlet nozzles to the sphere, information from this point

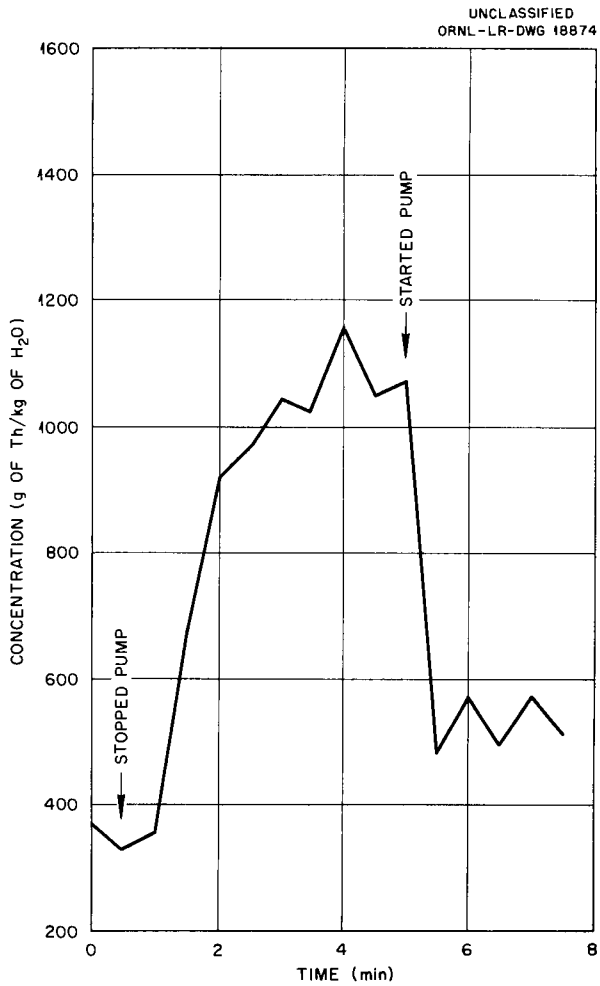

Fig. 9.9. Variation of Concentration from Lower Blanket Sample Point with Time as Pump Is Stopped and Restarted, System Temperature 195°C.

is not necessarily representative of general conditions in the lower hemisphere. Additional sampling points are to be installed.

9.5.4 Analytical Data

A plot of iron and thorium concentrations vs time during run SM-2 is shown in Fig. 9.10. From the iron analyses the generalized corrosion rate is calculated to be about 0.7 mpy. Chromium and nickel pickup is very slightly above the minimum determinable levels.

Microscopic examination of slurry from all sampling points has failed to reveal any evidence of sphere formation in the slurry. The slides were prepared by dispersing the sample in sodium pyrophosphate solution before it was mounted.

[12] R. B. Korsmeyer *et al.*, *HRP Quar. Prog. Rep. Oct. 31, 1956*, ORNL-2222, p 62.

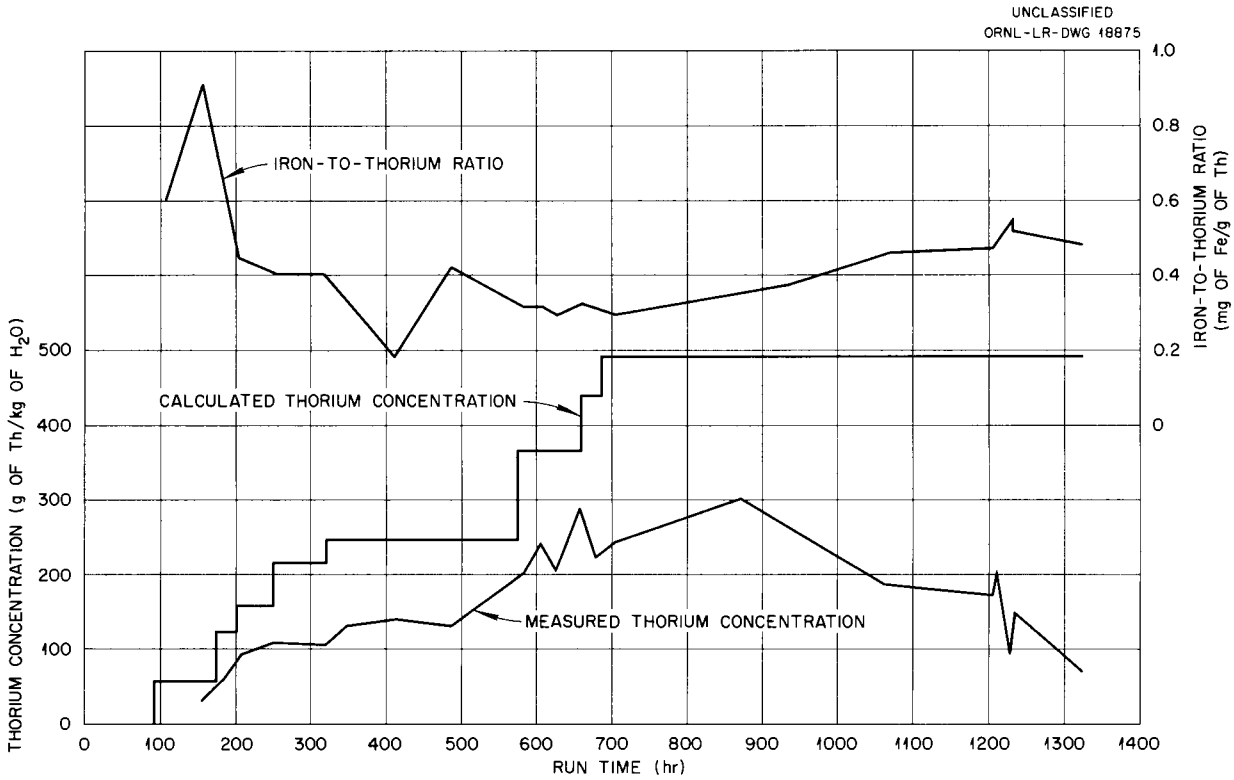

Fig. 9.10. Slurry Blanket Test, Run SM-2, Variation of Thorium and Iron Concentration with Time.

10. VALVE DEVELOPMENT

D. S. Toomb

E. H. Bell A. M. Billings

10.1 SEALING BELLOWS

A type 347 stainless steel bellows (Fulton Sylphon No. 10717-R3) of the type used in the HRT for sealing valve stems[1] was gold-plated at ORNL in an attempt to increase its corrosion resistance. This type of bellows, because of its thinness, is subject to short-term failure when exposed to oxygen-deficient uranyl sulfate solutions at elevated temperatures. Upon being tested in uranyl sulfate at 2000 psi and 300°C, the bellows failed after 3500 cycles with a stroke of $\frac{1}{8}$ in. Prior to plating, however, it was overstressed when the convolutions were spread so that the plating solution could penetrate to the inner folds. Another test is planned in which the bellows will be plated before the final mechanical forming operation which compresses the bellows.

10.2 VALVE TRIM

Two sets of valve trim, designed (Fig. 10.1) for tight shutoff, incorporating a gold gasket recessed in a groove in the plug and mating with an annular ring on the seat have now been tested in the valve test loop. The first set failed to perform satisfactorily because of insufficient clearance between the tongue-and-groove mating surfaces. The second set, in which this clearance was increased, withstood 404 dumping cycles with uranyl sulfate at 1250 psi and 275°C. Leakage after test, as denoted by pressure rise in a vacuum system of known volume, was approximately 10 μ/min. A representative pressure rise for the more conventional type 347 stainless steel trim is approximately 30 μ/min.

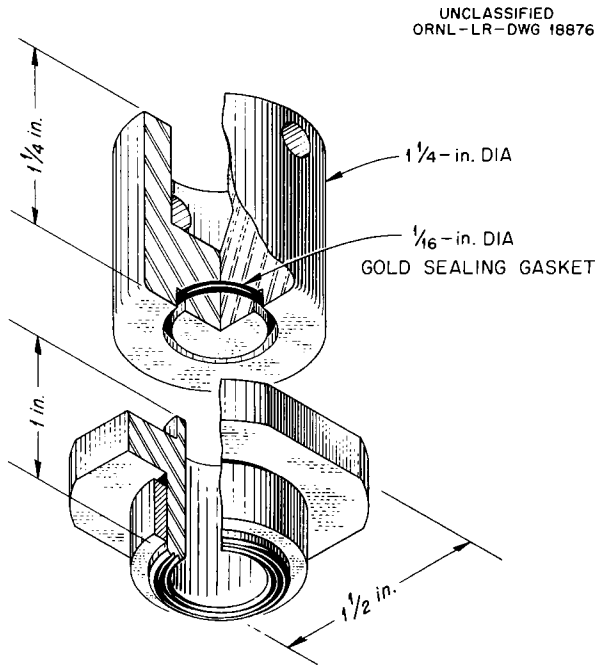

Fig. 10.1. Gold-Gasket-Sealed Valve Trim.

[1] D. S. Toomb *et al.*, *HRP Quar. Prog. Rep. July 31, 1956*, ORNL-2148, p 23.

Part IV

REACTOR MATERIALS RESEARCH

E. G. Bohlmann

11. SOLUTION CORROSION[1]

J. C. Griess H. C. Savage
S. R. Buxton D. N. Hess
J. L. English E. F. House
R. S. Greeley T. H. Mauney
W. C. Ulrich

11.1 PUMP LOOP TEST RESULTS

11.1.1 Mockup of the Zircaloy–Stainless Steel Transition and Expansion Joint

A second test of the mockup of the Zircaloy–stainless steel transition and expansion joint, previously mentioned,[2,3] used in the HRT reactor vessel, was made in 100A dynamic corrosion loop F. A detailed report on the first test is to be issued.[4]

When the test-vessel flanged joint was reassembled after the first test, the loop was filled with water to the desired volume and concentrated fuel solution was added to give a solution of the composition 0.04 *m* UO_2SO_4, 0.005 *m* $CuSO_4$, and 0.02 *m* H_2SO_4.

The thermal cycling was performed as before between 100°C at 100 psig and 300°C at 1550 psig. Mechanical deflections of the bellows through a total traverse of $\frac{5}{8}$ in., $\frac{5}{16}$-in. extension and $\frac{5}{16}$-in. compression relative to the neutral point, were made during each thermal cycle. An additional mechanical deflection of the bellows of $\frac{5}{8}$ in., from the fully extended position to fully compressed and return, made in $\frac{1}{8}$-in. increments over a period of about 15 min was imposed during each 16-hr period that the system was at 300°C and 1550 psig.

The test was of 1200 hr duration, during which time the bellows underwent 50 complete thermal cycles and mechanical deflections, plus 47 additional mechanical deflections during the time that the system was at 300°C and 1550 psig. Since installation the bellows has been subjected to a total of 104 thermal cycles and 148 mechanical deflections.

A differential pressure across the bellows from outside to inside and across the gasket in the transition joint was maintained at about 45 to 50 psia. The interior of the bellows was kept full of water from the condensate tank, and daily samples of the water were taken in order to detect any leakage of the fuel solution across the test gasket or the expansion joint. No leakage was detected at any time during the run. At the end of the run the housing surrounding the test assembly was removed, and an additional leak test was made by applying 50 psig of helium inside the expansion joint and bellows and "sniffing" the exterior with a mass-spectrograph-type leak detector; no leakage was detected.

Prior to disassembly the 10-in.-IPS 1500-lb test-vessel oval-ring joint was leak-tested at 200 psig of helium with a mass-spectrograph-type leak detector. No leakage was observed.

Examination of the bottom groove of the 10-in.-IPS flange showed that no leakage of solution into the groove had occurred; leakage into this groove had occurred during the previous test.[3] The oval-ring gasket was removed from the flange top groove for the first time since the original assembly. No solution had ever leaked into the top groove. No significant attack of the oval-ring gasket was apparent under 10X magnification.

The pitted areas on the bellows at the edges of the reinforcing rings, mentioned previously,[3] were examined closely by moving the rings to reveal the entire crevice area between the rings and the bellows. Figure 11.1 illustrates the appearance of the pits after the first run and after the second run. As can be seen, one new pit (No. 6) developed at the edge of the top ring during the second run, and two small pits (Nos. 2 and 3) spread into a long collection of pits. The pitting at the lower edge of the bottom ring did not continue during the second run.

---

[1] Reported in greater detail by J. C. Griess *et al.*, *Quarterly Report of the Solution Corrosion Group for the Quarter Ending January 31, 1957*, ORNL CF-57-1-144 (to be issued).

[2] J. C. Griess *et al.*, *HRP Quar. Prog. Rep. July 31, 1956*, ORNL-2148, p 73.

[3] H. C. Savage *et al.*, *HRP Quar. Prog. Rep. Oct. 31, 1956*, ORNL-2222, p 75.

[4] T. H. Mauney *et al.*, *Operating Test of HRT Core Vessel Transition Joint and Expansion Bellows Mock-up*, ORNL CF-57-1-68 (to be issued).

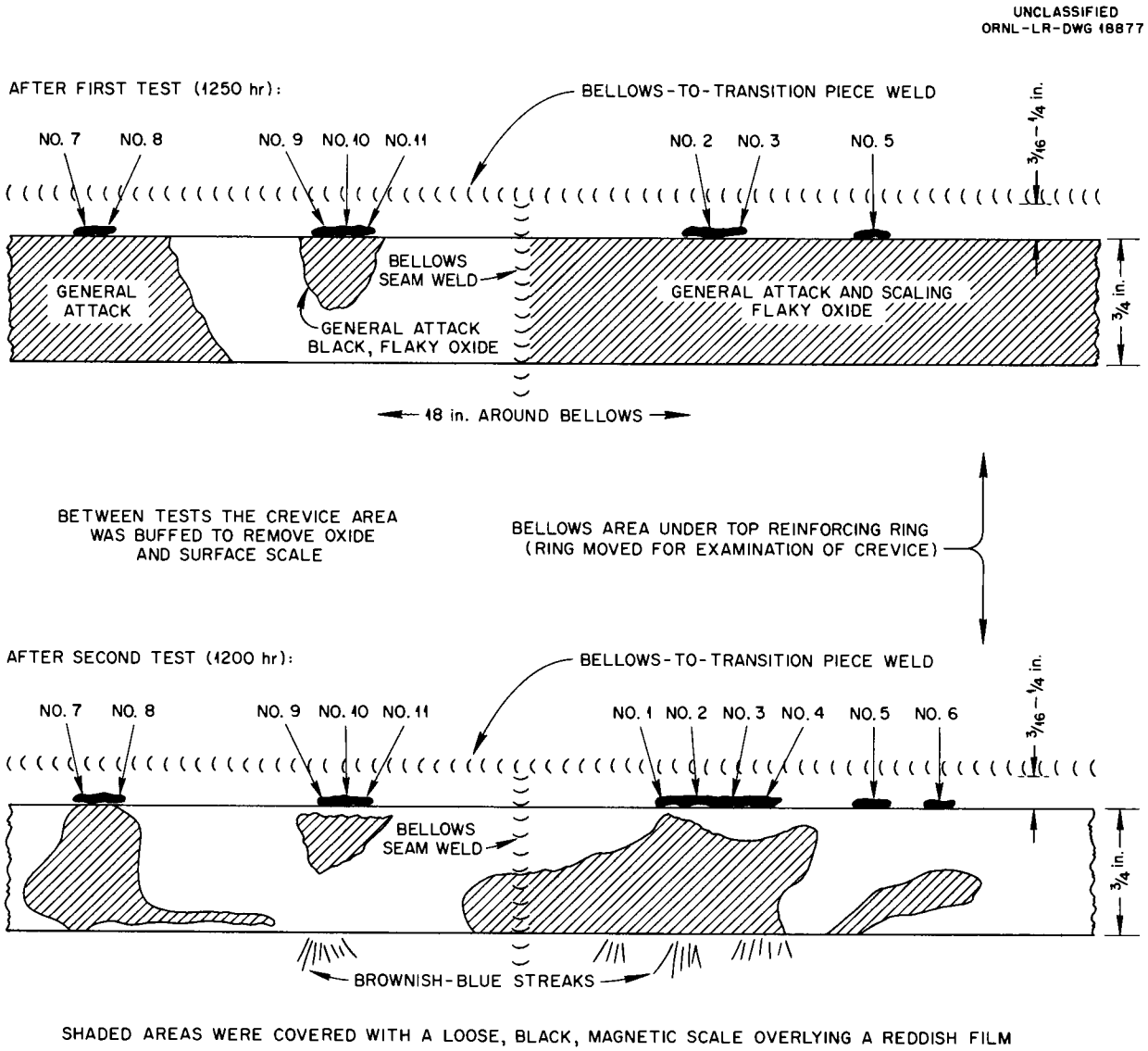

AVERAGE PIT DEPTH (in.) IN PITTED AREAS (SHADED BLACK ON DIAGRAMS ABOVE):

	AFTER FIRST TEST	AFTER SECOND TEST		AFTER FIRST TEST	AFTER SECOND TEST
NO. 1	NOT ATTACKED	0.015	NO. 7	0.008 – 0.010	0.019
NO. 2	0.008 MAX	0.019	NO. 8	0.008 – 0.010	0.023
NO. 3	0.008 MAX	0.019	NO. 9	0.013	0.020
NO. 4	NOT ATTACKED	0.014	NO. 10	0.016	0.017
NO. 5	0.008 MAX	0.016	NO. 11	0.013	0.013
NO. 6	NOT ATTACKED	0.018			

Fig. 11.1. Appearance of Area Under Top Reinforcing Ring on HRT Core–Pressure Vessel Bellows Mockup After Operation in Simulated Fuel Solution.

The pit depths were measured with a microscope–dial-gage-indicator assembly by focusing the microscope on the edge of a pit and then on the bottom of the pit and noting on the dial indicator the microscope carriage travel. Although this method gave pit depths accurate to only ±0.002 to ±0.003 in., the following conclusions were drawn:

1. The average pit depth at the edge of the top band roughly doubled during the second run. The pitting at the lower edge of the bottom band did not continue. No measurable crevice corrosion was observed under either band.

2. The pit depth increased from 0.008 to 0.016 in. to about 0.015 to 0.020 in., with one pit giving an average depth measurement of 0.023 in. (The bellows is of two-ply construction, each ply being 0.050 in. thick.)

3. The rate of pitting attack remained approximately the same as in the first test, about 100 mpy, even though the frequency and total number of mechanical deflections of the bellows were doubled in the second run.

The exact cause of the pitting is not known, but in view of the severity of the attack, further testing is planned to investigate the factors involved.

11.1.2 Studies with the Proposed HRT Fuel Solution

Long-term runs at 200, 250, and 300°C with a solution containing 0.04 *m* UO_2SO_4, 0.02 *m* H_2SO_4, and 0.005 *m* $CuSO_4$, the solution proposed for use in the HRT, were terminated during the past quarter. The run at 200°C lasted for 3683 hr; at 250°C, 3660 hr; and at 300°C, 3841 hr. The solutions were stable with regard to hydrolytic precipitation of uranium and copper with one possible exception. At 300°C after 2740 hr, there was a sudden unexplained 12% decrease in copper concentration. After this decrease the copper-ion concentration remained constant. It seems unlikely that the copper loss was due to hydrolysis, since the loss was very sudden and since no pH change of the solution was observed.

The average corrosion rates of pin specimens of several alloys and metals exposed in the above-mentioned runs are shown in Table 11.1. The critical velocities for type 347 stainless steel

Table 11.1. Corrosion Rates in Long-Term Runs with 0.04 *m* UO_2SO_4 Containing 0.02 *m* H_2SO_4, 0.005 *m* $CuSO_4$, and 500 to 1500 ppm O_2

Materials	Flow Rate (fps)	Corrosion Rates (mpy)		
		L-35 (200°C)	M-29 (250°C)	K-17 (300°C)
Average stainless steels[a]	8	1.7		
(new pins)	12	4.9	0.75	0.23
	20		1.1	0.31
	26		0.93	0.42
	34	12	1.3	0.47
	42	16		
Niobium	8	0.01		
	12		0.35	
	34		0.81	
	42	5.4		
Titanium[b]	8–42	0	0	0
Zirconium[c]	8–42	0	0	0.05
Titanium[d]	20–34	0	0.09–0.18	0.33–0.42

[a]Include types 304, 304 cast, 304 sensitized, 304L, 309 SCb, 347, 347 cast, 347 sensitized, 430, and 446.
[b]Include types RC-55, 75A, 100A, and 150A.
[c]Include crystal-bar zirconium, Zr–2.5% Sn, and Zircaloy-2.
[d]Include Ti–3% Al–5% Cr; Ti–6% Al–4% V; Ti–5% Al–2.5% Sn; and Ti–4% Al–4% Mn.

coupon-type specimens were 15 to 20 fps at 200°C, 25 to 35 fps at 250°C, and 35 to 40 fps at 300°C.

From examination of Table 11.1 it can be seen that the total attack was relatively severe at 8 to 12 fps at 200°C and at 20 to 34 fps at 250°C, even though the pins eventually filmed over and stopped corroding. At 34 to 42 fps at 200°C the corrosion rate was high, but a partially protective film formed which offered some protection as the run progressed.

Not included in Table 11.1 are data from a number of pins which had been exposed in previous runs also. All these specimens, even those exposed at flow rates above the critical velocity, retained their original protective coatings and actually gained weight as a result of the deposition of corrosion products from other parts of the system on their surfaces. This observation has been made previously[5] and shows that certain pretreatments may be useful in extending the critical velocity of a system for prolonged periods of time.

An additional run, in which 0.04 *m* UO_2SO_4 containing 0.02 *m* H_2SO_4, 0.005 *m* $CuSO_4$, and 500 to 1000 ppm O_2 was circulated in loop N at temperatures ranging from 175 to 300°C, was also completed. Prior to the run the system was defilmed with chromous sulfate[6] in order to study how corrosion rates of new stainless steel specimens would change with temperature in an essentially new stainless steel system. The operating temperatures for the run are shown below; the asterisk denotes times at which corrosion specimens were examined.

Temperature (°C)	Time (hr)
175	292*
	148
200	573*
	457*
	672
225	1734*
250	366*
300	339*

[5] H. C. Savage *et al.*, *HRP Quar. Prog. Rep. Oct. 31, 1956*, ORNL-2222, p 77.

[6] J. C. Griess *et al.*, *HRP Quar. Prog. Rep. April 30, 1956*, ORNL-2096, p 84.

The corrosion specimens were defilmed only at the conclusion of the run; the corrosion rates of the specimens during each period of operation were calculated from weight changes in the as-removed condition in order to show what would happen at each higher temperature to a surface that had become filmed over at low temperatures on startup.

Corrosion rates as high as 5 mpy were observed for stainless steel pins at 23 fps and as high as 23 mpy for stainless steel coupons and pins at 44 to 50 fps at 200 to 255°C. Corrosion rates at 175°C were about the same as those at 250°C, being no higher than 2 mpy at 23 fps and 9 mpy at 50 fps. Corrosion rates at all velocities at 300°C were between 2 and 4 mpy, and it is possible that this represents not a loss of metal but a dehydration or change in character of the film at high temperature.

The stability of the proposed HRT fuel solution in heavy water instead of normal water was also investigated. One run was made in which a heavy-water solution containing 0.04 *m* UO_2SO_4, 0.02 *m* D_2SO_4, and 0.005 *m* $CuSO_4$ was circulated at 300°C for 1000 hr. Throughout the run the solution was completely stable, and the corrosion results were no different from those observed in a similar solution with normal water as the solvent.

11.1.3 Studies on the Effectiveness of Pretreatments

The long-term runs described above demonstrated that under certain conditions a preformed film on stainless steel would retain its integrity for long periods of time at flow rates in excess of the critical velocity. In view of this observation three attempts have been made to pretreat stainless steel corrosion specimens with different Cr(VI)-containing solutions.

The pretreating solutions contained (1) 50 ppm chromium as potassium dichromate, (2) 50 ppm chromium as chromium trioxide, and (3) 100 ppm chromium as chromium trioxide. Each solution was circulated in a loop containing type 347 stainless steel coupons for 100 hr at 250°C with 1000 to 2000 ppm oxygen. The loop was then drained, rinsed with water, charged with uranyl sulfate solution, and operated at 250°C.

The pretreatment with the solution containing 50 ppm chromium as potassium dichromate was ineffective. The critical velocity for the type 347

stainless steel specimens in 0.17 *m* UO_2SO_4 at 250°C for 200 hr was approximately the same as in a run without pretreatment, 20 to 30 fps. The pretreating solution with 50 ppm chromium as chromium trioxide was partially effective, since, under the same conditions, the critical velocity was 35 to 40 fps. The difference between potassium dichromate and chromium trioxide may lie in the lower pH of the chromium trioxide solution.

The pretreatment with a solution containing 100 ppm chromium as chromium trioxide was very effective. The film on the type 347 stainless steel coupons withstood attack by 0.17 *m* UO_2SO_4 at 250°C for 1000 hr at flow rates as high as 55 to 60 fps. At the end of the 1000-hr period, the 0.17 *m* UO_2SO_4 was replaced by 1.3 *m* UO_2SO_4, and the run was continued for 100 hr at 250°C; no change in the critical velocity was observed. Further experiments are in progress to determine how effective these films will be over extended periods of time and to determine the mechanism of film breakdown in cases where it occurs.

11.1.4 Use of Titanium Inserts in Stainless Steel Loops

The use of titanium inserts to protect stainless steel from corrosion in highly turbulent areas has frequently been proposed. One 100A loop was equipped with two such inserts to determine their effectiveness and to determine the extent of crevice corrosion on stainless steel. The inserts were made from 75A titanium pipe machined to fit snugly inside the stainless steel piping.

After the loop had been used for 9900 hr with uranyl sulfate solutions ranging in concentration from 0.04 to 1.3 *m* at 175 and 300°C, the inserts were removed and the stainless steel pipe was examined for corrosion. In both cases it was necessary to split the pipe to remove the insert. In one case the oxide between the titanium and the stainless steel contained some UO_2 and Fe_3O_4, whereas in the other case only Fe_2O_3 was found. In neither case was the stainless steel corroded appreciably. Apparently, in the case where the reduced iron oxide had formed, oxygen was completely absent and some, if not all, of the uranium in the crevice had precipitated. It seems reasonable to conclude that the acid that formed as a result of the precipitation was consumed in the corrosion of a small amount of stainless steel, the corrosion products of which plugged the crevice and prevented more solution from entering. With the second insert the clearance between the stainless steel and the titanium insert was sufficient to allow enough oxygen in the crevice so that uranium did not precipitate, and corrosion was no greater than would be found in an essentially static system. Thus it may be concluded that titanium liners in areas of high turbulence can protect the underlying steel piping and that the crevice formed need not lead to severe attack.

11.1.5 Corrosion of Stainless Steel in Beryllium Sulfate Solutions Containing Uranium

Solutions containing beryllium sulfate have been circulated in loop O to determine the usefulness of beryllium sulfate as an additive to aqueous fuel solutions. Loop O, which was built to handle beryllium solutions safely, has been described previously.[7]

The first series of runs was made at 250°C with 1.0 *m* $BeSO_4$ solutions in which uranium trioxide had been dissolved (runs O-3, -5, and -6). The coupons were of type 347 stainless steel. The properties of the solutions are listed in Table 11.2. The results obtained are shown in Fig. 11.2 and are compared with results obtained in standard uranyl sulfate solutions under similar conditions. With 0.17 *m* UO_3 dissolved in 1.0 *m* $BeSO_4$ (run O-3) no regular velocity dependence was observed, whereas with 0.25 *m* UO_3 (run O-5) a sharp critical velocity at 10 to 15 fps was found. With 0.36 *m* UO_3 (run O-6) the solution was not completely stable at 250°C, and at the end of the run small amounts of beryllium oxide and uranium trioxide were found in the loop; at the highest uranium concentration the weight loss of the coupons decreased with increasing velocity. In all the above $BeSO_4$ solutions the weight losses of the specimens exposed at low velocity were as great as or greater than in uranyl sulfate solutions with the same uranium concentration, but at high flow rates the weight losses were considerably lower than in uranyl sulfate solutions.

One run (run O-7) was made in which 0.17 *m* UO_3 was dissolved in 0.5 *m* $BeSO_4$ and the resulting solution circulated at 250°C. The results showed that the weight losses of type 347 stainless steel at low velocity were still greater than in 0.17 *m*

[7] *Ibid.*, p 82.

Table 11.2. Properties of Beryllium Sulfate Solutions Used in Loop O

Run No.	Concentration (m)			pH at 28°C	Temperature (°C) at Which Second Liquid Phase Appeared	Remarks
	$BeSO_4$	Uranium as UO_3	$CuSO_4$			
3	1.0	0.17		2.8	302	Stable for 87 hr at 250°C
5	1.0	0.25		3.1	290*	Stable for 176 hr at 250°C
6	1.0	0.36		3.3	278	Slight precipitation of BeO and UO_3 occurred at 250°C in 200 hr
7	0.5	0.17		3.5	275	Stable for 177 hr at 250°C
8, 9	0.2	0.04	0.005	3.4	295	Precipitation of Be and decrease in pH occurred at 280°C in 200 hr
10, 11**	0.04	0.04	0.005	2.8	317	Stable for 200 hr at 300°C

*Interpolated value.
**Uranium as UO_2SO_4.

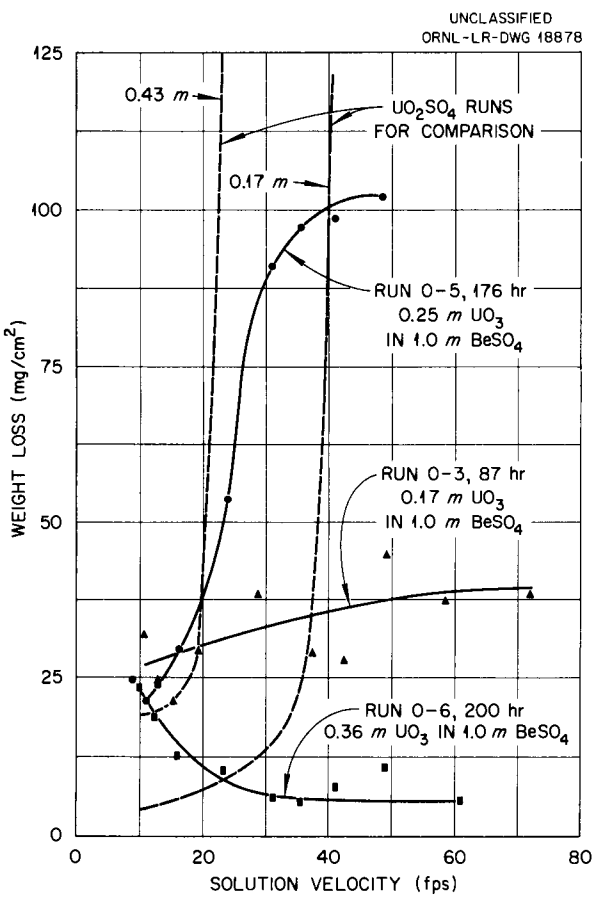

Fig. 11.2. Comparison of Weight Losses of Type 347 Stainless Steel Coupons in UO_3-$BeSO_4$ Solutions and in UO_2SO_4 Solutions at 250°C.

UO_2SO_4. Solutions of 0.17 m UO_3 in beryllium sulfate less than 0.5 m could not be used, since the solubility limit would be exceeded at temperatures below 250°C. Approximately 0.2 m $BeSO_4$ was necessary to dissolve sufficient uranium trioxide to give a solution containing 0.04 m uranium, the concentration proposed for use in the HRT. Therefore runs were also made with 0.2 m $BeSO_4$ containing 0.04 m UO_3 and 0.005 m $CuSO_4$ at 250 and 280°C (runs O-8 and -9, Table 11.2). Higher temperatures were not studied, since the solution separated into two liquid phases at 295°C. In addition, when at 280°C, the solution was not completely stable, as shown by the fact that some beryllium was lost from solution during the 200-hr run. The weight losses of the type 347 stainless steel coupons from runs O-8 and -9 are shown in Fig. 11.3 and are compared with those from runs made with 0.04 m UO_2SO_4 containing 0.02 m H_2SO_4 and 0.005 m $CuSO_4$. The composition of the latter solution is the same as that to be used in the HRT.

It can be seen that generally the results in the 0.04 m UO_3–0.2 m $BeSO_4$ solution were worse than in the 0.04 m UO_2SO_4–0.02 m H_2SO_4 solution, although the difference at 250°C was not great. Thus it appears that solutions of uranium trioxide in beryllium sulfate offer no advantage over uranyl sulfate solutions in the range 0.04 to 0.17 m uranium as far as out-of-pile corrosion of stainless steel is concerned.

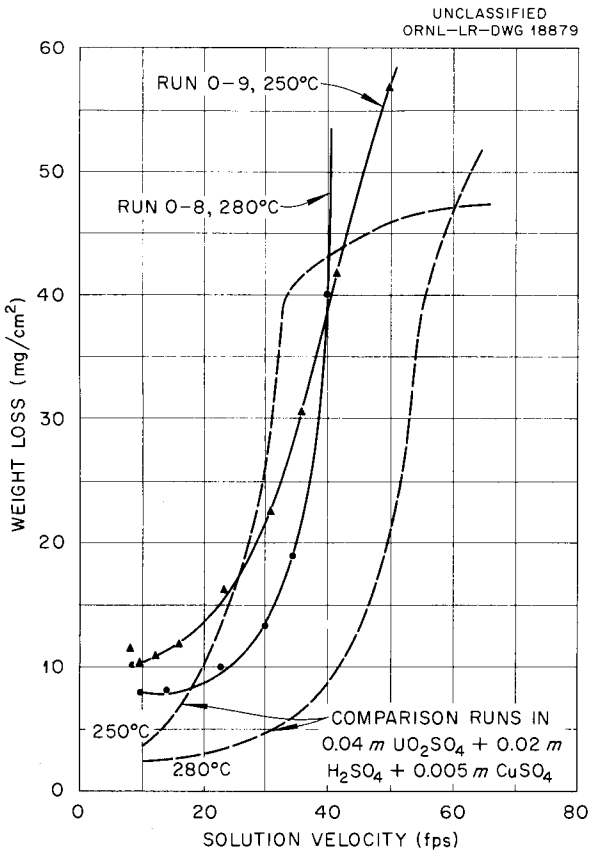

Fig. 11.3. Comparison of Weight Losses of Type 347 Stainless Steel Coupons in 0.2 *m* $BeSO_4$ Containing 0.04 *m* UO_3 and 0.005 *m* $CuSO_4$ and in 0.04 *m* UO_2SO_4 Containing 0.02 *m* H_2SO_4 and 0.005 *m* $CuSO_4$ (200-hr Runs).

Previous attempts[8] to circulate equimolal uranyl sulfate–lithium sulfate solutions at the 0.04 *m* level resulted in hydrolytic precipitation of some uranium and lithium even at 250°C. Since beryllium sulfate solutions are acidic, it was felt that equimolal uranyl sulfate–beryllium sulfate solutions at the 0.04 *m* level might be stable at high temperatures. Quartz-tube experiments showed that a solution of 0.04 *m* UO_2SO_4, 0.04 *m* $BeSO_4$, and 0.005 *m* $CuSO_4$ was stable at 300°C for 3 hr and that the solution separated into two liquid phases at 317°C.

[8] J. C. Griess *et al.*, *HRP Dynamic Corrosion Studies: Quarter Ending July 31, 1956*, ORNL CF-56-7-52, p 29 (Classified).

Two runs, each of 200 hr duration, have been made with the UO_2SO_4–$BeSO_4$ solution; one run was made at 250°C (run O-10), and the other at 300°C (run O-11). The corrosion results were similar to those observed in 0.04 *m* UO_2SO_4–0.02 *m* H_2SO_4–0.005 *m* $CuSO_4$ at the same temperature. The solution in both runs was stable for the 200-hr period, although longer runs might show a slow hydrolytic precipitation, since the pH decreased between 0.2 and 0.3 during both runs. The weight losses of the type 347 stainless steel coupons are plotted in Fig. 11.4; for comparison, data obtained in runs with 0.04 *m* UO_2SO_4–0.02 *m* H_2SO_4–0.005 *m* $CuSO_4$ solutions are included.

The room-temperature pH of a solution containing 0.04 *m* UO_2SO_4, 0.02 *m* H_2SO_4, and 0.005 *m* $CuSO_4$ is 1.5, whereas that of a solution containing 0.04 *m* $BeSO_4$ and 0.04 *m* UO_2SO_4 is 2.8. Since

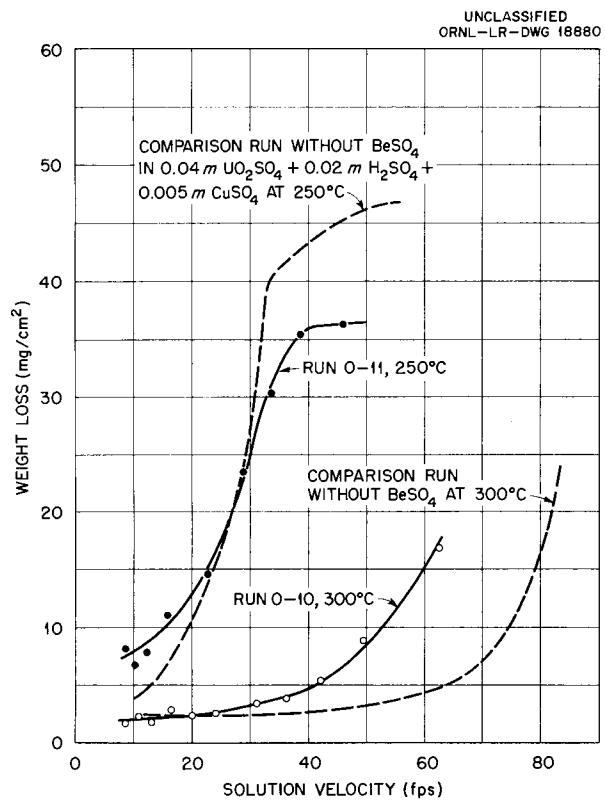

Fig. 11.4. Comparison of Weight Losses of Type 347 Stainless Steel Coupons in 0.04 *m* UO_2SO_4 plus 0.04 *m* $BeSO_4$ plus 0.005 *m* $CuSO_4$ and in 0.04 *m* UO_2SO_4 plus 0.02 *m* H_2SO_4 plus 0.005 *m* $CuSO_4$ (200-hr Runs).

both solutions appear to be stable at high temperatures, it is possible that the hydrolysis of beryllium sulfate increases with rising temperature to an extent sufficient to supply the acid necessary to stabilize the uranyl sulfate. If the above reasoning is correct, the equimolal uranyl sulfate–beryllium sulfate solutions should be less corrosive than a uranyl sulfate solution containing sulfuric acid at temperatures in the range of 150 to 250°C. Tests to determine the accuracy of the above hypothesis are in progress.

11.1.6 Effect of Cr(VI) on the Corrosion of Stainless Steel

In the last quarterly report,[9] data were presented on the effect of Cr(VI) in uranyl sulfate solutions on the corrosion of stainless steel at 250 and 275°C. During the past quarter a similar study was made at 300°C. The results paralleled those at the lower temperatures; that is, the higher the Cr(VI) concentration, the higher the corrosion rate at flow rates in excess of the critical velocity and the less the quantity of metal dissolved during film formation at low flow rates.

11.1.7 Effect of Copper Sulfate on the Corrosion of Stainless Steel

A study aimed at determining the effect of cupric sulfate in uranyl sulfate solutions on the corrosion of stainless steel has been made. The test conditions were 0.17 *m* UO_2SO_4 at 250°C with concentrations of copper between 0 and 1150 ppm. A titanium loop was used to minimize the Cr(VI) content of the solution. The results indicated that copper had no effect on the corrosion at flow rates less than the critical velocity; above the critical velocity the corrosion rate increased approximately linearly with copper concentration. With no copper in the system the film-free corrosion rate was 160 mpy; with 1150 ppm copper present the rate was 250 mpy.

11.2 LABORATORY CORROSION STUDIES

11.2.1 Stress-Corrosion Cracking in Chloride-containing Uranyl Sulfate Solutions

Tests to determine the susceptibility of type 347 stainless steel to stress-corrosion cracking in boiling 0.04 *m* UO_2SO_4 solutions containing 0.02 *m* H_2SO_4, 0.005 *m* $CuSO_4$, and various concentrations of halide ions have been continued. Previous data[10] have shown that the addition of iodide or bromide ions to the solution did not produce cracking, although the presence of bromide ions did accelerate the general attack. Studies during the past quarter confirmed the above results; uranyl sulfate solutions containing bromide ions in the range 50 to 200 ppm have failed to produce cracking in highly stressed type 347 stainless steel.

The concentrations of chloride ions that have been shown[10] to produce cracking of stressed type 347 stainless steel in 0.04 *m* UO_2SO_4 solution are 25 and 50 ppm. On the other hand, chloride concentrations of 0, 5, 10, and 100 ppm did not produce cracking under the conditions of the test. During the past quarter chloride concentrations of 200 and 500 ppm were added to the uranyl sulfate solution, and during a 500-hr test period no definite indications of cracking were observed; however, at the 500-ppm chloride level, suspected cracking was observed. Additional exposure time will be required to verify the existence of actual cracks. No cracking was found after 2000 hr of exposure at chloride levels of 0, 5, 10, and 100 ppm.

The effect of chloride ions on the generalized corrosion attack of unstressed type 347 stainless steel in 0.04 *m* UO_2SO_4–0.02 *m* H_2SO_4–0.005 *m* $CuSO_4$ solution is shown in Fig. 11.5. The weight-loss data were for duplicate specimens exposed for a total of 500 hr in the respective test media. The 500-hr weight-loss data for chloride concentrations from 0 to 100 ppm were reported previously, and they indicated a leveling-off in the rate of attack with increased chloride concentrations.[10] However, the recent longer time data with solutions containing 200 and 500 ppm of chloride showed that the rate of corrosion attack increased in linear fashion over the range of chloride concentrations from 50 to 500 ppm.

11.2.2 Stress-Corrosion Cracking Produced by Tap Water

Previously reported data[11] showed that cold-bent type 347 stainless steel pipes through which 60-

[9] H. C. Savage *et al.*, *HRP Quar. Prog. Rep. Oct. 31, 1956*, ORNL-2222, p 78.

[10] J. L. English and J. C. Griess, *HRP Dynamic Corrosion Studies: Quarter Ending July 31, 1956*, ORNL CF-56-7-52, p 36–43 (Classified).

[11] J. L. English and J. C. Griess, *Quarterly Report of the Solution Corrosion Group for the Period Ending April 30, 1956*, ORNL CF-56-4-138, p 31–36 (Classified).

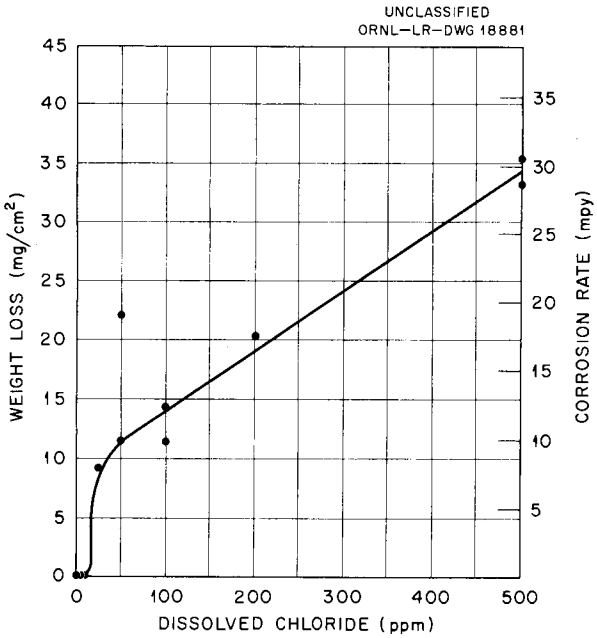

Fig. 11.5. Effect of Chloride Ion Concentration on the Corrosion of Unstressed Type 347 Stainless Steel After 500 hr in Boiling and Aerated 0.04 *m* UO_2SO_4 Solution Containing 0.02 *m* H_2SO_4 and 0.005 *m* $CuSO_4$.

psig steam was being passed would undergo transgranular stress-corrosion cracking if Y-12 plant chloride-containing potable water was sprayed on their surfaces. At that time it was reported that during a 11,000-hr test period all exposed pipes (six in number) had numerous deep cracks. The cracking was attributed to the chloride ions in the tap water. Although the water contained only between 3 and 7 ppm chloride, the thick scale that formed on the surface of the pipes contained 760 ppm chloride.

Recent 1000-hr experiments were carried out in a spray test unit, under conditions similar to those described above, to determine the effect of various stress-relief treatments on the stress-corrosion-cracking susceptibility of cold-formed type 347 stainless steel. (All the type 347 stainless steel was from the same heat of steel, and specimens subjected to the boiling 65% HNO_3 test corroded at rates of less than 2.0 mils/month.) The manner in which the stainless steel was treated after bending and the results of the test are shown in Table 11.3. In addition to the type 347 stainless steel, a cold-formed titanium pipe and a modified type 430 stainless steel pipe were tested. (The modified type 430 stainless steel was supplied by Babcock & Wilcox Co. and contained 16.1% Cr, 0.86% Ni, 0.024% C.) Throughout the tests 60-psig steam was passed through the pipes, and tap water was sprayed on their surfaces.

Examination of the pipes after test by the Super-Pentrex dye-penetrant technique showed cracking of all the type 347 stainless steel pipes, except the two pipes which had been fully annealed after bending and the one pipe which had been shot-peened to place the surface under compressive stresses. It was interesting to note that the greatest cracking frequency was observed on the pipes which had been subjected after bending to a sensitizing temperature of 1250°F. There appeared to be fewer cracks in the specimens that had been subjected to 750°F than in the specimens that had received a 600°F treatment. The cracks were on the tension side of the stressed pipes; no cracks were found on inner surfaces that were under compressive stress. A considerable amount of pitting attack was present on all type 347 stainless steel pipes, and, in instances where cracks were formed, the pits were intimately associated with the crack area. Numerous cracks passed directly through pit sites, but there was no positive indication that cracking originated from pit sites.

Modified type 430 stainless steel and titanium did not develop cracks, although pitting was apparent in both materials. These two materials will be subjected to further testing, as will type 347 stainless steel.

11.2.3 Stress-Corrosion Cracking in High-Temperature, Chloride-containing Water

Preliminary studies have begun on methods of reducing or eliminating stress-corrosion cracking of austenitic stainless steel in high-temperature waters containing low concentrations of chloride ions. To date it has been demonstrated that annealed type 347 stainless steel sheet cold-formed into U-bends, with the open ends drawn partially closed by means of stainless steel tie bolts, will crack consistently in a solution containing 100 ppm chloride (50 ppm chloride added as sodium chloride and 50 ppm added as hydrochloric acid, pH = 2.8) and oxygen at 300°C. All 26 specimens exposed in the solution phase cracked in 100 to 300 hr. Of the 22 specimens

Table 11.3. Stress-Corrosion Cracking of Steam-Heater Type 347 Stainless Steel and Other Materials Externally Cooled for 1000 hr by Chloride-containing Filtered Water

Material	Number of U-Bends	Initial Treatment	Observations
Type 347 stainless steel	3	Cold formed; no heat treatment; lightly pickled in HNO_3-HF	Numerous cracks on all three U-bends; many pits in crack areas
Type 347 stainless steel	2	Cold formed; sensitized for 1 hr at 1250°F; air cooled; pickled in HNO_3-HF	Cracking frequency greater than on as-bent pipes; many deep pits associated with cracks and elsewhere
Type 347 stainless steel	2	Cold formed; heated for 24 hr at 600°F; air cooled; pickled in HNO_3-HF	Numerous cracks on both specimens; many deep pits in crack areas
Type 347 stainless steel	2	Cold formed; heated for 12 hr at 750°F; air cooled; pickled in HNO_3-HF	Less cracking than observed on 600°F-treated U-bends; many pits
Type 347 stainless steel	2	Cold formed; annealed for ½ hr at 1950°F; water cooled; pickled in HNO_3-HF	No apparent cracks; many pits
Type 347 stainless steel	1	Cold formed; lightly grit-blasted; shot-peened	No apparent cracks; some pitting attack
Type 430 stainless steel (modified)*	1	Cold formed; pickled in HNO_3-HF	No apparent cracks; some pitting attack
MST Gr 3 Ti	1	Cold formed	No apparent cracks; random pitting

*Chemical composition: 16.1% Cr, 0.86% Ni, 0.024% C.

exposed in the vapor phase, 14 developed cracks and 8 did not. Oxygen partial pressures ranging from a few psi to 150 psi have been used, and no direct correlation seems to exist between oxygen concentration and cracking.

Further work is in progress to define the conditions necessary to produce cracking and to evaluate the effectiveness of inhibitors, cathodic protection, preformed films, removal of oxygen, etc., in preventing stress-corrosion cracking of type 347 stainless steel in chloride-containing environments.

11.2.4 Testing of Zirconium Alloys

In cooperation with the HRP Metallurgy Group a number of different zirconium-base alloys have been tested in oxygenated uranyl sulfate solution. In addition to supplying information on the general corrosion resistance of the various alloys, the test program was designed to furnish corrosion specimens for study of the oxide film structure by x-ray and electron diffraction techniques. Specimens were exposed for two periods, 100 hr and a maximum of 1000 hr. Results of the electron and x-ray examinations are not yet available.

The specimens were exposed in oxygenated 0.04 *m* UO_2SO_4 solution containing 0.02 *m* H_2SO_4 and 0.005 *m* $CuSO_4$ at 300°C. In some cases both mechanically polished and chemically polished surfaces were used. The mechanically polished specimens were abraded on 180-grit paper; the chemical polishing was done in a nitric-sulfuric-hydrofluoric acid solution.

The observed corrosion data for the longer exposure periods are shown in Table 11.4. The weight changes were obtained in the as-removed condition; no attempt was made to defilm the specimens. From the table it is apparent that all the alloys showed reasonably good corrosion resistance and exhibited no localized attack.

Table 11.4. Corrosion of Zirconium-Base Alloys by Oxygenated 0.04 *m* UO_2SO_4–0.02 *m* H_2SO_4–0.005 *m* $CuSO_4$ Solution at 300°C

Test No.	Material Identity	Alloy Composition (wt %)	Heat Treatment	Specimen Condition	Total Time (hr)	Observed Weight Change (mg/cm^2)	Specimen Condition
S-74	Zr-42	33 Nb–67 Zr	No heat treatment; cold-rolled directly from casting to 0.06 in. thick	Mechanically polished	804	+0.3* +0.1*	Dull, medium-dark-gray uniform film; uniform attack
S-16	Zr-42	33 Nb–67 Zr	Same as above	Chemically polished	1000	+0.5	Lustrous brown and gray thin film; uniform attack
S-78	Zr-18	10 Mo–90 Zr	Hot-rolled at 700°C to 0.1 in.; cold-rolled to 0.06 in.	Chemically polished	804	–5.8* –7.4*	Mottled green and brown film; surfaces heavily roughened; uniform attack
S-71	Zr-12	5 Mo–10 Nb–85 Zr	Homogeneized for 7 hr at 1175°C; water quenched; cold-rolled to 0.1 in.	Mechanically polished	804	–0.2 Negligible*	Dull yellow and brown streaked film; uniform attack
S-13	Zr-12	5 Mo–10 Nb–85 Zr	Same as above	Chemically polished	1000	–3.0	Mottled gray and green film; uniform attack
S-73	Zr-17	5 Mo–15 Nb–80 Zr	Homogeneized for 2 hr at 1175°C; water quenched; cold-rolled to 0.1 in.	Mechanically polished	804	+0.3	Semilustrous dark-brown and black film; uniform attack
S-15	Zr-17	5 Mo–15 Nb–80 Zr	Same as above	Chemically polished	1000	–1.9	Mottled gray and black film; uniform attack
S-81	Zr-47	7 Mo–20 Nb–73 Zr	No heat treatment; cold-rolled directly from casting to 0.1 in.	Chemically polished	804	+0.1	Lustrous dark-gray film with yellow streaks; uniform attack
S-72	Zr-14	5 Mo–10 Nb–5 Ta–80 Zr	Homogeneized for 7 hr at 1175°C; water quenched; cold-rolled to 0.1 in.	Mechanically polished	804	+0.2	Dull dark-brown and black film; uniform attack
S-14	Zr-14	5 Mo–10 Nb–5 Ta–80 Zr	Same as above	Chemically polished	1000	–1.9	Mottled dark-gray and black film; uniform attack
S-75	Zr-67	3 Sn–15 Nb–82 Zr	No heat treatment; cold-rolled directly from casting to 0.06 in.	Mechanically polished	804	+0.4* +0.5*	Dark-gray film with white streaks; uniform attack
S-17	Zr-67	3 Sn–15 Nb–82 Zr	Same as above	Chemically polished	1000	+0.8	Mottled gray and black film; uniform attack

*Duplicate specimens.

However, previous experience showed that Zircaloy-2, under similar conditions, undergoes less attack than any of the alloys listed. The corrosion behavior of binary alloys of zirconium with palladium, manganese, titanium, indium, uranium, platinum, chromium, and silicon will also be tested.

11.2.5 Effect of Heat Treatment and Surface Finish on the Corrosion of Elgiloy

The behavior of Elgiloy (a spring material considered for use in the HRT liquid-level controller, with a nominal chemical composition in weight per cent of 20 Cr–15 Ni–2 Mn–7 Mo–40 Co) in oxygenated uranyl sulfate solution at 300°C has been described previously.[12] Although the alloy was found to possess satisfactory general corrosion resistance in both solution and vapor phases of 0.04 *m* UO_2SO_4 solution containing 0.02 *m* H_2SO_4 and 0.005 *m* $CuSO_4$, later tests showed the alloy to be susceptible to stress-corrosion cracking. Tests during the past quarter were carried out to determine the effects of surface and heat treatments on the susceptibility of the alloy to stress-corrosion cracking.

The results of the tests, with one exception, showed that surface treatment of the Elgiloy had no effect on the cracking tendency. The one exception was the electropolishing of hardened specimens, which prevented cracking in the solution and vapor phases, possibly due to removal of surface stresses. The as-received material, which showed repeated cracking in high-temperature uranyl sulfate solutions, had a hardness of 50 to 51 on the Rockwell C scale; after the alloy was treated at 900°F for 5 hr, it had a hardness of 56 Rockwell C and showed a definite susceptibility to cracking, except when electropolished. On the other hand, annealing the material at 2100°F produced a material in which stress-corrosion cracks have not been observed; the hardness of the annealed material is 85 on the Rockwell B scale. It should be pointed out that no stress had been applied to any of the specimens; hence it is not surprising that the fully annealed material did not show cracks. Further corrosion studies with Elgiloy will depend on whether or not the alloy can be successfully used as a spring material in the annealed condition. If it can, further testing must be done to determine its susceptibility to stress-corrosion cracking when moderate stresses are applied.

11.2.6 Corrosion Tests Related to the HRT Chemical Processing Plant

Corrosion studies related to the chemical processing plant of the HRT have been continued.[13] With the decision to use stabilized Carpenter-20 stainless steel for fabrication of a number of components, such as tanks, pumps, and valves, studies were initiated during the past quarter to examine the corrosion behavior of Carpenter 20-Cb specimens that were representative of the materials being used in the fabrication of the above components. The corrosive environment was a solution of boiling and oxygenated 4 *M* H_2SO_4 containing the following simulated fission and corrosion products:

	Concentration (g/liter)		Concentration (g/liter)
$Zr(SO_4)_2$	56	$Ru(SO_4)_2$	0.4
Fe_2SO_4	75	UO_2SO_4	28
Cr_2SO_4	24	$CuSO_4$	1.5

Table 11.5 gives a description of the original form of the material and the observed corrosion rates. All the specimens, with the exception of the welded pipe joint and specimen B, showed uniform corrosion attack, with no evidence of cracking at locally stressed areas. At the end of the report period the observed corrosion rates were either decreasing slightly or remaining constant with time.

The welded pipe joint was ¾-in. sched-40 Carpenter 20-Cb stainless steel welded with Carpenter 20-Cb rod to type 347 stainless steel pipe of comparable size. The circumferential weld metal exhibited crater corrosion attack at several sites. The longitudinal weld in the Carpenter 20-Cb pipe showed a prominent knife-line attack in the base metal immediately adjacent to the weld. The weld metal also exhibited a narrow band of highly localized attack extending along the center of the weld. At the end of the report

[12] J. L. English and J. C. Griess, *HRP Quar. Prog. Rep. Jan. 31, 1956*, ORNL-2057, p 86.

[13] H. C. Savage *et al.*, *Quarterly Report of the Solution Corrosion Group for the Period Ending October 31, 1956*, ORNL CF-56-10-13, p 18–23.

Table 11.5. Corrosion of Carpenter 20-Cb Stainless Steel in 4 *M* H_2SO_4 Solution Containing Simulated Fission and Corrosion Products

Temperature: Boiling (111°C)
Atmosphere: Oxygen

Specimen Identification	Original Material Description	Total Test Time (hr)	Corrosion Rate (mpy)
B	$2\frac{1}{4}$-in. square bar	214	7.5
O	$3\frac{1}{4}$-in. square bar	214	3.2
Ⓑ	$3\frac{1}{4}$-in. square bar	214	3.3
P	$2\frac{1}{4}$-in. square bar	214	3.1
M	$2\frac{1}{4}$-in. square bar	214	2.8
Welded joint of Carpenter 20-Cb and type 347 stainless steel		266	20.4

period the observed corrosion rate of 20 mpy for 266 hr was decreasing with increased exposure time. One of the duplicate specimens identified as B in Table 11.5 had two deep pits on one surface and apparent cracking across an edge. The network of cracks also extended into the flat surface of the specimen. Neither pitting nor cracking was observed on any of the other Carpenter 20-Cb stainless steel specimens.

Other tests carried out with a variety of materials in boiling and oxygenated 4 *M* sulfuric acid free of added fission and corrosion products produced corrosion results similar to those previously reported for the same solutions free of oxygen.[13] The corrosion rates observed in the oxygen-containing solutions were, with the exception of Carpenter 20-Cb, which exhibited improved general corrosion resistance, a factor of 2 to 50 times greater than in the 4 *M* H_2SO_4 solution free of oxygen. Even though the over-all corrosion rate of Carpenter 20-Cb was lowered in the presence of oxygen, its susceptibility to stress corrosion was not reduced. Numerous cracks were observed in highly stressed areas of Carpenter 20-Cb stainless steel.

Some of the Carpenter 20-Cb specimens referred to in this report are undergoing further testing. In addition, numerous specimens will be tested in 4 *M* H_2SO_4 solutions at 100°F, both with and without added fission and corrosion products. Since the decay storage tanks of the chemical plant will be cooled, it is probable that the 100°F tests will be more indicative of the corrosion rates to be expected in the chemical plant than are the boiling tests.

12. SLURRY CORROSION

E. L. Compere
H. C. Savage
S. R. Buxton
S. A. Reed
G. E. Moore
J. A. Russell, Jr.
R. M. Pierce[1]
R. M. Warner
W. C. Ulrich

12.1 PUMP LOOPS

12.1.1 100A Pump Loops

Four additional dynamic slurry corrosion tests were made in 100A pump loops BS and CS during the quarter. In loop BS, two tests – BS-7, a 194-hr test, and BS-8, a 334-hr test – were made at 300°C with oxygen added at charge concentrations of approximately 500 g of thorium per kilogram of H_2O; the slurry was made from 800°C-calcined thorium oxide prepared at ORNL. In both tests the 100A pump was operated at half the normal rotational speed to minimize bearing wear and possible caking on the pump impeller by centrifugal action. In run BS-8 a solution of Na_2SO_4 was added to the loop to provide about a 0.02 *m* concentration of SO_4^{--}.

Runs CS-32 and CS-33, of 139- and 190-hr duration, respectively, were made in loop CS at 300°C with the addition of hydrogen (and hydrazine) to determine the corrosion effects of aqueous slurry under reducing conditions. The charge concentration for each test was approximately 500 g of thorium per kilogram of H_2O. Slurry for these tests was prepared from a different batch of 800°C-calcined, ORNL-produced thorium oxide. Specimen corrosion rates for the four runs are given in Table 12.1.

The slurry used in runs BS-7 and BS-8 was prepared from batch LO-14 thorium oxide, which was made at ORNL by oxalate precipitation of thorium nitrate and final calcination at 800°C. This same slurry, which was circulated in two previous tests[2] at 250°C, had formed spheroidal agglomerates ranging in size from 7 to 20 μ during circulation and had been deposited as hard, tenacious cakes in the centrifugal pump and in the loop piping. Run BS-7 was made to determine whether similar effects would occur at 300°C. To minimize possible centrifugal deposition of slurry in the pump and to prevent severe damage to the Al_2O_3 pump bearings should such deposits occur, the pump was operated at half speed, 1800 rpm, with 30-cycle current provided by a motor-generator set.

Two sets of pin-type corrosion specimens in holders of different annuli were placed in the main line at a flow of 13 gpm (11 and 22 fps), and one set of pin specimens was placed in the return line at a flow of 25 gpm (31 fps). Flow through the mixing line was 12 gpm. All flow measurements were made with water at room temperature with the pump operating at 1725 rpm. A 32-hr performance test on oxygenated water at 300°C was made before slurry was charged to the system. Slurry was added to the loop in a routine manner while it was operating at 300°C and 1350 psi pressure. Two additions were required to charge the 9.73 kg of thorium oxide to provide a calculated load concentration of 645 g of thorium per kilogram of H_2O.

The sampled concentration of the system varied widely during the test. Also, slurry spheroids were formed during circulation. By chemical analysis the circulating slurry varied from an initial concentration of 722 g of thorium per kilogram of H_2O to a maximum of 1052 g/kg after 25 hr of circulation. It was found that coincident with these fluctuations in concentration the slurry interface, detected by a G-M survey meter, in the vertical loop pressurizer rose or fell with decreasing or increasing concentration. Also, the larger spheroids were detected in samples of highest concentration. By microscopic examination, some slurry samples were found to contain spheroids as large as 80 μ.

Presumably, the concentration effects were caused by spheroid growth. It can be shown that, under the conditions of operation, spheroids of 25 to 80 μ entering the pressurizer via the system mixing line would settle at a more rapid rate than the net downward flow of liquid through the pressurizer, which would effectively strip part of the solids from the vertical pressurizer and cause them to be concentrated in the main loop piping.

[1] On loan from TVA.

[2] E. L. Compere *et al.*, *HRP Quar. Prog. Rep. Oct. 31, 1956*, ORNL-2222, p 81; *HRP Dynamic Slurry Corrosion Studies: Quarter Ending October 31, 1956*, ORNL CF-56-10-14 (to be issued).

Table 12.1. Corrosion of Metal Specimens by Thorium Oxide Slurries in Various 100A Loop Runs at 300°C

Run			BS-7	BS-8	CS-32	CS-33
Grams of Th per kilogram of H_2O (av)			841	484	410	347
Oxide batch			LO-14	LO-14	LO-2A	LO-2A
Additives			O_2	O_2, Na_2SO_4	A + H_2; N_2H_4	A + H_2; N_2H_4
Hours			194.2	334.8	139.3	190.4
Alloy	Specimen Type	Velocity (fps)	Mean Attack Rate (mpy) (defilmed)			
Austenitic stainless steels	Pin	10–12	2.3	2.2	0.4	0.8
	Pin	20–23	4.7	9	1.1	0.8
	Pin	29–31	4.9	10		
	Coupon	41–43			15	8
Armco iron and A212 B carbon steel	Pin	10–12	19	18	25	17
	Pin	20–23	19	14	47	34
	Pin	29–31	24	13		
	Coupon	41–43			110	48
Titanium and alloys	Pin	10–12	WG;* 1.6	5	WG	2.4
	Pin	20–23	0.9	7	2.6	2.1
	Pin	29–31	4.5	9		
	Coupon	41–43			10	6
Zircaloy-2 and zirconium	Pin	10–12	WG	0.2	WG	WG
	Pin	20–23	1.0	1.1	WG	0.5
	Pin	29–31	1.5	1.4		
	Coupon	41–43			7	2.8

*WG = Weight gain shown by defilmed specimens.

The run was terminated after 194 hr of slurry circulation because of increased pump power demand and a pulsating noise in the pump. Inspection of the system after it was drained and then rinsed with water revealed deposits of thoria on the pump impeller and in the pump suction nozzle. The deposits in this run at 300°C appeared identical to those that formed in previous runs[2] at 250°C with the same slurry, LO-14.

In general, the attack of all specimens was substantially lower than the rates observed in past tests under the same conditions and with the use of a similarly prepared thoria. Attack of system components, with the exception of the front sintered Al_2O_3 pump bearing, was moderate. The front Al_2O_3 bearing was not re-usable. Wear was severe but uniform with no evidence of grooving or chipping. The associated Al_2O_3 journal was unaffected. The bearing and journal had run for 230 hr in slurry and for 445 hr in water before failure occurred. Generalized loop attack, based on analysis of slurry samples, was 0.6 mpy.

Run BS-8 was the first test of a series of three proposed runs in loop BS in which an intentional addition of sulfate ion will be made to slurry prepared from batch LO-14 thorium oxide. For run BS-8, SO_4^{--} was added as sodium sulfate. In subsequent tests sulfate will be added as sulfuric acid and as thorium sulfate.

Three sets of pin corrosion specimens were inserted in the test loop. Two sets were placed in the main line at a flow of 12 gpm (10 and 20 fps), and one set was placed in the return line at a flow of 24 gpm (29 fps). Flow through the mixing line

was 12 gpm. Pump operation was at 1725 rpm. A 77-hr performance test with oxygenated water at 300°C was made before the slurry was charged.

Thirty minutes before the slurry was charged, a solution containing approximately 45 g of sodium sulfate was injected into the loop to provide approximately 4000 ppm of SO_4^{--} (based on thorium oxide). The system was then charged with 7.9 kg of batch LO-14 thorium oxide for a load of 512 g of thorium per kilogram of H_2O. Slurry was circulated for a period of 334.8 hr at an average concentration of 484 g of thorium per kilogram of H_2O.

By microscopic examination, slurry spheroids ranging from 4 to 16 μ were detected in the first sample, withdrawn from the system after 4 hr of circulation. No apparent spheroid growth was noted in the samples taken after 22.6 and 46.4 hr of circulation. However, in the fourth sample, taken after 94.1 hr of slurry circulation, the majority of the spherical bodies were 8 to 30 μ. At this time about 90% of the sample was composed of spheroids. Another sample, taken 72.1 hr later (166.2 total circulation hours), contained only spheroids of 5 to 20 μ. No further sphere growth was noted during the balance of the run. The cause of this phenomenon is not known.

The austenitic stainless steels and titanium specimens showed higher attack rates than in previous tests without sulfate, but none of the observed rates were excessive. The generalized loop attack rate was 4.2 mpy, of which about 90% could be attributed to attack on the pump impeller.

The pump was found to be in excellent condition after the test, except that the cast stainless steel impeller had lost 32 g, with no localized attack. Graphitar 14 bearings and Stellite journals were employed in this run and were undamaged. The pump was operated with 30-cycle current.

The slurry charge for runs CS-32 and CS-33 was prepared from a different lot of 800°C-calcined, ORNL-produced thoria designated as batch LO-2A. Material from this batch had been circulated in one previous test[3] in loop CS at 300°C with an oxygen overpressure. No spheroid formation had been observed.

Runs CS-32 and CS-33 were made in order to observe the corrosion effects of aqueous thoria slurry in a reducing atmosphere. For these tests the loop was charged with the appropriate volume of water and then alternately evacuated and purged with argon to remove residual air in the system. Ten milliliters of 85% hydrazine hydrate was then injected into the loop to destroy traces of oxygen dissolved in the water. The quantity of hydrazine added, approximately 400 ppm, was a twentyfold excess over the calculated quantity needed to react with dissolved and residual gaseous oxygen. Then, 30 psig of hydrogen and 90 psig of argon were charged to the system at room temperature. Argon was used to prevent gas binding and to ensure thermal circulation through the condenser in the pump purge system.

Before the slurry was added in run CS-32, a 72-hr performance test at 300°C and 1400 psig was made. A gas sample taken during this period contained, by chemical analysis, <1 ppm of oxygen. Two batch additions of slurry, containing a total of 8.22 kg of LO-2A thorium oxide, were charged to the system to provide a calculated load concentration of 498 g of thorium per kilogram of H_2O. Five milliliters of 85% hydrazine hydrate was added to each slurry charge.

Slurry circulation proceeded routinely for 134 hr. After 135 hr of circulation the system pressure fell rapidly, pump cavitation began, and a small leak was located in the top flange of the loop pressurizer. Therefore the test was terminated after 139.3 hr of slurry circulation.

No spheroid formation or particle growth was noted during the test. The average particle size of the final sample of slurry withdrawn from the loop just before shutdown was <0.7 μ. With the addition of hydrazine, which was partially decomposed to ammonia at the operating temperature, the room-temperature pH values of slurry samples ranged from an initial 10.2 to a final 9.3.

A gradual decrease in the circulating slurry concentration, from an original 493 to a final 404 g of thorium per kilogram of H_2O, occurred during the run. This gradual loss of solids during circulation has been typical of CS-loop runs. It is known that slurry accumulates in the annulus in each sample barrel in the system and that the extent of the accumulations varies with both slurry concentration and velocity. The deposits are not cakes or plugs. Flushing of these areas with water during the regular loop rinsing procedure normally removes the accumulations readily. The loop piping is being revised to prevent solids holdup in these areas.

[3] E. L. Compere *et al.*, *HRP Quar. Prog. Rep. July 31, 1956*, ORNL-2148, p 83.

Attack of pin specimens of the austenitic stainless steels, titanium, and Zircaloy at flow velocities of 11 and 23 fps was quite low. The carbon-steel pins reflected a definite velocity effect, and the defilmed rates were lower than rates observed previously at the same velocities in oxygenated runs.

Coupon specimens exposed at 41 fps showed rather high corrosion rates. Weight-loss data of type 347 stainless steel and of mild-steel coupons placed in the first two upstream positions of the specimen holder, when compared with duplicate specimens in downstream positions, reflected marked entrance effects. However, attack of the leading coupons was quite uniform.

Corrosion rates of type 347 stainless steel and Zircaloy-2 coupons, which were fabricated with weld beads placed at right angles to slurry flow, were generally higher than rates obtained with smooth coupons in the same holder. Examination of the welded specimens revealed areas of localized attack immediately behind the weld beads.

Run CS-33 was a duplicate of run CS-32. The purging, charging procedure and conditions of operation were identical. The loop was charged with slurry prepared from batch LO-2A thoria to provide a calculated load concentration of 529 g of thorium per kilogram of H_2O. A 27-hr performance run on water was made at 300°C before the slurry was charged.

Operation was routine for the initial 189 hr, at which time the fifth slurry sample was withdrawn from the loop. After sampling, the high-pressure sample valve could not be properly secured; so the run was terminated.

Microscopic examination of slurry samples taken periodically during the test revealed the formation of small spheroids estimated to be between 4 and 8 μ. No apparent growth took place.

There was a gradual downward trend in circulating concentration during the run period, which was attributed to holdup in the annuli of the vertical specimen holders. No cakes or deposits were found in the system after it was rinsed.

In general, pin attack rates of the austenitic stainless steels, titanium, Zircaloy-2, and mild steels at 12 and 23 fps were low and in good agreement with previously observed rates. Attack rates of coupon specimens at 43 fps were also in good agreement with previously observed rates. Entrance effects were notable on the type 347 steel leading coupon. Some abrasive attack was evident.

The two sets of titanium wear rings used in the 100A pump during runs CS-32 and CS-33 appeared to be quite brittle when the pump was dismantled for inspection. The rings are currently being examined by the Metallurgy Group for evidence of hydrogen embrittlement. Preliminary vacuum-fusion analyses of several of the rings indicated considerable hydrogen pickup.

In both runs CS-32 and CS-33 the same Al_2O_3 bearings and journals were used, and the pump was operated on 60-cycle current. No damage to the bearings was observed in these runs, and they were in suitable condition for use in subsequent runs.

12.2 TOROIDS

The physical examination of a type 347 stainless steel toroid that had circulated aqueous thorium oxide slurries for approximately 4000 hr has been described.[4] A metallographic examination of this toroid has now been completed, and another toroid of similar operating history has also been examined in detail.

The effect of circulating time on the degradation of two thorium oxides of different maximum calcination temperature by circulation of their aqueous slurries in toroids has been studied. Also investigated was the correlation between circulating time, particle size, and attack rate on selected corrosion pin specimens.

Due to the observation of spheroid formation in 100A loops by batch LO-14 thorium oxide (reported in the last quarterly report), this oxide was studied in toroids and compared with the "standard" oxide, which also had shown this unusual behavior in loops and in toroids.

12.2.1 Toroid Examination

The results of a superficial, physical examination of the interior surfaces of a type 347 stainless steel toroid, in which various aqueous thorium oxide slurries had been circulated for 4883 hr, were previously reported.[4,5] A metallographic examination of this toroid (toroid N) has now been

[4] E. L. Compere *et al.*, *HRP Quar. Prog. Rep. Oct. 31, 1956*, ORNL-2222, p 81.

[5] E. L. Compere *et al.*, *HRP Dynamic Slurry Corrosion Studies: Quarter Ending October 31, 1956*, ORNL CF-56-10-14 (to be issued).

completed,[6] as well as a physical and metallographic examination of another type 347 stainless steel toroid (toroid E) exposed to circulating aqueous thorium oxide slurries for 3860 hr.

Examination of the interior surfaces of toroid N revealed that areas downstream of protuberances were subject to a relatively greater attack than were areas upstream from such projections. The protuberances themselves (the excess metal of the circumferential weld) showed some metal loss. The interior of the pipe contained comet-shaped pits and striae. Metallographic examinations of several sections of toroid N revealed transgranular cracks, which could best be attributed to stress corrosion, probably arising from the presence of chloride ions in one of the aqueous environments. Figure 12.1 illustrates the transgranular nature of the cracks. The larger opening of the crack at the surface of the metal coincided with a stria observed on the surface.

[6]The metallography was carried out by T. M. Kegley, Jr., of the Y-12 Metallography Section of the ORNL Metallurgy Division.

Fig. 12.1 Photomicrograph of Area of Toroid N Showing Transgranular Crack. 250X. Reduced 11%.

The interior of toroid E was not nearly so attacked as that of toroid N. The surfaces were generally covered with a brown film that was considerably darker upstream of protuberances and much lighter downstream. A very slight loss of surface metal appeared to have occurred just downstream from projections (excess metal of circumferential weld and corrosion pin specimens), which resulted in a roughened appearance; small teardrop-shaped depressions were observed more frequently downstream than just upstream from such protuberances. Very few striae were observed. Figure 12.2 shows the extent and nature of the attack on the excess metal of the circumferential weld. Metallographic examination of sections of toroid E, taken from the same relative locations as examined in toroid N, did not reveal any cracks.

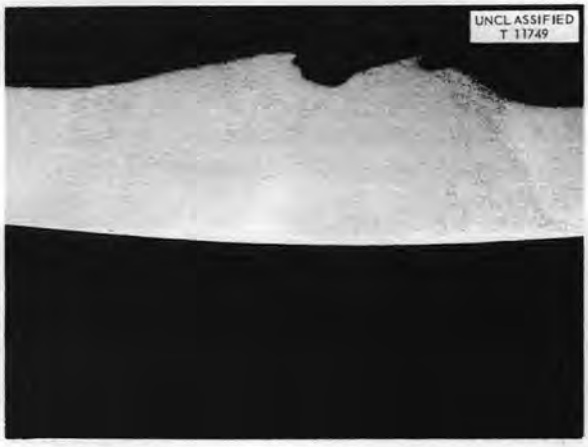

Fig. 12.2 Longitudinal Section of Circumferential Weld of Toroid E. 16X. Reduced 33%.

It is impossible to assign the cause of the stress-corrosion cracking in toroid N to any specific thoria because the toroid was exposed to many environments before it was examined. However, the toroid did circulate a thorium oxide of exceptionally high chloride content (probably 0.3 to 0.8 mg of chloride per gram of thorium oxide) from which a supernatant solution of 963 mg of chloride per liter was obtained after 142 hr of circulation. The oxides circulated in toroid E were all of production-grade material and contained 0.04 to 0.05 mg of chloride, or less, per gram of thorium oxide. Through metallographic examinations of

toroids of history similar to those of toroids N and E, it may be possible to assign unequivocally the cause of this stress-corrosion cracking to a specific thoria.

12.2.2 Effect of Circulation Time

One of the properties of thorium oxide slurries generally noticeably affected by circulation is the size distribution of the oxide particles.[7,8] The influence of the particle size on the erosiveness of thoria slurries was anticipated by Thomas[9] and others,[10] and a positive correlation between size and attack rate was indeed observed.[7]

Because the size of the oxide particles generally decreased during circulation, a greater rate of attack was expected early in the run when the size of the particle was relatively large. As degradation of the particles occurred during circulation, the rate of attack was expected to fall off; some constant level of attack would probably be reached as the dimensions of the oxide became smaller than some "critical" size.

To test this hypothesis, a series of experiments in toroids was made in which the effect that the length of circulation might have on the slurry behavior was studied and the extent of the oxide particle degradation and the rate of attack by the slurry on selected corrosion pin materials were determined. During the tests the following variables were maintained constant: the slurry concentration was approximately 1000 g of thorium per kilogram of H_2O, an oxygen atmosphere was used, and a constant relative velocity of circulation at 26 fps was maintained. Among the variables studied were the length of circulation (50 to 200 hr), the temperature during circulation (100 and 250°C), the maximum calcination temperature of the thorium oxide (800 and 1200°C), the alloy under test (type 347 stainless steel and titanium 75A), and the difference between raw slurry and slurry previously circulated in toroids.

Oxygen was supplied to the toroids by the thermal decomposition of hydrogen peroxide, a reaction that apparently occurred in this system even at 100°C. The 100°C temperature resulted merely from slurries of 1000 g of thorium per kilogram of H_2O being circulated at 26 fps relative velocity in toroids; no heat from an external source was added. After the desired period of circulation all the corrosion pin specimens were removed for evaluation and were replaced with new specimens. Instead of replacing each of the slurries after every run, some were recirculated in the next run in order to compare the effects of a precirculated slurry with those of a raw (not circulated) slurry.

The particle-size distribution of the circulated slurries was determined[11] by gravitational sedimentation in 0.001 *M* $Na_4P_2O_7$. Such results showed that degradation of any particular oxide to a constant size under the described conditions was accomplished within 50 hr. The temperature during the circulation had little effect upon the ultimate size of the oxide. As reported previously,[7] the oxide calcined at the lower temperature (800°C) appeared to be degraded to a slightly greater extent (from an average particle diameter of ~2.1 to ~0.6 μ) than the oxide calcined at the higher temperature (1200°C; from ~2.3 to ~0.9 μ).

The pH of the slurries after the runs varied from about 5.5 to 8.2. All the circulated slurries seemed thick at room temperature, which agreed with previous results correlating slurry thickness and particle size.[4] The slurry of the 800°C oxide which had circulated at 100°C appeared considerably thicker at room temperature than when the circulation had been carried out at 250°C or when the 1200°C oxide was circulated at either 100 or 250°C.

Except for a single case (discussed below) the defilmed weight losses of the corrosion pin specimens of type 347 stainless steel and titanium 75A were quite small. The weight-loss data per unit of exposed area (mg/dm^2) were plotted against time (hours) in order to evaluate the attack rates. Almost all the data yielded straight lines on such a plot when the precision of such measurements was taken into account (estimated to be about ±14 mg/dm^2); the slope of these lines yielded the corrosion rate. The weight-loss data of type 347 stainless steel exposed to raw slurry (800 and 1200°C calcination) at 250°C did not show such a

[7] E. L. Compere *et al.*, *HRP Dynamic Slurry Corrosion Studies: Quarter Ending July 31, 1956*, ORNL CF-56-7-51, p 20 ff.

[8] C. E. Schilling, *HRP Quar. Prog. Rep. Oct. 31, 1955*, ORNL-2004, p 179.

[9] D. G. Thomas, *Comments on the Erosiveness of ThO_2 Slurries*, ORNL CF-55-4-36 (April 5, 1955).

[10] G. E. Moore and E. L. Compere, *HRP Quar. Prog. Rep. July 31, 1955*, ORNL-1943, p 140.

[11] G. W. Leddicotte and H. H. Miller, *Anal. Chem. Semiann. Prog. Rep. Oct. 20, 1954*, ORNL-1788, p 21 (Classified).

linear dependence on time until a transient initial period was completed; the corrosion rates in these cases were calculated from the straight lines obtained by neglecting the first 50 hr of exposure.

The corrosion rates calculated as just described are given in Table 12.2. Included in the table are the average particle diameters either determined directly or inferred from comparable experiments. Inspection of the table reveals that those runs carried out near 100°C gave attack rates on both type 347 stainless steel and titanium 75A that were consistently smaller than obtained under similar conditions but when the circulating temperature was near 250°C; the differences were small, however. The slurries of 1200°C oxide gave the same or smaller attack rates than slurries of the 800°C oxide; again the differences were small.

The correlation between particle size (degradation of the thorium oxide) and the attack rate can best be shown by consideration of short exposure times (for example, 50 hr) as demonstrated in Table 12.3. Thus a slurry containing thorium oxide of relatively small and constant average particle diameter (a precirculated slurry) gave attack rates on type 347 stainless steel of about 1 mpy (800°C oxide) or 6 mpy (1200°C oxide) for a raw slurry which was degraded during the exposure. Similar but less pronounced results were obtained with titanium.

For longer periods of circulation (147 hr) there was little difference in rates between a precirculated and a raw slurry, probably because the time which was required to degrade the particles (and during which enhanced attack took place) was small compared with the total elapsed time of the run.

Thus the parabolic curves, obtained on plotting the weight loss per unit of exposed area vs time, may be explained. The weight loss was rapid until degradation of the oxide below the critical size had occurred; the loss of metal then took place much more slowly and linearly with time.

Observations and conclusions similar to those presented above were reported in 100A loop slurry studies.[12]

The only exception to the general statement that the attack rates were relatively low occurred in a single run in which it is believed that oxygen was absent. Both the stainless steel and titanium pins were much more severely attacked (about 28 mpy

[12] E. L. Compere *et al.*, *HRP Quar. Prog. Rep. Oct. 31, 1956*, ORNL-2222, p 81.

Table 12.2. Summary of Toroid Experiments Studying the Effect of Circulation Time of Aqueous Thorium Oxide Slurries

Concentration: 1000 g of Th per kg of H_2O; D-17 thorium oxide
Relative velocity: 26 fps
Atmosphere: Oxygen

Oxide Calcination Temperature (°C)	History	Range Circulation Time (hr)	Nominal Temperature (°C)	Average Particle Diameter* (μ)		Graphical Attack Rate** (mpy)	
				Original	Final	347 SS	Ti-75A
800	Raw	50–195	100	2.1	0.6	2	1.5
		50–147	250	2.1	0.6	1.5	8
	Precirculated	121–195	100	0.6	0.6	1.0	1.0
		50–208	250	0.6	0.6	4	8
1200	Raw	50–195	100	2.3	0.8	0.5	1.0
		50–208	250	2.3	1.0	2	2
	Precirculated	121–195	100	0.8	0.8	0.5	1.0
		50–208	250	0.8	0.9	3	1.5

*By gravitational sedimentation in 0.001 *M* $Na_4P_2O_7$ (see ref 8).

**Slope of weight loss per unit exposed area vs time plots; incremental rate values for indicated time periods are given.

Table 12.3. Effect of the Thorium Oxide Particle Size in Circulating Aqueous Slurries on the Rates of Attack of Selected Alloys

Concentration: 1000 g of Th per kg of H_2O; D-17 ThO_2
Relative velocity: 26 fps
Temperature: 250°C
Atmosphere: 100-psi oxygen (250°C)
Toroid: Type 347 stainless steel

Circulation (hr)	Calcination Temperature (°C)	Average Particle Diameter (μ)		Particles (wt %) >3-μ Diameter		Pin Specimen Attack Rate (mpy)	
		Original	Final	Original	Final	347 SS	Ti-75A
50	800	2.1	0.6	37	14	11,12	7,8
		0.6	0.6	10	10	1,1	4
	1200	2.3	1.1	39	15	5,6	4,6
		0.9	1.0	13	15	0,0	1,3
147	800	2.1	0.6	37	10	2,5	7
		0.6	0.6	12	10	3,4	4,7
	1200	2.3	0.9	39	13	2,3	2,3
		0.9	0.9	9	13	0,3	2,2

for the steel and 10 mpy for the titanium) than pins from other runs and in appearance suggested immediately that little or no oxygen had been present during the run. The slurry in this run also suggested a lack of oxygen (gray rather than cream in color). The observed rates for the stainless steel agreed with values previously obtained in oxygen-depleted or absent systems.[7,13]

12.2.3 Batch LO-14 Thorium Oxide

Tests with aqueous thorium oxide slurries had been carried out in 100A loops with batch LO-14 thorium oxide and gave results that were unique compared with those from runs with other LO-batch oxides.[12] The runs with the batch LO-14 oxide, however, were similar to tests with the "standard" slurry in that both materials produced hard deposits and gave high attack rates. Circulation of the batch LO-14 slurry in 100A loops led to particle growth, which, at the time, was believed to be a most unusual occurrence.

The rather unique behavior of slurries of the batch LO-14 oxide in 100A loops led to its investigation in toroids. The present section describes a few tests evaluating the batch LO-14 oxide; the tests and the results are summarized in Table 12.4.

The first runs with batch LO-14 thorium oxide in toroids were carried out at low velocities (10 fps) in an attempt to produce particle growth as was shown to occur under these conditions with the standard slurry.[4,5] The batch LO-14 oxide behaved in a perfectly "normal" manner: it became degraded during circulation even though corrosion pin specimens were absent in some runs in order to eliminate impacts (and, therefore, fracturing) of the particles during circulation; it gave attack rates on type 347 stainless steel corrosion pin specimens comparable to those produced by batches D-17 and LO-12 oxides under similar conditions; it did not give deposits of thoria. There was no evidence that batch LO-14 thorium oxide possessed unique properties.

The presence of impurities in the thorium oxide (probably added during circulation) was suggested as a possible cause of the unusual behavior shown by the standard oxide.[5] Aluminum had been considered as one of several ions whose presence might alter the behavior of an aqueous thorium oxide slurry. This hypothesis was tested by adding calcined aluminum oxide to a slurry of batch LO-14

[13] G. E. Moore and E. L. Compere, *HRP Quar. Prog. Rep. Oct. 31, 1954*, ORNL-1813, p 100.

Table 12.4. Effect of Circulation of Batch LO-14 Thorium Oxide Slurries in Toroids

Concentration: 1000 g of Th per kg of H_2O
Atmosphere: 90-psi oxygen (200°C)
Temperature: 200°C
Circulation time: 100 hr
Toroids: Type 347 stainless steel

Relative Velocity (fps)	Oxide	Additive	Average Particle Diameter[a] (μ)		Type 347 SS Attack Rate (mpy)
			Original	Final	
10	LO-14		3.2	2.0	1[b]
	LO-14		3.2	2.3	c
	LO-14	Al_2O_3[d]	3.2	2.7	1[b]
	LO-14	Al_2O_3[d]	3.2	1.7	c
26	LO-14		3.2	4.2[e]	c
	LO-14	Al_2O_3[d]	3.2	0.8	c
	Standard		9–15	0.8[f]	c
	Standard		9–15	0.7	2[b]

[a]By gravitational sedimentation in 0.001 *M* $Na_4P_2O_8$ (see ref 8).
[b]Average of four corrosion pin specimens.
[c]No corrosion pins present.
[d]At concentration of 130 mg of aluminum per kilogram of thorium oxide.
[e]See Figs. 12.4 and 12.5.
[f]See Fig. 12.3.

oxide in an amount to provide an aluminum concentration of about 130 mg per kilogram of thorium oxide (130 ppm, thorium oxide basis). Such an addition did not noticeably affect the behavior of the oxide.

The batch LO-14 oxide was also compared with the standard oxide by circulating them as aqueous slurries at 26 fps relative velocity. The standard slurry behaved in a fashion similar to that previously observed for it under these conditions.[4,5] On the other hand, the batch LO-14 oxide under these conditions behaved in a manner different from that observed for any oxide previously; this unusual behavior may partly be explained by the absence of corrosion pin specimens. Analysis of the particle-size distribution by gravitational sedimentation indicated particle growth, a phenomenon not previously observed at 26 fps relative velocity in the presence of pins. Figures 12.3 and 12.4 are optical photographs[14] of the slurries of standard oxide and batch LO-14 oxide circulated under identical conditions. Probably the most unusual observation of the run was the detection of several exceedingly large particles that were formed during the circulation. Figure 12.5 is a photograph of one of these giant ellipsoids, estimated to be approximately 150 by 200 μ. These particles were relatively easily fractured by slight pressure on the cover glass after they were mounted for photography; they appeared whole, without fractures or cracks, when removed from the toroid prior to mounting.

The presence of about 130 ppm aluminum (as-calcined aluminum oxide based on thorium oxide) produced a more "normal" behavior, although it would be hazardous to attach too great significance to this apparent effect on the basis of only one run. This is especially true since the behavior of pure batch LO-14 oxide by itself was erratic: at

[14]The optical photography was performed by R. S. Crouse of the Y-12 Metallography Section of the ORNL Metallurgy Division.

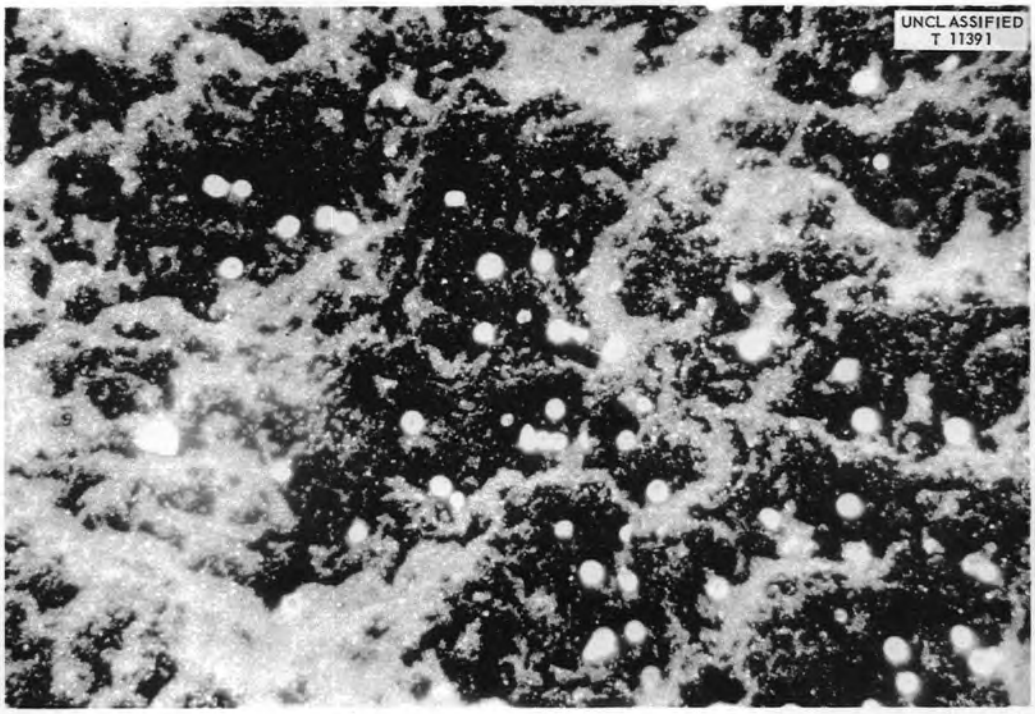

Fig. 12.3. 200A Standard Slurry After Circulation in Toroid at 26 fps Relative Velocity, 200°C, 1000 g of Thorium per Kilogram of Water with Oxygen for 100 hr (No Corrosion Pin Specimens Present). 400X. Reduced 17%.

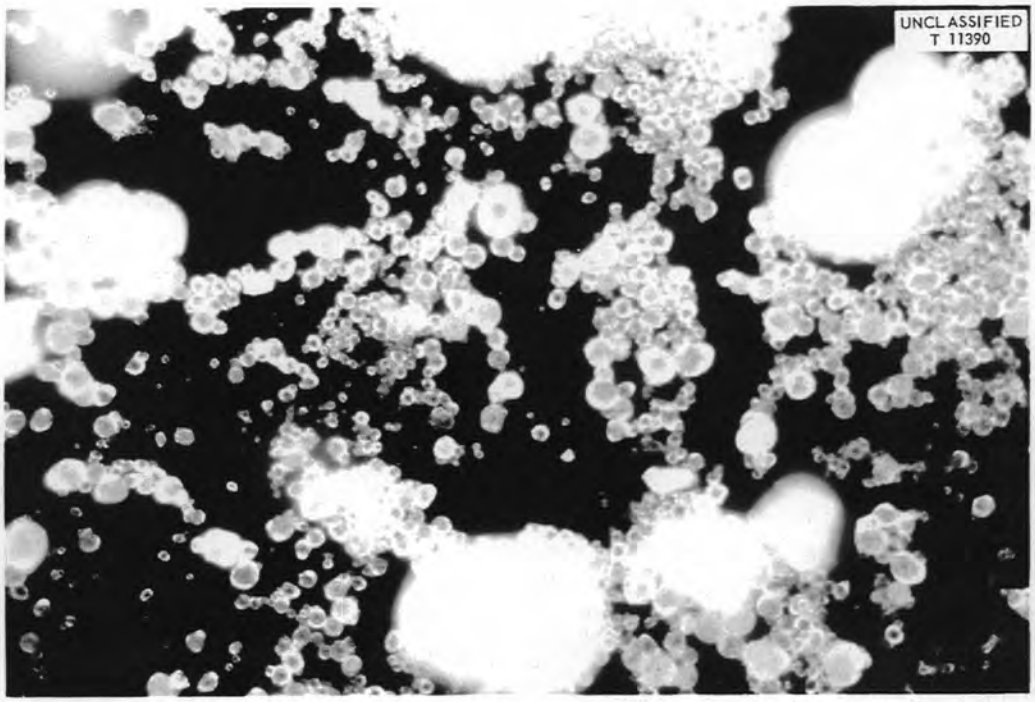

Fig. 12.4. Batch LO-14 Thorium Oxide After Circulation in Toroid at 26 fps Relative Velocity, 200°C, 1000 g of Thorium per Kilogram of Water with Oxygen for 100 hr (No Corrosion Pin Specimens Present). 400X. Reduced 17%.

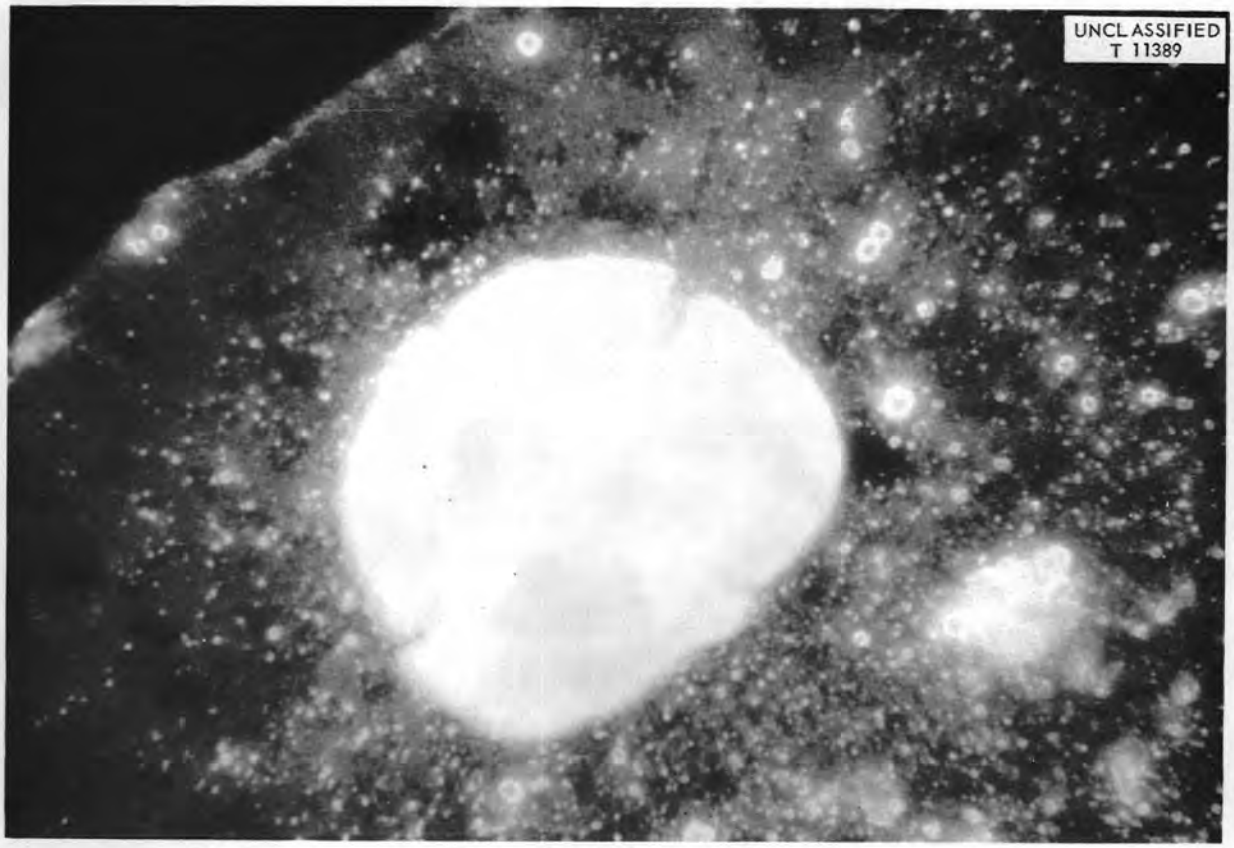

Fig. 12.5. Another Field of Fig. 12.4. 400X. Reduced 2%.

10 fps it behaved as did many "normal" oxides, while at 26 fps it behaved in a completely singular fashion. The influence of the amount and kind of electrolyte associated with thorium oxide (in solution and adsorbed) on the behavior of an aqueous thoria slurry has been reported many times. Many such substances may be generated during circulation and, even though present in small amount, may influence the behavior of the slurry.

12.3 IN-PILE SLURRY TOROID DEVELOPMENT

Since the toroid rotators[15,16] were used successfully in the slurry corrosion program and since they can circulate slurries without pumps, the development of a toroid rotator for radiation-corrosion studies was initiated. During the past quarter, emphasis shifted from the in-pile slurry loop[17] to the in-pile toroid rotator.

The preliminary design effort on the in-pile toroid rotator has been to provide an assembly which will operate within a reactor beam hole, approximately 10 in. in diameter, in the Oak Ridge Research Reactor. A feasibility report[18] on the use of toroids for in-pile dynamic corrosion testing by the British Atomic Energy Research Establishment served as an initial design guide. One experimental model of a toroid rotator has been constructed and is shown in Fig. 12.6. Briefly, the unit consists of two toroids mounted on a suitable holding fixture. Motion is applied to the toroids by means of a drive shaft and gear train. An air-driven motor is used as the power source. This

[15] E. L. Compere *et al.*, *HRP Quar. Prog. Rep. Oct. 31, 1956*, ORNL-2222, pp 88, 92–93.

[16] E. L. Compere *et al.*, *HRP Dynamic Slurry Corrosion Studies: Quarter Ending October 31, 1956*, ORNL CF-56-10-14 (to be issued).

[17] E. L. Compere *et al.*, *HRP Quar. Prog. Rep. Oct. 31, 1956*, ORNL-2222, p 88.

[18] J. R. Cossey and R. Littlewood, *Feasibility Tests on the Use of Toroids for Dynamic Corrosion Testing In-Pile*, AERE-C/M-281 (June 5, 1956).

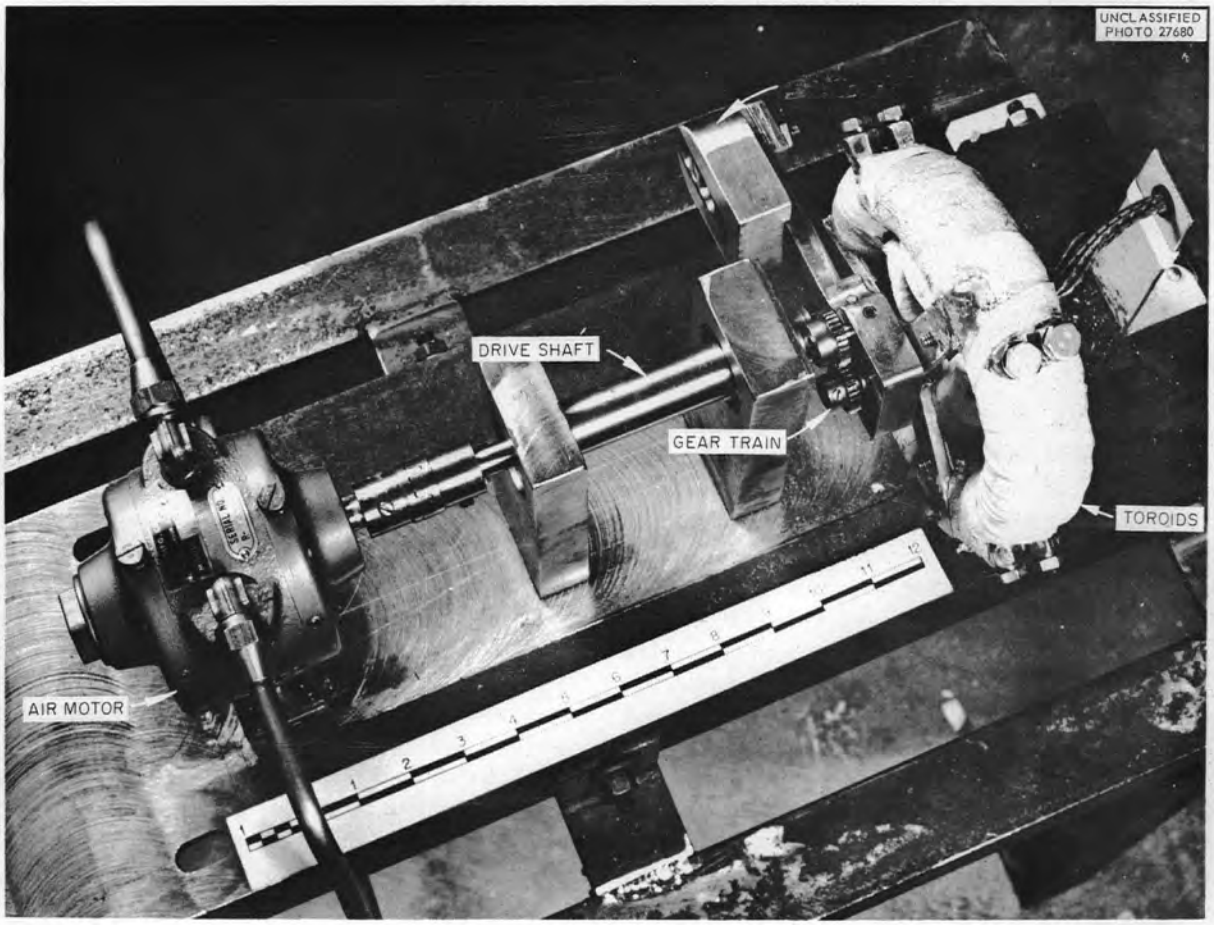

Fig. 12.6. Experimental In-Pile Toroid Rotator.

motor is advantageous because of its small size and ease of speed variation. Speed changes are accomplished by varying the air supply to the motor.

This experimental model has been operated briefly to date, with encouraging results. Operational speeds up to 1100 rpm (which result in slurry velocities of approximately 25 fps) have been attained. While other designs of an in-pile toroid are under investigation, the present experimental model will be useful in test evaluation of temperature control, pressure measurement, and operating performance required for in-pile operation.

13. RADIATION CORROSION

G. H. Jenks H. C. Savage

A. L. Bacarella
J. E. Baker
S. E. Bolt
R. J. Davis
V. A. DeCarlo
D. T. Jones
R. A. Lorenz
T. H. Mauney
J. R. McWherter
A. R. Olsen
R. M. Pierce
J. A. Russell
M. D. Silverman
F. J. Walter
K. S. Warren
D. B. Weaver[1]
S. H. Wheeler
L. F. Woo
W. C. Yee

13.1 IN-PILE LOOPS

13.1.1 Development and Construction

(a) General. – Construction of in-pile loop assemblies for operation in beam holes HB-2 and HB-4 at the LITR is continuing. Design, fabrication, and testing of component parts for use in the loop assembly to be installed in beam hole HN-1 at the ORR are under way.

(b) HB-4 Loop Package. – Construction and testing of loop L-4-16 were completed during the past quarter.[2] The loop is now in operation in beam hole HB-4 of the LITR.

Components parts are being fabricated for stainless steel loop L-4-18, the next loop scheduled for insertion in beam hole HB-4. A canned aluminum-cobalt alloy wire will be incorporated in the core section of this loop as a separate neutron-flux monitor. The wire will be removed and counted for flux exposure at the conclusion of the experiment. In previous loops a determination of the neutron flux at various locations in the core has been obtained from induced-activity measurements of corrosion specimens.

(c) HB-2 Loop Package. – The all-titanium loop,[3,4] L-2-14, is undergoing additional testing in the mockup facility, prior to insertion in beam hole HB-2.

Loop L-2-17 is now being constructed. This is a stainless steel loop containing coupon corrosion specimens and stress specimens. Zircaloy-2 tapered-channel coupon holders in the core and line contain titanium-55AX, Zircaloy-2, and type 347 stainless steel coupons. In addition, six ladder coupon holders[2] in the core, five in the line, and two in the pressurizer contain a variety of stainless steel, titanium alloys, and zirconium alloys. One Zircaloy-2 and one titanium-55AX stress-specimen assembly are included in the core sample array. A titanium-55AX stress-specimen assembly is located in the in-line holder. A canned aluminum-cobalt alloy wire will also be placed in the core section of loop L-2-17 as a separate flux monitor.

(d) Byron Jackson Pumps. – Eight Byron Jackson 5-gpm canned-rotor pumps for use in in-pile loops have been received from the vendor. One of these has undergone extensive out-of-pile tests during the past quarter in development loop DV-9, circulating a solution of 0.17 *m* UO_2SO_4, 0.03 *m* $CuSO_4$, 0.04 *m* H_2SO_4 for 943 hr at 250°C. The performance of the pump during this run was satisfactory. Testing of this pump and others will continue after modifications to test-loop DV-9 are completed. These modifications are required to incorporate component parts of the ORR loop package for test evaluation. The design layout of a loop package incorporating the Byron Jackson 5-gpm pump has been completed, but assembly of the loop is being delayed pending completion of the pump performance tests.

(e) ORR Loop Package. – Design and development work for a dynamic-loop radiation-corrosion test facility in the ORR continued this past quarter. The ORR loop and its associated equipment have been modeled closely after the LITR in-pile corrosion test loops. The major changes have been necessitated by the higher radiation intensities which will be encountered in the ORR.

A cooler has been designed for removing gamma heat from the core wall in order to prevent boiling

[1] On loan from TVA.

[2] G. H. Jenks *et al.*, *HRP Quar. Prog. Rep. Oct. 31, 1956*, ORNL-2222, p 100.

[3] G. H. Jenks *et al.*, *HRP Quar. Prog. Rep. July 31, 1956*, ORNL-2148, p 92.

[4] G. H. Jenks *et al.*, *HRP Quar. Prog. Rep. April 30, 1956*, ORNL-2096, p 90.

of solution in contact with the inner surface of the core wall. It has been calculated that approximately 4 kw of heat should be removed from the core wall.[5] Two test models of the cooler have been constructed; one was designed for testing in the laboratory, and the other, for testing on development loop DV-9 (ref 5). These coolers consisted of about 6 ft of ¼-in. stainless steel tubing wrapped around the core and cast in aluminum. The laboratory model was tested through a cooling range from 0.2 to 2.8 kw, and the development-loop model was tested through a range from 0.3 to 3.3 kw of heat removal at 250°C (ref 5). This variation in cooling was accomplished by using either air, water, or air-water mixtures as the cooling medium. A wide range of cooling rate can be attained by varying the air-to-water ratio as required. On the basis of these test results the cooler appears satisfactory. In-pile operation of loop L-2-15 with an air-water coolant proved the reliability of this type of cooling. A loop core with a cooler is being fabricated for installation in the first ORR development loop. The cooler is similar to the test models, with minor modifications in the length and geometry of the tubing to improve the temperature distribution.

The ORR loop package will be required to handle up to approximately 20 kw of fission and gamma heat during in-pile operation, as compared with 1 to 3 kw in the present LITR loops. New loop coolers and heaters have been proposed to meet this requirement. To provide maximum loop heating and cooling capacity in the limited heat-transfer area available, a combination heater-cooler has been designed. This unit consists of Calrod-type electric heaters embedded in an aluminum casting around the ⅜-in. pipe of the loop. A jacketed annulus external to the casting is used for cooling. An alternate design consists in casting cooling coils in the aluminum around the ⅜-in. pipe along with the electric heaters. Tests are under way to evaluate the performance of these units and to determine the better of the two designs. Calculations and preliminary tests of a similar loop cooler indicate that the cooling capacities of these new units should be adequate. Air, water, or air-water mixtures will be used as cooling media to provide a wide range of cooling capacity.

[5] R. A. Lorenz and D. T. Jones, *Laboratory Test of a Core Cooler for ORR Loop HN-1*, ORNL CF-56-12-65 (Dec. 18, 1956).

A new system of loop temperature control is being investigated. The problem is not only to compensate for the large total change in fission and gamma heat between reactor shutdown and full-power operation, but also to accomplish this rapidly in order to prevent a large drop in the loop temperature when the reactor is scrammed. The system being investigated is one which automatically adjusts the amount of water in the air-water coolant mixture according to the reactor power. Fine temperature control will be accomplished with electrical heaters. Adjustment of the air-water mixture will be controlled by a reactor power signal and will be either stepwise or continuous. The electric heating system will make up the difference between fission and gamma power change and the compensation made by the air-water coolant change.

The volume of the pressurizer in the ORR loop package has been increased to approximately 750 cc from the present 520-cc volume of the LITR loop pressurizer. This was done to provide more fuel-solution expansion volume and to provide additional oxygen space.

(f) ORR Loop Auxiliary Equipment. – Shielding on the equipment chambers, sample carriers, and loop carrier will be increased to protect personnel from the higher radioactivity of solution and loop components. The glass reservoirs will be enclosed in a leak-tight enclosure and shielded with 2 in. of lead. A neutron shield of paraffin and cadmium will be used around the small equipment chamber to reduce the fast-neutron flux encountered during solution sampling.

In addition to the above shielding improvements, many of the "hot" operations have been streamlined to reduce both radiation intensity and time required in the working area. For example, lead shielding on the front of the equipment chambers will be in the form of sliding doors so that a portion of the front of either chamber may be opened, worked through, and closed quickly without exposing the entire face of the equipment chamber. The sample platform has been equipped with wheels and a screw adjustment so that the sample carrier may be positioned accurately and quickly. Piping inside the small equipment chamber has been revised to permit rapid disconnection with remotely operated tools working from a distance of 4 ft or more. Clamping of the capillary tubes after draining the loop has been made simpler and more positive. The dummy shielding plug for the HN-1 beam hole

has been designed so that neutron-flux monitors may be inserted, exposed, and removed with the reactor operating at full power.

In order to prevent the precipitation of uranyl peroxide in the fuel solution removed for loop samples, it is considered necessary to maintain the temperature of the lines and valves in the loop sample system at a temperature of ~70°C while the lines contain the radioactive solution. The shielded sample carrier will be maintained at 60°C minimum. Electrical heating will be used for the valves, lines, and sample carrier.

Engineering design of the equipment chambers, sample carriers, and other auxiliary equipment is 75% complete. One-third of the drawings for these components have been issued for purchase of materials and construction. Fabrication of components at ORNL is scheduled to begin March 1.

13.1.2 General Description of In-Pile Loop Experiment L-2-10

Except for metallographic examination, the eighth in-pile loop experiment, L-2-10, has been completed. Details of this experiment and the results will be reported.[6] A summary is presented below.

This was the first loop experiment exposed in LITR beam hole HB-2. The available unperturbed thermal-neutron flux in this hole is $\sim 3 \times 10^{13}$ neutrons·cm^{-2}·sec^{-1}, which is 2 to 3 times that available in beam hole HB-4, where previous experiments have been conducted. The uranyl sulfate concentration in this experiment was the same as that proposed for use in the HRT, 0.04 *m*, which is about one-fourth that used in previous loops. The operating temperatures of the main stream and pressurizer were increased to 280 and 305°C, respectively, in this experiment. Previous experiments had been conducted at 250°C in the main stream and at 280°C in the pressurizer. Otherwise, the equipment, methods, and procedures used in this experiment are similar to those reported for previous experiments.[7]

This loop was constructed from type 347 stainless steel, and for the first time stainless steel coupon holders were used. Identical sets of corrosion coupons (24 each) in type 347 stainless steel tapered-channel coupon holders were installed in the core and in-line positions. These coupons consisted of type 347 stainless steel, Zircaloy-2, and titanium-55AX specimens. Six impact specimens and six tensile specimens of Zircaloy-2 were contained in the loop, three of each in the special line holder and three of each arranged around the core coupon holder. Also included in the specimen array surrounding the core coupon holder were two assemblies of rod coupons fabricated of types 347 and 309 SCb stainless steel, Zircaloy-2, and platinum. These specimens were ½ × ½ × 0.060 in. coupons spaced evenly on 0.20-in.-dia rods. The rods, nuts, and spacers were of type 347 stainless steel.

The structure of the loop was essentially the same as for the previous experiments. The circulating pump was an ORNL 5-gpm model of the outboard-bearing type with pure sintered aluminum oxide bearings and journal bushings.

Difficulty with operation of the fuel circulation pump necessitated termination of the experiment after 1672 hr of fuel circulation time. A sharp increase in pump power requirements produced a "fast-setback" signal and scrammed the reactor. Solution circulation was not completely lost but was decreased to such an extent that the pressurizer temperature started rising, and the pressurizer heater power decreased sharply. The pump and heaters were cut off manually. The pump was restarted, but its operation was still faulty and circulation could not be increased. The pump was again shut off, and the emergency loop-drain procedure was carried out.

The loop was operated with enriched solution for a period of 1672 hr, 216 hr of which were accumulated before the reactor went to power. The energy output of the LITR during the 1456 hr of circulation at power was 3765 Mwhr. Essentially all the power was accumulated at the 3-Mw reactor level.

The solution charged to the loop for in-pile operation was of the following composition:

UO_2SO_4 (enriched)	0.04 *m*
$CuSO_4$	0.0075 *m*
H_2SO_4	0.02 *m*

The solution used as makeup to replace solution withdrawn as samples from the loop during operation contained 0.04 *m* excess acid to replace acid

[6] J. R. McWherter *et al.*, *HRP Radiation Corrosion Studies – In-Pile Loop L-2-10*, ORNL-2250 (in press).

[7] G. H. Jenks *et al.*, *HRP Quar. Prog. Rep. Oct. 31, 1956*, ORNL-2222, p 101–106.

consumed in corrosion and 130 ppm chromium to inhibit corrosion of the type 420 stainless steel valve stems during solution additions.

The average fission power during operation as determined from cesium analyses was 462 w. The power density at a given specimen position in the core was determined from measurements of the induced activities of the type 347 stainless steel core coupons, core rod coupons, and core rod spacers. Measurements were also made of the type 309 SCb stainless steel core rod coupons and of three pieces cut from the type 347 stainless steel wall of the core body. For the first time in a loop experiment, an apparent radial neutron-flux gradient was observed in the core. The core rod coupons, located outside the core coupon holder, appeared to have been exposed to a neutron flux about 25% higher than that to which the coupons located inside the holder at equal axial positions had been exposed. The radial flux gradient may have been the result of the use of stainless steel holders in this experiment, although this is not certain. With the exception of L-4-12, which had titanium holders, all previous loop experiments had Zircaloy-2 holders.

The power densities determined from induced activities ranged from 4.7 w/ml for the leading core coupon to 0.9 w/ml for the rear core coupon, while the power-density values for the core rod coupons ranged from 3.6 to 1.9 w/ml. The power density in the solution at the nose of the core was 6.2 w/ml. Because of the high fast-neutron flux (>1.0 Mev) in beam hole HB-2, the power-density values reported below were corrected to include the estimated power-density contribution from this source. The estimated values were based on fast-neutron measurements in hole HB-2 by Trice,[8] and ranged from 0.5 w/ml at the leading edge of the first core coupon to 0.1 w/ml at the rear core coupon position. Since all previous experiments were conducted in beam hole HB-4, where the fast-neutron flux is appreciably lower, this correction has not been applied previously.

The average over-all corrosion rate of stainless steel as calculated from the oxygen data remained almost constant throughout the period of operation, including the period prior to reactor startup. The rate for the first 300 hr following the reactor startup was 0.5 mpy, while the rate for the total period of exposure to radiation was 0.4 mpy. The rates for the same periods based on nickel-in-solution data were 0.4 and 0.2 mpy, respectively. Part of the difference between the oxygen and nickel values, but not all of it, may be accounted for by the difference between the quantities which are measured by the two methods. The over-all rate obtained from oxygen data is the apparent rate which is calculated when it is assumed that oxygen is consumed only in the corrosion of steel and that all steel surfaces in contact with high-temperature solution corrode uniformly. At least part of these assumptions are not valid, since oxygen is also consumed in corrosion of zirconium and titanium. For the rate calculations from nickel data, no contribution by metals other than nickel-bearing alloys need be considered. The assumption with respect to uniformity of steel corrosion is the same as with the oxygen rate calculations.

13.1.3 Qualitative Results of Inspection and Evaluation of Loop L-2-10

The loop was dismantled routinely and without incident. The core, two in-line sample holders, the pressurizer, two sections from the pressurizer heater, a section of piping adjacent to the pump outlet, and the pump were removed from the loop. The remainder of the loop was buried.

Before removal of the pump from the loop the impeller was rotated manually but only with difficulty. This experience is considered evidence of binding. Following removal of the pump, the volute was cut away. Examination of this component and of the impeller revealed no indications of localized attack or presence of foreign material. Further examination showed the rotor end play to have been adequate and the rear bearing housing to have been pinned securely in place. However, the bearings themselves had not been mechanically fixed in the housing other than by an interference fit. From these observations and from pump experience gained out-of-pile, it was concluded that faulty bearing movement and possibly distortion of the rotor can were the causes of the pump failure.

There was no evidence of localized corrosion in this loop. All component surfaces outside the core region were covered with a heavy black rust-like scale. The scale was of a darker color than that found in similar locations in previous loops. This

[8] J. B. Trice, *Solid State Quar. Prog. Rep. Aug. 10, 1952*, ORNL-1359, p 10–13 (Classified).

result may be tentatively ascribed to the higher loop temperatures encountered in this experiment. The scale deposit was heavier on the wall in the liquid-phase region of the pressurizer than in the vapor-phase region. Also, the scale in the vapor-phase region presented an appearance which was more gray than black.

Unlike previous loops,[7] some stainless steel surfaces in the core region were not covered with the usual black scale. The type 347 stainless steel core coupon holder was essentially free from any bulk scale on the forward or high-flux end but gradually acquired a black velvety-appearing scale from approximately the mid-point to the rear of the holder. This scale was present on both the outer and inner holder surfaces. The same graduation of scale thickness was observed on the type 347 stainless steel coupons contained in the core holder. The scale deposit on most of the inside wall of the type 347 stainless steel core body ranged from a rust-red in appearance at the high-flux end to a heavy black deposit at the low-flux end. This scale also showed several spots of discoloration in areas adjacent to the core rod coupons contained in rod assembly A. These discolorations were not in evidence on areas of the core wall adjacent to rod assembly B. Rods A and B were located in the core annulus below and above the core center line, respectively. The center lines of the rods were parallel to the core axis and were in a plane which passed through the axis and which made a 30-deg angle with the horizontal. Rod A appeared to be much closer than rod B to the core body wall. The local discolorations of the core wall can be correlated with the adjacent rod A coupons as follows:

1. In the regions adjacent to the stainless steel coupons the scale was heavy and dull gray in color.
2. Scale in the regions adjacent to Zircaloy-2 coupons was heavy and black.
3. The areas adjacent to platinum coupons were generally rust-red in color, with the scale becoming thinner toward the center of the discolored areas. In the exact center of each of these areas was located a thin, black band of scale approximately $\frac{1}{16}$ in. in width.
4. A noticeable rust-red spot of film was found in the core cap near the end of the rod A assembly.

The two core rod coupon assemblies differed in their as-removed appearance. Rod B assembly was covered with a rust-like scale, which became heavier toward the low-flux end. Rod A assembly had a very much thinner scale deposit, particularly in the high-flux regions. On rod A, the type 347 stainless steel spacers which were located on either side of each of the two platinum rod coupons exhibited a hard, glossy, black scale instead of the rough, rust-like scale which covered the remaining spacers. All the rod B spacers exhibited the rough, rust-like scale.

The Zircaloy-2 impact and tensile specimens occupying the remaining six core-annulus specimen locations were free from any scale and were covered with a thin irridescent film. This same type of film was previously noted on the Zircaloy-2 impact specimens located in the loop L-4-12 core annulus.[7]

The Zircaloy-2 and titanium core coupons had only slight amounts of scale deposit; those located in the high-flux regions had practically none.

As with previous loops[7] the standard cathodic defilming was not entirely effective, and some film was retained by some specimens after this treatment, particularly the zirconium and titanium coupons from the in-line positions. In fact, all Zircaloy-2 in-line coupons showed weight increases or no weight change following the final defilming.

The core impact and tensile specimens were not defilmed but were transferred to the Metallurgy Group for remote testing. Several coupons of each material from the core and in-line holders, core rod assemblies, and sections from the core cap, pressurizer, pressurizer heater, and main loop piping have been set aside for metallographic examination. Two Zircaloy-2 coupons, one from the core coupon array and one from the core rod B coupon array, are to be analyzed for hydrogen content.

13.1.4 Quantitative Results of Inspection and Evaluation of Loop L-2-10

All corrosion-rate values reported below were calculated from weight-loss data, with the exposed specimen area and total radiation time (equivalent to 1255 hr of LITR operation at 3 Mw) used as the basis for the calculations. Average solution velocities across the coupons contained in the tapered type 347 stainless steel core and in-line holders were from 8.9 to 41.9 fps. The solution velocity across the rod coupons in the core annulus was less than 1 fps. As mentioned previously, power-density values include contributions from the fast neutrons.

(a) Zircaloy-2. – As in previous experiments, the corrosion rates of the core specimens were power-density dependent. Observed rates for the core holder coupons varied from 3.6 mpy at 1.7 w/ml to 5.2 mpy at 2.9 w/ml. The core rod coupons exhibited higher rates, varying from 5.7 mpy at 2 w/ml to 9.1 mpy at 3.6 w/ml. The in-line Zircaloy-2 coupons showed either weight increases or no weight changes following the defilming.

(b) Titanium-55AX. – The three titanium core specimens which were exposed at less than 2 w/ml exhibited corrosion rates of approximately 1 mpy. The coupon exposed to the highest power density, 3.3 w/ml, and a solution velocity of 14 fps exhibited a rate of 0.8 mpy. The other two coupons, at 2.7 and 2.1 w/ml and at solution velocities of 22 and 35 fps, exhibited corrosion rates of 2.0 and 5.4 mpy, respectively. From these results it appears that power density and velocity interact to produce an acceleration of corrosion. The average corrosion rate for the in-line coupons was 1.1 mpy. There was no apparent effect of velocity on the attack of the in-line specimens.

(c) Platinum. – Platinum corroded very slightly. The four core rod coupons gave corrosion rates of from 0 to 0.03 mpy. Loop L-4-11 was the only previous experiment to contain platinum core or core rod coupons. Specimens in that experiment exposed to the same power density as the specimens in loop L-2-10 exhibited rates of 0.2 to 0.4 mpy. No platinum was included among the in-line specimens in this loop.

(d) Type 347 Stainless Steel. – Thirteen type 347 stainless steel specimens were located in the core coupon holder. Corrosion rates for these coupons varied from 2.8 mpy at 4.7 w/ml to 0.12 mpy at 1.0 w/ml. The solution velocity across the specimens varied from 9 to 38 fps and produced no apparent effect on the corrosion rates.

Three type 347 stainless steel coupons on rod A in the core annulus at power densities of 3.9, 2.8, and 2.0 w/ml corroded at rates of 6.6, 5.4, and 2.6 mpy, respectively. Three similar coupons on rod B in the core annulus at power densities of 3.3, 2.4, and 2.1 w/ml corroded at rates of 0.6, 0.1, and 0.1 mpy, respectively.

The average corrosion rate of in-line specimens was 0.2 mpy, with no indication of velocity effect at velocities ranging from 9 to 38 fps.

(e) Type 309 SCb Stainless Steel. – The two specimens of type 309 SCb stainless steel contained in the rod A assembly, exposed to power densities of 3.6 and 2.6 w/ml, exhibited corrosion rates of 9.7 and 7.9 mpy, respectively. The two specimens from rod B, exposed to power densities of 3.1 and 2.0 w/ml, corroded at rates of only 0.6 and 0.1 mpy, respectively.

13.1.5 Discussion of Results from Loop L-2-10

In a previous discussion of Zircaloy-2 in-pile corrosion data,[9] the relationship of corrosion rate to power density over the range studied was shown to be expressed by

$$CR = APD\left(1 - e^{-B/CR^{1.5}}\right) ,$$

where

CR = corrosion rate, mpy,
PD = power density, w/ml,
A = constant, depending on solution composition and temperature,
B = constant, depending on temperature.

For the in-pile experiments containing 0.17 m UO_2SO_4 with excess acid (0.04 m initially) at 250°C, the values for constants A and B as determined from the data are 1.25 and 8.3, respectively. For the same solution in-pile at 280°C, the values as determined from autoclave data are 2.2 and 40, respectively. As defined, the constant B for L-2-10 data should be the same as that for the 0.17 m UO_2SO_4 solution at 280°C (i.e., equal to 40). Assuming this value for B, the L-2-10 core rod coupon data are expressed reasonably well by the above equation with A equal to 3.2. The results[10] of autoclave experiment Z-12, which, with the exception of velocity, was carried out under similar conditions, are also expressed by the equation for the L-2-10 rod data. The reason for the lower rates observed on the core holder coupons in L-2-10 is unknown.

Since the conditions for experiment L-2-10 simulate the proposed operating conditions of the HRT more closely than any of the loop experiments conducted previously, the results of this experiment provide the best basis for estimating Zircaloy-2 corrosion in the HRT. Employing 17 w/ml at 280°C

[9] G. H. Jenks *et al.*, *HRP Quar. Prog. Rep. Oct. 31, 1956*, ORNL-2222, p 111.

[10] G. H. Jenks *et al.*, *HRP Quar. Prog. Rep. July 31, 1955*, ORNL-1943, p 129.

as an example of an HRT condition, extrapolation from the highest rates found in L-2-10, that is, those for the core rod coupons, predicts a corrosion rate of 20 mpy. The use of D_2O rather than H_2O as the solvent for the HRT solution may increase this predicted rate somewhat. As observed[11] in autoclave experiment Z-20, the corrosion rate for Zircaloy-2 with heavy water as the solvent was 30% higher than that in similar experiments with light water as the solvent.

In the case of steel the results are not so consistent as those for Zircaloy-2, and a confident extrapolation to HRT conditions cannot be made. The radiation intensities which will prevail on the steel in the HRT will be lower than the highest intensities to which steel specimens in this loop were exposed. However, the average solution power density in this experiment was about 0.4 w/ml, whereas that in the HRT will be about 10 w/ml. Present experimental results are inadequate to permit evaluation of the effect of this difference on corrosion. Also unevaluated are effects which may arise due to differences in operating conditions between the HRT and the loops.

In order to check the corrosion data in this loop, an oxygen balance has been made. The measured oxygen consumption during operation based on pressure measurements was 1922 cc (STP). Based on weight changes of coupons, the Zircaloy-2 and titanium surfaces account for 709 and 19 cc, respectively. Assuming that all steel surfaces outside the core corroded at the same rate as the in-line steel coupons, average 0.16 mpy, these surfaces account for 507 cc. The 687 cc remaining would be accounted for by an average corrosion rate of the exposed steel in the core of 1.1 mpy. In comparison, the average corrosion rate of the steel coupons in the core holder based on weight changes was 0.96 mpy. This indicates that the average rate of the steel core wall was not significantly higher than the average of these core holder coupons.

There was no evidence of solution instability in this experiment. The loop was exposed to reactor radiation for a total of about 1255 hr. The nickel concentration in solution at the end of the experiment was about 0.006 *m*. The calculated concentration of excess acid at this time was 0.016 *m*. The results of analyses of the six samples taken during the final 400 hr of operation gave an average uranium concentration of 0.045 *m*; the initial concentration was 0.44 *m*. The average copper concentration in these six samples was 0.0071 *m*, compared with an original concentration of 0.0078 *m*.

13.1.6 In-Pile Loop L-4-13

Exposure of in-pile stainless steel experiment L-4-13 in the LITR has been completed. Total circulation time for the experiment was 1042 hr, of which 73 hr were accumulated outside the reactor. The energy output of the LITR during in-pile operation was 2362 Mwhr, and essentially all this energy was liberated at the 3-Mw level. Disassembly of the loop and examination of the loop and specimens are in progress. Corrosion specimens for this loop included type 347 stainless steel, type 309 stainless steel, titanium A-40, Zircaloy-2, crystal-bar zirconium, and a zirconium alloy containing 20% niobium. Coupon specimens, as well as impact and tensile specimens of these materials, were located in the core, while the in-line position contained coupon and impact specimens. The coupon specimens in both positions were contained in tapered-channel type 347 stainless steel holders.

This is the first loop that has been irradiated in either the HB-4 or HB-2 beam holes at the LITR in which a D_2O fuel solution was used. The solution charged to loop L-4-13 for in-pile operation was of the following composition:

UO_2SO_4	0.17 *m* (enriched)
$CuSO_4$	0.03 *m*
H_2SO_4	0.02 *m*

The solution used as makeup to replace solution withdrawn as samples from the loop during operation contained 0.04 *m* excess acid to replace acid consumed in corrosion and 100 ppm chromium to inhibit corrosion of the stainless steel stems in the valves used during solution additions. The operating temperatures of the loop were the same as for most previous loops: main stream, 250°C; pressurizer, 280°C.

Over-all stainless steel corrosion rates obtained from nickel and oxygen data show some changes

[11] G. H. Jenks *et al.*, *HRP Quar. Prog. Rep. Oct. 31, 1956*, ORNL-2222, p 107–111.

with operating time. As calculated from oxygen data, the corrosion rate during the first 300 hr in-pile was 2.0 mpy. During the final 670 hr the average rate was 1.0 mpy. The rates calculated for the same periods of time from the amounts of nickel found in solution were 2.3 and 0.4 mpy, respectively.

13.1.7 In-Pile Loop L-2-15

Stainless steel loop L-2-15 has been exposed in beam hole HB-2 at the LITR. Total circulation time for the experiment was 792 hr, of which 75 hr were accumulated outside the reactor. The energy output of the LITR during in-pile operation was 1632 Mwhr. Almost all this energy was liberated at the 3-Mw level. After 470 hr of circulation time it was necessary to halt operation temporarily to drain the solution from the loop in order to replace a malfunctioning valve located in the line between the fuel expansion chamber and the fuel reservoir. Subsequent examination of the valve showed the valve-stem tip to be cleanly broken off. The loop was recharged with fresh solution, and operation was continued for an additional 322 hr, when operation of the loop was halted by failure of the fuel circulation pump. Disassembly of the loop and examination of the loop and specimens are in progress.

This loop contained coupon, tensile, impact, and stress-corrosion specimens. Zircaloy-2 tapered-channel coupon holders in the core and line positions contained Zircaloy-2, titanium-55AX, and type 347 stainless steel coupons. Ladder holders in both positions contained type 347 stainless steel, Zircaloy-2, type 309 SCb stainless steel, titanium type 110-AT, nickel-clad Zircaloy-2, platinum-clad Zircaloy-2, and platinum coupons. Tensile specimens of crystal-bar zirconium and Zircaloy-2, as well as stress assemblies of titanium type 55AX, were located in both positions.

The solution charged to loop L-2-15 for both periods of in-pile operation was of the following composition:

UO_2SO_4	0.17 *m* (enriched)
$CuSO_4$	0.015 *m*
H_2SO_4	0.03 *m*

Two different solutions were employed as makeup to replace solution withdrawn as samples during loop operation. One contained excess H_2SO_4 at a concentration of 0.02 *m*, and the other, at 0.07 *m*. Chromium(VI) at a concentration of 100 ppm was added to both solutions for protection of stainless valve stems in the fuel system. Otherwise, the solutions were the same as the charge solution. The appropriate makeup solution was employed as required to maintain the calculated concentration of excess H_2SO_4 in the loop at 0.03 *m*. The mainstream operating temperature was 278°C; the pressurizer temperature was 298°C.

No evidence of solution instability was observed at these operating conditions. The over-all stainless steel corrosion rate was 1.5 mpy based on oxygen data and 0.5 mpy based on nickel in solution. If the oxygen data are corrected for the amount consumed in zirconium oxidation, the corrosion rate, based on the corrected data, is 1.3 mpy.

13.1.8 In-Pile Loop L-4-16

Stainless steel loop L-4-16 is now being exposed in beam hole HB-4 at the LITR. The core and in-line coupon holders are tapered-channel holders fabricated from type 347 stainless steel and contain coupon specimens of type 347 stainless steel, titanium 55AX, and Zircaloy-2. Two ladder coupon assemblies are located in the core and one is in the in-line sample position. The ladder holders were fabricated from type 347 stainless steel, and each contains 15 coupon specimens. The ladder coupons are comprised of 17 different specimen materials: type 347 stainless steel, Zircaloy-2, and 15 alloys of sponge or crystal-bar zirconium with niobium, palladium, and platinum. Eight impact specimens were also contained in the loop: five in the core and three in the in-line position. These specimens were fabricated of titanium 110-AT, titanium 55AX, Zircaloy-2, and a zirconium–15% Nb alloy. In addition, one tensile specimen of titanium 110-AT was contained in the core and one in the in-line sample holder. The solution composition for L-4-16 is as follows:

UO_2SO_4	0.17 *m* (enriched)
$CuSO_4$	0.015 *m*
H_2SO_4	0.025 *m*

The solution used as makeup to replace samples withdrawn from the loop is the same as above except that it contains 0.07 *m* H_2SO_4 to replace

acid consumed in corrosion and 100 ppm Cr as a corrosion inhibitor to protect the stainless steel valve stems during solution addition.

Operating temperatures for this loop are 280°C in the main stream and 295°C in the pressurizer.

13.2 IN-PILE AUTOCLAVE TEST, LITR

13.2.1 Development and Construction

The present in-pile autoclave facility of beam hole HB-5 of the LITR, which provides for only one test at a time, has been redesigned to provide for the simultaneous exposure of up to three autoclaves. The rocking-bomb shielding plug, beam-hole liner, autoclave, auxiliary equipment, and instrumentation have all been redesigned, and a mockup of the new facility has been constructed in Building 9204-1, Y-12. This mockup is now being used to check the new equipment prior to installation in beam hole HB-5 of the LITR and will be used in the future to test and pretreat the autoclaves prior to in-pile operation.

The construction of the instrument panel board, shielding plug, autoclave plugs, rocking mechanism, and beam-hole liner has been completed. Figure 13.1 is a photograph of the mockup facility, showing panel board, rocking mechanism, and external auxiliary equipment containers for three autoclaves. Figure 13.2 shows the autoclave, which contains nine rectangular, flat-plate corrosion specimens $\frac{1}{4} \times 0.4 \times \frac{1}{16}$ in. thick. Figure 13.3 is a photograph of two equipment chambers, in which are located the pressure cells, valves, and service connections. The dummy plug shown in the third position is used for shielding when any hole is not in use.

13.2.2 In-Pile Tests

Three Zircaloy-2 experiments, Z-26, Z-27, and L6Z-101, and one type 347 stainless steel experiment, H-97-2, are reported. The data are summarized in Table 13.1. A column indicating the presence or absence of atmospheric nitrogen in a bomb is included in the table.

Excepting five Zircaloy-2 experiments, all rocking-bomb experiments have been assembled in such a way that an amount of nitrogen, equivalent to the room-temperature gas volume of the bomb filled with air, was included. This amount of nitrogen could conceivably affect the corrosion data significantly: first by invalidating the assumptions made in calculating corrosion penetration from oxygen consumption, and second by affecting the nature of the corroding solution. For instance, the approximately 2 cc (STP) of nitrogen included, if oxidized completely to nitric acid during the in-pile exposure, would consume 5 cc (STP) of oxygen. This amount of oxygen would be calculated as about 0.025 mil penetration in a Zircaloy system or about 0.02 mil in stainless steel. Furthermore, the nitric acid concentration in the solution would become about 0.04 *m*.

Nitrogen apparently is not completely oxidized to any large extent in the bomb system. The values for the penetration in H-97-2, for instance, calculated from oxygen consumption and pin weight

Table 13.1. LITR In-Pile Bomb Data

Bomb No.	LITR Beam Hole	Bomb Material	Solution Composition (*m*)				Atmospheric N_2 Excluded	Enrichment (% U^{235})	Exposure Temperature (°C)	Fission Power Density (w/ml)	Irradiation Time (hr) (1 hr = 3 Mwhr)	Penetration (mils)		Corrosion Rate, O_2 Data (mpy)
			UO_2SO_4	$CuSO_4$	H_2SO_4	$MgSO_4$						O_2 Data	Pin Weight Data	
Z-26	HB-5	Zr-2	0.173	0.040	0.040	0.170	No	93.2	250	16.4	109.2	0.107	0.115	9.1
Z-27	HB-5	Zr-2	0.044	0.005	0.031		Yes	93.2	250	4.5	119.9	0.354	0.406	7.7
									280	4.3	64.2			14.5
									330	3.7	34.2			22.6
									300	4.1	57.4			12.5
H-97-2	HB-6	347 SS	0.171	0.040	0.030	0.170	No	93.2	250	6.6	580.2	0.031	0.037	0.45
L6Z-101	HB-6	Zr-2	0.172	0.040	0.040		Yes	93.2	250	8.7	128.3	0.225	0.255*	5.1
									280	8.2	120.2		0.197**	10.3

*Zr-2 pins.
**80% Zr–20% Nb pins.

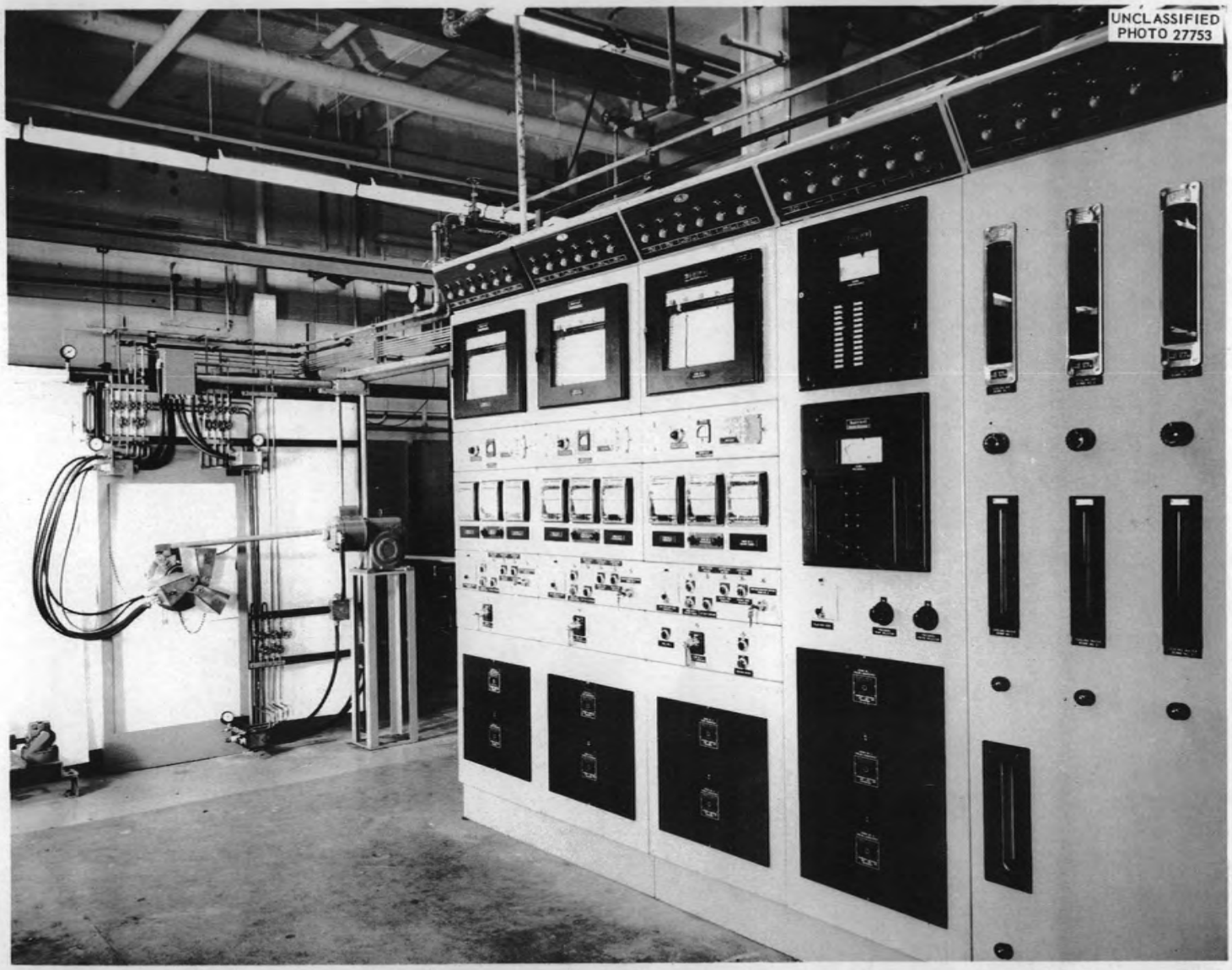

Fig. 13.1. Mockup Facility.

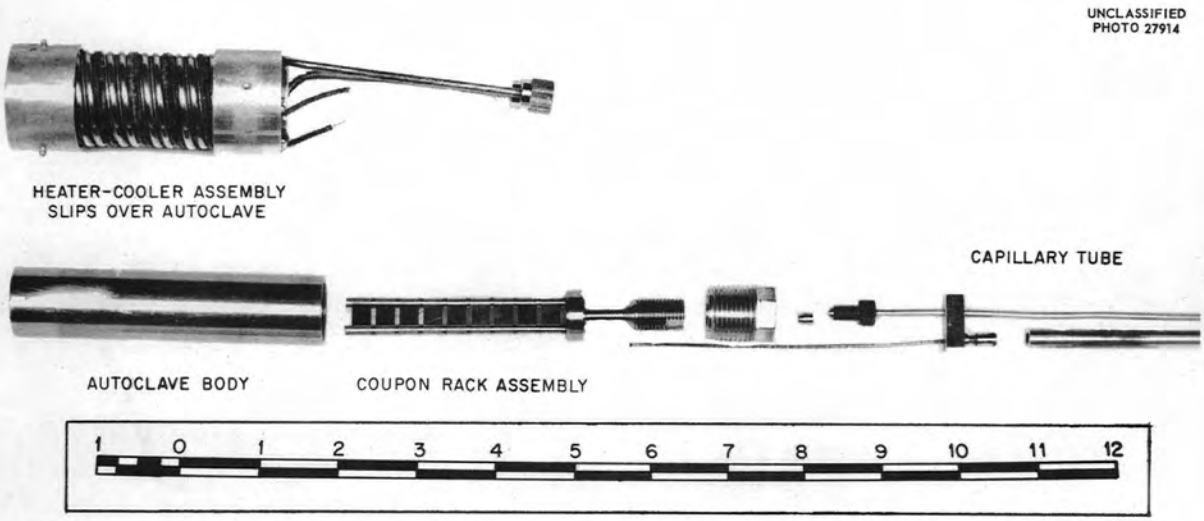

Fig. 13.2. Autoclave Assembly.

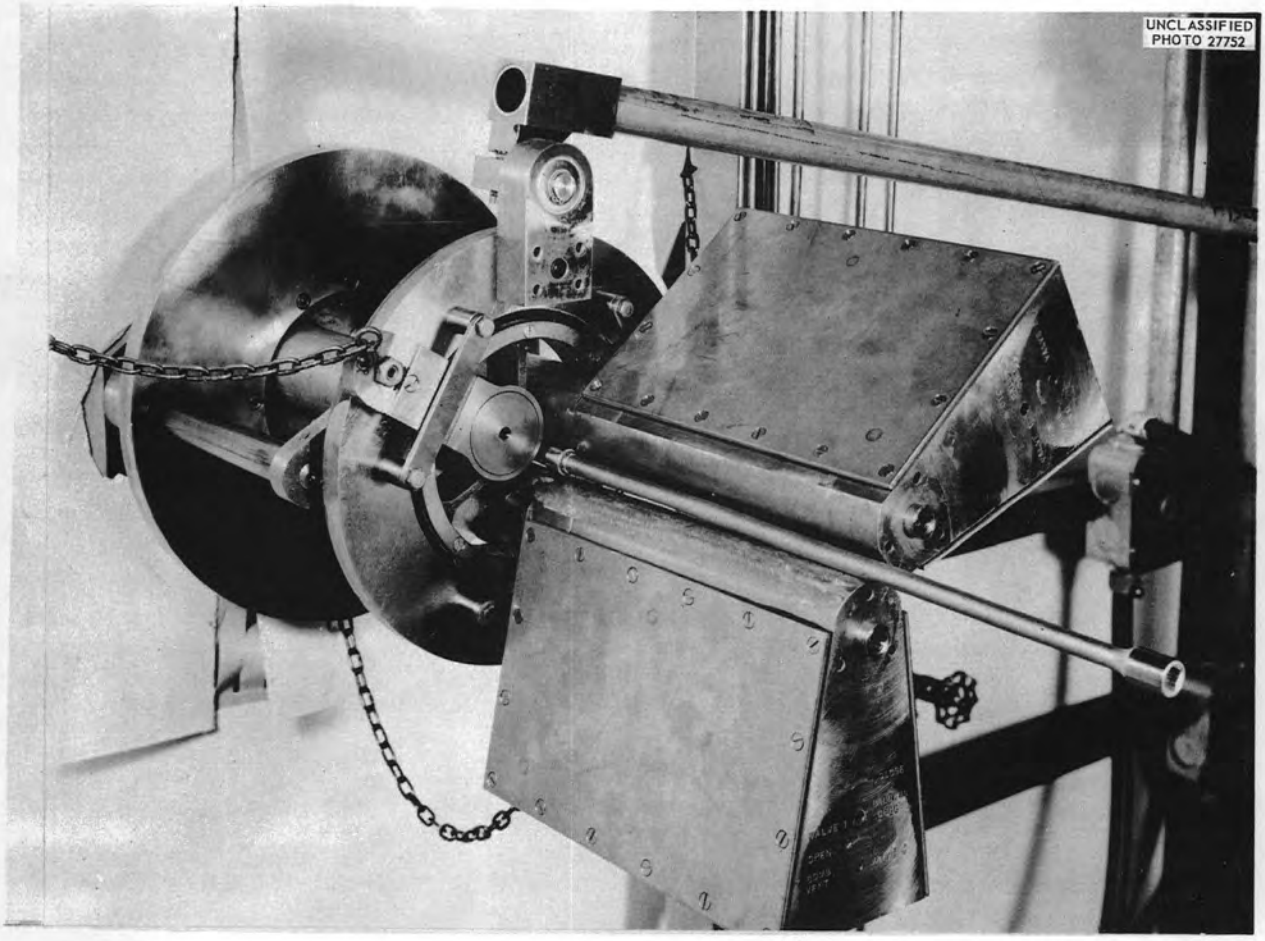

Fig. 13.3. Equipment Chambers.

losses agree very well, although the total penetration is only 0.03 to 0.04 mil. Furthermore, analysis of the solution removed from H-97-2 indicated that essentially no nitrate was present. A colorimetric method with phenyl disulfonic acid as the color-forming material was used. A Kjeldahl determination showed no NH_3 was present, but a total nitrogen determination using the Devarda method indicated 969 ppm of nitrogen. This concentration of nitrogen is of the same order as that corresponding to total fixation of the gaseous nitrogen included in the bomb (~650 ppm). It appears, then, that the gaseous nitrogen becomes combined in an unidentified form during exposure in the reactor.

Of the Zircaloy-2 experiments that have been run, five (Z-1, L6Z-101, Z-24, Z-27, and Z-25) were assembled in such a way as to exclude atmospheric nitrogen. Runs Z-1 (ref 12) and L6Z-101 were similar in that they both employed 0.17 *m* UO_2SO_4 and 0.04 *m* excess H_2SO_4, and the corrosion results from these two experiments are in line with those from similar experiments which contained nitrogen (with the possible exception of the corrosion rate of L6Z-101 at 280°C, as mentioned below). Experiment Z-24 (ref 13), in which 0.17 *m* UO_2SO_4 was used without excess acid, showed a corrosion rate of 27 mpy, as compared with 20 mpy predicted from results of experiments in which nitrogen was contained. Experiment Z-27 (discussed below) contained 0.04 *m* UO_2SO_4 with 0.03 *m* excess H_2SO_4, but there are insufficient data to ascertain an effect of the lack of nitrogen on corrosion in this system. A UO_2CO_3 experiment, Z-25, is not comparable with any other experiment.

Although no precise conclusion is warranted, it appears that a decrease in the corrosion rate of Zircaloy-2 from nitrogen contained in the bomb occurs in systems containing no excess acid. This suggests that the nitrogen either forms an acid or functions as excess acid does in reducing corrosion.

(*a*) Experiment Z-26. – This all-Zircaloy-2 experiment was conducted with a solution containing 0.17 *m* $MgSO_4$ in addition to 0.17 *m* UO_2SO_4, 0.04 *m* excess H_2SO_4, and 0.04 *m* $CuSO_4$. The equation proposed by Jenks,[14]

$$CR = 1.25PD\left(1 - e^{-8.3/CR^{1.5}}\right) ,$$

where CR is the corrosion rate in mpy and PD is the power density in w/ml, predicts a corrosion rate of 7.2 mpy. Jenks' equation is applicable to a system similar to that in Z-26, but without $MgSO_4$. The observed corrosion rate of 9.1 mpy, judging from past experience in reproducing Zircaloy-2 corrosion, is significantly higher than would be predicted.

A previously reported experiment, Z-21 (ref 13), contained excess sulfate as Li_2SO_4. The corrosion rate observed was about half that predicted for a similar system without Li_2SO_4; Z-21 was operated at 280°C and contained no excess acid. In comparison, Z-26 was run at 250°C with 0.04 *m* excess H_2SO_4.

Analysis of the solution removed from the Z-26 bomb indicated that about one-third the magnesium was lost from the solution during the experiment. However, no magnesium was detected in chemical analyses of the scale and precipitate. It may be noted that in the Li_2SO_4 experiment also, the analytical results indicated that about one-third the lithium was lost from the solution. Again, however, no lithium was detected in the scale, and no precipitate was found in this experiment.

(*b*) Experiment Z-27. – An all-Zircaloy-2 system was operated with 0.04 *m* UO_2SO_4, 0.03 *m* H_2SO_4, and 0.005 *m* $CuSO_4$ at four different temperatures, in the following sequence: 250, 280, 330, and 300°C. The primary purpose of the experiment was to extend the operating temperature to 330°C, or 30°C higher than any previous autoclave experiment. The temperature dependence of corrosion rate observed in Z-27 is shown graphically in Fig. 13.4, and data obtained earlier in Z-10 (ref 15), a 0.17 *m* UO_2SO_4 experiment, are included for comparison. As shown, the results obtained at 250 and 280°C in Z-27 lie on a line which is roughly parallel to that drawn through the Z-10 data. However, the 300 and 330°C data lie on a second lower line, which is again roughly parallel

[12] G. H. Jenks *et al.*, *HRP Quar. Prog. Rep. Jan. 31, 1955*, ORNL-1853, p 112.

[13] G. H. Jenks *et al.*, *HRP Quar. Prog. Rep. Oct. 31, 1956*, ORNL-2222, p 107–111.

[14] *Ibid.*, p 111.

[15] G. H. Jenks *et al.*, *HRP Quar. Prog. Rep. Jan. 31, 1956*, ORNL-2057, p 97.

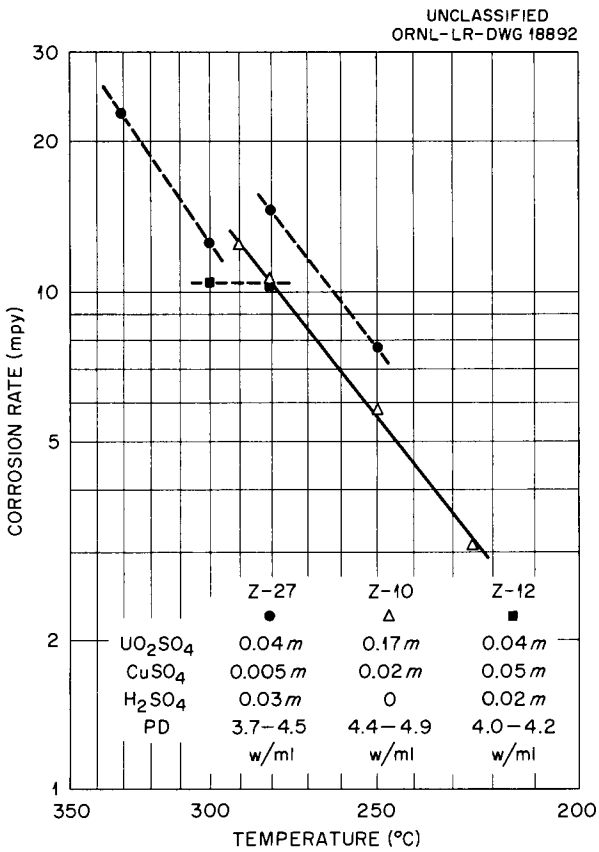

Fig. 13.4. Temperature Effect on Radiation Corrosion of Zircaloy-2.

to the other lines. This difference between the results obtained at the lower and higher temperatures is not adequately explained as spread of the experimental data. Furthermore, the Z-12 experiment,[15] which also contained 0.04 *m* UO_2SO_4 and which was exposed first at 280°C and then at 300°C, showed a rate of 10.3 mpy at both temperatures, that is, a similar anomalous temperature effect in the same temperature range. The Z-12 data are plotted in Fig. 13.4. No such discontinuity has been observed with 0.17 *m* UO_2SO_4 systems up to 300°C (ref 13), the highest temperature to which this system has been exposed.

As has been the case with all Zircaloy-2 bomb experiments, uranium was lost from solution during the exposure of Z-27. The fraction lost, about 40%, is greater than that usually observed with systems employing an initial uranium concentration of 0.17 *m*. Two factors probably account for the high percentage loss in this experiment. First, the concentration of uranium found in the scale which covers the Zircaloy surfaces is roughly the same for 0.04 *m* UO_2SO_4 systems as for 0.17 *m* systems; hence for the same amount of scale there results a factor of 4 increase in the percentage loss from solution of the lower concentration. Second, the exposure in this experiment was to a total penetration of about 0.4 mil, which is on the high side of the range of penetration values for previous experiments; hence the amount of scale formed in the experiment was greater than usual.

The rate of 14.5 mpy at 280°C in Z-27 is about 40% greater than that anticipated from the results of previous bomb experiment Z-12 (0.04 *m* UO_2SO_4, 0.02 *m* H_2SO_4, 0.05 *m* $CuSO_4$, 280°C, 4.2 w/ml). The explanation of this difference is unknown. However, the differences in the systems which may have had some effect on the differing rates may be listed: (1) nitrogen was excluded from Z-27 but was included in Z-12, (2) the concentration of excess H_2SO_4 was 0.03 *m* in Z-27 and 0.02 *m* in Z-12, and (3) Z-27 was exposed initially at 250°C to a penetration of about 0.1 mil before exposure at 280°C, whereas the initial exposure of Z-12 was at 280°C. Sufficient data are not available to determine the difference between the importance of these factors. It may be noted, however, that the corrosion rate of 10.3 mpy observed in Z-12 agrees very well with the core rod coupon data from loop experiment L-2-10 (see Sec 13.1.4). The solution for the loop experiment was 0.007 *m* in $CuSO_4$ and contained nitrogen at an estimated concentration of about 50 ppm; otherwise, the solutions employed in L-2-10 and Z-12 were the same.

(c) Experiment H-97-2. – A type 347 stainless steel experiment was operated with a solution containing 0.17 *m* $MgSO_4$, 0.17 *m* UO_2SO_4, 0.04 *m* $CuSO_4$, and 0.03 *m* H_2SO_4. This solution was shown to be stable above 280°C in a quartz tube even when sufficient NiO was dissolved in it to produce a nickel concentration of 0.008 *m*. However, analysis of the solution removed from the bomb after the experiment indicated that about two-thirds the magnesium initially included in the solution was no longer there. Some magnesium was detected in chemical analysis of scale from this bomb.

The corrosion rate observed in H-97-2 of 0.45 mpy at 250°C and 6.6 w/ml is similar to the steady-state rates observed in H-93 (0.54 mpy at 7.8 w/ml) and H-94 (0.51 mpy at 7.7 w/ml). Experiments

H-93 and H-94 contained solutions similar to the one in H-97-2, except that no $MgSO_4$ was used and the $CuSO_4$ concentration was 0.01 *m*. Although it appears that the addition of $MgSO_4$ had little effect on the corrosion rate, one difference in the corrosion behavior of H-97-2 as compared with the rates in the earlier experiments should be noted. In H-93 and H-94 the corrosion rates for an initial period of 200 to 250 hr were relatively high (1.3 and 2.2 mpy, respectively), and following this period the rates were apparently constant at 0.54 and 0.51 mpy, respectively. Experiment H-97-2, in contrast, showed a constant rate during the entire 580-hr exposure.

(*d*) Experiment L6Z-101. – This was the first experiment run in facility HB-6 following the installation of new equipment. The bomb and plug are essentially of the same design as those presently employed in hole HB-5.

The purpose of this Zircaloy-2 experiment was to obtain data in a previously unexplored power-density region to check the corrosion rate vs power-density relation recently proposed by Jenks.[14] The solution was 0.17 *m* UO_2SO_4, 0.04 *m* $CuSO_4$, and 0.04 *m* H_2SO_4, and the power density was 8.7 w/ml at 250°C and 8.2 at 280°C. The corrosion rate at 250°C agrees very well with the equation; 5.1 mpy was observed and 5.3 mpy predicted. At 280°C the appropriate equation predicts 11.5 mpy, which is somewhat higher than the 10.3 observed.

Experiment L6Z-101 contained two pins fabricated from an alloy containing 80% Zr and 20% Nb. The corrosion penetration, as measured by pin weight losses, was about 77% of that found in the Zircaloy-2 pins. This improvement in corrosion behavior is less than that found in Z-19, which was operated at 280 and 300°C and contained 0.17 *m* UO_2SO_4 without excess acid but with about 500 ppm of molybdenum. The pins in Z-19 contained 15% Nb and corroded about half as much as the Zircaloy-2 specimens.

13.3 SUPPORTING RESEARCH

13.3.1 Corrosion of Type 347 Stainless Steel in a System Free from the Products of Corrosion

The study of the out-of-pile corrosion behavior of pin-type specimens of type 347 stainless steel in a system free from the products of corrosion has continued. Further experiments have been made with solutions of UO_2SO_4 in which the total uranium was about 0.17 *m* and in which the acidity was affected by additions as follows: (1) none, (2) 0.017 *m* H_2SO_4, (3) 0.008 *m* H_2SO_4, and (4) 0.008 *m* UO_3. Solutions 1 and 2 have been run at temperatures of 250 and 290°C. The 250°C experiments with solution 1 were reported previously.[16] Experiments with the other solutions were at 250°C. All the solutions were pressurized with 300 to 400 psi of oxygen at the test temperatures. The results are given in Table 13.2. Values for the concentration of acid appearing in parentheses were calculated from the analytical data for U and SO_4. Those solutions for which the pH is not reported have not been analyzed. Experiments 25 to 28 are of uncertain quantitative value. All the specimens suffered nonuniform attack. When an estimate was made of the area which suffered attack, along with the assumption that the attack was uniform, the results indicated that the rate was 20 ± 1 mpy for all. Information on the amount of adherent oxide formed on the steel specimens is listed in Table 13.3. Similar information was not obtained for the earlier experiments 1 to 12.

A plot of the corrosion-vs-time data is shown in Fig. 13.5; included for comparison are the previously reported results for the 0.17 *m* UO_2SO_4 experiments at 250°C.

The same general corrosion behavior was obtained in all cases. After a varying amount of corrosion, a protective film was formed, and the rate of attack became low. The amount of metal attacked prior to the formation of a protective film varies with the acidity and the temperature. The variation with acidity is shown clearly by comparison of the results at conditions E, A, F, and C in Fig. 13.5. The concentration of excess acid for these experiments increased from that prevailing in the solution with 0.008 *m* UO_3 (acid deficient) to 0.017 *m* in the order listed. The temperature for each of these solutions was 250°C. The amount of metal involved in the formation of a protective film varied from about 0.04 mil for condition E to about 0.4 mil for condition C. The temperature effect is evident by comparison of the results at conditions A vs B and C vs D. It is seen that the amount of metal

[16] A. L. Bacarella, *Corrosion of Stainless Steel by Uranyl Sulfate Solutions Free of Stainless Steel Corrosion Products*, ORNL CF-56-2-3 (Feb. 9, 1956) (Classified).

Table 13.2. Type 347 Stainless Steel Corrosion Data

Run No.	Solution Composition	pH	Temperature (°C)	Exposure Time (hr)	Penetration (mils)	Over-all Rate (mpy)
12	0.168 m UO_2SO_4	2.50	$267 \leq T \leq 273$	43.5	0.025	5.1
13	0.168 m UO_2SO_4	2.52	290	44.0	0.034	6.7
14	0.168 m UO_2SO_4	2.51	290	89.0	0.040	4.0
15	0.168 m UO_2SO_4	2.51	290	188.7	0.033	1.5
16	0.161 m UO_2SO_4 (0.020 m H_2SO_4) 0.017 m H_2SO_4	1.62	250	78.0	0.45	50.3
17	0.167 m UO_2SO_4 (0.018 m H_2SO_4) 0.017 m H_2SO_4	1.75	250	187.5	0.40	18.7
18	0.167 m UO_2SO_4 0.017 m H_2SO_4		250	96.0	0.43	39.0
19	0.166 m UO_2SO_4 (0.020 m H_2SO_4) 0.017 m H_2SO_4	1.80	290	96.3	0.038	3.9
20	0.166 m UO_2SO_4 0.017 m H_2SO_4		290	4.1	0.030	62.9
21	0.161 m UO_2SO_4 (0.022 m H_2SO_4) 0.017 m H_2SO_4	1.72	250	4.0	Nonuniform corrosion, ~50% unattacked	
22*	0.155 m UO_2SO_4 0.008 m UO_3	2.94	250	48.0	0.038	6.9
23*	0.161 m UO_2SO_4 0.008 m UO_3	2.96	250	96.0	0.041	3.7
24*	0.161 m UO_2SO_4 0.008 m UO_3		250	24.0	0.023	8.4
25	0.161 m UO_2SO_4 0.008 m H_2SO_4	1.98	250	24.0	~0.05	~18
26	0.161 m UO_2SO_4 0.008 m H_2SO_4	1.98	250	24.0	~0.07	~23
27	0.161 m UO_2SO_4 0.008 m H_2SO_4	1.98	250	48.0	~0.10	~20
28	0.161 m UO_2SO_4 0.008 m H_2SO_4	1.98	250	4.0	~0.01	~20

*Acid deficiency of 0.008 m H_2SO_4.

Table 13.3. Amounts of Adherent Oxide Formed on Type 347 Stainless Steel Specimens

Run No.	Exposure Time (hr)	Weight of Oxide (mg/cm^2)
13	44.0	0.62 ± 0.04
14	89.0	0.63 ± 0.04
15	188.7	0.62 ± 0.04
16	78.0	7.1 ± 0.1
17	187.5	6.3 ± 0.1
18	96.0	5.9 ± 0.1
19	96.3	0.84 ± 0.05
20	4.1	0.35 ± 0.05
21	4.0	Not calculated – nonuniform corrosion
22	48.0	0.74 ± 0.04
23	96.0	0.82 ± 0.04
24	24.0	0.41 ± 0.04

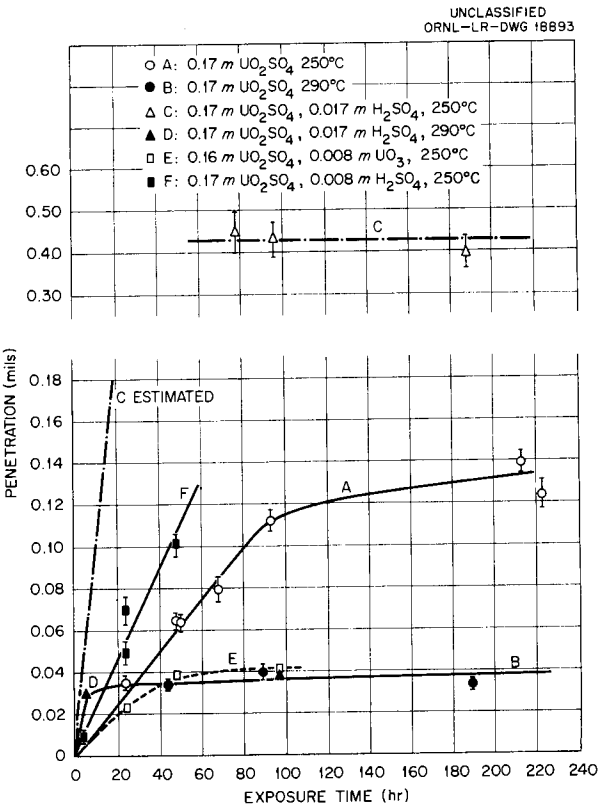

Fig. 13.5. Corrosion of Type 347 Stainless Steel in Solutions Free of Corrosion Products.

involved in film formation decreased markedly in both solutions when the exposure temperature was increased from 250 to 290°C. Furthermore, the results indicate that the effect of acid was negligible at the higher temperature, as is shown by comparison of the results at conditions B and D.

The rate of attack at the start of exposure is also affected by the concentration of excess acid, the rate increasing with increasing acidity. This may be seen by again referring to the results at conditions E, A, F, and C (Fig. 13.5). The experimental results to date, however, are insufficient to establish whether the initial rate also changes with temperature.

It should again be noted that the corrosion prior to passivation in this system, where the solutions are free of corrosion products, is appreciably greater than in static autoclave experiments.[16] As discussed previously, this difference is probably due to the difference in concentration of the corrosion product, chromium(VI). It is interesting to compare these results with those of a loop experiment[17] designed to minimize the concentration of corrosion products in solution. Four steel pin specimens were installed in an all-titanium loop and exposed at 250°C to a solution 0.17 *m* in UO_2SO_4 and 0.02 *m* in H_2SO_4 for 200 hr. Two of the pins, situated at a fluid flow velocity of 12 fps, gave rates of 385 and 190 mpy. Two other pins at 70 fps both gave rates of 770 mpy. The rates at 12 fps were higher than those experienced by similarly located specimens in a stainless steel loop experiment with a similar solution condition. Also, they are much higher than the rate reported here for the same temperature and solution composition. Comparison of these various results leads to the conclusion that the corrosion of steel is increased by the removal of corrosion products from the bulk of the solution. However, there is superimposed on this effect an accelerating effect due to rapid flow of solution.

[17] R. S. Greeley and J. C. Griess, private communication.

As has been speculated by Griess,[18] this velocity effect may, in part, be associated with the rate of transfer of corrosion products from the laminar film into the bulk solution. In view of this possibility, the study of velocity effects in the region between 0 and 10 fps is considered to be of interest. It is in this velocity range that the characteristics of flow transform from viscous to turbulent. A program of study is being considered in which flow in this velocity region is included as a variable in the present type of experiments.

13.3.2 Radiation Stability of Triethyl Phosphate and Amsco 125-82

Triethyl phosphate and Amsco 125-82 were examined[19] as possible HRT secondary refrigerants. Both these materials, which possess satisfactory physical properties for the already-installed refrigerating system, were irradiated at room temperature with Van de Graaff electrons to a dose level of 3.7×10^{22} ev/ml, comparable with that which the HRT secondary refrigerant will undergo over a two-year period. The results of this study indicate that either of the materials may be satisfactorily employed as the HRT secondary refrigerant in the cold traps. It is recommended that the refrigerant should be replaced about every three months and that the lines should be flushed out with fresh material to dissolve and remove any "polymer" formed.

A similar irradiation of Amsco 125-82 at its boiling point (165°C) revealed that approximately twice as much material was decomposed as that observed for room-temperature irradiation. Calculations have been made which indicate that, averaged over the total volume of refrigerant, the energy absorbed per milliliter due to irradiation in a freeze-plug section will be less by a factor of 10^3 than that due to irradiation in the cold traps when equal exposure periods are assumed. If it can be assumed that the coils of the freeze-plug sections will be completely freed of refrigerant following a freezing operation, then it appears that decomposition in this usage will not appreciably increase the average rate of decomposition of the refrigerant. Difficulties which may arise from the combination of radiation and thermal effects if some refrigerant remains in the coils have not been evaluated.

[18] J. C. Griess, *HRP Quar. Prog. Rep. Nov. 15, 1951*, ORNL-1221, p 21–23.

[19] M. D. Silverman, *The HRT Refrigerating System*, ORNL CF-57-1-28 (Jan. 9, 1957).

14. METALLURGY

G. M. Adamson

R. G. Berggren
J. P. Hammond
W. J. Leonard
M. L. Picklesimer
J. J. Prislinger
P. L. Rittenhouse
R. L. Stephenson
J. K. White
J. C. Wilson
C. H. Wodtke

14.1 PHYSICAL METALLURGY

14.1.1 Zirconium-Alloy Development

The objective of the zirconium-alloy development program is the development of a zirconium-base alloy with better radiation-corrosion resistance to fuel solutions than Zircaloy-2 has. Zirconium-niobium alloys have shown the most promise, and most of the work has been and will continue to be concentrated on the Zr–15% Nb base alloys. Alloys with bases of sponge and crystal-bar zirconium are being studied. A portion of the work to date was discussed in the last report.[1]

Specimens of the alloys 85 Zr–15 Nb, 85 Zr (sponge)–15 Nb, 84 Zr–15 Nb–1 Fe, 83 Zr–15 Nb–2 Pd, and 83 Zr–15 Nb–2 Pt (compositions in wt %) have been beta-quenched (at 900°C for 3 hr, water-quenched) and reheated to 300 to 600°C for times from 30 min to two weeks. The aging-hardness curves are presented in Figs. 14.1 to 14.5. Heating for times shorter than 30 min is

[1] G. M. Adamson *et al.*, *HRP Quar. Prog. Rep. Oct. 31, 1956*, ORNL-2222, p 114–116.

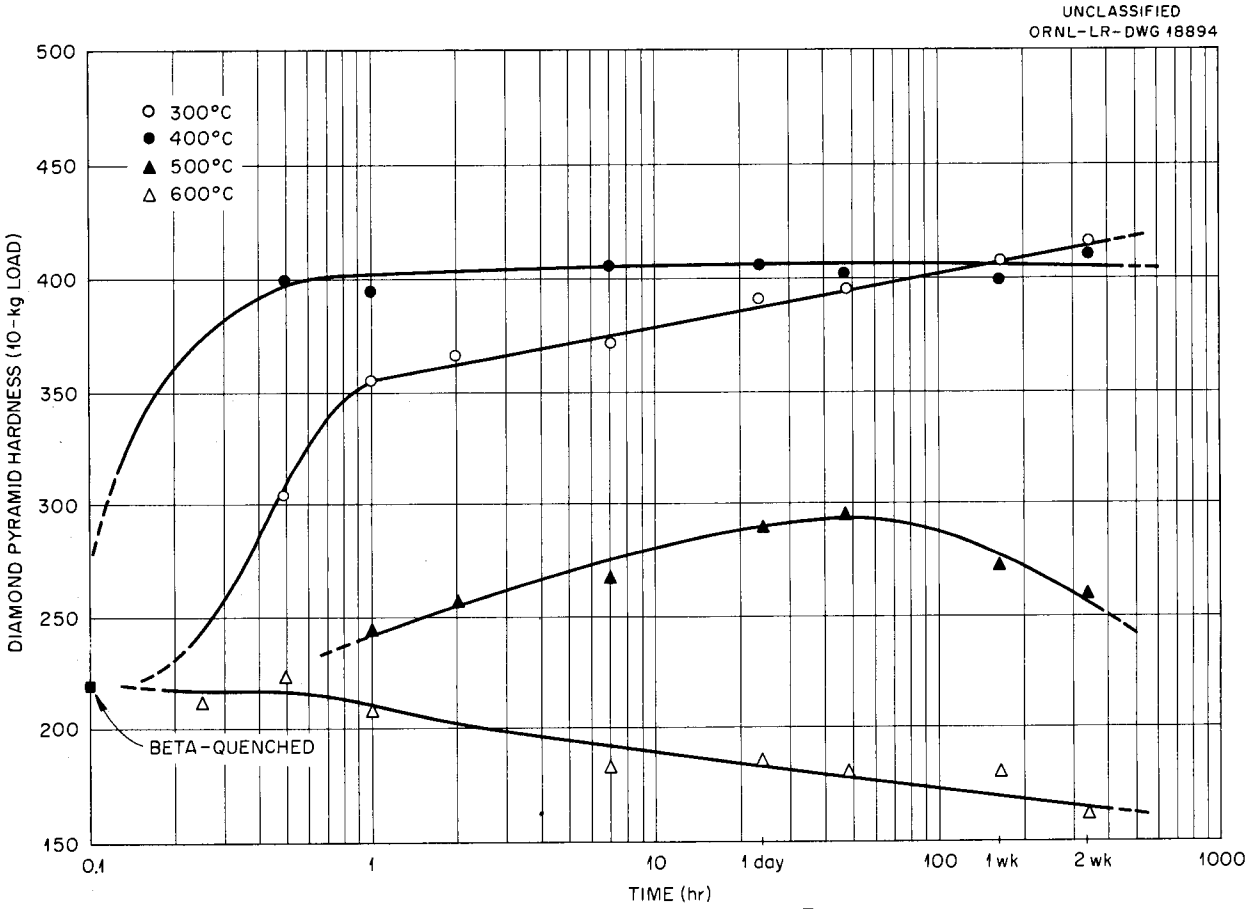

Fig. 14.1. Time-Temperature-Hardness Curves for Zr (Iodide)–15% Nb, Beta Quenched (900°C) and Reheated.

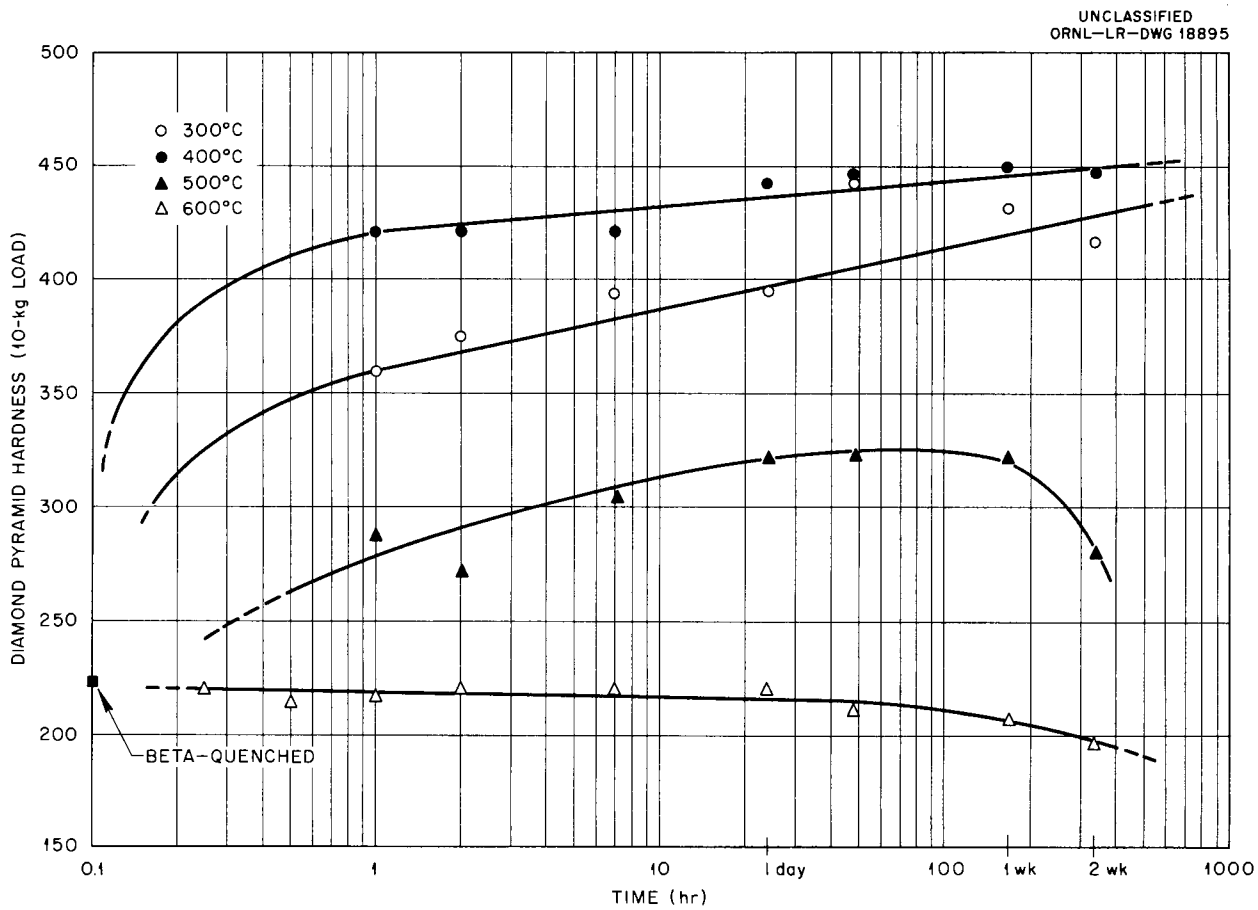

Fig. 14.2. Time-Temperature-Hardness Curves for Zr (Sponge)–15% Nb, Beta Quenched (900°C) and Reheated.

not practical in the method used (i.e., capsulating in vacuum or a partial pressure of argon in quartz or Vycor) but will be practical in the isothermal transformation machine in the near future. Microstructural examination of these specimens is under way, but few photomicrographs have been made to date. Analyses of the aging-hardness curves, the microstructures of the specimens, a preliminary apparent-specific-heat curve determined at the University of Tennessee in an adiabatic dynamic calorimeter, and preliminary x-ray diffraction examinations of some of the specimens permit the drawing of the following tentative conclusions:

1. Except for the hardening that occurs after the specimen is quenched and reheated to 400°C, all the transformations of the beta phase of the Zr–15 Nb base alloys are quite sluggish.

2. Transformation of retained beta, occurring at 500°C and below, in the beta-quenched and reheated specimens is quite similar to the age-hardening transformation occurring in age-hardenable alloys, showing the usual effect of temperature on the aging curves. Only those specimens aged at 500°C showed overaging in two weeks. The addition of the ternary elements, Fe, Pd, and Pt, causes a shift in the curves similar to that caused by some ternary additions to age-hardenable alloys. The addition of 2% Pd to the Zr–15 Nb alloy increased the incubation time of "omega" phase formation to 1 hr, while the addition of 1% Fe or 2% Pt increased the incubation time to 2 hr, at 500°C. These additions also appear to shift, to longer times, the hardness curves at 300 and 400°C, but no values can be given for the increase

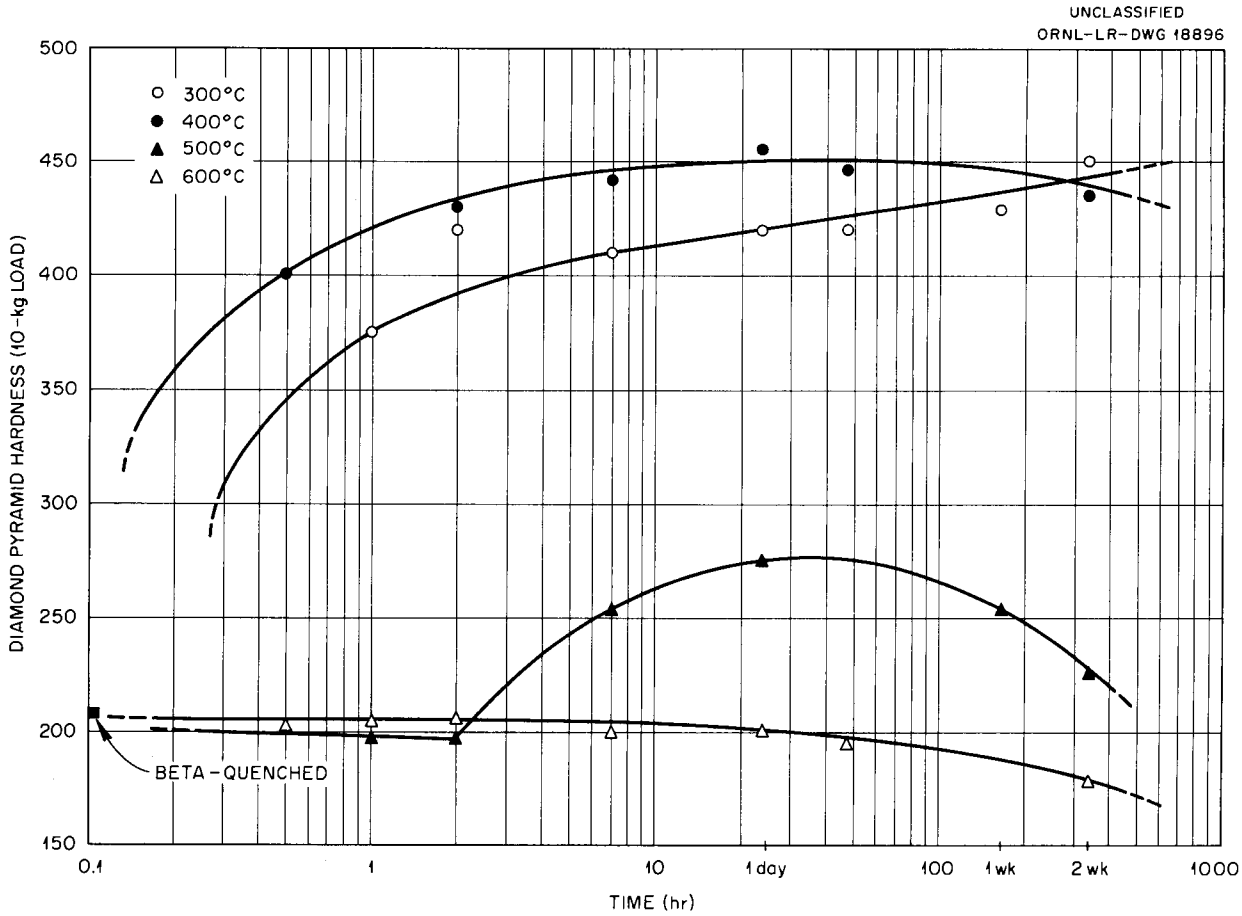

Fig. 14.3. Time-Temperature-Hardness Curves for Zr (Iodide)–15% Nb–1% Fe, Beta Quenched (900°C) and Reheated.

in these incubation times, since times shorter than 30 min have not yet been run. It is hoped that these increases in incubation time on quench and reheat indicate that the formation of "omega" phase may be sufficiently delayed to permit welding without serious embrittlement in the heat-affected zone.

3. The transformation of the retained beta on cooling is delayed by the addition of Fe, Pt, and Pd, as shown by the hardnesses (Table 14.1) of specimens which were water-quenched, step-cooled (100°C every 24 hr), or furnace-cooled. The microstructures of the ternary alloys show an amount of transformation, primarily grain boundary, equivalent to their increase in hardness. The step-cooled binary alloys show a reduction in hardness caused by overaging. The 2% Pt and

Table 14.1. Change in Hardness of Heat-treated Zirconium-Base Alloys with Cooling Rate

Alloy	Diamond Pyramid Hardness, 10-kg Load		
	Furnace Cooled	Step Cooled*	Beta Quenched
Zr–15 Nb	295	225	218
Zr–15 Nb (sponge)	260	224	220
Zr–15 Nb–1 Fe	232	272	208
Zr–15 Nb–2 Pd	197	266	195
Zr–15 Nb–2 Pt	205	305	200

*Furnace controller turned down 100°C every 24 hr.

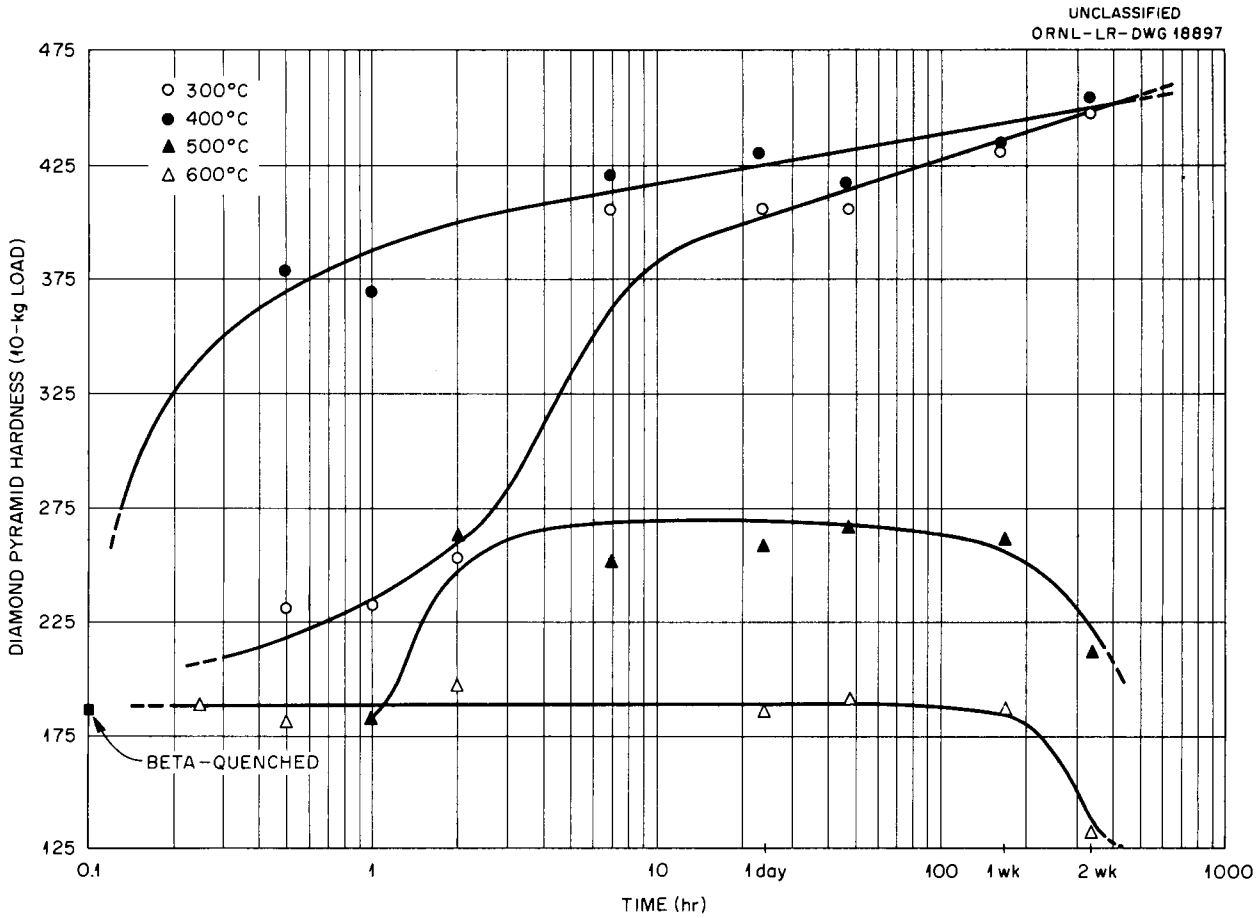

Fig. 14.4. Time-Temperature-Hardness Curves for Zr (Iodide)–15% Nb–2% Pd, Beta Quenched (900°C) and Reheated.

2% Pd alloys show essentially the same microstructure whether quenched or furnace cooled, except that grain boundaries are more apparent in the furnace-cooled specimens. No photomicrographs have been made as yet.

4. The Widmanstätten platelet transformation structure has not yet been identified by x-ray examination and seems to form and to be stable only below approximately 250°C. The structure dissolves on reheating a quenched specimen to 300 to 600°C, the rate of solution being greater at the higher temperatures. The structure seems to form during the quench and is not seen in air- or furnace-cooled 15% Nb specimens, but is seen in the 1 Fe, 2 Pd, and 2 Pt–15 Nb alloys. An analysis of the specific-heat curve indicates that the platelet phase starts dissolving at about 250°C, and is completely dissolved at 350°C, with a heating rate of approximately 8°C per minute in the calorimeter.

5. The formation of the "omega" phase, on quench-and-reheat heat treatment, occurs between 300 and 530°C, with the greatest precipitation occurring near 400°C and the phase dissolving on further heating until all the "omega" phase is redissolved at 530°C, again at a heating rate of 8°C per minute in the calorimeter. No eutectoid transformation was detectable either on heating or on cooling in the calorimeter. A very sluggish transformation of the decomposition products (for a specimen previously heated at 600°C for two weeks) to beta was observed, starting at about 580°C and continuing to 800°C at a heating rate of 8°C per minute.

Chemical polishing and etching techniques have been worked out so that all specimens prepared

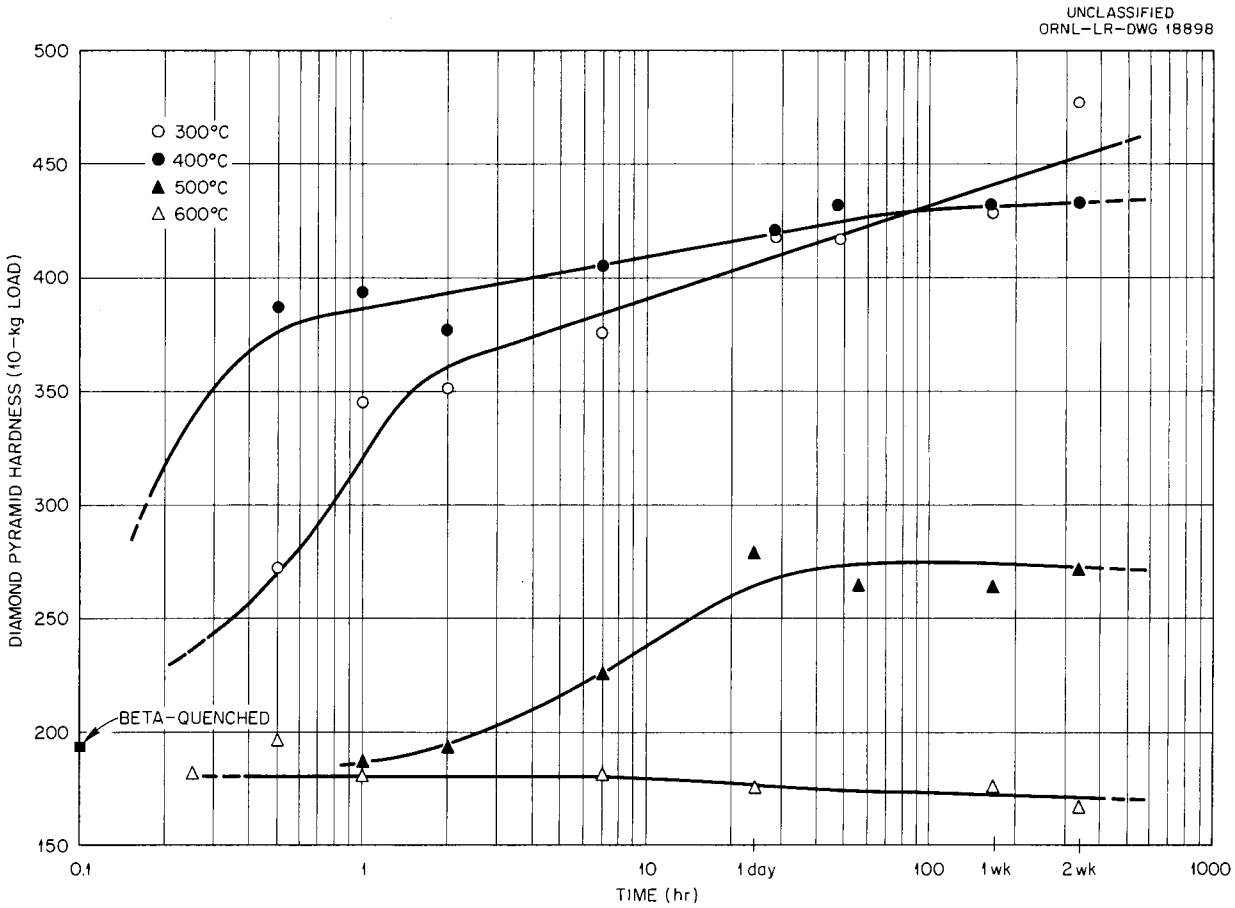

Fig. 14.5. Time-Temperature-Hardness Curves for Zr (Iodide)–15% Nb–2% Pt, Beta Quenched (900°C) and Reheated.

to date can be examined metallographically and photomicrographs made. Cathodic etching experiments are being carried out on certain specimens to serve as a check on the microstructures as revealed by chemical polishing and to prepare specimens for examination by electron microscopy. Three specimens have been successfully cathodically etched, and the microstructures are in essential agreement with those shown by chemical polishing. No electron microscopy has been done as yet.

14.1.2 Special Zirconium Alloys – Mechanical Properties

The Armour Research Foundation of the Illinois Institute of Technology during the past year has been investigating, under a research contract, the stability of all-beta and all-alpha zirconium-base alloys for application under stress at temperatures up to approximately 300°C. These alloys are to be weldable, and the deterioration of the corrosion resistance, impact strength, and tensile ductility is being studied as a function of time at operating temperatures, stresses, and heat treatment.

Alloys being studied are iodide Zr, unalloyed sponge Zr, iodide- and sponge-base Zr–1.5% Sn alloys, and iodide- and sponge-base Zr–Nb alloys with and without small ternary additions. Tensile, tensile-impact, as-heat-treated, and as-welded studies will be made. Hardness and metallographic studies of the Zr-Nb alloys will be made as a preliminary to the mechanical-property determinations.

The following indications are given as a summary of the work to date on the all-alpha alloys:

1. Unalloyed iodide Zr is superior in tensile

impact tests to unalloyed sponge Zr, especially in the welded condition.

2. The presence of 1.8% Sn has little effect on the strength of iodide Zr in the as-quenched (1000°C) as well as in the welded condition.

3. The presence of 1.7% Sn enhances the tensile impact strength of sponge Zr in the as-quenched (1000°C) condition; no welded specimens were prepared because of insufficient stock.

A small amount of work has been done with the iodide Zr–15 Nb and Zr–15 Nb–2 Pd alloys. The Zr–15 Nb alloy shows consistent brittleness in the as-quenched (1000°C) and in the quenched-and-aged (600°C) conditions. The Zr–15 Nb–2 Pb alloy, however, shows considerable ductility and fairly high strengths in both conditions: 1000°C water quenched, 89,600 and 92,500 psi ultimate tensile strength with 14% elongation in 1 in.; 1000°C water quenched followed by aging at 600°C for 24 hr and water quenching, 98,000 and 94,000 psi ultimate tensile strength with 12 and 6% elongation in 1 in. No tensile impact results have been reported.

14.1.3 Zirconium-Hydrogen System

The modified Sievert's apparatus,[2] for the addition of H_2 to Zr and Ti specimens and for equilibrium H_2 pressure determinations over Zr and Ti alloys, has been plagued with leaks that will not permit a leak rate of less than 5 μ in 2 hr. Since many of the equilibrium studies desired will involve pressures not greater than 100 μ and since times on the order of 24 hr will be required to establish equilibrium conditions, a leak rate of less than 5 μ in 24 hr is desired. The primary source of leaks has been the grease-type ground-glass taper valves used in the system. A new type of valve, requiring no grease and completely enclosed in glass, has been designed, built, and tested satisfactorily. A design modification of the apparatus incorporating the new-type valves is under way.

14.2 MECHANICAL METALLURGY

14.2.1 Effect of Hydrogen on Embrittlement of Titanium at 300°C

An investigation is being made to determine the effect of hydrogen content on the room-temperature impact strength of commercially pure A55 titanium plate that has been aged at 300°C for various periods of time.

Subsize cylindrical-shaped Izod specimens having a circumferential 45-deg V-notch were machined from a ¼-in. plate of A55 titanium, care being taken to ensure that all the specimens had the same orientation with respect to the plate.

The information obtained to date is from vacuum-annealed, as-received, and hydrogen-charged A55 titanium plate. The vacuum-annealing cycle consisted in heating the titanium specimens to 800°C, maintaining that temperature for 20 hr at a pressure of less than 0.1 μ, and cooling slowly to room temperature. The charged specimens were first vacuum-annealed, reheated to 800°C in a vacuum of less than 0.1 μ, charged with a calculated amount of hydrogen, and then slow-cooled to room temperature.

Figure 14.6 shows the variation in impact strength with increasing hydrogen content of as-received specimens and others aged for 2520 hr at 300°C. The aging does not seem to have any adverse effects on the impact properties. All values for the aged specimens are above the as-received curve, but are within the limits of error.

14.2.2 Drop-Weight and Charpy V Impact Studies of Steel, Titanium, and Zirconium

The drop-weight test[3] is used to determine the lowest temperature at which a material is ductile. Values are expressed in terms of the nil ductility temperature (NDT), which is the temperature at which the metal loses its ability to deform in the presence of a sharp crack.

As an aid to the radiation-damage program, a study was made on a vacuum-melted steel, Crucible Steel's Ferro-Vac-10, to determine the relationship between the Charpy V impact curve and the NDT. The dimensions of the drop-weight specimens were 1 × ½ × 14 in. instead of the usual 3½ × ½ × 14 in. The crack-starter material was Haynes Stellite hard-facing material. The NDT was approximately +10°F for the as-received condition and –20°F for the normalized material (heated at 1700°F for 1 hr and air cooled to room temperature). Full-size Charpy V specimens were machined from the used drop-weight specimens. The relationship

[2] W. O. Harms, J. I. Federer, and G. B. Wadsworth, *HRP Quar. Prog. Rep. Jan. 31, 1955*, ORNL-1853, p 158.

[3] P. P. Puzak, M. E. Schuster, and W. S. Pellini, *Welding J.* **33**, 481S–495S (1954).

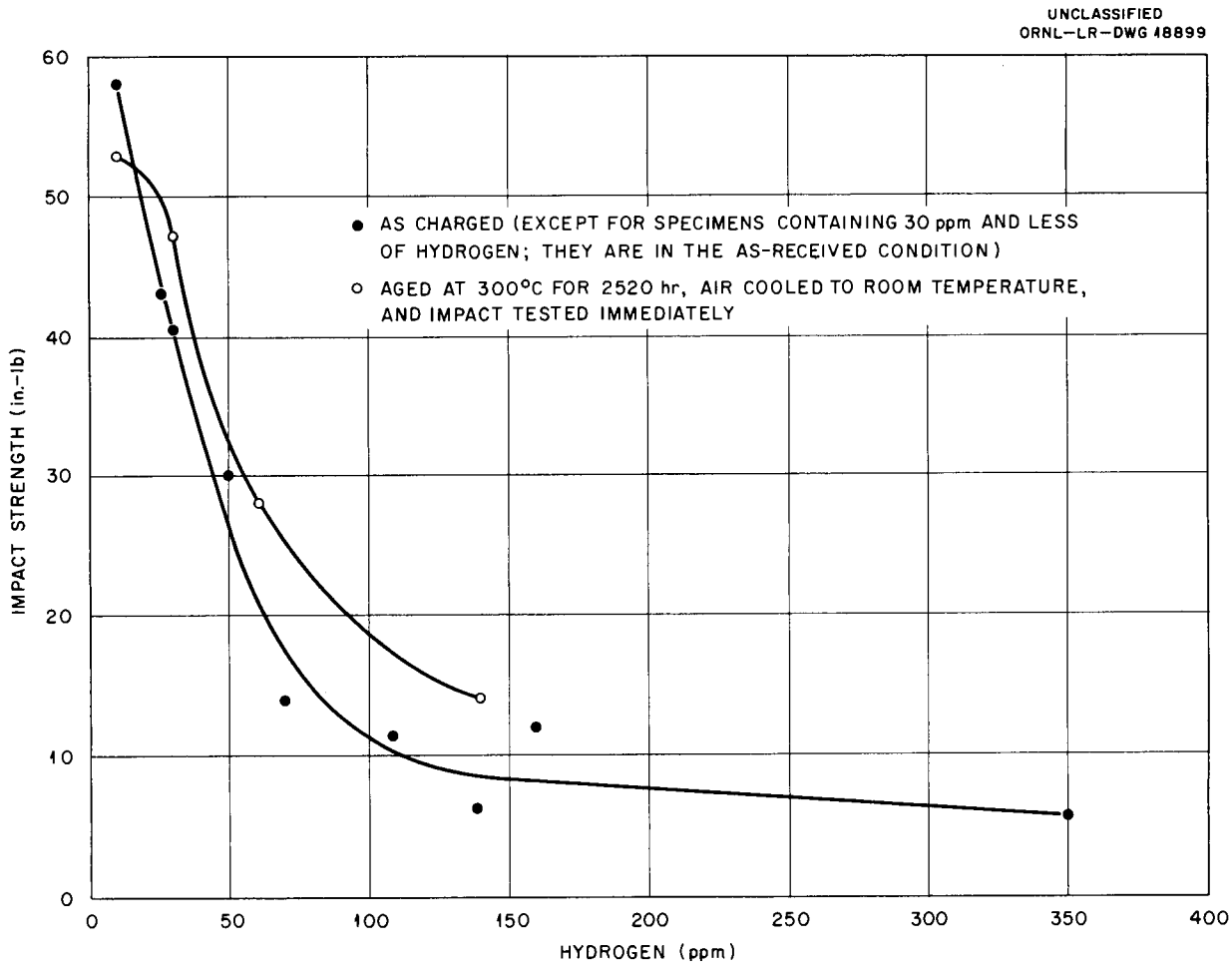

Fig. 14.6. Variation in Impact Strength with Hydrogen Content of Aged A55 Titanium.

between the NDT and its position on the Charpy V impact curve is demonstrated in Fig. 14.7.

These curves demonstrate the unacceptability of Charpy curves in determining brittle characteristics of metals. The normalized material is brittle at temperatures below −20°F, even with impact values of 30 ft-lb; the as-received material is brittle below 10°F, while above it is ductile, but with values of only 5 ft-lb.

Drop-weight testing of titanium alloys has continued during this period. Samples of A55 titanium have been tested in the range of 22 to −196°C, with no brittle failures. Cracks have progressed only through the heat-affected zone near the crack-starter weld. Charpy V specimens are being machined from the broken plates. A single plate of A75 titanium was tested at −70°C and was brittle at this temperature.

The relationship between the Charpy impact curve and the NDT for 6 Al–4 V titanium is demonstrated in Fig. 14.8. The dimensions of the drop-weight specimens used were $3\frac{1}{2} \times \frac{1}{2} \times 14$ in. This relationship is very similar to that found in steels, with the NDT near the inflection at the lower end of the curve. Although sufficient points were not determined, it is possible that a break does exist in the center of the curve. During drop-weight testing, this material broke in a brittle manner below −139°F and was ductile above this temperature. The material exhibited a very pronounced shear lip, which decreased somewhat with decreasing test temperature. An interesting observation was that the shear lip was present

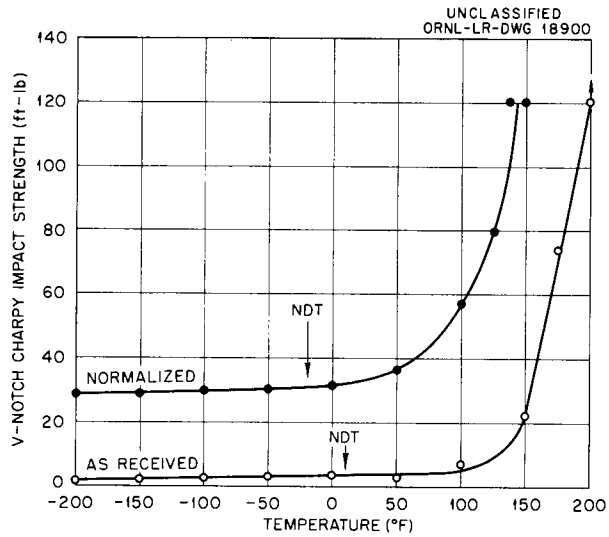

Fig. 14.7 Charpy V Transition Curves for Ferro-Vac-10 Steel.

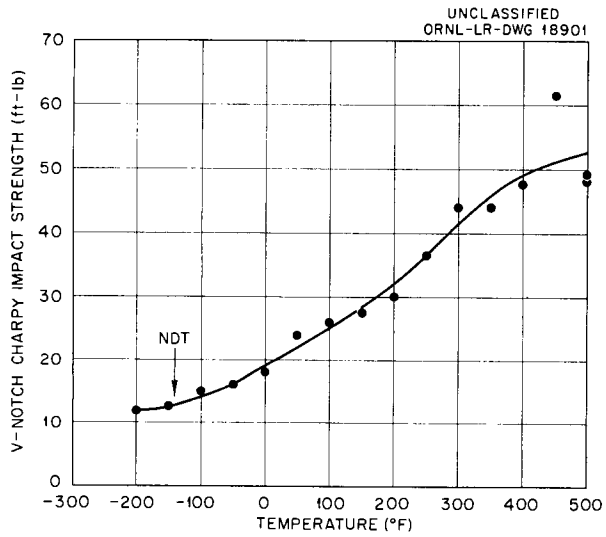

Fig. 14.8. Charpy V Transition Curve for 6 Al–4 V Titanium.

below the NDT, which is contrary to what would normally be found in steel.

A modified vise for the Charpy V (full-size) impact apparatus is being machined at present. The new vise will permit the impact specimen to be heated in place by carbon electrodes at each end of the specimen. A thermocouple will be spot-welded to the specimen as close to the root of the notch as possible by means of a capacitor discharge welder. A network of thermocouples connected to a selector switch gives the temperature of any particular specimen. Preliminary tests with a borrowed welding transformer, which provided the necessary voltage to ensure an adequate heat supply, have proved very successful; an order has been placed for a welding transformer.

14.3 WELDING DEVELOPMENT

Work has been under way on establishing and qualifying a procedure for welding the Carpenter 20 stainless steel for HRT chemical plant components. The alloy contains nominally 20 Cr, 29 Ni, 3 Cu, 3 Mo, 1 Nb max (wt %) and is completely austenitic in the as-welded condition.

Cracking was found in the initial tungsten arc welds, which had been made under conditions normally used for welding type 347. The interdendritic cracks were typical of those found in completely austenitic welds in the 300-series steels.

As dictated by the necessity for preventing hot cracking, welding current was limited to the range of 60 to 100 amp. Weld cracking, previously shown by guided bend test, was curtailed, but welding speed was drastically reduced.

A single-welded joint without backing strip was satisfactorily completed in 6-in. sched-40 pipe. Welding was done with the tungsten arc process, in the horizontal position (pipe axis vertical). In the standard guided bend tests, four welds satisfactorily passed both the root and face-type bend tests, with a $2T$ radius. Three tension specimens gave values of 93,600, 96,000, and 91,600 psi, and in each case a shear-type failure occurred in the weld zone.

14.4 METALLURGICAL DEVELOPMENT AND SERVICE

14.4.1 Roll Cladding Titanium on Steel

The Armour Research Institute demonstrated[4] experimentally the feasibility of roll cladding titanium on plain carbon steel and on stainless steel. By use of an intervening 0.025-in. sheet of vanadium as a diffusion barrier, titanium-clad carbon-steel samples (about 3 × 9½ in.) were successfully prepared with substantial bonding strengths. Total reductions of 80% or more were

[4] Armour Research Institute, *Summary Report, Feasibility of Roll Cladding Titanium on Steel* (Dec. 31, 1956).

found necessary; the rolling temperature was from 850 to 1000°C.

It was shown that the quality of the bond, as reflected by rather severe bend tests, is not seriously affected by protracted anneals at from 300 to 750°C.

A phase, very probably sigma, detected at the vanadium-steel interface does not seem to be a serious threat to the stability of the bond. A thin layer of pure copper interposed between the vanadium and the plain-carbon-steel base proved effective in eliminating this phase and lending some improvement to the quality of the clad. However, smaller individual roll reductions are necessary.

Titanium can be clad on stainless steel by procedures much the same as those employed for plain-carbon-steel clads. Although the quality of stainless-base clads is not so good as that of carbon-steel-base clads, even when a copper barrier is placed between the vanadium and the stainless steel, the clads nevertheless are sound and would be satisfactory for some applications.

14.5 INSPECTION DEVELOPMENT

14.5.1 Development of an Eddy-Current Test for Heat Exchanger Tubing

The development of an eddy-current test for the detection of flaws in type 347 stainless steel $\frac{3}{8} \times 0.065$ in. tubing and $\frac{3}{8} \times 0.49$ in. tubing was the subject of a recently concluded development project contracted to American Testing and Control Company (AT&C) of Berkeley, California. A successful test was to have detected No. 80 drill holes, and notches on either the outside or the inside diameter at a depth of 3% of the wall thickness.

AT&C designed an all-transistorized eddy-current instrument known as the Metron V for this inspection problem. In the AT&C test system a tandem or differential arrangement of small-outside-diameter coils is operated at 260 kc. This high frequency gives good sensitivity and resolution to certain types of defect. A No. 80 drill hole gives a recorder deflection of almost full scale, and resolution is sufficient to separate two No. 80 drill holes $\frac{1}{4}$ in. apart. The tandem coil arrangement causes some lack of sensitivity to a uniform 3% notch, except at its ends, because this system differentiates the signal and hence only gives indications from discontinuities that occur suddenly. This implies that certain types of cracks may go completely unnoticed. AT&C contends that natural defects are not as uniform as the notch and therefore might be detectable.

The biggest gap in the technique is the ID inspection. There is inherently bad penetration of eddy currents through the tube wall at the high frequency employed. AT&C proposed a double inspection, one with encircling coils to show the outer part of the tube, and another with a bobbin-type coil to inspect the inside, but their final report did not mention any ID work. Subsequent to this report, an oral agreement was reached to have this phase of the investigation completed.

14.6 EFFECTS OF RADIATION ON STRUCTURAL METALS AND ALLOYS

14.6.1 Equipment and Facilities

Irradiation of 187 impact and 79 tensile specimens of 14 alloys is under way in facility HB-3 of the MTR; the irradiation will continue through four three-week cycles. The irradiation apparatus was designed to provide data on the effect of irradiation temperature on the changes in strength and ductility of the specimens. The three temperatures at which neutron exposures are being made were calculated to be 702, 558, and 365°F and were measured to be 694, 600, and 482°F.

The apparatus (Fig. 14.9) utilizes gamma-ray heating to elevate specimen temperatures during irradiation. A massive stainless steel wedge (shape dictated by the gamma-ray heating gradient in the MTR beam hole) is used as a heat generator; one face of the wedge carries tensile specimens (three deep) and the other face, notch-impact specimens. The outer surfaces of the specimens are forced against mating surfaces of the water jacket. During reactor operation the heat generated in the wedge is conducted through the specimens to the water jacket. Thus a gradient is established across the stack of specimens. About 30 thermocouples at various locations monitor typical specimen temperatures.

14.6.2 Results of Irradiation Experiments

The first known data on the effects of irradiation on Zircaloy-2 and high- and low-ferrite austenitic stainless steel weld metals have been obtained. Table 14.2 gives the result of tension tests on these materials. The effect of irradiation is to cause a greater loss of ductility in the weld metal

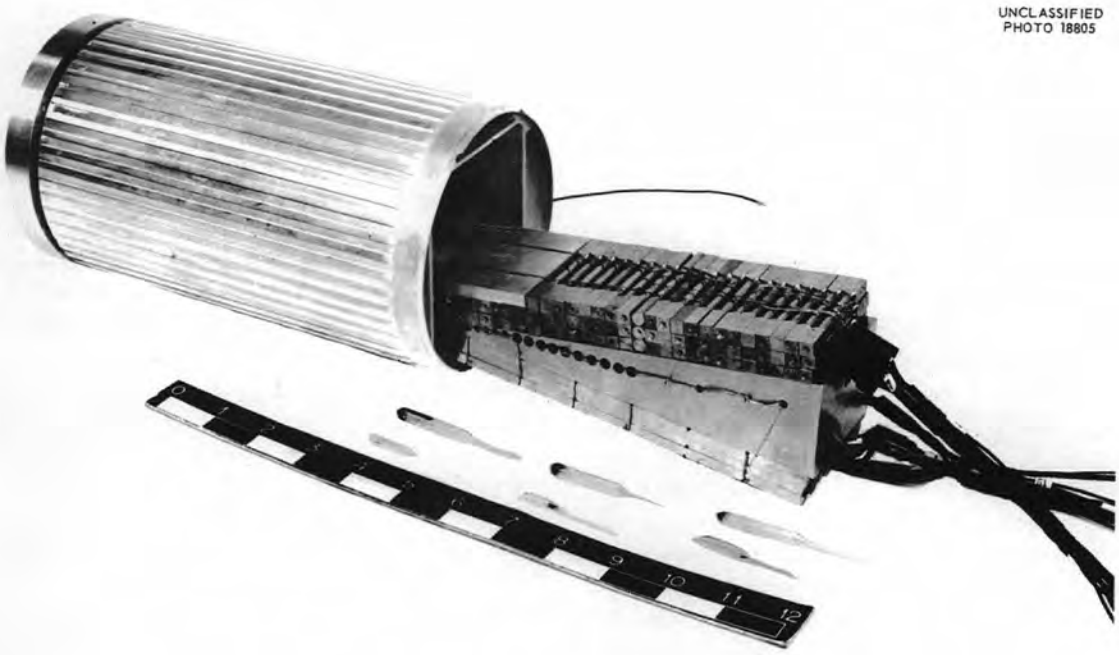

Fig. 14.9. Elevated-Temperature Irradiation Apparatus.

Table 14.2. Tensile Properties of Irradiated Weld Metals

Material	Dose, Fast (*nvt*)	Yield Strength (psi)	Tensile Strength (psi)	Uniform Elongation (%)	Total Elongation (%)
Zircaloy-2	0	64,500	77,000	10.5	16.3
	3.6×10^{19}	86,600	91,300	2.4	10.2
Austenitic stainless steel (low-ferrite weld)	0	55,100	90,100	38.5	43.5
	1×10^{20}	101,600	112,700	16.0	22.2
Austenitic stainless steel (high-ferrite weld)	0	56,300	92,900	41.5	48
	1×10^{20}	107,000	116,000	20.2	29

than in wrought material of similar composition. The specimens were cut across the weld zone in ¼-in.-thick plates; accordingly, the weld metal and the heat-affected zone constitute only a portion of the gage length. Thicker weldments are required to produce specimens in which the gage length is all weld metal.

High-purity vacuum-melted iron specimens were used to determine whether radiation effects might be reduced in iron or iron alloys by removing the greatest possible number of impurity elements. Subcritical and supercritical anneals were used to produce both fine- and coarse-grained specimens.

Irradiation to 3.6×10^{19} *nvt* (fast) at about 175°F produced normal changes in properties. The effect of strain rate was then determined by pulling specimens at 2 in.·in.$^{-1}$·min^{-1}, about 40 times as fast as the normal strain rate. At the higher strain rate, neither the coarse-grained nor the fine-grained iron showed appreciable uniform elongation before the maximum load was reached;

all elongation took place after necking began. Strain rate, over the limited values employed here, has little effect on the unirradiated material. The E-7016 weld-metal specimens tested earlier showed a great loss in uniform elongation at relatively low doses;[5] a strain-rate effect was sought by pulling tests at 0.002 in. $in.^{-1} \cdot min^{-1}$, but none was observed. The data indicate that the mechanical properties of high-purity iron are much more strain-rate-sensitive than those of carbon steels.

A few preliminary irradiations of full-size Charpy V specimens in the LITR have been completed. The fast-neutron dose was 4×10^{18} *nvt*. In an A212, grade B steel, tests were run at 32°F after irradiations at 600°F and at about 150°F. Three control specimens broke at an average of 24.0 ft-lb; the 600°F irradiated specimens at 17.2 ft-lb (two specimens); and the 150°F irradiated specimens at 3.2 ft-lb (two specimens). The control fractures were ductile, but all irradiated fractures had a rather unusual appearance of mixed brittle and ductile effects that had not been observed before. Besides illustrating the effect of irradiation temperature, these preliminary experiments suggest that closer attention should be paid to fracture appearance in evaluating test results.

[5] R. G. Berggren and J. C. Wilson, *Recent Data on the Effects of Neutron Irradiation on Structural Metals and Alloys*, ORNL CF-56-11-1 (Jan. 30, 1957).

Part V

CHEMICAL ENGINEERING DEVELOPMENT

F. R. Bruce

15. FUEL PROCESSING

D. E. Ferguson E. O. Nurmi
R. W. Horton R. A. McNees
S. Peterson

15.1 BEHAVIOR OF SOLIDS IN THE HRT MOCKUP

Solids recovered from the HRT mockup loop were coarser than the synthetic corrosion-product solids introduced into the loop (Fig. 15.1). A probable explanation is that the fine particles tended to agglomerate either while being held for several days in the hydroclone underflow pot or while in the loop system itself. If the latter explanation is correct, particle growth in the HRT fuel system may prevent accumulation in the fuel of extremely fine particles that cannot be separated by the hydroclone.

Many variations in method of preparation were tried in an effort to synthesize corrosion-product solids with the lowest possible halide content. Analytical difficulties, however, made the exact halide content doubtful, as evidenced by material balances on halides ranging from 5% to more than 200%. In a series of tests in which UO_2SO_4 solutions containing 150 to 500 g of solids per liter of solution were heated to 300°C for 72 hr, the fluoride content of the solution increased from a blank value of 6 to 7 ppm to only 9 to 10 ppm. The chloride content in all cases was too low (<10 ppm) to be measured accurately with the amount of liquid available. These results indicated that, despite possibly adverse analytical data, use of dilute suspensions of the solids in the HRT chemical plant would not introduce dangerous amounts of halides into the system.

15.2 IODINE CHEMISTRY

The behavior of iodine in simulated fuel solution under irradiation was studied further. The

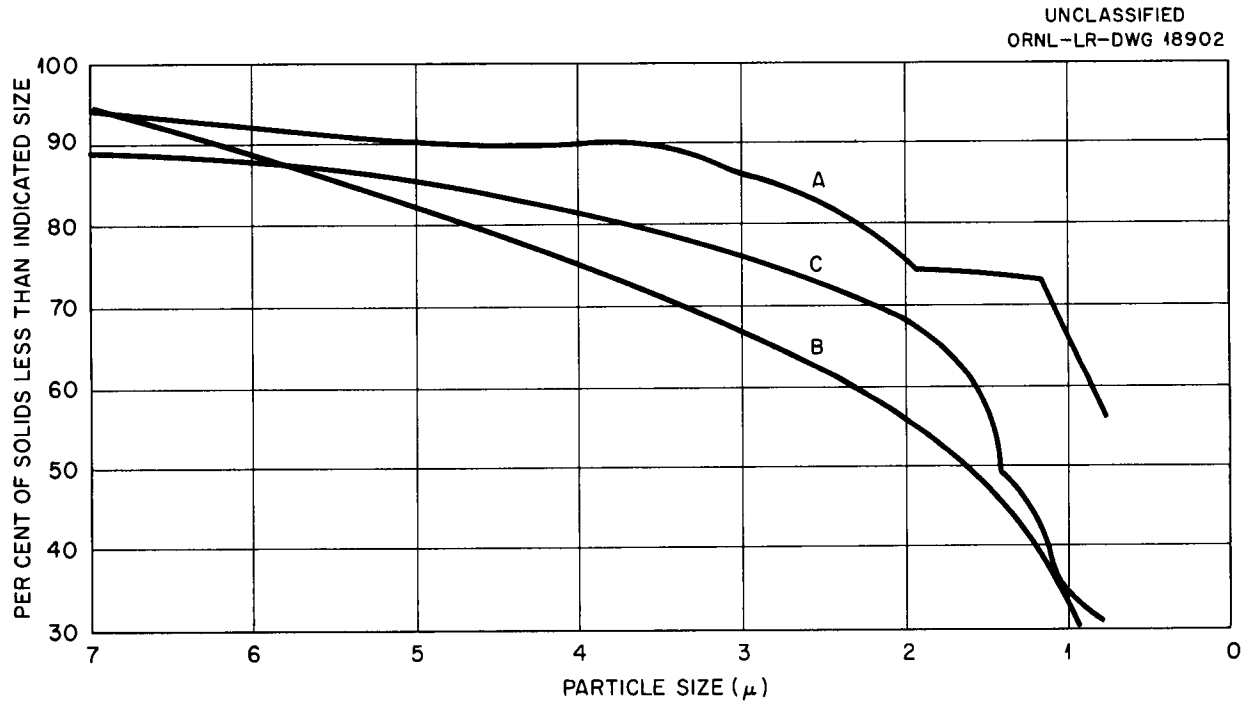

Fig. 15.1. Particle Size of Solids in HRT Mockup Loop. (A) Solids injected into loop; (B) solids were removed from the system after the hydroclone had been operating for 11 days and were assumed to be representative of corrosion-product solids; (C) solids collected in 14 hr of operation during a 200°C temperature cycle.

following variables were considered: composition of the atmosphere over the fuel solution, iodine concentration, and temperature in the range 100 to 120°C.

Small variations in the H_2/O_2 mole ratio in the vicinity of 2/1 markedly affected the valence state, with increasing H_2 content decreasing the stability of the iodate. Increasing the temperature from 100 to 110°C did not measurably affect the iodate stability, but a further increase to 120°C decreased the amount of iodate present. Variation in iodine concentration in the range 10^{-5} to 10^{-6} *m* had no measurable effect. These results suggest that, in the low-pressure system of a homogeneous reactor, maintenance of iodine in its volatile elemental state would be favored by H_2/O_2 ratios greater than 2/1 or by maintaining a temperature of 120°C in the system.

The experimental method used in these studies was to load synthetic fuel solution (0.02 *m* UO_2SO_4, 0.005 *m* H_2SO_4, 0.005 *m* $CuSO_4$, 10^{-5} or 10^{-6} *m* HIO_3) into a stainless steel bomb with the desired mixture of hydrogen and oxygen at a total pressure near 1 atm. The bomb was heated to the desired temperature and then exposed to Co^{60} gamma radiation at an intensity of 2 w/liter. Samples taken immediately before starting the irradiation and at various times during each irradiation were analyzed to determine the proportions of iodide ion, elemental iodine, and iodate ion.

Previous experiments with the iodine initially present as iodide and as elemental iodine[1] showed slow oxidation to iodate when the H_2/O_2 mole ratio was less than 2/1. In the present work, with iodine initially present chiefly as iodate, reduction was to a mixture of iodide and free iodine, largely the latter (Fig. 15.2). As a result of the two opposing processes, that is, oxidation of elemental iodine and reduction of iodate, the iodate proportion should reach a steady-state value. This was not achieved in a few hours of irradiation at this intensity, unless the steady-state value was not greatly different from the initial value. Often the iodate content dropped below the steady-state value and then rose. This probably reflects a more rapid approach to dissolution equilibrium for hydrogen than for oxygen, favoring reduction in the early part of the experiment.

[1] D. E. Ferguson *et al.*, *HRP Quar. Prog. Rep. Oct. 31, 1956*, ORNL-2222, p 136–137.

For the conditions in Fig. 15.2, an estimate of the steady-state iodate value is given in Fig. 15.3 as a function of the H_2/O_2 ratio. When the initial iodine concentration was a factor of 10 lower (10^{-6} *m* IO_3^-), the concentrations were within the accuracy of the experiments, with the estimated steady-state values fitting the graph of Fig. 15.3.

When the solution was heated in the absence of radiation, the iodate was reduced to a mixture of iodide and free iodine; no attempt was made to

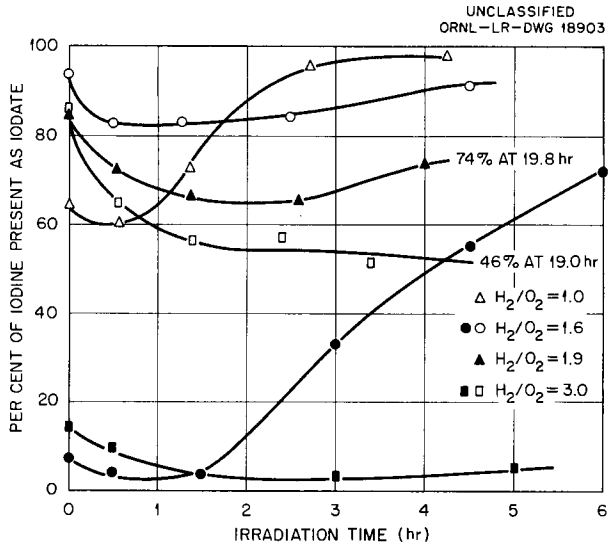

Fig. 15.2. Behavior of Iodine in Simulated HR Fuel at 100°C. Iodine concentration, 10^{-5} *m*.

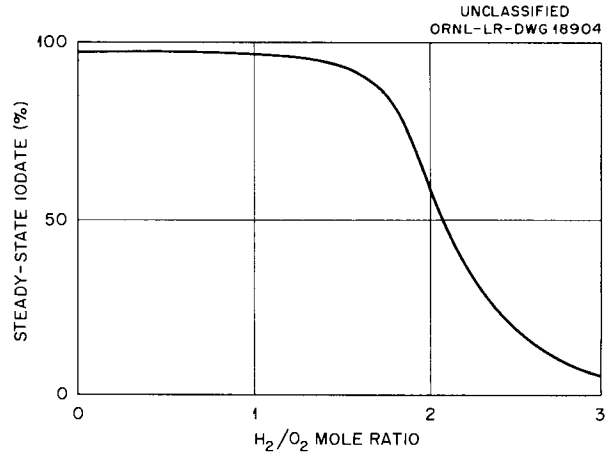

Fig. 15.3. Dependence of Solution Iodate Steady-State Value on Gas Composition.

determine the extent and rate of this reaction. In experiments in which overnight heating was followed by irradiation, the iodide diminished and the iodine-iodate proportions approached the steady-state values determined by the gas composition. This is shown for low H_2/O_2 ratios in Fig. 15.2 and for H_2/O_2 near stoichiometric proportions in Fig. 15.4.

Iodate stability was relatively unaffected by increasing the temperature from 100 to 110°C, but it was greatly decreased by a further increase to 120°C (Fig. 15.5). This effect also held at higher oxygen concentrations (Fig. 15.6).

15.3 VOLATILITY OF IODINE UNDER REACTOR CONDITIONS[2]

In a continuation of the dynamic loop runs[3] the effect of iron on the extractability of iodine under simulated reactor conditions was negligible. In two tests sufficient $Fe_2(SO_4)_3$ was added to give a total iron concentration of 30 or 300 mg/liter. In both cases 11 min was required to lower the iodine concentration to half its original value at 285°C. Allowing for variations in flow rates during the two experiments leads to values of 10.9 and 9.5 for the vapor-liquid distribution coefficient and indicates that the presence of iron as a corrosion product in a homogeneous reactor fuel system will not prevent the iodine from being scrubbed out of such a solution by a circulating gas.

Preliminary data[3] indicated that the platinized alundum pellets used in the radiolytic-gas recombiner system would absorb and hold more iodine at 500 than at 350°C. Further experiments showed that equilibrium conditions had not been obtained in the previous experiments and that iodine is absorbed more strongly at 350 than at 500°C. Better values are 31 mg of iodine per kilogram of pellets at 350°C and 6.5 mg of iodine per kilogram of pellets at 500°C when the gas contained no hydrogen. Addition of hydrogen to the gas stream carrying iodine over the hot, platinized alundum pellets increased the amount of iodine held up on the pellets. At 500°C the iodine absorbed was 26 mg per kilogram of pellets, or about four times the amount when no hydrogen

[2] R. A. Keeler, *Homogeneous Reactor Fuel Reprocessing Quarterly Progress Report: October 1–December 31, 1956*, KLX-10060.

[3] D. E. Ferguson *et al.*, *HRP Quar. Prog. Rep. Oct. 31, 1956*, ORNL-2222, p 137–139.

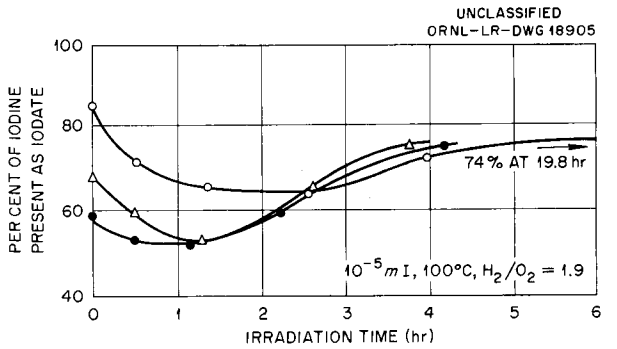

Fig. 15.4. Iodate Behavior for Different Pre-irradiation Iodate Contents.

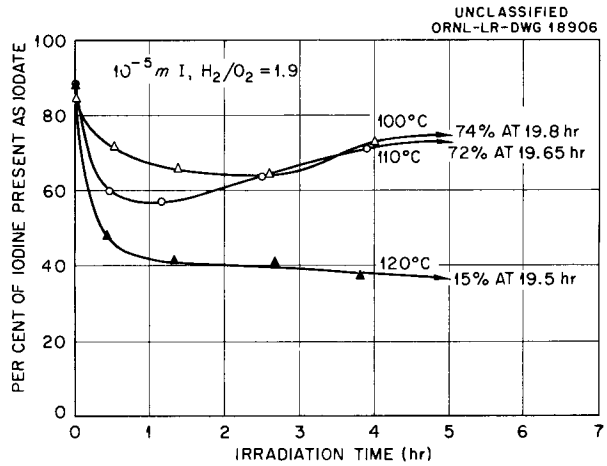

Fig. 15.5. Effect of Temperature on Iodate Radiation Stability.

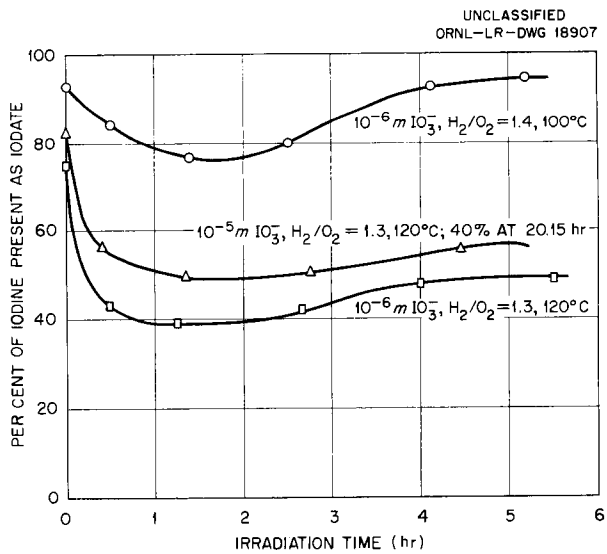

Fig. 15.6. Effect of Temperature on Iodate Stability at Low H_2/O_2 Ratios.

was present. At 350°C absorption ranged from 100 to 500 mg of iodine per kilogram of pellets in different sections of the absorption tube during two separate runs. In both runs the gas flow over the pellets was stopped while the pellets were at 350°C. Shortly after the gas flow was stopped, a violet color appeared in the vapor space within the tube and then disappeared as the temperature continued to drop. It is postulated that after the gas flow was stopped, the recombination of hydrogen and oxygen continued until all the hydrogen was oxidized. The absorbent thus became "supersaturated" with respect to a hydrogen-free atmosphere, and iodine volatilized from the pellets as a result of oxidation of iodide to free iodine. Further cooling resulted in reabsorption of iodine on the platinized pellets. Such behavior was not observed at 500°C, probably because the amount of iodine liberated upon cooling from 500°C was not sufficient to color the vapor.

Further studies on the behavior of iodine on silver-alundum pellets showed that the method of contacting iodine with the pellets did not affect the earlier observations.[3] Iodine introduced into silvered alundum pellets by passing tagged iodine vapor with steam and oxygen over the pellets at 300°C did not exchange with untagged iodine subsequently used in the same way. Exchange, and hence dissociation, became evident in the temperature range 350 to 400°C.

15.4 BEHAVIOR OF FISSION PRODUCTS IN CIRCULATING LOOP TESTS

In a 500-hr run in loop A, zirconium "plated out" almost quantitatively on metal surfaces as the oxide when introduced into 0.04 *m* UO_2SO_4 solution at 300°C as zirconium sulfate solution. A suspension of zirconium oxide which had been externally precipitated was used as a feed solution under the same conditions, and essentially no zirconium oxide plating-out resulted. Material balances for the two zirconium salts are shown in Table 15.1. The major constituent of the scale

Table 15.1. Zirconium Material Balance in Circulating Loop Runs

	Zirconium (g)		Balance
	Input	Recovery	(%)
First Test			
48.7 liters of feed, 0.69 g of Zr per liter as $Zr(SO_4)_2$	33.66		
Samples, 48.2 liters		0.666	
Underflow pot drains		5.240	
Loop drains		4.855	
Scale from pump		5.089	
		15.85	47
Second test			
7.7 liters of feed, Zr as ZrO_2			
2.0 liters, 1.71 g of Zr per liter	3.42		
2.0 liters, 2.26 g of Zr per liter	4.52		
3.7 liters, 2.02 g of Zr per liter	7.48		
	15.42		
Samples, 7.7 liters		0.540	
Underflow pot drains		11.710	
Underflow pot rinse		1.610	
Loop drain		1.470	
		15.330	99
Total	49.08	31.18	64

scraped from the pump was zirconium (Table 15.2). Measurements of the scale thickness ranged from 3 to 5 mils but were not very accurate. If the scale thickness throughout the loop is taken as 3 mils, the missing zirconium from the over-all material balance of 64% is easily accounted for.

Table 15.2. Analysis of Scale from Pump in Circulating Loop Run

Sample	Amount (%)					
	Zr	Fe	Cr	Ni	U	SO_4
1	61.3	6.45	0.29	0.17	5.5	2.47
2	52.0	7.27	0.32	0.09	4.8	2.87
3	67.5	5.88	0.34	0.06	4.5	1.87

16. URANYL SULFATE BLANKET PROCESSING

D. E. Ferguson
R. D. Baybarz
N. A. Brown
J. M. Chilton
S. D. Clinton
E. O. Nurmi
W. J. Clossey
P. A. Haas
S. S. Kirslis
R. E. Leuze

The study of the chemistry of plutonium in uranyl sulfate solution included investigation of plutonium behavior in uranyl sulfate at 250°C, dissolution of corrosion-product oxides, and development of analytical procedures for irradiated uranyl sulfate solutions.

16.1 PLUTONIUM BEHAVIOR IN UO_2SO_4 SOLUTION AT 250°C

Plutonium formed in the uranyl sulfate blanket of the HRT can be expected to be distributed as follows: (1) in solution primarily as Pu(IV) and Pu(VI), (2) as a loose precipitate, primarily PuO_2, and (3) attached to vessel walls either as adsorbed ionic plutonium or as PuO_2. The amount of plutonium that will be in each of these forms depends on a large number of variables.

Laboratory experiments were carried out to determine the effect of some of these variables on plutonium behavior in 1.4 *m* UO_2SO_4 at 250°C in the absence of radiation. In general, the procedure was as follows: addition of $Pu(SO_4)_2$ to 1.4 *m* UO_2SO_4 at room temperature, addition of either 200 psi of oxygen or 200 psi of a mixture of 2 parts hydrogen and 1 part oxygen, heating the solution to 250°C, and cooling to room temperature for analysis. As previously reported,[1] the amount of Pu(IV) remaining in solution varied with the initial plutonium concentration: from 20 mg per kilogram of H_2O with an initial concentration of 20 to 30 mg per kilogram of H_2O to <3 mg per kilogram of H_2O with an initial concentration of 100 mg per kilogram of H_2O. The reason for this variation is not fully understood. The presence of preformed PuO_2 crystals reduced the apparent solubility of Pu(IV). Four solutions, containing 15 to 23 mg of plutonium per kilogram of H_2O, were spiked with a slurry of PuO_2 crystals and then heated to 250°C under a stoichiometric H_2-O_2 overpressure. Plutonium precipitated in all solutions, leaving 3 to 8 mg per kilogram of H_2O in solution. The possibility that some unknown material added in the plutonium spike was responsible for lower Pu(IV) solubilities with higher initial plutonium concentration was eliminated by the following experiment. A solution of uranyl sulfate containing 50 mg of plutonium per kilogram of H_2O was heated at 250°C to precipitate PuO_2, leaving 6 mg per kilogram of H_2O in solution. The precipitate was removed and more plutonium sulfate was added to bring the concentration of the supernatant up to 15 mg per kilogram of H_2O. When heated at 250°C, all the plutonium remained in solution. That the peculiar solubility behavior was not a result of increased alpha activity in the solution was shown by the fact that plutonium did not precipitate at 250°C from a 1.4 *m* UO_2SO_4 solution containing 15 mg of plutonium per kilogram of H_2O plus sufficient Am^{241} to provide alpha activity equal to that of 65 mg of plutonium per kilogram of H_2O.

The total amount of plutonium remaining in 1.4 *m* UO_2SO_4 after being heated to 250°C depended on the amount of plutonium oxidized to Pu(VI). In pyrex containers, Pu(IV) was readily oxidized to Pu(VI) under 200 psi O_2. However, under 100 psi O_2 plus 200 psi H_2, Pu(IV) was stable. In type 347 stainless steel containers under either 200 psi O_2 or 100 psi O_2 plus 200 psi H_2, Pu(IV) was readily oxidized to Pu(VI). It has been shown[2] that chromium from stainless steel corrosion is an effective catalyst for oxidation of Pu(IV) when heated under a stoichiometric H_2-O_2 overpressure. The oxidation depends on the availability of dissolved oxygen. In static bomb tests, uranium was reduced when the solution depth was more than a few centimeters. This was apparently due to oxygen being consumed by stainless steel

[1] D. E. Ferguson *et al.*, *HRP Quar. Prog. Rep. July 31, 1956*, ORNL-2148, p 121–122.

[2] D. E. Ferguson *et al.*, *HRP Quar. Prog. Rep. Oct. 31, 1956*, ORNL-2222, p 143.

corrosion more rapidly than it was replaced by diffusion from the gas-liquid interface.

The solubility of Pu(VI) is not known. However, when 1.4 *m* UO_2SO_4 containing plutonium was heated at 250°C under oxygen in pyrex, the plutonium remaining in solution was 100 mg per kilogram of H_2O or more, approximately 97% Pu(VI) and 3% Pu(IV). In all experiments made in stainless steel under either pure oxygen or stoichiometric hydrogen plus oxygen, much less than 100 mg of plutonium per kilogram of H_2O remained in solution, but it was essentially all Pu(VI). In a series of experiments, 1.4 *m* UO_2SO_4 solutions containing initial Pu(IV) concentrations of 17.5, 36, 52, and 70 mg per kilogram of H_2O were heated to 250°C in type 347 stainless steel under 200 psi H_2 and 100 psi O_2. In all cases about 16 mg of plutonium per kilogram of H_2O, essentially all Pu(VI), remained in solution. When plutonium was added gradually at the rate of 5 mg per kilogram of H_2O per day, all the plutonium was oxidized to Pu(VI) and remained in solution until the concentration exceeded 33 mg per kilogram of H_2O. When the plutonium was increased to 37 mg per kilogram of H_2O and heated at 250°C, only 7.5 mg per kilogram of H_2O remained in solution. After further additions and heating, 6 to 9 mg of plutonium per kilogram of H_2O remained in solution. The reason for this behavior and the lower apparent solubility of Pu(VI) when heated in stainless steel is not known.

When 1.4 *m* UO_2SO_4 containing plutonium was heated to 250°C, plutonium that did not stay in solution formed a loose PuO_2 precipitate or was adsorbed on the container walls. In pyrex containers plutonium adsorption was negligible, and essentially all the nonsoluble plutonium was loose PuO_2 precipitate. Adsorption on stainless steel sometimes accounted for all the plutonium lost from solution, and in all experiments in stainless steel adsorption was significant. The variables involving the retention of plutonium on container walls are not well understood. Plutonium is apparently held on stainless steel in two ways – by ionic adsorption and by trapping of PuO_2 particles in the corrosion film. It was reported[2] that during the first part of an experiment in which plutonium was added to 1.4 *m* UO_2SO_4 in stainless steel at the rate of 5 mg per kilogram of H_2O per day, plutonium adsorption was ~0.001 $\mu g/cm^2/hr$. As this experiment was continued, all the plutonium removed from solution during the rapid decrease in dissolved plutonium from 37 to 7.5 mg per kilogram of H_2O was adsorbed on the stainless steel, and no loose PuO_2 precipitate was formed. As the gradual addition of plutonium was continued, the adsorbed plutonium was increased to 40 $\mu g/cm^2$, with no indication of leveling off. Autoradiographs showed this plutonium to be uniformly distributed with no evidence of high-concentration areas characteristic of trapped PuO_2 crystals. In a series of experiments, 1.4 *m* UO_2SO_4 solutions containing initial Pu(IV) concentrations of 17.5, 36, 52, and 70 mg per kilogram of H_2O were heated to 250°C in type 347 stainless steel under 200 psi H_2 and 100 psi O_2. The plutonium remaining in solution was about 16 mg per kilogram of H_2O in all cases. The amount of plutonium adsorbed was 0.3, 6, 9, and 10 $\mu g/cm^2$, respectively, and the amount of plutonium as loose PuO_2 was 0, 0.8, 10.5, and 25 mg per kilogram of H_2O, respectively. Although more plutonium was adsorbed from solutions with higher initial concentrations, the fraction of precipitated plutonium that was adsorbed actually decreased.

16.2 BLANKET SOLIDS DISSOLUTION

Additional studies were made of a method for completely dissolving the solids expected to be removed during operation of the HRT blanket chemical processing plant. The studies reported previously[1] were made with only the separated solids. During operation of the HRT chemical plant, the underflow-pot contents will be discharged periodically. After each discharge the pot will be rinsed and these solutions combined to give a solution about 0.8 *M* in UO_2SO_4 containing about 0.5 mole of corrosion-product oxides per liter. This solution will be evaporated to dryness to recover heavy water, and the resulting solids, including the uranium, must be dissolved. Satisfactory dissolution of simulated solids in phosphoric acid was demonstrated on a laboratory scale.

In these experiments, 100 ml of a simulated hydroclone underflow-pot slurry was evaporated to dryness, and the solids were dissolved in 85% H_3PO_4. The solution was 0.825 *M* in UO_2SO_4 and 0.49 *M* in corrosion-product oxides. The slurry was evaporated to dryness and baked at 250°C for 30 min. A total of 75 ml of 85% H_3PO_4 was added, and the mixture was heated to 225°C,

at which point the solids were completely dissolved, with a final volume of 62 ml. Water, 150 ml, was added to dilute the solution, which was then evaporated to a final volume of 150 ml. The phosphoric acid concentration in the diluted solution was 5.8 *M*, with a total phosphate concentration of 7.3 *M*. The solution was stable on boiling at the 7.3 *M* phosphate concentration.

16.3 ANALYSIS OF IRRADIATED URANYL SULFATE

During previous in-pile experiments, standard methods available for plutonium and neptunium analyses gave erroneous results. The principal difficulty with plutonium analyses was caused by the high beta activity from Np^{239}, which jammed the alpha counter. The Analytical Chemistry Division[3] has developed tentative methods for both neptunium and plutonium analyses. These methods will be useful for in-pile bomb studies and also for determining neptunium and plutonium behavior in the HRT uranyl sulfate blanket.

The suggested procedure for total plutonium involves (1) fluoride precipitation of plutonium and neptunium from a reduced solution with lanthanum carrier, (2) solution of the precipitate in H_3BO_3-HCl and reduction of the plutonium to Pu(III), (3) extraction of the solution with thenoyltrifluoroacetone (TTA) in xylene, discarding the neptunium-containing organic phase, (4) a second fluoride precipitation of plutonium with lanthanum carrier, and (5) counting of the plutonium alpha activity in the total LaF_3 precipitate on a proportional alpha counter adjusted to be insensitive to beta rays. The average deviation of six determinations by the above procedure on known concentrations of plutonium in 1.5 *M* UO_2SO_4 also containing neptunium was 3.3%.

The tentative procedure for total neptunium comprised (1) fluoride precipitation of neptunium from a reduced solution with lanthanum carrier and zirconium holdback, (2) solution of the precipitate in $Al(NO_3)_3$-HCl and reduction of the plutonium to Pu(III), (3) extraction of the solution with TTA-xylene, discarding the plutonium-containing aqueous phase, (4) stripping of neptunium from the organic phase with 10 *M* HNO_3, and (5) counting of an aliquot of nitric acid solution for Np^{239} gamma activity. The average deviation of five determinations on known concentrations of neptunium in 1.5 *M* UO_2SO_4 was 6.6%.

Work is in progress on the development of plutonium valence determinations.

16.4 LOOP P-1 TESTS

Initial operating tests were started on loop P-1. The first two runs were made with H_2O and an O_2 overpressure; loop temperatures of 150 and 200°C were attained. The third run was made for cleaning purposes with a 3 wt % Na_3PO_4 solution and O_2 overpressure in the loop, and a temperature of 240°C was reached. The Westinghouse 150-A pump has run for three different periods of approximately 4 hr each.

Before the pump was started, the loop was pressure-tested with nitrogen. The continuously operated part of the loop was made leak-tight up to a pressure of 1500 psi. A gold wire gasket between the scroll case and the pump stator casing allowed leakage at pressures greater than 1500 psi, which was the only difficulty encountered during operation. After two thermal cycles the torque on the scroll-case bolts had dropped from 300 to 40 ft-lb, indicating that the gold wire had been considerably flattened. The bolts were retightened to 200 ft-lb, and, upon cooling at the completion of the third run, the torque required to loosen the bolts was approximately 80 ft-lb. A gold-plated stainless steel gasket is being made in the shop to replace the gold wire.

The loop was initially filled with 14.0 liters of water. This experimentally determined volume agrees to within 2% with the calculated loop volume of 14.2 liters. Approximately 1.2 liters of H_2O was not recovered when the loop was drained. About 0.3 liter of this volume could be attributed to holdup behind the loop flow restrictors, but loss of the remaining 0.9 liter could not be explained.

Since there are no loop heaters, all heat to the loop solution must be supplied by the 150-A pump. After the first two runs, with the loop uninsulated, it was decided that an aluminum-foil insulation around the pressurizer and main loop piping would be necessary in order to reach an operating temperature of 260°C. After two layers of aluminum-foil insulation were applied, the loop temperature (240°C) was still increasing when the loop pump

[3] Development work by F. Moore and H. Wright, Analytical Chemistry Division.

was shut off to end the third run. No trouble is expected in reaching the operating temperature when the loop container is sealed and evacuated to minimize the convection heat losses.

Tests[4] on the pressurizer were completed with a series of runs in which there was no water spray and therefore no forced mixing of the gas phase. They indicated that the loop can be operated safely with the proposed overpressure of 100 psi of both oxygen and hydrogen. Spontaneous combustion reactions did not occur in H_2O-H_2-O_2 systems when the vapor contained less than 50% of a stoichiometric mixture of H_2-O_2. When small nickel or platinum coils were inserted and heated electrically, explosive reactions were obtained with vapor that was calculated to contain more than 30% of the stoichiometric mixture. The reactions were occasionally rapid with vapor calculated to contain 20 to 30% $2H_2$-O_2.

[4] D. E. Ferguson *et al.*, *HRP Quar. Prog. Rep. Oct. 31, 1956*, ORNL-2222, p 142.

None of the observed reactions resulted in equipment damage. The final, most severe tests of shock damage to the pressurizer were made by exploding 300 psi of H_2 and 150 psi of O_2 mixed in the pressurizer at below 100°C to give essentially 100% explosive gas undiluted by steam. These tests gave sharp reports heard outside the cell wall.

Tests with a fast recorder indicated pressure peaks of 800 to 1500 psi at the pressure element.

16.5 LOOP P-2 COMPONENT TESTS

16.5.1 Titanium Canned-Rotor Pump

Room-temperature tests on a modified ORNL canned-rotor pump (Fig. 16.1) were completed. All parts (Fig. 16.2) exposed to the fluid pumped are titanium, with the exception of high-density aluminum oxide bearings and journals. The design (ORNL Dwg. D-27001) incorporates a 4-in.-dia impeller and three-phase stator windings to give shutoff heads of 53 ft at 60 cps and 113 ft at 95 cps electrical input.

UNCLASSIFIED
PHOTO 19539

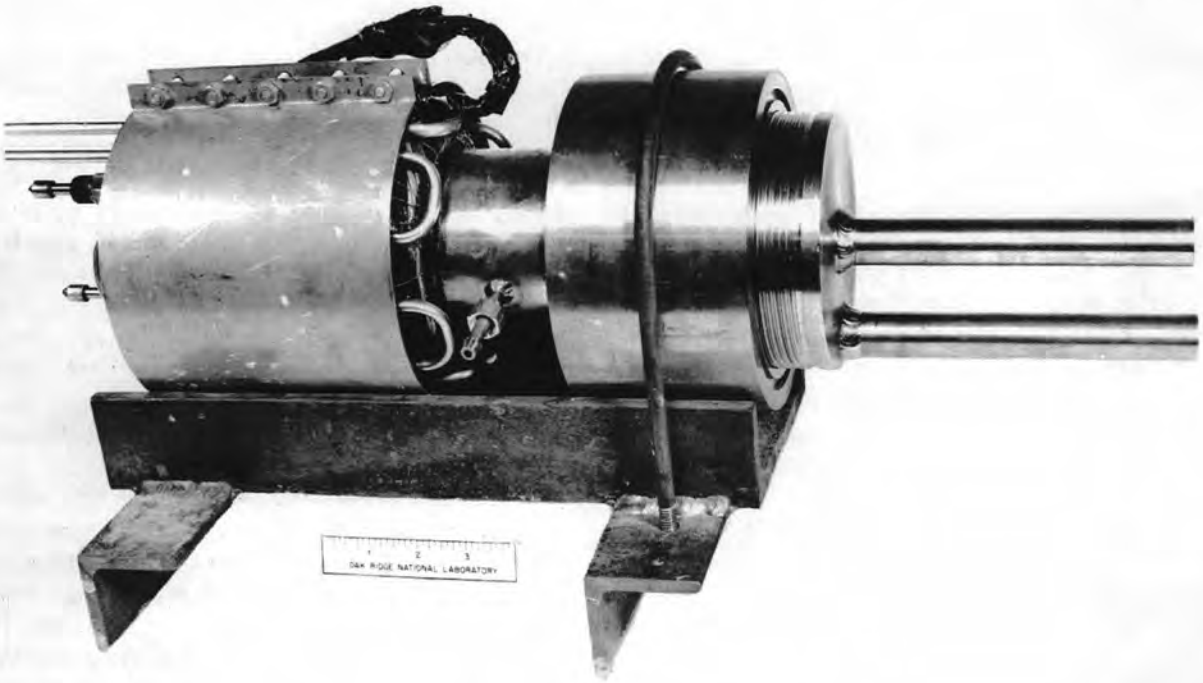

Fig. 16.1. All-Titanium Pump – 5 gpm.

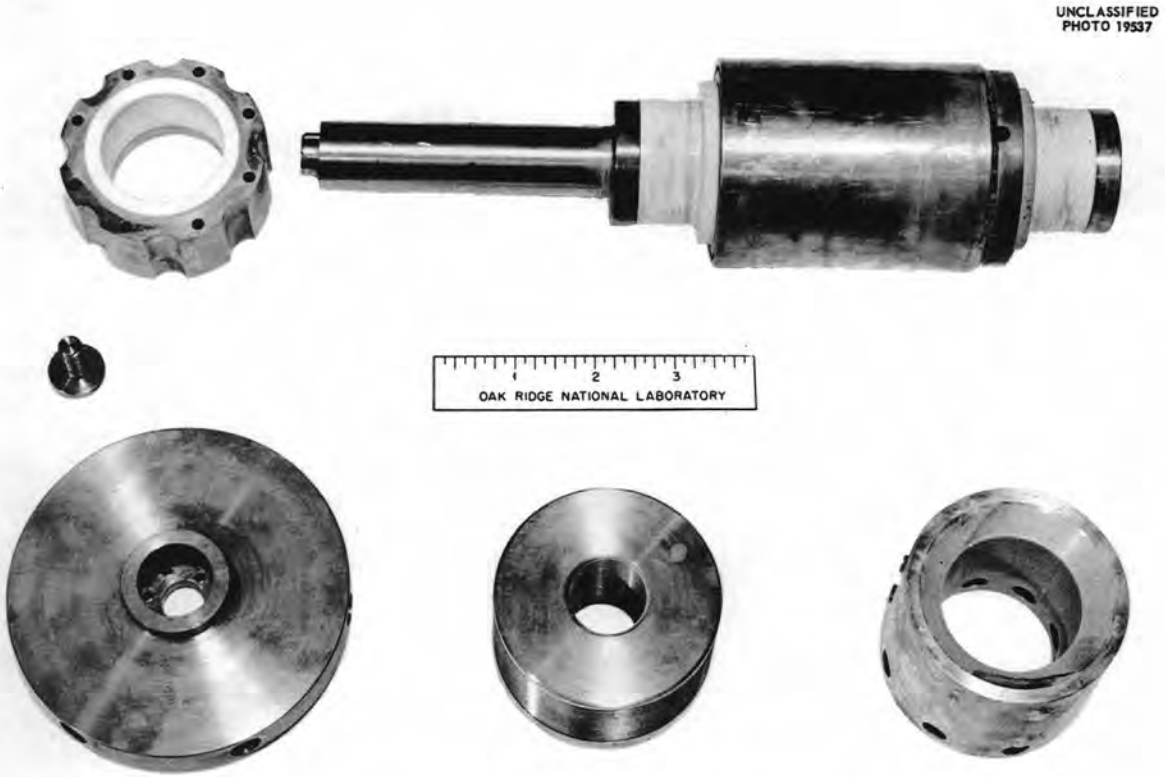

Fig. 16.2. Parts for All-Titanium Pump.

The aluminum oxide bearings and journals showed no wear during the 30 hr of test operation with H_2O at room temperature. The measured differences between the outside diameters of the journals and the inside diameters of the bearings were 0.0020 to 0.0028 in. when the pump was fabricated and 0.0018 to 0.0022 in. at the end of the test operation. The suction head necessary to prevent cavitation was about 10 ft at 1 gpm and 20 ft at 5 gpm.

16.5.2 Core Tank

The 4-in.-dia spherical titanium core tank with an aluminum jacket designed to remove 3 kw of gamma heat has been received.

16.5.3 Heat Exchanger

A heat exchanger designed to permit removal of 10 kw of heat from loop solution at 260°C was tested with several variations of air and H_2O coolant combinations. This heat exchanger has three parallel ¼-in. IPS sched-80 titanium pipes for the UO_2SO_4 solution side cast in aluminum with three parallel ¼-in. IPS sched-40 stainless steel coolant pipes. This geometry has the following advantages:

1. The double wall between the loop solution and the coolant minimizes the possibility of coolant contamination.
2. The increased area per unit of length minimizes the heat flux.
3. The increased area and thinner pipe walls, as compared with those of a single larger pipe, minimize the thermal stresses in the titanium.

Either water sprayed into air or a coolant water stream of about 4 gpm entering at 30°C or less could remove 7 to 10 kw of heat from the loop solution at 260°C. Either 100-psia air or water sprayed into air could remove 0 to 3 kw. There does not seem to be any arrangement which would

give continuous, smooth control with this heat exchanger for heat-removal rates of 3 to 7 kw. The air with water sprayed into it does not give completely reproducible heat-removal rates for water inputs of 20 to 120 cc/min. When this range is approached from the high water-rate side, the heat transfer remains high, probably because the walls remain wetted down. When the water rate is gradually increased starting with initially dry tubes, the high heat-transfer rate is not obtained until the water rate exceeds 100 cc/min. There are liquid water droplets in the exit air stream throughout all the tests with water rates of over 20 cc/min.

16.6 ELECTROLYSIS AS A METHOD OF H_2-O_2 ADDITION FOR LOOPS P-1 AND P-2

Because of high corrosion rates (over 1 in./year) and low current efficiencies (15 to 50%), electrolysis does not appear to be a practical method for adding a stoichiometric H_2-O_2 mixture to a high-pressure high-temperature loop system.

16.7 HYDROCLONE DEVELOPMENT STUDIES

Two 0.16-in.-dia hydroclones with dimensions the same as those of hydroclones proposed for loops P-2 and P-3 have been given flow-rate and efficiency tests. The observed capacity for each hydroclone was 0.12 gpm for 100 ft of liquid pressure drop (Fig. 16.3). The efficiency of one unit was 48% for the TM-Y ThO_2, for which 0.40- and 0.25-in.-dia units have efficiencies of about 35 and 42%.

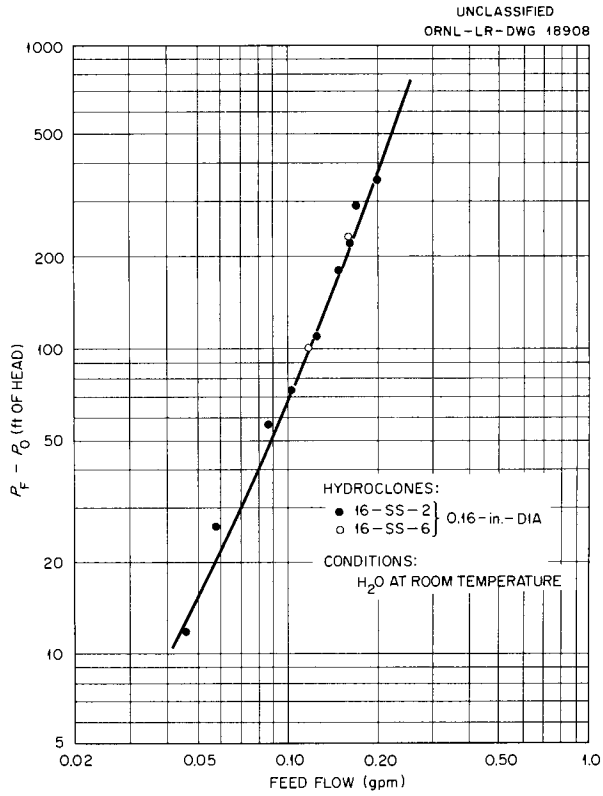

Fig. 16.3. Flow vs ΔP for 0.16-in.-dia Hydroclones.

17. THORIUM OXIDE SLURRY DEVELOPMENT

D. E. Ferguson
E. V. Jones
N. A. Krohn
L. E. Morse
J. P. McBride
R. L. Pearson
C. E. Schilling
W. M. Woods

17.1 SLURRY IRRADIATION STUDIES

17.1.1 Slurry Irradiations in the LITR

Extensive revision of the instrumentation for hole C-44 of the LITR and installation of new instrumentation for hole C-43, a new irradiation facility, prevented any slurry irradiations during the past quarter. The new facility, which will enter the reactor through a diagonal tube in the side of the tank, will permit long-term slurry irradiations to be carried out without interfering with the operating schedule of the LITR.

17.1.2 Postirradiation Examination of Slurries

Two slurries of pure thorium oxide and seven slurries of thorium–0.5% uranium oxide (93% enriched uranium) which had been irradiated at 300°C in the LITR during the past year were recovered for examination (Table 17.1). None appeared to have been grossly affected by the irradiation. The calculated power density under irradiation for the slurries containing the enriched uranium was approximately 5 kw/liter (the average power density expected in the TBR blanket).

One of the pure thorium oxide slurries contained oxide prepared by the precipitation of thorium oxalate at 10°C followed by a multistage calcination ending at 900°C (TO-10-900-24);[1] the other was an aliquot of an oxide slurry which had been pumped for 100 hr at 200°C in loop 200A at Y-12 (200A-6).[2,3] Two of the mixed oxides were prepared by wet autoclaving ThO_2 and enriched $UO_3 \cdot H_2O$ at 300°C and calcining the recovered solids at 900°C; the others were prepared by coprecipitating the thorium and uranous oxalates and calcining the mixtures, two at 800°C and three at 900°C.

All slurries were readily recovered from the irradiation bombs and all were brownish in color except 200A-6, which was cream-colored. One of the slurries had lost water during storage and was quite thick, but was readily suspended on the addition of fresh water. The settling rates of the irradiated slurries appeared normal, and there were no gross changes in the volumes of the settled solids. Aliquots of the slurries have been submitted for physical, chemical, and radiochemical analyses.

17.1.3 Corrosion-Erosion Effects in Operation of the Dash-Pot-Stirred Irradiation Bomb

Out-of-pile tests to determine the pickup of corrosion products during operation of the dash-pot-stirred irradiation bomb were continued. For a constant slurry concentration the rate of iron pickup increased with increasing calcination temperature of the oxide (Fig. 17.1). Previous results[4] have indicated that the attack is primarily abrasive in character; hence it should be possible to detect any increase in abrasive-hardness of the slurry particles resulting from in-pile irradiation.

17.2 GAS-RECOMBINATION STUDIES

Investigation of the catalytic recombination of hydrogen and oxygen by thorium-uranium oxide slurries containing 0.05 *m* molybdenum oxide was continued with studies on the effect of sulfate and rare-earth additions on the reaction rate. While the addition of both sulfate and rare earths decreased the catalytic activity of the slurries, the reaction rates in the presence of 6000 ppm of sulfate (based on ThO_2) and 1268 ppm of rare earths were sufficiently fast to recombine the radiolytic gases that would be produced in a TBR blanket slurry and to maintain a steady-state pressure less than 2000 psi (Tables 17.2 and 17.3).

The experiments were carried out with thorium–0.5% uranium oxide slurries containing 1000 g of thorium per kilogram of H_2O. They were prepared by tumbling the dry powders (i.e., ThO_2, $UO_3 \cdot H_2O$,

[1] V. D. Allred, E. V. Jones, and J. P. McBride, *HRP Quar. Prog. Rep. Jan. 31, 1956*, ORNL-2057, p 115.

[2] R. B. Gallaher and A. S. Kitzes, *Preparation of Standard Oxide*, ORNL CF-56-10-8 (Oct. 3, 1956).

[3] D. E. Ferguson *et al.*, *HRP Quar. Prog. Rep. Oct. 31, 1956*, ORNL-2222, p 145.

[4] *Ibid.*, p 147–148.

Table 17.1. Postirradiation Examination of Slurries

Irradiation conditions: 300°C, $\sim 3 \times 10^{13}$ neutrons·cm^{-2}·sec^{-1}

Experiment No.	Material	Preparation	Additives	Th Concentration (g per kg of H_2O)	Irradiation Time (hr)	Color	Settling Rate (cm/sec)	Supernatant	Settled Volume (ml)[a]	
									Irradiated	Control
LITR-26[b]	ThO_2, TO-10-900-24	10°C precipitated $Th(C_2O_4)_2$; calcined at 900°C	None	750	198	Gray-brown	0.05	Cloudy	2.3	
LITR-27[b]	ThO_2, 200A-6	Pilot-plant oxide pumped 100 hr	None	750	344	Cream	0.05	Cloudy	2.4	2.5
LITR-17[c]	ThO_2–0.5% UO_3; 93% enriched	Wet autoclaved at 300°C; calcined at 900°C	1000 ppm PdO	1000	92	Brown	Very slow	Cloudy	2.6	2.8
LITR-18[c]	ThO_2–0.5% UO_3; 93% enriched	Wet autoclaved at 300°C; calcined at 900°C	1000 ppm PdO	1000	20	Gray-brown	0.05	Clear	2.9	2.8
LITR-28[b]	ThO_2–0.5% UO_3; 93% enriched	Coprecipitated oxalates; calcined at 800°C	20,000 ppm MoO_3	750	136	Brown	Very slow	Cloudy	Not settled in 24 hr	3.0
LITR-29[b]	ThO_2–0.5% UO_3; 93% enriched	Coprecipitated oxalates; calcined at 800°C	20,000 ppm MoO_3	750	314	Brown	Very slow	Cloudy	2.7	3.0
LITR-19[c]	ThO_2–0.5% UO_3; 93% enriched	Coprecipitated oxalates; calcined at 900°C	1000 ppm PdO	1000	210[d]	Gray-brown	0.01	Clear	1.1	
LITR-21[e]	ThO_2–0.5% UO_3; 93% enriched	Coprecipitated oxalates; calcined at 900°C	1000 ppm PdO	750	168	Brown	Very slow	Clear	2.6	
LITR-25[e]	ThO_2–0.5% UO_3; 93% enriched	Coprecipitated oxalates; calcined at 900°C	20,000 ppm MoO_3	750	192	Brown	0.01	Clear	3.1	

[a]A 3-ml settled volume is equivalent to 1000 g of Th per liter for the slurries containing 750 g of Th per kg of H_2O and to 1250 g of Th per liter for the slurries containing 1000 g of Th per kg of H_2O.

[b]*HRP Quar. Prog. Rep. Oct. 31, 1956*, ORNL-2222, p 145.

[c]*HRP Quar. Prog. Rep. July 31, 1956*, ORNL-2148, p 123–124.

[d]Irradiated in settled condition.

[e]*HRP Quar. Prog. Rep. April 30, 1956*, ORNL-2096, p 107.

MoO_3) for 1 hr, dispersing them in water, and subsequently heating the slurry at 280°C for 3 hr in the presence of oxygen. The sulfate was added to the slurry as $Th(SO_4)_2 \cdot xH_2O$. The rare earths were added to the slurry as a rare-earth sulfate solution which was prepared by dissolving Lindsay rare-earth sulfate mixture 302 in water.

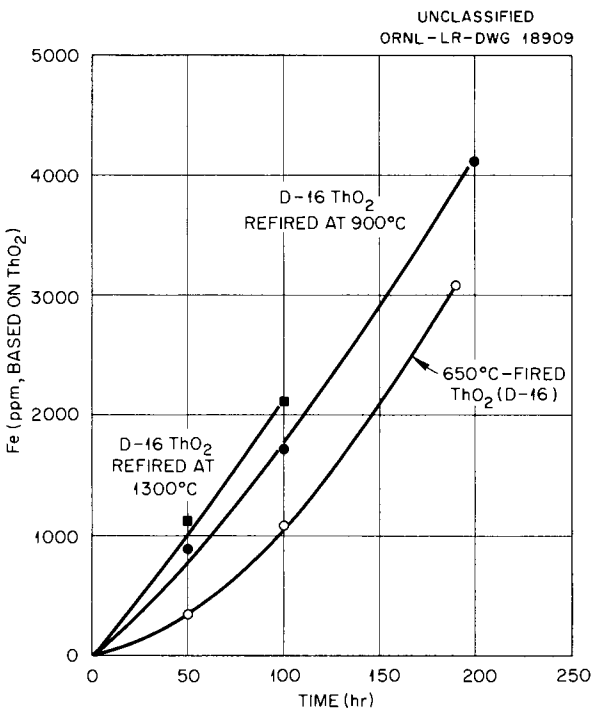

Fig. 17.1. Corrosion-Product Pickup in the Out-of-Pile Operation of the Dash-Pot Irradiation Bomb. Conditions: 750 g of Th per kg of H_2O; 300°C; stirring frequency, 3.5 cps.

Stoichiometric mixtures of hydrogen and oxygen were added to the slurries, in small stainless steel autoclaves, and brought to temperatures while being vigorously agitated. The rate of hydrogen consumption was obtained from the rate of total pressure decrease with time, assuming the perfect gas law to apply.

17.2.1 Effect of Sulfate

The combination rate of a hydrogen-oxygen mixture over the slurry as prepared and to which 2000 ppm of sulfate (based on ThO_2) had been added as thorium sulfate was 1.8 moles of hydrogen per hour per liter of slurry at 277°C and 500 psi hydrogen, somewhat less than has been observed in the absence of sulfate. When heated for 70 min at 285°C under H_2 (1000 psi at room temperature), the combination rate was 36 moles of H_2 per hour per liter at 170°C with P_{H_2} = 500 psi, comparable to that observed in the absence of sulfate. Increasing the sulfate concentration to 4000 ppm in the activated slurry resulted in about a 20% decrease in the combination rate. Increasing the sulfate concentration to 6000 ppm did not further decrease the reaction rate (Table 17.2).

17.2.2 Effect of Rare Earths

The addition of 634 ppm of rare earths as sulfate to an activated slurry did not decrease its cata-

Table 17.2. Effect of Sulfate on Reaction Rate of Stoichiometric H_2-O_2 Mixtures in Aqueous Thorium-Uranium Oxide Slurries

Slurry composition: Thorium, 1000 g per kg of H_2O (900°C ThO_2)
Uranium, 0.5 g per kg of H_2O
MoO_3, 0.05 *m*

Slurry	Sulfate Concentration (ppm, based on ThO_2)	Temperature (°C)	H_2 Reaction Rate, P_{H_2} = 500 psi (moles/hr/liter)
As prepared	2000	277	1.8
Activated*	2000	170	36.4
	4000	176	29.4
	6000	174	30.6

*Slurry heated with H_2 (1000 psi at 250°C) for 70 min at 285°C.

Table 17.3. Effect of Rare-Earth Accumulation on Reaction Rate of Stoichiometric H_2-O_2 Mixtures in Aqueous Thorium-Uranium Oxide Slurries

Slurry composition: Thorium, 1000 g per kg of H_2O (900°C ThO_2)
Uranium, 0.5 g per kg of H_2O
MoO_3, 0.05 *m*

Slurry	Rare-Earth Oxide Concentration (ppm, based on ThO_2)	Temperature (°C)	H_2 Reaction Rate, P_{H_2} = 500 psi (moles/hr/liter)
As prepared		277	5.17
Activated*		167	29.2
	634	166	29.1
	1268	172	20.6

*Slurry heated with H_2 (1000 psi at 25°C) for 60 min at 280°C.

lytic activity. A combination rate of 29 moles of hydrogen per hour per liter of slurry at 166 to 167°C with P_{H_2} = 500 psi was observed both before and after the addition of the rare earths. Doubling the rare-earth concentration lowered the reaction rate about 30% (Table 17.3).

The concentration of rare earths in the first experiment (634 ppm) was determined by adjusting the cerium concentration to that which would be present under steady-state conditions of blanket operation, assuming 5×10^{13} neutrons·cm^{-2}·sec^{-1} as the flux and continuous processing over a 249.2-day cycle.[5] Since the amounts of the other rare earths relative to the cerium were greater in the mixture used than would be the case for the rare earths at equilibrium in a blanket system, the total rare-earth concentration was probably greater than would actually be the case for a blanket slurry.

17.3 STUDIES WITH THORIUM OXIDE SLURRIES CONTAINING SODIUM SILICATE

Early investigation of the effect of additives on slurry behavior indicated that sodium silicate was a good dispersing agent for aqueous thorium oxide suspensions.[6] More recently, loop tests with thorium oxide slurries containing sodium metasilicate indicated that the silicate additions improved the handling characteristics of the slurry at elevated temperatures.[7] Hence laboratory experiments were undertaken to delineate the chemistry of the silicate-slurry systems and to determine the effect of silicate additions on the viscosity and hindered-settling rates.

17.3.1 Adsorption Studies

(a) Room Temperature. – The room-temperature adsorption of sodium and silicon from sodium metasilicate solution by thorium oxide was studied as a function of silicate concentration. The adsorption of silicon was disproportionately greater than that of sodium. At silicate and thoria concentrations of interest in the slurry development program, the silicate was almost completely adsorbed by the thoria (Table 17.4).

The experiments were carried out with slurries of ACDC-13 thorium oxide (800°C-fired pilot-plant production), containing 350 g of thorium per kilogram of H_2O, in sodium metasilicate solutions. The slurries were tumbled overnight and then allowed to settle for 24 to 72 hr before samples of the supernatants were withdrawn for sodium and silicon analyses. The amounts of sodium and silicon adsorbed were estimated by difference.

[5] A. T. Gresky and E. D. Arnold, *Products Produced in Continuous Neutron Irradiation of Thorium*, ORNL-1817 (Feb. 6, 1956).

[6] D. E. Ferguson *et al.*, *HRP Quar. Prog. Rep. Oct. 31, 1954*, ORNL-1813, p 146.

[7] P. H. Hayes and D. G. Thomas, *Thermal Stability of Sodium Silicate Treated Thorium Oxide Slurry in Dynamic Tests (100-A Loop Run T-79)*, ORNL CF-56-11-2 (Nov. 12, 1956).

Table 17.4. Room-Temperature Adsorption Data for Thorium Oxide Slurries Containing Sodium Silicate

Slurry: ACDC-13 ThO_2, 350 g of thorium per kilogram of H_2O
Tumbled overnight
Settled 24 to 72 hr

Original Supernatant Concentration			Final Supernatant Concentration (mg/ml)		Amounts Adsorbed* on ThO_2 (mg/g)		Mole Ratio of Si/Na Adsorbed on ThO_2
$Na_2O \cdot SiO_2$ (moles/liter)	Na (mg/ml)	Si (mg/ml)	Na	Si	Na	Si	
0.005	0.23	0.14	0.123	0.006	0.268	0.336	1.02
0.025	1.15	0.70	0.773	0.016	0.942	1.71	1.49
0.050	2.30	1.40	1.60	0.080	1.75	3.30	1.55
0.250	11.5	7.0	9.70	3.53	4.5	8.67	1.57
			9.31	4.03	5.5	7.42	1.11
			9.33	4.19	5.5	7.26	1.08
0.500	23.0	14.0	22.2	5.03	2.0	22.5	9.25
			21.9	5.03	2.75	22.5	6.71
			22.1	3.27	2.25	22.5	9.75

*Calculated by difference from supernatant analyses.

Pronounced dispersion effects were noted at silicate concentrations less than 0.05 *M*. At higher silicate concentrations, up to 0.5 *M*, the supernatants were crystal clear.

(*b*) Effect of Autoclaving. – A slurry of ACDC-13 thorium oxide, 250 g of thorium per kilogram of H_2O, in a 0.0044 *M* sodium metasilicate solution (1000 ppm SiO_2, based on ThO_2) was autoclaved at 285°C for 108 hr. The recovered slurry was dispersed and allowed to settle slowly to a dense bed. The concentrations of sodium and silicon in the supernatant of the recovered and original slurry were as follows:

	Recovered (mg/ml)	Original (mg/ml)
Sodium	0.127	0.200
Silicon	0.006	0.12

The slurry solids contained 0.240 mg of sodium and 0.200 mg of silicon per gram of thorium oxide. The results indicate again essentially complete adsorption of the silicon and disproportionately less adsorption of sodium.

A material balance calculated from the analytical data showed nearly 50% of the silicon unaccounted for. Since the analytical method determines only ionic species containing silicon, it appears that a large fraction of the silicate originally present had been hydrolyzed by the autoclaving treatment to a form not readily soluble.

Dialysis of an aliquot of the slurry for 24 hr gave a flocculated slurry that settled with a clear supernatant. The concentration of sodium in the dialyzed slurry supernatant was 0.017 mg/ml. The solid contained 0.060 mg of sodium and 0.017 mg of silicon per gram of thorium oxide, indicating that most of the adsorbed ionic species were removed by the dialysis.

17.3.2 Equilibrium Studies

Erratic results obtained in hindered-settling-rate and pumping studies at elevated temperatures with thorium oxide slurries containing silicate prompted an investigation of the rate of approach to equilibrium in such systems. As the initial part of such a study, slurries of thorium oxide, 250 g of thorium per kilogram of H_2O, and thorium-uranium oxide were autoclaved for 108 hr at 285°C in the presence of 1000 ppm of SiO_2 (based on ThO_2) added as sodium metasilicate ($Na_2O \cdot SiO_2$). Hindered-settling-rate and dash-pot-stirred-bomb data

were obtained on the recovered slurries from room temperature to 300°C.

Slow settling rates and pronounced dispersion effects were noted in the treated slurries at temperatures less than 100°C, but above this temperature (to 300°C) little change was observed in the hindered-settling rates for the treated slurries when compared with the untreated slurries (Fig. 17.2). Both the treated slurries, however, were much more fluid than the untreated slurries at all temperatures (100 to 300°C), as indicated by a much shorter stirrer rise time when they were stirred in the dash-pot bomb (Fig. 17.3). The effect of the silicate treatment on the viscosity of the thorium-uranium oxide slurry was much more pronounced than in the case of the thorium oxide slurry. In fact, the stirrer rise times for the treated mixed-oxide slurry were less than those observed for the stirrer on air.

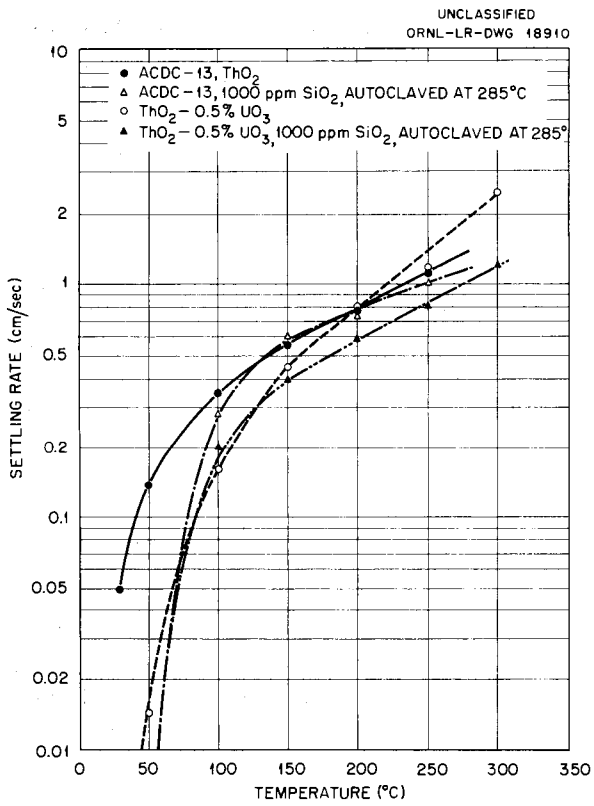

Fig. 17.2. Effect of Autoclaving at 285°C on the Hindered Settling Rates of Thorium and Thorium-Uranium Oxide Slurries.

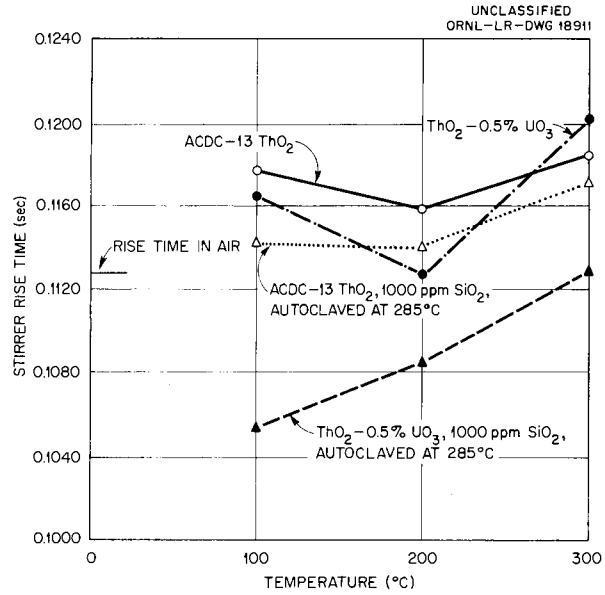

Fig. 17.3. Stirrer Rise Time in the Dash-Pot Bomb for Slurries of Thorium and Thorium-Uranium Oxide.

The thorium oxide used in the experiment was ACDC-13, an 800°C-fired pilot-plant oxide. The thorium-uranium mixed oxide contained 0.5% U and was prepared by an 800°C firing of the co-precipitated oxalate.

17.3.3 Viscosity Studies

The effects of sodium metasilicate additions on the viscosities of a thorium oxide slurry and a thorium-uranium oxide slurry were investigated in the dash-pot-stirred irradiation bomb. The experiments were carried out with slurries of a standard pilot-plant oxide (ACDC-13) fired at 800°C and of a mixed thorium-uranium oxide, containing 0.5% U, prepared by an 800°C firing of a coprecipitated thorium-uranous oxalate; both contained 750 g of thorium per kilogram of H_2O. Slurries of both oxides showed a decrease in apparent viscosity with increasing sodium metasilicate concentration in the temperature range 100 to 300°C (Figs. 17.4 and 17.5).

The apparent viscosity of the pure thorium oxide in the absence of silicate was 10 centistokes at 100 and 200°C and 12 centistokes at 300°C, decreasing at all temperatures with increasing SiO_2 concentration until at a concentration of 7000 ppm the apparent viscosity was zero. X-ray fluoroscopic

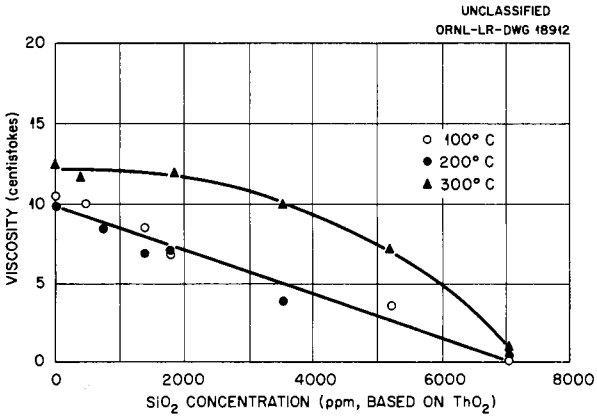

Fig. 17.4. Effect of $Na_2O{\cdot}SiO_2$ on the Viscosity of a ThO_2 Slurry.

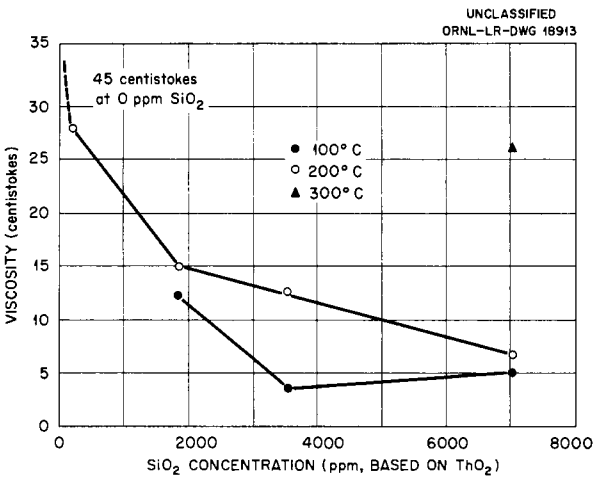

Fig. 17.5. Effect of $Na_2O{\cdot}SiO_2$ on the Viscosity of a Thorium–0.5% Uranium Oxide Slurry.

examination of the dash-pot-stirred bomb containing this slurry revealed pronounced foaming.

The viscosity of the mixed oxide slurry was very much greater than that of the pure oxide slurry for all silicate concentrations and at all three temperatures. At 300°C the mixed oxide slurry was too thick for a viscosity measurement to be obtained at all SiO_2 concentrations less than 7000 ppm SiO_2, where the viscosity was 26 centistokes.

In all experiments the sodium metasilicate was added to the slurry in the dash-pot bomb and the slurry heated with stirring at 200°C for 2 hr before making a viscosity measurement at this temperature. Viscosity measurements were then made at 100 and 300°C (in that order), the slurry being stirred for 2 hr at each temperature prior to the viscosity measurements. On occasion the temperature was again lowered to 200°C and a second viscosity measurement was made. In most cases the original measurement was reproduced.

17.3.4 High-Temperature Hindered-Settling-Rate Studies

The effect of sodium silicate $[Na_2O(SiO_2)_{2.9}]$ additions on the hindered-settling rate of a slurry of the standard oxide[8,9] containing 250 g of thorium per kilogram of H_2O was determined over the temperature range 25 to 300°C by an x-ray technique.[10] Silicate concentrations up to 1000 ppm SiO_2, based on ThO_2, had little effect on the settling rate at any temperature. Higher concentrations of SiO_2, up to 20,000 ppm, did not affect the room-temperature settling rate but resulted in pronounced decreases in the settling rate at slurry temperatures of 100 to 250°C, the relative effect of a given concentration of silicate depending on the slurry temperature (Fig. 17.6). At 100°C marked decreases in the settling rates occurred at SiO_2 concentrations of 2000 and 10,000 ppm. Similar changes in settling rates were observed for slurry temperatures of 150 and 200°C at 6500 and 10,000 ppm SiO_2, respectively.

All slurries were heated at 300°C for an hour or more prior to the settling studies. Since the studies were carried out with standard slurry oxide, the bulk of which is in the form of spherical aggregates 10 to 20 μ in size, the settling results are not generally applicable to other thorium oxide slurries with markedly different particulate properties. Additional studies on the effect of silicate additions on slurry settling rates are being carried out with the 800°C-fired pilot-plant oxide, both as prepared and after being ground in the micropulverizer.

Pronounced foaming was observed in the slurry containing 21,000 ppm SiO_2 at 100 and 150°C, making it impossible to measure a settling rate. Both an air-foam and a water-foam interface formed when agitation ceased. It was also observed that

[8] R. B. Gallaher and A. S. Kitzes, *Preparation of Standard Oxide*, ORNL CF-56-10-8 (Oct. 3, 1956).

[9] D. E. Ferguson *et al.*, *HRP Quar. Prog. Rep. Oct. 31, 1956*, ORNL-2222, p 145.

[10] V. D. Allred, E. V. Jones, and J. P. McBride, *HRP Quar. Prog. Rep. April 30, 1956*, ORNL-2096, p 112.

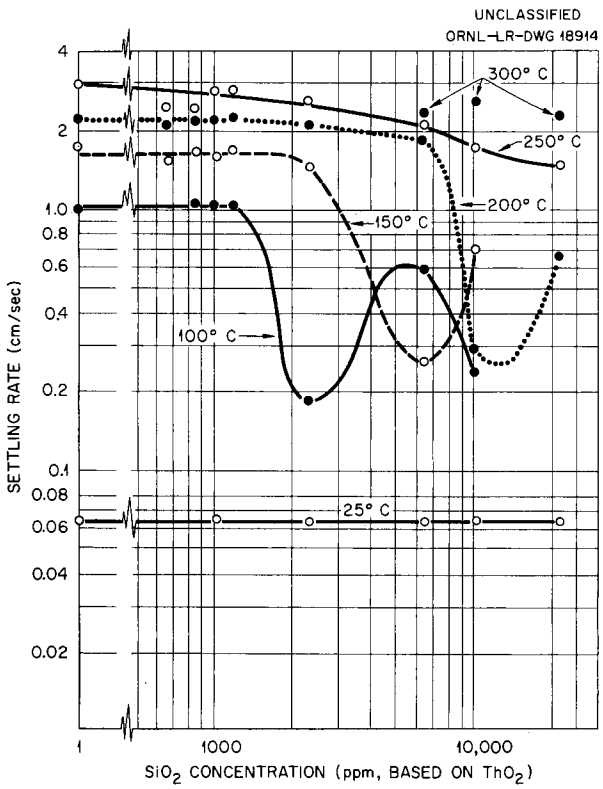

Fig. 17.6. Effect of Temperature and $Na_2O{\cdot}SiO_2$ Additions on the Hindered-settling Rates of Aqueous Thorium Oxide Slurries.

the settling rates for some slurries at higher temperatures changed with time at temperature, indicating that the systems were not at equilibrium. Experiments to determine the rate of approach to equilibrium in silicated slurry systems are under way (Sec 17.3.2), and particular attention will be paid to this aspect of silicate addition in future settling studies.

17.4 EFFECT OF ALUMINUM OXIDE ON THORIUM OXIDE PROPERTIES

The effect of aluminum oxide contamination on the properties of thorium oxide prepared by the coprecipitation of the oxalates and subsequent firing was determined for aluminum concentrations of 250, 500, 1000, and 10,000 ppm (based on ThO_2). The addition of the aluminum resulted in oxide products with increased crystallite sizes and proportionately lower specific surface areas, as well as smaller average particle sizes when compared with the pure oxides (Table 17.5). Properties of aqueous slurries of the thorium-aluminum oxides, both as prepared and after being autoclaved at 300°C, appeared very little different from room-temperature sedimentation characteristics of slurries of pure oxide similarly treated (Table 17.6). Adding the aluminum as $Al(OH)_3$ to the thorium oxide and autoclaving at 300°C yielded slurries with comparable properties (Table 17.7).

Table 17.5. Characteristic Properties of Thorium-Aluminum Oxides

Preparation method: 900°C calcination of coprecipitated oxalates

Oxide Designation	Al Concentration (ppm)	d_g, Geometric Mean Particle Size (μ)	σ_g, Geometric Standard Deviation	X-Ray Crystallite Size (Å)	Nitrogen Adsorption Surface Area (m^2/g)	S/θ, Relative* Surface Available for N_2 Adsorption
D-16-900	0	2.5**	4.4**	470	7.9	0.62
$Th\text{-}Al_4$	258	1.4	1.3	753	4.5	0.57
$Th\text{-}Al_3$	515	1.3	1.2	748	3.7	0.46
$Th\text{-}Al_1$	1,030	1.3	1.2	608	5.0	0.51
$Th\text{-}Al_2$	10,100	1.3	1.2	654	4.2	0.46

*Calculated from the crystallite size, assuming a cubic crystal.

**After being autoclaved at 300°C.

Table 17.6. Room-Temperature Settling Properties of Aqueous Slurries of Thorium-Aluminum Oxide Prepared from the Coprecipitated Oxalates: 900°C Calcination

Slurry thorium Concentration: 250 g of Th per kg of H_2O

Slurry Preparation	Oxide Designation	Al Concentration (ppm, based on ThO_2)	pH	U_0, Settling Rate (cm/sec)	Critical[a] Concentration (g of Th per liter)	Settled[b] Concentration (g of Th per liter)
Tumbled 2 hr	D-16-900	0	9.0	0.138	900	1450
	$Th\text{-}Al_4$	258	9.4	0.132	750	1350
	$Th\text{-}Al_3$	515	9.2	0.166	850	1550
	$Th\text{-}Al_1$	1,031	9.4	0.170	800	1300
	$Th\text{-}Al_2$	10,100	9.2	0.135	650	1100
Autoclaved 22 hr at 300°C	D-16-900	0	6.7	0.058	850	1450
	$Th\text{-}Al_4$	258	7.5	0.063	750	1200
	$Th\text{-}Al_3$	515	7.1[c]	0.066[c]	750[c]	1250[c]
	$Th\text{-}Al_1$	1,031	7.4	0.078	700	1200
	$Th\text{-}Al_2$	10,100	6.8	0.040	650	1200

[a]Concentration at which slurry enters the compaction region of settling.
[b]After settling 48 or more hours.
[c]Average for two experiments.

Table 17.7. Room-Temperature Settling Properties of Aqueous Thorium Oxide–Aluminum Oxide Slurries

Slurry preparation: D-16-900 ThO_2; $Al(OH)_3$
250 g of Th per kg of H_2O
Autoclaved 22 hr at 300°C

Al Concentration (ppm, based on ThO_2)	pH	U_0, Settling Rate (cm/sec)	Critical[a] Concentration (g of Th per liter)	Settled[b] Concentration (g of Th per liter)
0	6.7	0.058	850	1450
250	6.8	0.079	950	1500
500	6.0	0.075	950	1550
1,000	6.0[c]	0.081[c]	950[c]	1550[c]
10,000	5.7	0.039	730	1300

[a]Concentration at which slurry enters the compaction region of settling.
[b]After settling 48 or more hours.
[c]Average for two experiments.

No marked changes in room-temperature slurry behavior were noted between the pure oxide slurries and the thorium-aluminum slurries which were autoclaved at 300°C in the presence of 1000 and 2500 ppm of sulfate (Table 17.8).

The thorium-aluminum oxalates were coprecipitated from a solution of the nitrates by the addition of excess oxalic acid and were decomposed to oxide by a multistage calcination ending at 900°C. For comparison purposes D-16 oxide (650°C calcination) was refired at 900°C. For studies with the simple mixtures, $Al(OH)_3$ was precipitated from the nitrate solution by the addition of NH_4OH, washed, and added to the D-16-900 oxide prior to the autoclaving at 300°C. The settling studies were carried out with slurries (250 g of thorium per kilogram of H_2O) of various oxides and mixtures. For settling studies on the slurries as prepared, they were first tumbled for 2 hr at room temperature. To determine the effect of autoclaving, the slurries were autoclaved for 22 hr at 300°C in stainless steel containers. Sulfate was added as thorium sulfate.

From the data of Table 17.5 it is apparent that the particles of the thorium-aluminum oxides prepared by the thermal decomposition of the coprecipitated oxalates are not only on the average much smaller than those of a pure oxide similarly prepared but are much more uniform (i.e., low value of σ_g). Electron micrographs of the mixed-oxide products indicated them to be cubical. The relative surface areas available for nitrogen adsorption calculated from the x-ray crystallite sizes are slightly less than is observed for pure oxide but not so low as those observed for thorium-uranium oxides prepared by thermal decomposition of the coprecipitated thorium-uranous oxalates (Table 17.9).

17.5 PREPARATION AND PROPERTIES OF THORIUM-URANIUM OXIDE

The effect of the method of oxide preparation on the properties of thorium-uranium oxide with a uranium/thorium mole ratio of 0.005/1 was investigated. Three methods were studied: simple addition of UO_3 to ThO_2 followed by autoclaving

Table 17.8. Effect of Sulfate on the Room-Temperature Settling Properties of Thorium-Aluminum Oxide Slurries

Slurry preparation: 250 g of Th per kg of H_2O
Sulfate added as $Th(SO_4)_2$
Autoclaved 22 hr at 300°C

Sulfate Concentration (ppm, based on ThO_2)	Oxide Designation	Al Concentration (ppm, based on ThO_2)	pH	U_0, Settling Rate (cm/sec)	Critical[a] Concentration (g of Th per liter)	Settled[b] Concentration (g of Th per liter)
1000	D-16-900	0	6.5	0.070	950	1500
	$Th\text{-}Al_4$	258	5.0	0.059	750	1400
	$Th\text{-}Al_3$	515	5.5[c]	0.079[c]	850[c]	1500[c]
	$Th\text{-}Al_1$	1,031	5.3	0.065	800	1400
	$Th\text{-}Al_2$	10,100	5.6	0.033	650	1150
2500	D-16-900	0	3.0	0.027	750	1600
	$Th\text{-}Al_4$	258	4.6	0.079	750	1350
	$Th\text{-}Al_3$	515	3.2	0.059	800	1600
	$Th\text{-}Al_1$	1,031	5.1	0.070	800	1500
	$Th\text{-}Al_2$	10,100	4.1	0.047	750	1400

[a]Concentration at which slurry enters the compaction zone of settling.
[b]After settling 48 or more hours.
[c]Average for two experiments.

Table 17.9. Characteristic Properties of Thorium Oxide and Thorium-Uranium Oxides

Prepared (1) by wet-autoclaving the simple mixtures at 300°C, (2) by the thermal decomposition of the coprecipitated oxalates, (3) by the hydrothermal decomposition of the nitrate solutions, and (4) by the hydrothermal decomposition of the coprecipitated oxalates and subsequent firing.

Preparation No.	Preparation Conditions	Final Firing Conditions		Mean Stokes Diameter (μ)	Specific Surface Area (m^2/g)	X-Ray Crystallite Size (Å)	S/θ, Relative* Surface Available for N_2 Adsorption
		Temperature (°C)	Time (hr)				
D-16	ThO_2 from thorium oxalate thermal decomposition	650		2.1	34.7	103	0.59
		750	16.5	2.2	21.1	191	0.67
		900	4	2.5	7.9	412	0.54
		1100	24	3.2	6.0	898	0.90
		1300	24	2.7	2.2	1783	0.74
						Av	0.69
69	ThO_2–0.5% UO_3; prepared from D-16 (650°C) and $UO_3 \cdot H_2O$, wet-autoclaved at 300°C, dried and re-fired	750	18	1.4	18.9	195	0.62
		900	1		19.1	222	0.71
		900	8		13.5	306	0.69
		900	15.5	1.5	11.7	335	0.66
		900	29		11.3	362	0.68
		1000	18	1.6	5.8	483	0.47
						Av	0.64
81	ThO_2–0.6% UO_3; prepared by thermal decomposition of the coprecipitated oxalates	370	2		28.6	50	
		480	21.2		28.0	70	0.33
		640	2	(4–5)	13.1	105	0.23
		900	2		2.8	373	0.17
		900	3.2		2.6	395	0.17
		900	21.4		2.4	548	0.22
		900	44		2.4	580	0.23
						Av	0.22
N-4	ThO_2–0.4% UO_3; prepared by hydrothermal decomposition of the nitrate solutions at 300°C	400	1		28.6	144	0.69
		650	1		29.7	133	0.66
		650	24	2.6	27.7	145	0.67
		800	1		20.7	136	0.47
		900	1		20.6	149	0.51
		900	24		16.0	174	0.46
		1000	1		16.5	158	0.43
						Av	0.56
92	ThO_2–0.4% UO_3; prepared by hydrothermal decomposition of the coprecipitated oxalates at 300°C	900	17	~0.2 (93% < 1 μ)	19.1	227	0.72

*Calculated from the x-ray crystallite size.

in water at 300°C and subsequent firing; thermal decomposition of coprecipitated thorium-uranous oxalate; and hydrothermal decomposition of a thorium-uranium nitrate solution at 300°C. All mixed-oxide products appeared to be suitable slurry materials.

17.5.1 Characteristic Properties of Thorium-Uranium Oxides

The properties of thorium-uranium mixed oxides typical of the products from the various methods of preparation are shown in Table 17.9. The properties of a pure oxide prepared by the thermal decomposition of thorium oxalate are included for comparison. The particle size, specific surface area, and x-ray crystallite size of the mixed oxide prepared by autoclaving a simple mixture of the thorium and uranium oxides and firing are seen to be nearly the same as those obtained for the pure oxide under the same firing conditions. These materials both show the lack of growth of particle size with increasing firing temperature and the characteristic decrease in specific surface and increase in x-ray crystallite size typical of the oxide products prepared by the thermal decomposition of thorium oxalate.[11] The mixed oxide prepared by the thermal decomposition of the coprecipitated oxalates also shows a marked decrease in surface area and increase in crystallite size with increasing firing temperature. However, the ratio of specific surface area to a theoretical surface area calculated from the x-ray crystallite size for the oxide from the coprecipitated oxalates is lower by a factor of 3 than for the other preparations, indicating a more dense packing of the crystallites.

The mixed oxide prepared by the hydrothermal decomposition of the thorium-uranium nitrate solution shows the small x-ray crystallite size and nongrowth of the crystallites with increasing firing temperature, which are typical of the hydrothermally prepared oxides.[12] The specific surface area decreased with increasing firing temperature but not so much as for the thermally decomposed material. The decreases in specific surface area with increasing firing temperature for the thermally and hydrothermally prepared mixed oxides are very similar to those obtained for the pure oxide prepared by analogous methods (Fig. 17.7).

17.5.2 Abrasive Properties of Thorium-Uranium Mixed Oxides

The most striking difference in the properties of the various mixed oxides was in the abrasive properties of their aqueous suspensions. Table 17.10 shows the penetration rate for various slurries which were impinged as a jet against thin stainless steel plates.[13] The slurry of the mixed oxide prepared by thermal decomposition of the coprecipitated oxalates penetrated more than 10 times as fast as similar slurries of the pure oxide from the thermal or hydrothermal decomposition of

[11] V. D. Allred and S. R. Buxton, *HRP Quar. Prog. Rep. July 31, 1955*, ORNL-1943, p 184.

[12] E. V. Jones, *HRP Quar. Prog. Rep. Oct. 31, 1955*, ORNL-2004, p 175.

[13] J. P. McBride and W. L. Pattison, *HRP Quar. Prog. Rep. July 31, 1953*, ORNL-1605, p 139.

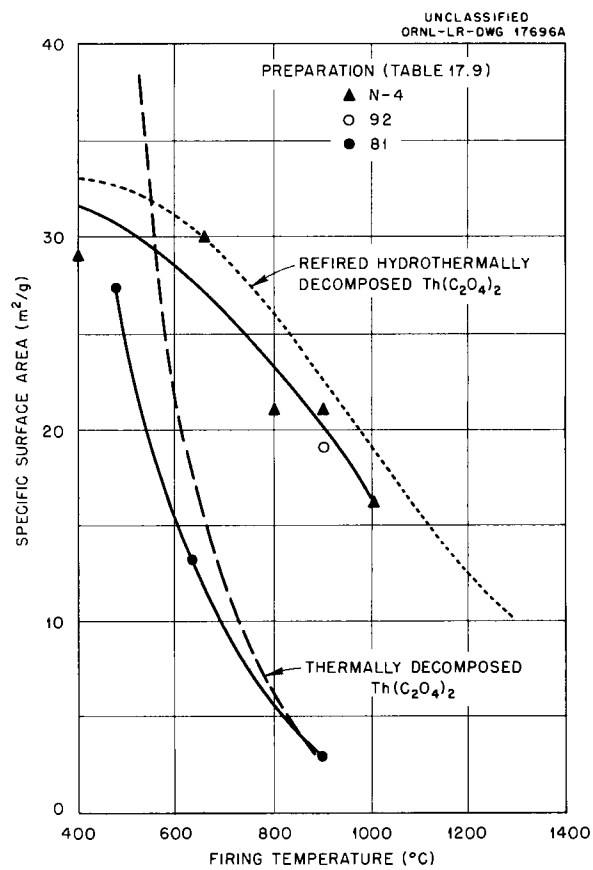

Fig. 17.7. Effect of Firing Temperature on Specific Surface Area of Thorium-Uranium Oxides.

Table 17.10. Abrasive Properties of Aqueous Thorium-Uranium Mixed Oxide Slurries

Oxides fired at 900°C
Slurry thorium concentration: 250 g/liter
Temperature: 250°C

Slurry Oxide	Penetration Rate (mils/min)
ThO_2 from thorium oxalate thermal decomposition	0.16
ThO_2–0.5% UO_3, prepared from 650°C-fired ThO_2 and $UO_3 \cdot H_2O$ wet-autoclaved at 300°C, dried and refired	0.11
ThO_2–0.4% UO_3, prepared by thermal decomposition of coprecipitated oxalates	1.72
ThO_2 prepared from thorium oxalate by hydrothermal decomposition at 300°C and firing	0.08
ThO_2–0.4% UO_3, prepared from coprecipitated oxalates by hydrothermal decomposition at 300°C and firing	0.14

thorium oxalate or mixed oxides prepared by autoclaving simple oxide mixtures or hydrothermally decomposing the coprecipitated oxalates.

17.5.3 Room-Temperature Settling Properties of Aqueous Thorium-Uranium Oxide Slurries

Tables 17.11 and 17.12 show the room-temperature hindered-settling properties for aqueous suspensions of pure ThO_2 from oxalate thermal decomposition and mixed oxides prepared by autoclaving simple oxide mixtures and thermally decomposing the coprecipitated oxalates. Prior to the settling studies the slurries were subjected to a variety of pretreatments, including autoclaving at 300°C with O_2, H_2, and CO_2 atmospheres and also in the presence of 1000 to 10,000 ppm of sulfate (based on ThO_2).

The mixed oxide from the coprecipitated oxalates settled much faster than the others and to a denser settled bed under all conditions of pretreatment. Little difference was observed in the settling characteristics of slurries of the pure oxide and of the mixed oxide prepared by autoclaving simple mixtures. Of interest is the fact that autoclaving at 300°C with the various gaseous overpressures did not markedly change the settling characteristics of any of the slurries.

Autoclaving at 300°C in the presence of sulfate resulted in lower supernatant pH's, much lower settling rates for all slurries at sulfate concentrations of 2500 ppm and higher, and slight increases in the settled concentrations. Despite the high solubility of UO_2SO_4 in water at 300°C, the addition of sulfate does not appear to affect the mixed-oxide slurries any differently from the pure oxide slurry. The lack of any gross change in the behavior of aqueous suspensions of the mixed oxide after the variety of autoclaving treatments indicated above constitutes the real importance of the settling results presented in the tables.

17.6 PREPARATION OF THORIA SOLS AND GELS[14]

Work is continuing on the preparation of thoria sols and of gels suitable for the preparation of slurry microspheres. It has been found that the micels in nitrate-stabilized thoria sols 0.25 *M* in ThO_2 and 0.125 *M* in nitrate ion, prepared by ultrafiltration from pH-adjusted thorium nitrate solutions, become smaller and more uniform in size on aging 210 hr at 100°C. Quick-settling thoria gels have been prepared by coagulation of thoria sols with thorium/nitrate ratios of 4/1 by hexamethylenetetramine solution. An ultrasonic device to locate the slurry-water interface by a pulse-echo technique is being manufactured for use in high-temperature high-pressure equipment.

[14]Work done by Houdry Process Corporation.

Table 17.11. Room-Temperature Sedimentation Characteristics of Aqueous Thorium and Thorium-Uranium Oxide Slurries

Slurry thorium concentration: 250 g per kg of H_2O

Slurry Treatment	Slurry Oxide[a]	Supernatant pH	Settling Rate (cm/sec)	Thorium Concentration (g/liter)	
				Critical[b]	Settled[c]
Tumbled 2 hr at 27°C	I	9.0	0.14	900	1500
	II	7.9	0.07	700	1300
	III	6.6	0.12	1100	1700
Autoclaved 22 hr at 300°C	I	6.7	0.06	800	1400
	II	6.8	0.08	800	1300
	III	6.1	0.12	1000	1900
Autoclaved 22 hr at 300°C,	I	6.5	0.10	900	1500
O_2 overpressure (300 psi	II	8.8	0.11	800	1500
at room temperature)	III	7.4	0.18	1300	2100
Autoclaved 22 hr at 300°C,	I	8.8	0.13	900	1600
H_2 overpressure (350 psi	II	9.5	0.11	900	1500
at room temperature)	III	8.8	0.16	1200	1900
Autoclaved 22 hr at 300°C,	I	4.7	0.06	900	1700
CO_2 overpressure (500 psi	II	4.4	0.06	800	1400
at room temperature)	III	5.1	0.12	1100	1900

[a](I) pure D-16 ThO_2 recalcined at 900°C; (II) $ThO_2 + UO_3$, prepared by wet-autoclaving D-16 (650°C) plus $UO_3 \cdot H_2O$ at 300°C, drying, and refiring at 900°C; (III) $ThO_2 + UO_3$, prepared from thorium-uranous oxalate coprecipitated at 40°C, calcined at 900°C.

[b]Critical concentration is concentration at which slurry enters the compaction region of settling as opposed to hindered-settling region.

[c]Settled concentration after 48 hr of settling.

Table 17.12. Effect of Autoclaving at 300°C with Added Sulfate on the Room-Temperature Sedimentation Characteristics of Thorium and Thorium-Uranium Oxide Slurries

Slurry thorium concentration: 250 g/liter
Autoclaved 22 hr at 300°C

Sulfate Concentration Added as H_2SO_4 (ppm, based on ThO_2)	Slurry Oxide[a]	Final Supernatant pH	Settling Rate (cm/sec)	Thorium Concentration (g/liter)	
				Critical[b]	Settled[c]
0	I	6.7	0.06	800	1400
	II	6.8	0.08	800	1300
	III	6.1	0.12	1000	1900
1000	I	6.5	0.07	900	1500
	II	5.9	0.05	800	1600
	III	6.0	0.11	1100	2100
2500	I	3.0	0.03	800	1600
	II	5.5	0.05	900	1600
	III	5.2	0.13	1100	2200
5000	I	3.3	0.04	900	1700
	II	3.2	0.03	800	1600
	III	3.2	0.06	1000	2200
10,000 (autoclave attacked in all cases)	I	4.8	0.05	1000	1900
	II	5.0	0.04	800	1700
	III	5.2	0.08	1000	2100

[a](I) pure D-16 ThO_2 recalcined at 900°C; (II) $ThO_2 + UO_3$, prepared by wet-autoclaving D-16 (650°C) plus $UO_3 \cdot H_2O$ at 300°C, drying, and refiring at 900°C; (III) $ThO_2 + UO_3$, prepared from thorium-uranous oxalate coprecipitated at 40°C, calcined at 900°C.

[b]Critical concentration is concentration at which slurry enters the compaction region of settling as opposed to hindered-settling region.

[c]Settled concentration after 48 hr of settling.

18. THORIUM OXIDE BLANKET PROCESSING

D. E. Ferguson

R. E. Leuze R. D. Baybarz

At the present time the only practical method for processing irradiated thorium oxide slurry is to convert the oxide to a natural-water nitrate solution and treat by the Thorex process. Although this method is adequate, it is expensive unless one plant can be built to process thorium oxide from several full-scale power reactors. Simple alternate methods of processing that can be incorporated as part of each reactor operation are therefore being investigated. Previous attempts[1] to leach protactinium and uranium from irradiated ThO_2 were only partially successful, since both are bound within the ThO_2 particles. Calculation shows that the recoil energy of fission fragments is sufficient to eject most fission products into the aqueous phase of a ThO_2 slurry if the ThO_2 particles are $<10\,\mu$ in diameter. This means that it may be possible to develop some method of removing most of the fission-product poisons together with an amount of Pa^{233} and U^{233} equal to the breeding gain without destroying the ThO_2 particles. Scouting studies were made to investigate this possibility.

18.1 ADSORPTION ON ThO_2

The behavior of fission products in ThO_2 slurries was tested by adding tracer quantities of Zr^{95}, Nd^{147}, Y^{91}, and Ru^{103} to the water phase. The tracers were rapidly adsorbed on the ThO_2, leaving <0.0001% in the water. The thorium oxide appeared to hold these cations irreversibly; they could not be eluted with dilute nitric or sulfuric acid. Further cation adsorption studies were made with ThO_2 slurried in dilute uranyl sulfate solution.

The nature of cation adsorption on ThO_2 is not completely understood; however, it appears to be similar to the double-layer effect common in colloid chemistry. Since the thorium atoms are located on the surface of the ThO_2 crystal, they attract and hold anions. In a water slurry the thorium oxide adsorbs hydroxyl groups, acquiring an excess negative charge. The excess hydroxyl groups then adsorb cations. For example, ThO_2 particles with a surface area of 35 m^2/g adsorbed 2000 ppm of uranium from dilute uranyl sulfate. Treatment of the ThO_2 slurry with dilute sulfuric acid replaced the hydroxyl ions with sulfate ions. The number of excess sulfate ions trapped on the ThO_2 was apparently small, since ThO_2 thus pretreated before being contacted with uranyl sulfate adsorbed only 10% as much uranium as untreated ThO_2. When the hydroxyl groups were replaced by phosphate or pyrophosphate ions, the amount of uranium adsorbed was increased to ~3500 ppm, and this uranium was not readily eluted with dilute acid. Replacement of the hydroxyl groups by silicate ions increased the uranium adsorption to 9000 ppm; however, about 90% of this uranium was eluted with dilute sulfuric acid.

Scouting tests showed that when freshly calcined ThO_2 was contacted with a saturated solution of sulfur in absolute alcohol, sulfur was adsorbed on the thoria, forming a protective film that decreased or eliminated hydroxyl adsorption when the treated ThO_2 was slurried in water. Thorium oxide treated in this way held about 50 ppm of sulfur. When the ThO_2 was slurried in dilute uranyl sulfate solution at 23 or 110°C, there was essentially no uranium adsorption. When ThO_2 was only partially saturated with sulfur in this manner, larger amounts of uranium were adsorbed (~800 ppm); however, this was readily eluted with dilute acid.

Further studies will be made on both uranium and fission-products adsorption to determine whether ThO_2 can be treated in some manner either to eliminate adsorption or to make the adsorption reversible.

[1] D. E. Ferguson, R. E. Leuze, and W. E. Tomlin, *HRP Quar. Prog. Rep. July 31, 1955*, ORNL-1943, p 221.

19. EQUIPMENT DECONTAMINATION

D. E. Ferguson

R. E. Leuze R. D. Baybarz

It was previously reported[1] that chromous sulfate–dilute sulfuric acid solutions were successful in defilming and decontaminating type 347 stainless steel that had been in contact with uranyl sulfate solutions containing fission products at 250 to 300°C. These chromous sulfate–sulfuric acid mixtures are the best descaling and decontaminating solutions now available. The reagent may be prepared by reduction of a higher-valence chromium salt, for example, chromium potassium sulfate.

Chromium(III) was satisfactorily reduced to Cr(II) in an electrolytic cell with lead anodes and cathodes separated by anion exchange membranes. The current density was 0.15 to 0.25 amp/in.^{2}. In a nine-chamber cell, with alternating anode and cathode compartments separated by Nalfilm-2, the chromic sulfate solution was pumped through at a rate of 1.5 liters/hr with >80% reduction. The cathode cell volume was 4 liters.

A chromic sulfate solution resulting from chromous sulfate descaling of a Y-12 corrosion loop (run I-38, see Sec 11.1) was reduced to the chromous state in the electrolytic cell with no difficulty. The original chromous sulfate descaling solution has been prepared by reduction of Cr(III) with zinc. However, reduction of the spent chromous sulfate solution with metallic zinc was difficult because of formation of a green hydrated chromic sulfate complex, but electrolytic reduction was not hindered by this material.

Chromous sulfate may also be prepared from the less expensive potassium or sodium dichromate. The Cr(VI) is reduced to Cr(III) with SO_2 and then electrolytically reduced to Cr(II). Electrolytic reduction of chromate to the chromic state is possible but difficult because of chromate precipitation on the lead electrodes, which reduces the current efficiency and removes chromium from solution; SO_2 reduction is rapid and inexpensive.

Nalfilm-2 so far seems to be the most stable membrane tried. No deterioration was noted in 0.1 to 1.0 *M* acid and chromium concentrations, or at temperatures up to 85°C. Above 90°C the film was not very stable. An Ionics film, PX43C-A111, became brittle and cracked after only a few hours of operation, necessitating shutdown of the cell.

[1] D. E. Ferguson, R. E. Leuze, and R. D. Baybarz, *HRP Quar. Prog. Rep. July 31, 1956*, ORNL-2148, p 132–133.

Part VI

SUPPORTING CHEMICAL RESEARCH

E. H. Taylor

20. AQUEOUS SYSTEMS AT ELEVATED TEMPERATURES

C. H. Secoy

F. E. Clark
H. F. McDuffie
R. Slusher
H. H. Stone

20.1 THE SYSTEM UO_2SO_4-$CuSO_4$-H_2SO_4-H_2O

An exploration of the phase behavior of mixtures of stoichiometric uranyl sulfate and copper sulfate solutions at 304°C was reported earlier.[1] This study disclosed that the entire composition map (represented graphically by plotting per cent $CuSO_4$ against per cent UO_2SO_4) was divided into three phenomenological regions: a region in which two liquid phases occurred, one in which solid and liquid existed, and a band, separating the first two, in which solid and two liquids were present.

Additional exploratory work of similar nature has confirmed several surmises concerning the qualitative behavior of the system. Before discussing these, however, an explanation of the system variables is required. For our purpose the system may be treated as a condensed system; that is to say, the vapor phase, even though it is always present, may be ignored. Pressure is therefore ignored as a variable, and composition values are the room-temperature values or, in other words, the values representing the total contents of the system. The actual variables are, therefore, temperature and three composition parameters.

The composition variables may be defined in several different ways open to arbitrary choice. The system composition is represented by the weight per cent of $CuSO_4$, the weight per cent of UO_2SO_4, and the mole per cent of excess H_2SO_4 based on the total moles of $CuSO_4$ plus UO_2SO_4. In order to proceed in a systematic manner, it is desirable to maintain a constant value for one of the variables while the others are varied over the range of interest. The manner chosen for expressing the amount of excess H_2SO_4 provides a precise experimental technique for holding this quantity constant while the concentrations of the salts are varied at will.

A concentrated solution of $CuSO_4$ was prepared, and to it was added an amount of sulfuric acid to approximate the desired mole per cent acid excess. The composition of this solution was accurately established by analysis for Cu^{++} and for SO_4^{--}. In a similar manner a concentrated master solution of UO_2SO_4 was prepared. The excess acidity of the two solutions was made as nearly identical as possible by repeated analyses and adjustments. Solutions of any desired concentrations of $CuSO_4$ and UO_2SO_4 (less than the concentrations of the master solutions) could then be prepared by mixing appropriate weight aliquots of the master solutions and of water. Thus any experimental errors in preparing the various mixtures would in no way affect the constancy of the excess acid, and analysis of the mixtures was considered unnecessary.

A study of solutions containing 29.11% excess acid has been completed, and work on solutions with approximately 20% and 40% excess acid, respectively, is in progress. Table 20.1 summarizes the experimental observations for the 29.11% excess acid system. The region in which a second liquid phase appears covers a large portion of the area investigated and extends to the $CuSO_4$ side of the diagram at $CuSO_4$ concentrations above about 11.5% $CuSO_4$. All experimental points in this region lie within 1 deg of a smooth curved surface when plotted in three-dimensional space (temperature vs per cent $CuSO_4$ vs per cent UO_2SO_4). Interpolations within the limits of this area are permissible and are readily made by a graphical method by separately plotting the rows and columns of Table 20.1. Table 20.2 gives the temperatures obtained by interpolation at whole-number values of the composition parameters. It is believed that these data have an absolute accuracy better than ±1°C and a relative accuracy within a few tenths of a degree. Curves depicting the interpolated data are shown in Fig. 20.1.

It is to be noted that the more dilute solutions studied yielded crystalline precipitates at temperatures more than 100°C below the two-liquid phase region. It is obvious that, starting at a composition point in the two-liquid phase region and moving in the direction of greater dilution at any temperature between about 200 and 300°C, a

[1] C. H. Secoy *et al.*, *HRP Quar. Prog. Rep. Oct. 31, 1956*, ORNL-2222, p 161.

Table 20.1. Phase Transition Temperatures (°C)

Master solutions: 16.69% $CuSO_4$, 29.11 mole % excess H_2SO_4[a]
45.63% UO_2SO_4, 29.11 mole % excess H_2SO_4

Weight Ratio, Solution/H_2O	Weight Ratio, $CuSO_4/UO_2SO_4$							
	10/0	9/1	8/2	7/3	6/4	5/5	4/6	0/10
10/0	345.5[b]	337.0	335.5	331.5	332.0	331.0	331.5	338.0
9/1	343.0			329.0	329.5	327.5	327.5	332.5
8/2	340.0			326.0	324.5	324.0		327.0
7/3	Solid,[c] 208	328.5		321.0	322.0	320.0		321.0
6/4	Solid, 198	327.0		319.0				316.5
5/5	Solid, 185	325.0						314.0
4/6	Solid, 175	324.5		B[a]				310.5
3/7	Solid, 173	Solid, 210						309.0
2/8	Solid, 170		320.0	317.0	315.5	314.0		311.0
1/9	Solid, 160	Solid, 180	Solid, 214	322.5	321.0	320.5		316.0

[a]Exact compositions for each solution may be calculated by taking the indicated fractions of the master solution values; e.g., for point B,

$$0.4 \times 0.7 \times 16.69 = 4.673\%\ CuSO_4,$$
$$0.4 \times 0.3 \times 45.63 = 5.476\%\ UO_2SO_4.$$

[b]All transitions not otherwise marked involved the appearance (rising temperature) of a second liquid phase.

[c]Solid redissolves with rising temperature at 325 ± 10°C. Second liquid phase appears at 336°C.

very steep cliff is encountered. A clear concept of this may be obtained from Fig. 20.2, which shows graphically the data of the first column of Table 20.1 (the $CuSO_4$-H_2SO_4-H_2O system).

Reliable data are very difficult to obtain in equilibrations involving the solid phases. The solutions in this region, particularly those not far from the liquidus surface, have a great tendency to remain supersaturated for hours. In general it was necessary to hold the solutions at 280 to 300°C for about 10 hr before the slightest trace of solid could be detected. The crystals would continue to grow for several hours after their initial appearance. All temperatures reported in Table 20.1 were obtained by varying the temperature at a rate of about 5°C per hour in the direction to cause the solid to redissolve. These observations are in general agreement with those reported earlier from rate studies in titanium vessels.[1] No effort has been made to determine the identity of the solid phases. The curves of Fig. 20.2 indicate at least three distinct phases, but this deduction is questionable. The indicated break at point B may not exist, or there may be as-yet-undetected breaks in the liquidus curve.

The following qualitative statements can be made concerning the effect of varying the per cent of excess acid. Increasing the amount of excess

Table 20.2. Smoothed Values for Two-Liquid Phase Temperatures (°C)

(29.11 mole % excess H_2SO_4)

$CuSO_4$ (wt %)	UO_2SO_4 (wt %)								
	0	5	10	15	20	25	30	35	40
0	*	315.5	310.4	309.3	311.4	315.1	319.8	325.3	331.2
1	*	313.8	310.5	310.8	313.2	317.1	322.1	327.6	333.3
2	*	313.8	311.3	312.3	315.1	319.3	324.2	329.7	335.6
3	*	314.7	312.7	314.1	317.1	321.5	326.4	331.9	337.7
4	*	316.1	314.4	316.1	319.2	323.7	328.5	334.0	339.9
5	*	317.7	316.1	318.1	321.4	325.9	330.7	336.0	**
6	*	319.3	318.1	320.3	323.6	328.0	332.8	338.1	
7	*	321.1	320.1	322.5	325.9	330.2	335.0		
8	*	322.9	322.3	324.7	328.1	332.4	337.2		
9	*	324.9	324.6	327.1	330.5	334.5	339.4		
10	*	326.9	327.0	329.5	332.8	336.7			
11	*	328.9	329.3	331.9	335.3	338.9			
12	336.9	331.0	331.7	334.3	337.7				
13	339.3	333.1	334.1	336.8					
14	341.2	335.3	336.5	339.3					
15	342.9	337.5	339.1						

*Solids precipitate at lower temperatures.

**Observations not extended above 340°C.

acid will cause the region, in which solid phases appear, to shrink toward more dilute solutions. The temperature of appearance of a solid phase at a particular concentration will be elevated. The scope of the two-liquid phase region will shrink, and the temperatures of appearance will be elevated. At a particular temperature the regions of homogeneity will increase in size. Continued study at other acidities should yield a measure of these effects.

20.2 HOMOGENEOUS CATALYSIS OF THE HYDROGEN-OXYGEN REACTION IN AQUEOUS SOLUTIONS

Study of the hydrogen-oxygen reaction, catalyzed by dissolved copper salts, was resumed during the past quarter after a lapse of several years. Although the previous work provided an adequate base for application of the reaction to the operation of the HRE and the operation of in-pile corrosion test apparatus, many details of the reaction remained to be elucidated. Questions concerning the effects of higher acidity on the reaction were raised as the Project sought to maintain the stability of dilute fuel solutions at progressively higher temperatures; information concerning reaction rates in heavy-water systems must be obtained before economical power-breeder reactors can be designed properly; the effects of various additives (e.g., lithium sulfate) for the control of corrosion in concentrated uranyl sulfate solutions must be known in order to permit evaluation of all possible fuel and blanket materials. In short, rates of reaction must be measured over all ranges of uranium concentration, acidity, additive concentration, and temperature likely to be of interest to the development of homogeneous reactors. Increased knowledge of the mechanism of the reaction

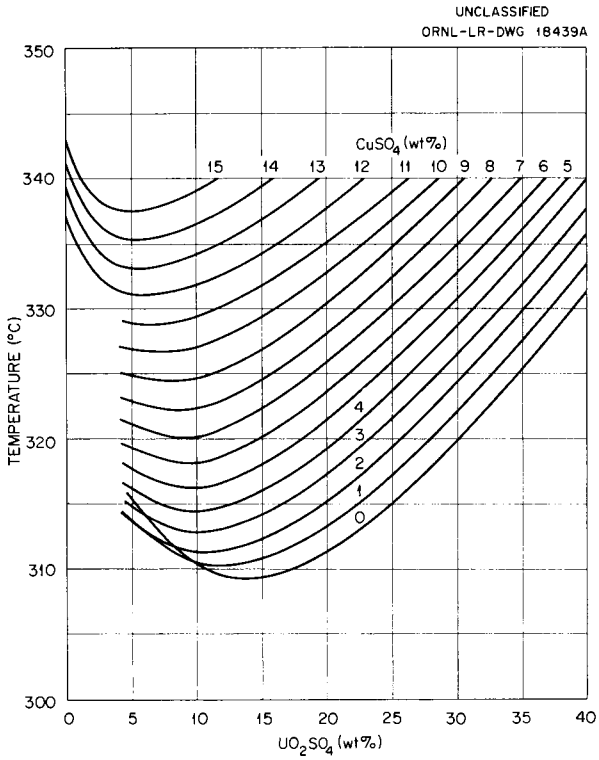

Fig. 20.1. Two-Liquid Phase Temperature in the System $CuSO_4$-UO_2SO_4-H_2SO_4-H_2O (29.11 mole % Excess H_2SO_4).

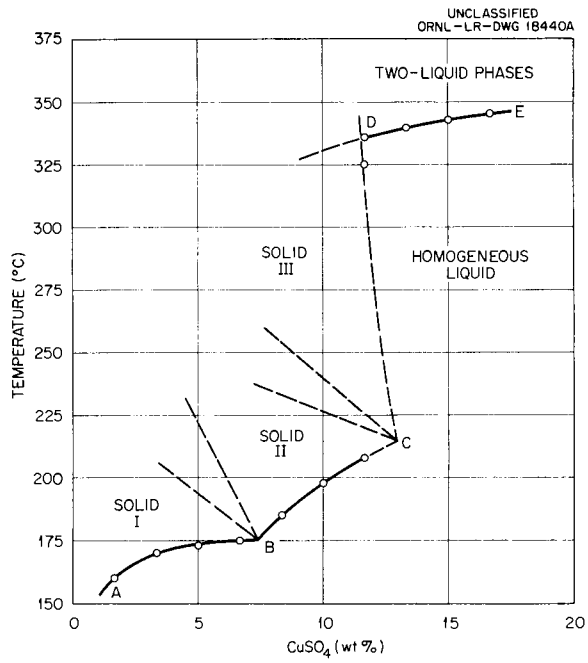

Fig. 20.2. The System $CuSO_4$-H_2SO_4-H_2O (29.11 mole % Excess H_2SO_4).

may be useful in connection with all these questions.

During the interim following publication of the then-classified but now-declassified recombination information,[2] there has been much interest in the homogeneous catalysis of reactions of dissolved molecular hydrogen. Winfield[3] has reviewed the general field of these reactions. Halpern and coworkers from the University of British Columbia have published extensive studies of the copper-catalyzed reactions of hydrogen in aqueous solutions – studies which, although at lower temperatures than those of reactor interest and under somewhat different conditions, have, nevertheless, confirmed and extended the ORNL results and have provided stimulating evidence in support of a proposed mechanism for the reaction. The ORNL laboratory and in-pile studies of recombination and its application to the HRE were recently the subject of declassified papers at an American Chemical Society symposium on nuclear energy.[4,5,6]

20.2.1 Cupric Perchlorate

The well-known usefulness of perchlorate in kinetic studies as a noncomplexing anion indicated that tests of cupric perchlorate might reveal the catalytic activity of the uncomplexed cupric ion. On the basis of tests at 250°C with solutions containing 0.001 *M* cupric perchlorate and 0.005

[2] H. F. McDuffie *et al.*, *The Radiation Chemistry of Homogeneous Reactor Systems. III. Homogeneous Catalysis of the Hydrogen-Oxygen Reaction*, ORNL CF-54-1-122 (Jan. 27, 1954).

[3] M. E. Winfield, *Rev. Pure Appl. Chem. (Australia)* 5, 217 (1955).

[4] H. F. McDuffie *et al.*, *Homogeneous Catalysis for Homogeneous Reactors*, paper presented at the Southeastern Section Meeting, American Chemical Society, Memphis, Tenn., Dec. 6, 1956.

[5] D. M. Richardson *et al.*, *In-Pile Studies of Homogeneous Reactor Solution Stability and Hydrogen-Oxygen Recombination*, paper presented at the Southeastern Section Meeting, American Chemical Society, Memphis, Tenn., Dec. 6, 1956.

[6] S. Visner, P. N. Haubenreich, and R. E. Aven, *Internal Recombination of Radiolytic Gas with a Homogeneous Catalyst in the Homogeneous Reactor Experiment*, paper presented at the Southeastern Section Meeting, American Chemical Society, Memphis, Tenn., Dec. 6, 1956.

to 0.050 M perchloric acid, it had been reported[2] that the specific reaction-rate constant for uncomplexed cupric ion was 5000 $M^{-1}\cdot hr^{-1}$ and that varying the acidity over the tenfold range of concentration did not affect the reaction rate; from this it was inferred that the hydrogen ion, H^+, did not participate in the rate-determining step of the reaction. Peters and Halpern[7] subsequently reported studies of the reaction of cupric perchlorate with hydrogen in aqueous solutions in the temperature range of 80 to 140°C. They used a constant overpressure of hydrogen and assumed that the solubility of hydrogen was constant over the range of temperature, with a value of $7.14 \times 10^{-4}\ M\cdot atm^{-1}$. The course of the reaction was followed by determining the zero-order rate of depletion of the oxidant, $Cr_2O_7^{--}$, which was present in the solution. From tests with solutions containing 0.1 M cupric perchlorate, 0.01 M perchloric acid, and 0.0005 M $Cr_2O_7^{--}$, they derived the following expression for the specific reaction-rate constant:

$$(1)\ k = 1.0 \times 10^{13} \exp \frac{-26{,}600}{RT}\ M^{-1}\cdot min^{-1}\ .$$

When this expression was converted to an Arrhenius plot of log k vs $1/T$ and extrapolated from 140°C to 250°C, it was possible to compare the agreement between the Peters and Halpern expression and the ORNL data. The agreement was found to be excellent, as indicated by Fig. 20.3.

When Halpern, Macgregor, and Peters[8] tested the effect of added perchloric acid (up to 1.0 M) upon the catalytic activity of cupric perchlorate at 110°C, they found a substantial lowering of the rate as the acidity was increased. Moreover, they found that at high acidity the rate was dependent upon the second power of the copper concentration, whereas it had been known that at low acidity the rate was dependent upon the first power of the copper concentration. They have interpreted their data in terms of a mechanism involving the species CuH^+ as a postulated intermediate, as indicated by the following equations:

$$(2)\qquad Cu^{++} + H_2 \underset{k_{-1}}{\overset{k_1}{\rightleftharpoons}} CuH^+ + H^+$$

[7] E. Peters and J. Halpern, *J. Phys. Chem.* **59**, 793 (1955).

[8] J. Halpern, E. R. Macgregor, and E. Peters, *J. Phys. Chem.* **60**, 1455 (1956).

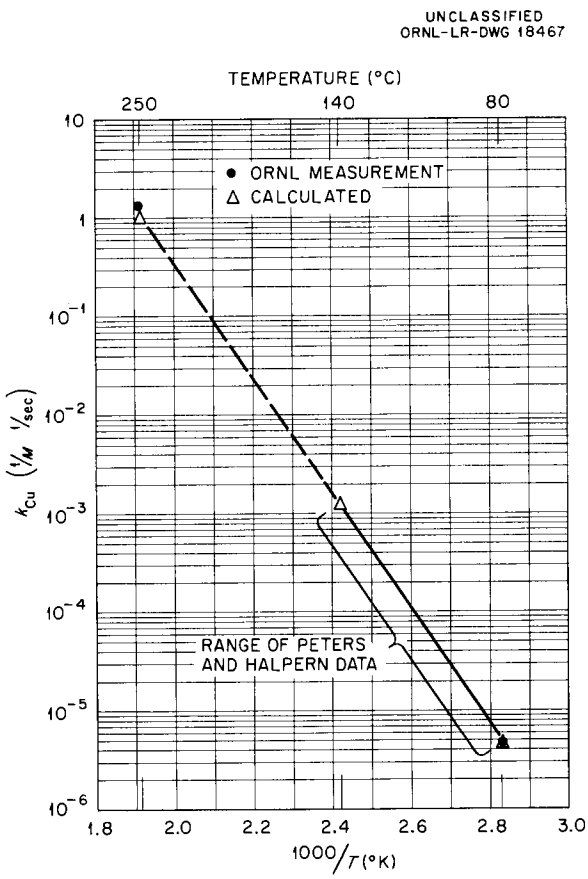

Fig. 20.3. Homogeneous Catalysis by Cupric Perchlorate.

$$(3)\qquad CuH^+ + Cu^{++} \xrightarrow{k_2} 2Cu^+ + H^+$$

$$(4)\qquad 2Cu^+ + \text{oxidant} \xrightarrow{\text{fast}} 2Cu^{++}$$

It will be observed that hydrogen ion, H^+, can participate in the reaction because of its presence in the equilibrium; the extent of its participation will depend on its concentration and the magnitude of the constant k_{-1} vs the concentration of Cu^{++} and the magnitude of the constant k_2. Based on a steady-state treatment of the intermediate CuH^+, Halpern *et al.* derived the following kinetic expression for the rate of the reaction:

$$(5)\qquad \text{Rate} = \frac{-d[H_2]}{dt} = \frac{k_1[Cu^{++}]^2[H_2]}{[Cu^{++}] + k_{-1}/k_2[H^+]}\ .$$

Inverting the above expression gives the following equation, which is in suitable form for displaying

and interpreting experimental results:

$$(6)\quad \frac{1}{R} = \frac{1}{k_1[Cu^{++}]\,[H_2]}\left[1 + \frac{k_{-1}}{k_2}\,\frac{[H^+]}{[Cu^{++}]}\right].$$

At low acidity the rate should be proportional to the first power of the copper concentration, and at high acidity the rate should become proportional to the second power of the concentration of copper; this was observed by Halpern *et al.* At a constant copper concentration a plot of $1/R$ vs acidity should give a straight line with a slope proportional to the ratio k_{-1}/k_2. Halpern's data indicated that, at 110°C, the value of this ratio was 0.25. The ORNL studies of cupric perchlorate plus perchloric acid (up to an acid-to-copper ratio of 50) did not show any indication of an acid effect; that is, the k_{-1}/k_2 ratio was zero. Although there is no demonstrated inconsistency, since the temperatures were different, it appears desirable to conduct additional work so as to provide confirmation of the mechanism or the basis for an alternative explanation of the data. It is not unlikely that the explanation lies in the effect of temperature upon the three rate constants involved; this effect could easily be such as to suppress k_{-1} relative to k_2 as the temperature is raised. Experiments with the perchlorate system at intermediate temperatures are planned which will furnish the desired information.

20.2.2 Cupric Sulfate

It had already been reported[2] that the addition of up to 0.05 *M* sulfuric acid to solutions containing 0.001 *M* cupric sulfate reduced the catalytic activity of these solutions at 250°C as the acidity was increased. A plot of the experimental data covering the range of 0.005 to 0.050 *M* sulfuric acid in the form of $10^5/k_{Cu}$ vs the molar concentration of acid is presented in Fig. 20.4. (Sulfuric acid is treated as a monobasic acid because the second ionization constant becomes very small at the elevated temperatures.) The observed relationship between $1/R$ and acidity appears quite linear, and would be consistent with the type of explanation for the reaction mechanism advanced by Halpern. The ratio of k_{-1}/k_2 calculated from these results is 0.0258, indicating that although the effect of acid is quite noticeable in the sulfate system at 250°C the actual value of k_2 is far larger (38.75 times) than k_{-1}. Since considerable experience had been obtained with the sulfate system and since it had been possible to find an acidity effect at 250°C in this system but not in the perchlorate system, a series of experiments at intermediate temperatures was planned to determine the effects of acidity and copper concentration.

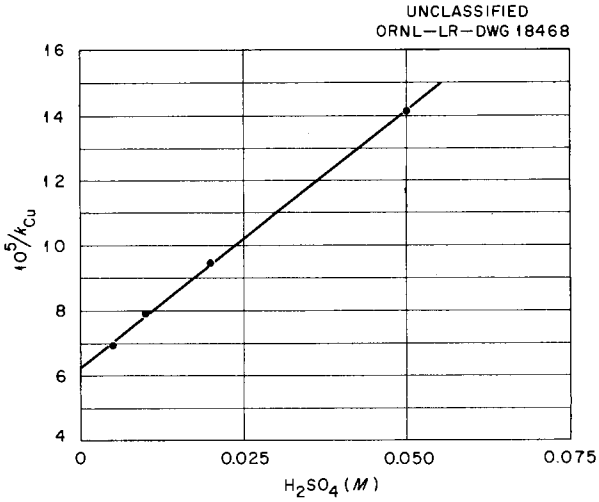

Fig. 20.4. Effect of Acidity upon the Catalytic Activity of 0.001 *M* Cupric Sulfate at 250°C.

The first tests in this series, at 200°C, were performed during the past quarter, and the relevant results are presented in Table 20.3. The techniques and nomenclature are the same as those previously reported[2] except that titanium bombs, fittings, and capillary tubes are being used to minimize the corrosive effects of high acid concentrations and the chloride released through slow thermal decomposition of perchlorate. It is obvious from consideration of the values of k_π (the experimentally observed first-order rate constant) at the same ratios of gas volume to liquid volume that the rate decreased as the acid concentration was increased. From plots of $1/k_\pi$ vs V_g/V_l, as shown by Figs. 20.5 through 20.8, linear relationships were obtained as required by the previous derivation of the effect of geometry.[2] The slopes of these lines are measures of α/RTk_{sol}, from which the values listed in Table 20.4 were obtained. The *ratios* of the solubility of hydrogen to the rate constant are known with much greater accuracy than either of the components separately, and it had

already been pointed out that rate constants should always be used together with the solubility values which were adopted in the kinetic calculations.

As a matter of practical interest to reactor engineers, the recombination equations will always contain the ratio of the solubility to the rate constant, and because of this the reactivity of the solution can always be related to the partial pressure of hydrogen in a useful way. For kinetic calculations, however, it is necessary to separate the influences of the environment on the solubility of hydrogen from those on the rate constants of the reaction. It can be assumed that the solubility of hydrogen is the same as that in water, as Halpern did, but it has recently been reported by Stephan *et al.*[9] that the presence of 1 *M* uranyl sulfate lowered the solubility of hydrogen at 275°F (near the temperatures of Halpern's experiments)

Table 20.3. Effect of Acidity on Hydrogen-Oxygen Reaction Rate

Temperature: 200°C
$CuSO_4$ concentration: 0.01 *M* [(a)]

Run No.	H_2SO_4 (*M*) [(a)]	V_g/V_l [(b)]	k_π (hr^{-1})	$1/k_\pi$ (hr)
C-12	0.025	0.324	1.17	0.855
26		0.61	0.637	1.63
16		1.02	0.403	2.48
31		1.34	0.296	3.38
5		1.60	0.257	3.88
21		3.31	0.138	7.25
1		3.42	0.141	7.1
C-17	0.050	0.453	0.518	1.93
3		0.48	0.578	1.73
8		1.16	0.204	4.9
19		1.17	0.221	4.52
24		2.41	0.117	8.56
13		3.52	0.072[(c)]	13.8
4		3.79	0.083	12.1
C-20	0.075	0.496	0.392	2.55
6, 14		0.665	0.272	3.68
22		1.23	0.158	6.33
11		1.17	0.176	5.68
7		2.53	0.0887	11.3
C- 9	0.100	0.363	0.443	2.26
23		0.692	0.233	4.3
25		1.25	0.143	7.0
2		1.31	0.177	5.66
18		2.66	0.0593	16.9
10		3.36	0.0502	19.9

(a) At room temperature.
(b) Corrected for change in density and loss of water to vapor phase at 200°C.
(c) Estimated.

[9] E. F. Stephan *et al.*, *The Solubility of Gases in Water and in Aqueous Uranyl Salt Solutions at Elevated Temperatures and Pressures*, BMI-1067 (Jan. 23, 1956).

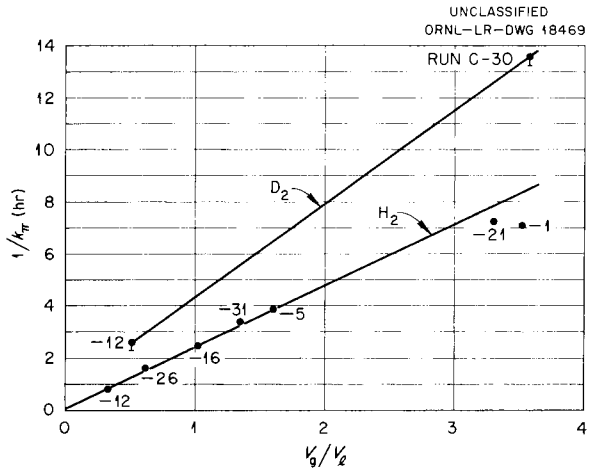

Fig. 20.5. Catalytic Activity of 0.01 *M* Cupric Sulfate in 0.025 *M* Sulfuric Acid at 200°C.

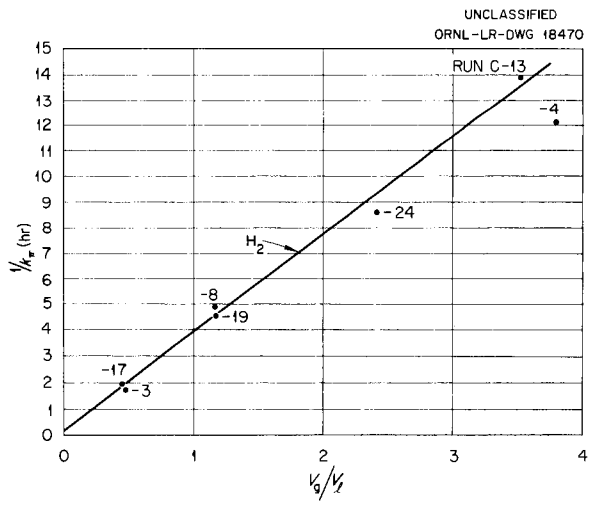

Fig. 20.6. Catalytic Activity of 0.01 *M* Cupric Sulfate in 0.050 *M* Sulfuric Acid at 200°C.

to about 45% of that in pure water. Information[10] concerning the solubility of hydrogen in water at 25°C indicates that sulfuric acid depresses the solubility slightly. Thus there is good reason to be cautious in accepting the proposition that all the effects are due to the rates and not to changes in solubility. If, however, for purposes of comparison with Halpern's treatment, the hydrogen solubility at 200°C is considered to be unchanged by the presence of 0.01 *M* cupric sulfate and up to 0.100 *M* sulfuric acid, the effect of the acid on the relative rates of the reaction can be presented as shown in Fig. 20.9. From the slope of the line it may be inferred that the ratio of k_{-1} to k_2 under these conditions was 0.33. The change from the ratio observed at 250°C is in the direction required for an explanation of the difference in acid effect observed in the perchlorate system at 250°C from that observed at 110°C. The additional experiments planned for lower temperatures and higher copper concentrations will provide additional information concerning this point.

[10] A. Seidell, *Solubilities of Inorganic and Metal Organic Compounds*, 3d ed., vol I, p 553–560, Van Nostrand, New York, 1940.

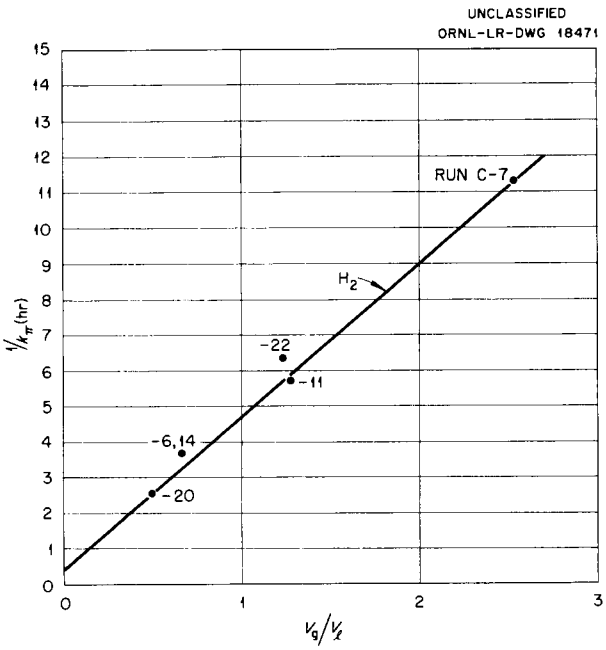

Fig. 20.7. Catalytic Activity of 0.01 *M* Cupric Sulfate in 0.075 *M* Sulfuric Acid at 200°C.

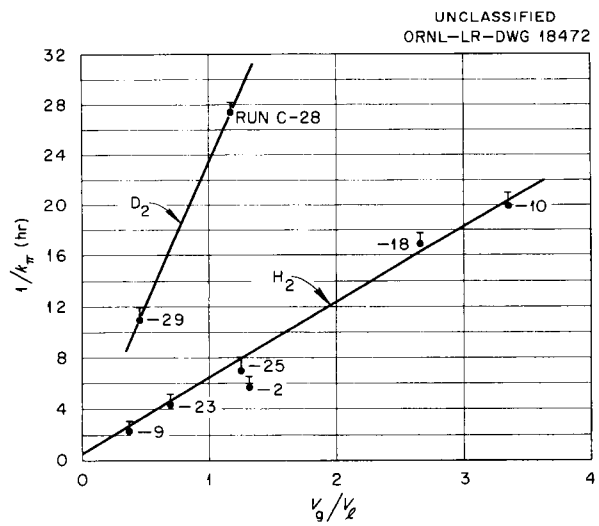

Fig. 20.8. Catalytic Activity of 0.01 *M* Cupric Sulfate in 0.100 *M* Sulfuric Acid at 200°C.

Table 20.4. Effect of Acidity on Catalytic Activity of Cupric Sulfate

Temperature: 200°C

$CuSO_4$ concentration: 0.01 *M**

Sulfuric Acid Concentration (*M*)*	α/k_{sol} (psi·hr·M^{-1})
0.025	1346
0.050	2168
0.075	2453
0.100	3372

*At room temperature.

20.2.3 The Deuterium-Oxygen Reaction

Homogeneous recombination in heavy-water reactor systems requires that deuterium, instead of hydrogen, react with the catalyst. It was previously reported[2] that under particular conditions at 250°C the combination of solubility and reaction-rate effects made deuterium only 60% as reactive as hydrogen for the same partial pressure of gas. During the past quarter, additional experiments with deuterium gas were conducted at 200°C and with the use of the solutions indicated in Table 20.3. Results of the tests with deuterium are presented in Table 20.5. These results indicate that with the solubility and rate effects combined,

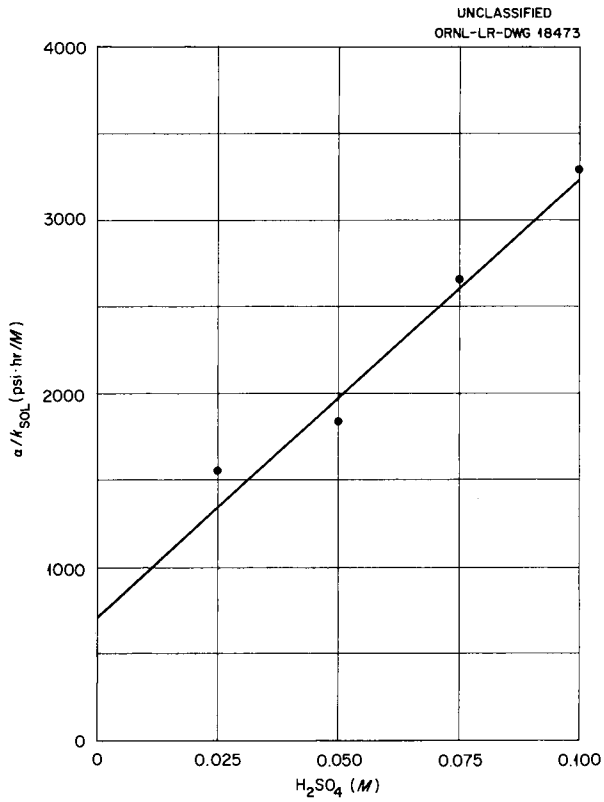

Fig. 20.9. Effect of Acidity upon the Catalytic Activity of 0.01 *M* Cupric Sulfate at 200°C.

the deuterium is only 30% as reactive as hydrogen in the presence of 0.100 *M* sulfuric acid but 66% as reactive in the presence of 0.025 *M* sulfuric acid. It remains to be determined whether the effect is due to the acid or to the change in isotope.

P. H. Emmett[11] has called attention to one implication of the equilibrium postulated as Eq. 2 of Halpern's mechanism. If deuterium gas is used in the presence of a light-water solution, any deuterium ions formed in the equilibrium exchange very rapidly with the hydrogen in the water; the subsequent reaction of hydrogen ions with the CuD^+ intermediate to regenerate the starting materials would furnish HD instead of D_2 and would ultimately convert the deuterium into hydrogen. Emmett pointed out that it should be possible

[11]ORNL Chemistry Division consultant.

Table 20.5. Effects of Acidity on Deuterium-Oxygen Reaction Rate

Temperature: 200°C
$CuSO_4$ concentration: 0.01 *M**

Run No.	H_2SO_4 (*M*)*	V_g/V_l **	k_π (hr^{-1})	$1/k_\pi$ (hr)
C-32	0.025	0.518	0.38	2.63
30	0.025	3.58	0.074	13.5
C-29	0.100	0.45	0.0918	10.9
28	0.100	1.17	0.0365	27.4
27	0.100	3.4	0.0151	66.1

*At room temperature.

**Corrected for change in density and loss of water to vapor phase at 200°C.

to detect the isotopic exchange by sampling the gas phase during the course of the reaction. Although such experiments have not yet been performed, other experiments had been performed with the use of deuterium gas and light-water solutions at 250°C, as indicated previously, and detailed rate data were available for the course of these reactions. If deuterium reacts more slowly than hydrogen and if the equilibrium with acid is such as to permit the k_{-1} reaction to compete with the k_2 reaction, then the conversion of a substantial amount of deuterium into hydrogen during the course of the reaction should lead to an accompanying increase in the experimentally measured rate constant. Examination of our plots of dP/dt vs P did not reveal the curvature which would have been expected. This finding is in agreement with the lack of acid effect in the perchlorate system and the relative unimportance of k_{-1} as compared with k_2 in the sulfate system at 250°C. If conditions can be established under which the acidity effect is so great as to represent a substantial competition with the forward reaction, the expected curvature in the rate plots will again be sought with experiments making use of deuterium gas and a light-water system.

21. RADIATION CHEMISTRY

J. W. Boyle H. A. Mahlman

21.1 FUNDAMENTAL PROCESSES IN THE RADIATION CHEMISTRY OF HEAVY WATER

Since the use of heavy water is becoming more prevalent, consideration of the fundamental processes of radiation-induced decomposition appears to be warranted. Therefore experiments were performed to ascertain the radical and molecular product yields in heavy water.

The heavy water was purified by distillation from an acid permanganate solution, from a basic permanganate solution, and finally from water in an all-silica system. The purified heavy water contained 0.26 wt % light water. The hydrogen of the final solutions (described below) was 98.8 mole % D.

The deuterium gas yield (G_{D_2}) from a 0.4 *M* H_2SO_4 heavy-water solution containing 10^{-4} *M* KBr exposed to Co^{60} radiation was determined to be 0.39 ± 0.01 molecule per 100 ev of absorbed energy. The ferric yield, $G_{Fe^{+++}(D_2O)}$, from an air-saturated 0.4 *M* H_2SO_4 heavy-water solution containing 0.001 *M* Fe^{++} and 0.001 *M* NaCl was determined to be 17.44 ± 0.08 molecules per 100 ev of absorbed energy.

The G_{D_2} from a 0.4 *M* H_2SO_4 heavy-water solution is identical with the G_{H_2} from its light-water counterpart,[1] namely, 0.39.[2] The $G_{Fe^{+++}(D_2O)}$ observed from a 0.4 *M* H_2SO_4 heavy-water solution of ferrous ions, however, is somewhat higher than the $G_{Fe^{+++}}$ = 15.6 determined[2] in a comparable light-water solution. The observed ferric yield is in good agreement with McDonell's[3] value [$G_{Fe^{+++}(D_2O)}$ = 17.5] but in disagreement with the value $G_{Fe^{+++}(D_2O)}$ = 18.6 reported by Trumbore and Aten.[4] The increased ferric yield may arise by alteration of reaction *E* or *R* of the usual scheme:[5]

$$(F) \qquad 2D_2O \rightsquigarrow D_2 + D_2O_2$$

$$(E) \qquad 2D_2O \rightsquigarrow D + D + D_2O_2$$

$$(R) \qquad D_2O \rightsquigarrow D + OD$$

It is anticipated that additional experiments will enable yields for the remaining molecular and radical products to be determined.

21.2 FIXATION OF NITROGEN BY RADIATION

Mixtures of nitrogen and oxygen and also of nitrogen and hydrogen were introduced at several hundred pounds' pressure into a platinum-lined autoclave and irradiated for one week in the ORNL Graphite Reactor at 150 to 175°C and a thermal-neutron flux of 3–4 × 10^{11} neutrons·cm^{-2}·sec^{-1}. In neither system was any decrease in pressure detected which could be ascribed to nitrogen fixation. The sensitivity of the equipment was such that a pressure change of a few pounds per week could be detected.

The autoclave (7.9-ml volume) which was used for these studies was originally ~70% filled with a solution 0.1 *m* in $Th(NO_3)_4$, UO_2SO_4 (U^{235}), and $Be(NO_3)_2$. The final volume of solution after seven weeks in the reactor was about 2 ml, a loss of 3 to 4 ml. This loss apparently occurred near the beginning of the run. Loss of thermal-decomposition products of the nitrate ion may have occurred, which would have caused hydrolytic precipitation of some or all of the cations. The autoclave was charged with nitrogen and oxygen during the sixth week and with nitrogen and hydrogen during the seventh week.

Nitrogen and oxygen are reported to react in the gas phase with an *M/N* = 1 for alpha irradiation[6] and $G_{NO_3^-}$ = 1.1 for reactor gamma rays and neutrons.[7] Nitrogen and hydrogen also react in the gas phase,[7] with a reported *M/N* = 0.2 for alpha particles.[6] Because of the small amount of energy absorbed in the gas phase from gamma rays and neutrons in the ORNL Graphite Reactor, gaseous fixation in our autoclave would amount to a pressure decrease of only a few pounds per square inch

[1] T. J. Sworski, *J. Am. Chem. Soc.* **76**, 4687 (1954).

[2] C. J. Hochanadel and J. A. Ghormley, *J. Chem. Phys.* **21**, 880 (1953).

[3] W. R. McDonell, *Radiation Chemistry of Normal and Heavy Water Solutions. I. Radiation Induced Oxidation of Ferrous Sulfate*, ANL-5206 (Jan. 12, 1954).

[4] C. N. Trumbore and A. H. W. Aten, Jr., *J. Am. Chem. Soc.* **78**, 4179 (1956).

[5] A. O. Allen, *Radiation Research* **1**, 85 (1954).

[6] S. C. Lind, *The Chemical Effects of Alpha Particles and Electrons*, p 100, Chemical Catalog Company, New York, 1928.

[7] J. Wright *et al.*, *Proceedings of the International Conference on the Peaceful Uses of Atomic Energy*, vol 7, p 560, United Nations, New York, 1956.

per week, the limit of detectability. Our results therefore do not disagree with the reported yields.

The fact that the summation of gaseous, heterogeneous, and liquid-phase fixation of nitrogen was below the detectability limit means that each mode of fixation alone was below the limit. From these limits of detection a maximum yield of liquid-phase fixation can be estimated to be <0.001 molecule of nitrogen fixed per 100 ev of energy absorbed in the liquid phase.

Part VII

ANALYTICAL CHEMISTRY

M. T. Kelley

22. ANALYTICAL CHEMISTRY

O. Menis

R. G. Ball
L. C. Bate
C. M. Boyd
G. Goldstein
H. P. House
G. W. Leddicotte
D. L. Manning
R. H. Powell
T. C. Rains
I. B. Rubin

R. M. Rush

22.1 ANALYSIS OF THORIUM OXIDE

Work was initiated on the development of a fluorometric method for the determination of aluminum in microgram quantities (<50 ppm) in thorium oxide. The fluorescent intensity of the aluminum–8-hydroxyquinoline complex which was selected for study was found experimentally to be directly proportional to the concentration of aluminum over the range of 0.5 to 10 μg in the 50 ml of solution which is used for the intensity measurement. The complex was formed in a 6 *M* acetate medium and then extracted into chloroform, following which the intensity of the fluorescence was measured. No interference was caused by the presence of as much as 1 g of thorium in the 6 *M* acetate solution from which the aluminum-oxine complex was extracted. Although interference from thorium is eliminated, this technique does not suffice to eliminate interference from iron and titanium. An attempt will be made to utilize 8-hydroxyquinaldine for the removal of iron and titanium, since Hynek and Wrangell[1] report that this reagent reacts with many elements, including iron and titanium, but not with aluminum.

A sensitive, spectrophotometric method has been developed for the determination of molybdenum in thorium oxide which contains uranium. Molybdenum is separated from thorium by extracting the former from a strongly acidic solution into a chloroform solution of α-benzoinoxime. The chromogenic reagent, quercetin (3,3′,4′,5,7-pentahydroxyflavone), is then added to the organic extract, after which the yellow color of the molybdenum-quercetin complex is measured at a wavelength of 420 mμ. Uranium can be determined in the raffinate without interference from molybdenum.

The method for the determination of titanium as the 8-quinolinol–hydrogen peroxide complex was applied to the analysis of slurries of thorium oxide.[2] It was found that a decrease in the absorbency index of the complex occurs when the initial test solution contains thorium; therefore, a study was initiated to determine a reason for this decrease. This study is as yet incomplete; however, indications are that a constant, but statistically insignificant, quantity of titanium is retained in the raffinate when thorium is present, while microgram quantities of thorium remain in the final organic solution. On the addition of hydrogen peroxide, the absorbency of the thorium–8-quinolinol complex is lessened, while that of the titanium complex is increased according to the amount of this element that is present. Since the estimation of titanium is based on the increase of absorbency as determined by a measurement of the combined absorbency of both the thorium and titanium complexes, before and after the addition of hydrogen peroxide, any decrease in the absorbency of the thorium–8-quinolinol complex would account for the apparent loss of titanium.

A study was made of the applicability of a colorimetric method for hydrazine, based on the use of *p*-diethylaminobenzaldehyde,[3] for the determination of microgram quantities of hydrazine in slurries of thorium oxide. As little as 0.2 ppm of hydrazine can thus be determined in the liquid phase. Determination of hydrazine in the whole slurry is difficult, because of either decomposition or adsorption of the hydrazine on the thorium oxide. Studies with spectrographically pure thorium oxide indicate that 25 to 30% of the hydrazine is lost over a period of 4 hr, after equilibration at room temperature.

A flame photometric method has been developed for the determination of microgram quantities of lanthanum. Calibration curves (radiant energy vs

[1] R. J. Hynek and L. J. Wrangell, *Anal. Chem.* **28**, 1520 (1956).

[2] I. B. Rubin and H. P. House, *Anal. Chem. Semiann. Prog. Rep. April 20, 1956*, ORNL-2070, p 38 (Classified).

[3] G. W. Watt and J. D. Chrisp, *Anal. Chem.* **24**, 2006 (1952).

concentration) were established for use in the determination of lanthanum in the concentration range of 4 to 20 μg/ml in nonaqueous media at three wavelengths corresponding to emission maximums for lanthanum, namely 442, 560, and 743 mμ. At a wavelength of 560 mμ, interference due to flame background is negligible, while the sensitivity is greater than at the two other wavelengths tested; therefore, this wavelength was selected for use in the flame photometric determination of lanthanum. The application of this flame spectrophotometric method to the determination of lanthanum in thorium oxide is now being studied.

A conductometric titration procedure, based on the work of Dawson and O'Connor,[4] was utilized to determine the acid- and base-exchange capacity of thorium oxide in order to correlate this property with the zeta potential and particle-size distribution. It was established that a carefully standardized procedure must be followed if the comparison of the results for different sample types is to have any significance.

22.2 DETERMINATION OF SUBMICRON PARTICLE SIZES BY AN ACTIVATION ANALYSIS–CENTRIFUGATION METHOD

The feasibility of determining submicron particle sizes in thorium oxide samples originating from the breeder blanket experiments has been demonstrated.[5] By this method, particle sizes can routinely be determined in the range of 0.07 micron, and the method could be used to determine particles as small as 0.05 micron. Basically, this method is used to analyze the supernatant slurry obtained after the activation analysis–sedimentation method[6] is completed at 0.70 micron. Measured portions of this slurry are centrifuged at various speeds and for different time intervals. Successive aliquots are removed from each sample at the completion of each of these operations. The particle-size distribution in each sample is calculated as a function of the centrifuge speed, time of centrifugation, and concentration of thorium oxide in the aliquots removed. The thorium concentration is determined by a radioactivity measurement in which the radioactivity in the aliquot analyzed is related to the total radioactivity of the sample. The radioactivity measured is Pa^{233}, 27.4-day, the product of the neutron reaction

$$Th^{232}(n,\gamma)Th^{233} \xrightarrow[23.5\ \text{min}]{\beta^-} Pa^{233} .$$

Measurements of the Pa^{233} radioactivity are made in a gamma counter.

The method is also adaptable to the particle-size analysis of sample materials, other than thorium oxide, in the submicron range.

22.3 DETERMINATION OF URANIUM BY MEANS OF A CONSTANT-POTENTIAL INTEGRATING COULOMETER

The constant-potential coulometer constructed by the Analytical Instrumentation Group has been applied to the determination of uranium in HRT fuel. The instrument itself has been calibrated and an electrolysis cell constructed which permits the determination of 5 mg of uranium in about 15 min. In a few preliminary experiments with pure uranyl sulfate solutions, the method appears to be capable of a precision better than 1%, although the use of empirical calibrations with known uranium solutions will probably be necessary at the 5-mg level. It also appears likely that both uranium and copper can be determined in a single sample.

[4] J. K. Dawson and D. J. O'Connor, *Chemical Aspects of the Homogeneous Aqueous Reactor Blanket*, AERE-C/M-255 (Sept. 1955) (Classified).

[5] L. C. Bate and G. W. Leddicotte, *Determination of Submicron Particle Sizes by an Activation Analysis – Centrifugation Method*, ORNL CF-57-1-116 (Jan. 29, 1957).

[6] G. W. Leddicotte and H. H. Miller, *Anal. Chem. Semiann. Prog. Rep. Oct. 20, 1954*, ORNL-1788, p 21 (Classified).

[redacted]

OAK RIDGE NATIONAL LABORATORY
HOMOGENEOUS REACTOR PROJECT

FEBRUARY 1, 1957

PROJECT DIRECTOR
R. B. BRIGGS — D

ASSOCIATE PROJECT DIRECTOR
C. E. WINTERS** — D
A. L. GUNNELS, SEC. — D

PROJECT EDITOR
W. D. REEL — I&R

DESIGN AND ENGINEERING
J. A. LANE, DIRECTOR
R. N. LYON, ASSISTANT DIRECTOR
REACTOR EXPERIMENTAL ENGINEERING DIVISION
T. S. CARLSMITH, SEC. — REE

DESIGN
W. R. GALL, SECTION CHIEF — REE
M. I. LUNDIN,* ASSISTANT SECTION CHIEF — REE

MECHANICAL DESIGN
F. C. ZAPP, GROUP LEADER — REE
F. C. BOWEN* — VITRO
C. A. BURCHSTED — REE
C. J. CLAFFEY — REE
C. W. COLLINS — REE
E. GUGLIELMO* — VITRO
R. C. MOREN — WESTINGHOUSE
R. G. PITKIN* — VITRO
R. E. SCHAPPEL — REE
D. O. TARR* — VITRO

LONG RANGE STUDIES
M. I. LUNDIN,* ACTING GROUP LEADER — REE
E. GIFT — REE
R. O. MAAK — FOSTER WHEELER

PLANT LAYOUT AND DRAFTING
C. L. SEGASER, GROUP LEADER — REE
F. C. BOWEN* — VITRO
E. GUGLIELMO* — VITRO
R. G. PITKIN* — VITRO
D. O. TARR* — VITRO
W. TERRY* — REE
R. W. BORGERS — REE
H. H. BRADFORD — REE
R. L. CAUBLE — REE
C. W. DAY — REE
J. P. DILORENZO — REE
R. L. HALE — REE
A. S. LUDLOW — REE
C. A. ROBERTS — REE
R. D. SATTERFIELD — REE
R. H. SIGLER — REE
W. T. STERLING — REE

PROCESS DESIGN
R. C. ROBERTSON, GROUP LEADER — REE
J. C. BOLGER — REE
H. A. MCLAIN — REE

STRESS ANALYSIS
R. D. CHEVERTON, GROUP LEADER — REE
J. N. ROBINSON — REE

ENGINEERING DEVELOPMENT
I. SPIEWAK, SECTION CHIEF — REE

HEAT EXCHANGERS, TITANIUM PROGRAM, MISCELLANEOUS EQUIPMENT
J. S. CULVER, GROUP LEADER — REE
B. D. DRAPER — TVA
P. P. HOLZ* — REE
I. K. NAMBA — REE

PUMPS
C. H. GARBARD, GROUP LEADER — REE
J. W. BAKER — REE
R. BLUMBERG — REE
E. C. HISE — REE
J. C. MOYERS — REE
J. P. HURST — REE
C. C. HURTT — REE
R. J. LOCKETT — REE

HRT MOCKUP, RECOMBINERS
P. H. HARLEY, GROUP LEADER — REE
B. A. HANNAFORD — REE
H. C. ROLLER — REE
D. E. WILLIS — REE
T. L. CASTILE — REE
A. B. DAFFRON — REE
R. GOODMAN — REE
W. M. PARKS — REE

SPECIAL ASSIGNMENT
P. P. HOLZ* — REE
T. M. CATE — REE
W. B. KRICK — REE
L. E. PENTON — REE
S. R. WEST — REE
T. R. WILSON — REE

INSTRUMENTATION AND CONTROLS
D. S. TOOMB, SECTION CHIEF — I&C

HRT AND INSTRUMENT DEVELOPMENT
R. L. MOORE, GROUP LEADER — I&C
J. C. GUNDLACH** — I&C
R. M. PIERCE — TVA
H. O. WILLS — REE
P. E. SMITH — I&C

HRP SUPPORTING FACILITIES
D. G. DAVIS, GROUP LEADER — I&C
G. W. GREENE — I&C
J. D. GRIMES — TVA
P. G. HERNDON — I&C
J. L. HORTON** — I&C
J. A. RUSSELL — I&C
R. M. BURNETT — I&C

VALVES AND ACTUATORS
A. M. BILLINGS, GROUP LEADER — I&C
E. H. BELL — I&C
P. F. HURAY — I&C
A. J. SHARONBERGER — I&C

ENGINEERING RESEARCH
R. B. KORSMEYER, SECTION CHIEF — REE

COMPONENT DEVELOPMENT
A. S. KITZES, GROUP LEADER — REE
R. B. GALLAHER — REE
M. RICHARDSON — REE
C. F. VANDEN BULCK — UCNC
R. P. WICHNER — REE

SLURRY SYSTEM DEVELOPMENT
L. F. PARSLEY, GROUP LEADER — REE
H. L. FALKENBERRY — TVA
I. M. MILLER — REE

SLURRY PROPERTIES
O. G. THOMAS, GROUP LEADER — REE
C. S. MORGAN — REE
R. H. NIMMO — REE

TECHNICIAN POOL
A. N. SMITH — REE
T. L. BOSWELL — REE
R. E. CARNES — REE
J. T. DICKIE — REE
C. M. FITZPATRICK — REE
C. A. GIFFORD — REE
P. H. HAYES — REE
C. A. MCLAUGHLIN — REE
H. G. MOORE — REE
R. E. POTTER — REE
R. M. SUMMERS — REE
B. J. SUTTON — REE
D. H. WALLACE — REE

REACTOR ANALYSIS
P. R. KASTEN, SECTION CHIEF — REE

REACTOR PHYSICS
T. B. FOWLER — REE
C. W. NESTOR, JR. — REE
M. W. ROSENTHAL — REE
M. TOBIAS — REE

LONG RANGE STUDIES
H. C. CLAIBORNE — REE
S. JAYE — REE
M. P. LIETZKE — REE

REACTOR MATERIALS RESEARCH
E. G. BOHLMANN, ASSISTANT DIRECTOR
REACTOR EXPERIMENTAL ENGINEERING DIVISION
T. F. KELLY, SEC. — REE
D. P. MALENFANT, STENO. — REE
R. E. WACKER, RECORDS — REE

SOLUTIONS
J. C. GRIESS, ASSISTANT SECTION CHIEF — REE
P. D. NEUMANN, SPECIAL ASSIGNMENT — REE

LOOPS
R. S. GREELEY — REE
S. R. BUXTON — REE
J. E. EVE — REE
W. H. HINDS — REE

LABORATORY STUDIES
J. L. ENGLISH, GROUP LEADER — REE
D. N. HESS — REE
E. F. HOUSE — REE
L. L. FAIRCHILD, LEADER — REE
H. L. BARKER — REE
P. B. DAVIS — REE
H. R. TINCH — REE
J. L. UNDERWOOD — REE

SLURRIES
E. L. COMPERE, ASSISTANT SECTION CHIEF — REE

LOOPS
S. A. REED — REE

TOROIDS
G. E. MOORE — C
R. F. BENSON — REE
F. E. MCDANIEL — REE

HRT LIAISON
D. M. RICHARDSON* — C

ENGINEERING
H. C. SAVAGE, ASSISTANT SECTION CHIEF — REE

SOLUTIONS
W. C. ULRICH — REE
J. F. WINESETTE, LEADER — REE
L. L. ALLEN — REE
C. R. BENSON — REE
C. M. BURCHELL — REE
C. L. FRANCIS — REE
J. B. FRENCH — REE
D. G. GATES — REE
J. W. GOOCH — REE
J. E. JACKSON — REE
G. A. MOORE — REE
L. G. PHELPS — REE
A. E. PUGH — REE
R. W. RAY — REE
T. R. RAYBURN — REE
W. H. WAGNER — REE

SLURRIES
R. M. WARNER — REE
B. W. SCOTT — REE

RADIATION
S. E. BOLT — REE
V. A. DECARLO — REE
T. H. MAUNEY — REE
J. D. BARNES — REE
C. H. BURBAGE — REE
J. R. HART — REE
H. F. HENDERSON — REE
B. H. PARKS — REE

RADIATION
G. H. JENKS, SECTION CHIEF — REE
D. T. JONES, ENGRG. COORDINATOR — REE
V. R. BULLINGTON — REE

IN-PILE LOOPS
J. R. MCWHERTER, GROUP LEADER — REE
J. E. BAKER — REE
J. W. BROWN — REE
R. A. LORENZ — REE
F. J. WALTER* — REE
S. H. WHEELER — REE
W. E. TEICHERT, A SHIFT LEADER — REE
K. G. CHANDLER — REE
R. M. WALLER — REE
E. H. GUNN, B SHIFT LEADER — REE
J. P. GORDON — REE
D. M. SMITH — REE
A. L. SUTTON, C SHIFT LEADER — REE
R. A. JONES — REE
C. E. ROBERTS — REE
J. W. MYERS, D SHIFT LEADER — REE
J. W. MOSIER — REE
R. G. ROSS — REE

IN-PILE BOMBS
R. J. DAVIS, GROUP LEADER — C
F. J. WALTER* — REE
K. S. WARREN — C
L. F. WOO — C
J. L. RUTHERFORD — REE
R. L. PLENONS — REE

SUPPORTING RESEARCH
A. L. BACARELLA — C
M. D. SILVERMAN — C
W. C. YEE — C

REMOTE EVALUATION
A. R. OLSEN — REE
B. W. MCCOLLUM, SHIFT LEADER — REE
W. J. SCHILL — REE
W. H. SMITH, JR. — REE
J. C. THOMPSON — REE

METALLURGY
G. M. ADAMSON, SECTION CHIEF — M

J. P. HAMMOND — M
W. J. LEONARD — M
M. L. PICKLESIMER — M
J. J. PRISLINGER — M
P. L. RITTENHOUSE — M
R. L. STEPHENSON — M
J. K. WHITE — M
P. J. JONES — M
G. C. NELSON — M
C. M. SMITH — M
M. A. WHEELER — M
J. J. WOODHOUSE — M

METALLOGRAPHY
R. S. CROUSE** — M
T. M. KEGLEY, JR. — M
E. R. BOYD — M
B. F. DAY** — M
L. G. SHRADER** — M

RADIATION DAMAGE
R. G. BERGGREN — SS
A. E. RICHT — SS
D. O. THOMPSON — SS
J. C. WILSON** — SS
F. M. GRIZZELL — SS

CHEMICAL TECHNOLOGY
F. R. BRUCE,** ASSOCIATE DIRECTOR
CHEMICAL TECHNOLOGY DIVISION
J. HOPPE, SEC. — CT

CHEMICAL DEVELOPMENT
D. E. FERGUSON, SECTION CHIEF — CT

BLANKET PROCESSING
R. E. LEUZE, PROBLEM LEADER — CT
R. D. BAYBARZ — CT
J. M. CHILTON — CT
S. S. KIRSLIS — CT
J. M. DELOZIER — CT
R. L. HICKEY — CT
O. K. TALLENT — CT

CORE PROCESSING
R. A. MCNEES, PROBLEM LEADER — CT
M. H. LLOYD — CT
S. PETERSON — CT
W. B. HOWERTON — CT

THORIUM BLANKET STUDIES
J. P. MCBRIDE, PROBLEM LEADER — CT
E. V. JONES — C
N. A. KROHN — CT
L. E. MORSE — CT
R. L. PEARSON — CT
C. E. SCHILLING — CT
W. M. WOODS — CT
C. W. GREENE — CT
P. E. NOVAK — CO-OP
W. L. PATTISON — CT
H. F. SOARD — CT

DESIGN
W. E. UNGER, ASSISTANT SECTION CHIEF — CT

PROCESS DESIGN
H. O. WEEREN — CT
B. F. BOTTENFIELD — CT

PROJECT DESIGN
A. M. ROM, PROBLEM LEADER — CT
G. B. BERRY — E&M
F. C. MCCULLOUGH — CT
E. B. BRIDGES — CATALYTIC CONSTRUCTION CO.
J. D. CUPP — CATALYTIC CONSTRUCTION CO.
H. W. FALLON — CATALYTIC CONSTRUCTION CO.
P. P. FEBBO — CATALYTIC CONSTRUCTION CO.
J. H. MANNEY — E&M
F. L. PEISHEL — E&M
J. PHILLIPS — CATALYTIC CONSTRUCTION CO.
K. F. STOOKSBURY — E&M
J. N. WHEELER — E&M

LOOP DESIGN
T. A. AREHART — CT
W. J. CLOSSEY — CATALYTIC CONSTRUCTION CO.
W. F. SCHAFFER — CT

INSTRUMENTATION
L. H. CHASE — I&C
C. S. LISSER — I&C

UNIT OPERATIONS
E. O. NURMI, GROUP LEADER — CT

BLANKET PROCESSING
P. A. HAAS — CT
S. D. CLINTON — CT
R. D. ARTHUR — CT
J. BEAMS — CT
R. C. EARLY — CT

SLURRY PREPARATION
C. C. HAWS — CT
V. L. FOWLER — CT

CORE PROCESSING
R. W. HORTON — CT
F. N. MCLAIN — CT
D. A. MCWHIRTER — CT
G. E. WOODALL — CT

PILOT PLANT
R. B. LINDAUER, SECTION CHIEF — CT

SLURRY PREPARATION
E. M. SHANK, PROBLEM LEADER — CT
J. R. PARROTT — CT

CHEMICAL RESEARCH
E. H. TAYLOR,** DIRECTOR
CHEMISTRY DIVISION
E. SCHAPPEL, SEC. — C

FUEL SOLUTION CHEMISTRY
C. H. SECOY, GROUP LEADER — C
F. E. CLARK — C
J. S. GILL — C
G. M. HEBERT — C
H. F. MCDUFFIE — C
D. W. SHERWOOD — C
R. SLUSHER — C
H. H. STONE — C
F. H. SWEETON — C

RADIATION CHEMISTRY
C. J. HOCHANADEL,** GROUP LEADER — C
J. W. BOYLE** — C
H. A. MAHLMAN** — C

HEAVY ELEMENT CHEMISTRY
R. W. STOUGHTON,** GROUP LEADER — C
J. HALPERIN** — C
M. H. LIETZKE** — C
W. C. WAGGENER** — C

INORGANIC SOLUTION CHEMISTRY
K. A. KRAUS,** GROUP LEADER — C
T. A. CARLSON** — C
H. O. PHILLIPS** — C

ANALYTICAL CHEMISTRY
MYRON T. KELLEY,** DIRECTOR
C. D. SUSANO,** ASSOCIATE DIRECTOR
K. ODOM, SEC. — AC

CORROSION ANALYTICAL LABORATORY
O. MENIS,* SUPERVISOR — AC
H. P. HOUSE, ASSISTANT SUPERVISOR — AC

RESEARCH
O. MENIS,* GROUP LEADER — AC
R. G. BALL — AC
C. M. BOYD — AC
G. GOLDSTEIN — AC
D. L. MANNING — AC
R. H. POWELL — AC
I. B. RUBIN — AC

SERVICES
C. K. TALBOTT, GROUP LEADER — AC
N. M. FERGUSON — AC
F. L. LAYTON — AC
T. C. RAINS — AC
T. P. BACON — AC
W. D. CLAPP, JR. — AC
C. A. CLARK — AC
C. G. FUSON — AC
P. S. GOODWIN — AC
T. G. MILLER — AC
V. S. NORMAN — AC
E. ONKST — AC

HRT AND IN-PILE LOOP ANALYSES
U. KOSKELA, SUPERVISOR — AC
L. G. FARRAR, ASSISTANT SUPERVISOR — AC
J. E. ATTRILL — AC
C. P. BAKER — AC
R. E. CORCORAN — AC
S. R. DINSMORE — AC
J. L. MOTTERN — AC
G. M. CAMPBELL — AC
G. I. GAULT — AC
B. D. HICKS — AC
M. H. MCCORQUODALE — AC
J. SLESSINGER, JR. — AC
W. R. WARREN — AC
H. L. WEBB — AC
H. L. WHITTINGTON — AC

HRT DEVELOPMENT
P. F. THOMASON, GROUP LEADER — AC
R. E. BIGGERS — AC
F. J. MILLER — AC
S. A. REYNOLDS, GROUP LEADER — AC
T. H. HANDLEY — AC

HIGH RADIATION LABORATORY
C. L. BURROS — AC

HOMOGENEOUS REACTOR TEST
S. E. BEALL, PROJECT ENGINEER — REE
B. EUBANK, SEC. — REE

OPERATIONS PLANNING
S. I. KAPLAN — REE

SPECIAL ASSIGNMENT
H. M. MCLEOD — CT

OPERATIONS
J. W. HILL, JR., CHIEF — REE
R. SMITH, JR. — REE

J. R. ENGEL, SUPERVISOR — CT
J. R. BUCHANAN — CT
H. K. SEARCH — PA. POWER AND LIGHT CO.
D. T. GODWIN — REE
A. L. JOHNSON — REE
C. E. WADDELL — CT

J. D. FLYNN, SUPERVISOR — REE
H. F. BAUMAN — CT
N. W. CURTIS — PA. POWER AND LIGHT CO.
W. T. BOSTIC — CT
E. W. BROWN — CT
T. G. HILL — REE

J. O. KOLB, SUPERVISOR — REE
H. A. BROWN — TVA
O. P. FRECH — REE
H. D. CURTIS — REE
R. J. SHANNON — CT
J. E. WOLFE — REE

G. W. RIVENBARK, SUPERVISOR — REE
T. H. GLADNEY — TVA
R. H. GUYMON — CT
R. J. HUNTER — REE
L. J. SHERSKY — CT
J. L. STEPP — REE

CHEMICAL PLANT COORDINATION
W. D. BURCH, PROBLEM LEADER — CT
W. L. ALBRECHT — TVA
N. C. BRADLEY — CT
R. H. WINGET — CT
W. A. SHANNON — CT

REACTOR COORDINATION
R. VAN WINKLE, GROUP LEADER — REE
R. R. WIETHAUP — CT
J. A. WATTS — REE

REACTOR ANALYSIS
P. N. HAUBENREICH, GROUP LEADER — REE

MAINTENANCE
W. TERRY,* SUPERVISOR — REE
R. W. JURGENSEN — AM. GAS AND ELEC. CO.
T. E. HAYNES — REE
G. H. JOHNSTONE — REE

REACTOR MATERIALS AND CHEMISTRY
D. M. RICHARDSON,* GROUP LEADER — C
J. D. JONES — REE

AC	ANALYTICAL CHEMISTRY DIVISION
C	CHEMISTRY DIVISION
CO-OP	STUDENT, NORTHWESTERN UNIVERSITY
CT	CHEMICAL TECHNOLOGY DIVISION
D	DIRECTOR'S DIVISION
E&M	ENGINEERING AND MECHANICAL DIVISION
I&C	INSTRUMENTATION AND CONTROLS DIVISION
I&R	INFORMATION AND REPORTS DIVISION
M	METALLURGY DIVISION
REE	REACTOR EXPERIMENTAL ENGINEERING DIVISION
SS	SOLID STATE DIVISION
TVA	TENNESSEE VALLEY AUTHORITY
UCNC	UNION CARBIDE NUCLEAR COMPANY, NEW YORK
*	DUAL CAPACITY
**	PART TIME

PERSONNEL SUMMARY

	FULL TIME	PART TIME	INDUSTRIAL PARTICIPANTS
ADMINISTRATION	6	5	
ANALYTICAL CHEMISTRY	41		
DESIGN AND ENGINEERING	97	2	7
CHEMICAL RESEARCH	9	10	
CHEMICAL TECHNOLOGY	57		
HOMOGENEOUS REACTOR TEST	37		6
REACTOR MATERIALS RESEARCH	100	4	
TOTAL	347	21	13

SUBCONTRACTS

ARMOUR RESEARCH FOUNDATION
AUBURN RESEARCH FOUNDATION
FOSTER WHEELER CORPORATION
HOUDRY PROCESS CORPORATION
OHIO STATE UNIVERSITY
RENSSELAER POLYTECHNIC INSTITUTE
SYRACUSE UNIVERSITY
TULANE UNIVERSITY
UNIVERSITY OF FLORIDA
UNIVERSITY OF VIRGINIA
VITRO CORPORATION